UC Irvine

UC Irvine Electronic Theses and Dissertations

Title

TLR Tri-Agonist and TLR-Antigen Conjugates as Modulators of Innate Immunity and as Adjuvants in a Q-Fever Vaccine

Permalink

https://escholarship.org/uc/item/6840b8s9

Author

Albin, Tyler James

Publication Date

2019

Peer reviewed|Thesis/dissertation

eScholarship.org Powered by the California Digital Library
University of California

UNIVERSITY OF CALIFORNIA,
IRVINE

TLR Tri-Agonist and TLR-Antigen Conjugates as Modulators of Innate Immunity and as Adjuvants in a Q-Fever Vaccine

DISSERTATION

submitted in partial satisfaction of the requirements
for the degree of

DOCTOR OF PHILOSOPHY

in Organic Chemistry

by

Tyler James Albin

Dissertation Committee:
Professor Aaron Esser-Kahn, Advisor
Professor Jennifer Prescher, Chair
Professor James Nowick
Professor Robert Spitale

2019

Portions of Chapters 1, 2, and 3 have been reproduced in part from: Albin, T.J.*; Tom, J.K.*; Manna, S.; Gilkes, A.P.; Stetkevich, S.A.; Katz, B.B.; Supnet, M.; Felgner, J.; Jain, A.; Nakajima, R.; Jasinskas, A.; Zlotnik, A.; Pearlman, E.; Davies, D.H.; Felgner, P.L.; Burkhardt, A.M.; Esser-Kahn, A.P. Covalently Linked Toll-Like Receptor Tri-Agonists Stimulate Distinct, Combination Dependent Innate Immune Responses. *ACS Central Science*, **2019**, Accepted. ***Co-first authors** © 2018 American Chemical Society.

Portions of Chapters 1 and 5 have been reproduced in part with permission from: Ignacio, B.J.*; Albin, T.J.*; Esser-Kahn, A.P.; Verdoes, M. TLR Agonist Conjugation: A Chemical Perspective. *Bioconjug. Chem.*, **2018**, *29* (3), 587-603. ***Co-first authors.** © 2018 American Chemical Society.

Portions of Chapter 1 have been reproduced in part with permission from: Tom, J.K.; Albin, T.J.; Manna, S.; Moser, B.A.; Steinhardt, R.; Esser-Kahn, A.P. Applications of Immunomodulatory Immune Synergies to Adjuvant Discovery and Vaccine Development. *Trends Biotechnol.*, **2018**, *37* (4), 373-388.© 2015 Cell Press.

All other materials © 2019 Tyler J. Albin

DEDICATION

To

My Mom, Dad, Family, Friends, and Mentors

For all of your love, support, and laughs

I couldn't have done it without you.

"**Follow your passion** — I know people tell you that, but I'm not kidding.

You will find your way to something that you really enjoy if you just keep looking,

and **you'll be surprised to see that you can change the world.**

So my advice is: pursue that — **leave the world better than you found it**,

and everybody's responsible for his or her own actions…"

Bill Nye

TABLE OF CONTENTS

LIST OF FIGURES

LIST OF SCHEMES

LIST OF TABLES

ACKNOWLEDGMENTS

First and foremost, I would like to thank my Ph.D. advisor, Professor Aaron Esser-Kahn. From the first time we spoke on the phone about coming to UCI, you have been incredibly supportive and encouraging. You have always encouraged me to take risks and try out new ideas and experiments. Although many of them didn't pan out, this has been incredibly influential in shaping my career development as an independent scientist. I deeply appreciate your guidance, both in the lab and in my career development, and enabling me to follow my passion. I look forward to seeing the amazing innovation and discoveries the lab develops in the years to come.

Next, I would like to thank my Thesis Committee. Thank you to Professor Jenn Prescher. You have always been supportive and provided advice I have found incredibly helpful throughout my time in graduate school. Thank you to Professor James Nowick. Your lab was one of the first I rotated in at UCI during the summer and I found it to be incredibly welcoming, making the transition to UCI an easy one. Thank you to Professor Rob Spitale. Your first year as a professor was also my first as a graduate student. I appreciate how you took a moment to ask how everything is going when we crossed paths, as well as your advice and insight.

Thank you to my collaborators. Professor Phil Felgner, you have always been very supportive over the last few years. I appreciate all of your our fun research endeavors, as well as your excellent taste in beer. Professor Amanda Burkhardt, getting all of our compounds tested has been a wild ride! Thankfully, I was fortunate enough to have you as a collaborator to be in the trenches with. I appreciate all of your help and will miss our coffee, cheese, and assorted tasty treat adventures. In addition, I would like to thank Professor Zhibin Guan and your lab members for providing a home for my final year. You have always made sure the lab was very welcoming and I appreciate you making this possible.

Thank you to the facilities and labs of UCI including Ben, Felix, Beniam, Phil, and Dima. Without your hard work and expertise, this work would not have been possible. Special thanks to Ben Katz for always being willing to help with every mass spec challenge I could think of.

Thank you to my previous mentors who have shaped my career. Thank you to Kirby Zornes and Bob Miller, my high school chemistry teachers. Your love of teaching and chemistry lit the spark that took me to where I am today. I really appreciate your excellence in teaching and inspiring to pursue this path. Thank you to Professor Amanda Murphy for being an amazing advisor to begin my research career with. You showed the patience and guidance that molded me into an effective researcher and I am very grateful for that. Thank you to Dr. Jack Sadowsky, my project manager during my internship at Genentech. I appreciate your guidance in working effectively in industry and transiting from academia. You lead by example and I know by following it I can also run a productive, supportive, and fun lab.

Thank you to my lab mates in the Esser-Kahn lab for all of the fun times over the years. Special thank you to my graduate mentor, Dr. Janine Tom. You are the best mentor and buddy I could have ever asked for. I miss all of our fun inside jokes from the first few years, but I am so happy to see you succeed in your career. Thank you to Dr. Saikat Manna, your help on the DTRA project has been incredibly important for us getting it over the finish line, all while being down to earth and a great coworker. Thank you to my undergraduate students, Sam Stetkevich and Arianna Mortavelli for working super hard and being excellent students. Special thanks to my labmates that also began grad school in 2014, Dr. Brittany Moser and Seong Min-Kim, both of you are so much fun to work with and have kept me sane for the last five years. Also, thank you to Dr. Alfred Chon for all of the fun times in and outside the lab, my food palate is far more cultured thanks to you. Thank you to Anna Love, Jainu Aijt, and Nihesh Naorem for all of your help on the various crazy product ideas we tried out together, you all are great scientists and I look forward to seeing your accomplishments. Thank you to Troy, Bethany, and Yoseline for being amazing lab managers.

Thank you to all of my friends I have made at UCI. Thank you to all of my roommates, Sam, Francesca, James, Mo, Zach, Majid, Chris, and David, for making life bearable through my time in graduate school. All of you have been great and I couldn't have been more lucky to room with such wonderful people. Special cheers to Sam Reifsnyder, my Brew-Bae. Way too many fun times to list, and I am glad I had such a great friend to help me through the bad times and to celebrate the good. Thank you to Dr. David Row, it's been fun enjoying coffee, beer, and our journey from Bellingham to Irvine together. Thanks to my childhood friends, particularly Shahar Golan and Max Luartes, for staying in touch and rooting for me the whole way though.

Thank you to Randi Lunquist. You have helped me through the end of this journey and I couldn't be more thankful to have met you. You remind me that there is more to enjoy in life than work, to appreciate nature and challenge me to be more adventurous. Your love, support, and understanding in helping me through these last few months mean the world to me and I can't wait to explore it with you.

Thank you to my family that is always there for me. Thank you to Nick and Kyah Albin for being awesome siblings. Thank you to Scott and Corey Sims for always being there when I needed to escape OC for a weekend for some family time. Thank you to my grandparents for your love, support, and always interested in hearing what's new.

Last but not least, I would like to express my deepest appreciation for my Mom and Dad. You have always supported me and encouraged me to follow my passion. You have always helped me through the stressful times and are always ready to celebrate my accomplishments. I couldn't imagine getting to this point without you both. Thank you!

To celebrate my newfound hobby in grad school, brewing, I have prepared a craft beer pairing guide that captures the character of each chapter to be enjoyed with this thesis.

Chapter 1: Deschutes Mirror Pond Pale Ale from Bend, Oregon
A welcoming beer. Like this chapter, it highlights years of previous work but with a Northwest twist.

Chapter 2: Elysian Dragonstooth Stout from Seattle, WA
A dense beer. This chapter goes deep into the synthetic details of our work.
Similarly, this beer is dense with flavor.

Chapter 3: Fremont Summer Ale from Fremont, WA
A lighter, yet interesting beer. A refreshing beer, that reveals more character as you go,
showing that all of that Stout was worth it.

Chapter 4: Nobel Ale Works Naughty Sauce Ale from Anaheim, CA
An intriguing beer. Full of unique flavor, just like our molecules.

Chapter 5: Lagunitas Super Cluster Ale, from Petaluma, CA
A beer unlike the others. This beer is full of twists and turns and keeps things exciting.

CURRICULUM VITAE

Tyler James Albin

EDUCATION

Ph.D. Chemistry. University of California, Irvine. 2014-2019
Advisor: Aaron Esser-Kahn.
Thesis title: "TLR Tri-Agonist and TLR-Antigen Conjugates as Modulators of Innate Immunity and as Adjuvants in a Q-Fever Vaccine."

B.S. Biochemistry and Minor in Materials Science Western Washington University. 2010-2014
Cum Laude, Departmental Honors, GPA: 3.89
Advisor: Amanda Murphy
Project title: "Functionalization of Conducting Polymers with Silk-Inspired Peptides."

RESEARCH EXPERIENCE

Esser-Kahn Lab. University of California, Irvine. Irvine, CA. 2014-2019
Graduate Student Researcher with Professor Aaron Esser-Kahn.

- Led chemistry efforts for synthesis, characterization, and testing of novel TLR agonist-based adjuvants for a novel Q-Fever vaccine within a highly collaborative, cross-functional project.
- Experienced in several steps of preclinical therapeutic development from taking a vaccine development project from chemical design to non-human primate testing in <3 years.
- Developed novel TLR agonist biomolecule-protein antigen conjugates for vaccine applications. This work is the basis of a spun out start company, Nanommune.
- Mentored two undergraduate students and three incoming graduate students.

Genentech. South San Francisco, CA. 2018
Summer Protein Chemistry Graduate Intern with Dr. Jack Sadowsky.

- Developed novel antibody-drug conjugate technology.

Murphy Lab. Western Washington University. Bellingham, WA. 2012-2014
Undergraduate Researcher with Professor Amanda Murphy.

- Pioneered project developing electrically-conductive biomaterials from silk peptides.
- Mentored two undergraduate students and developed a solid-phase peptide synthesis lab exercise for organic chemistry students.

SKILLS

Bioconjugation chemistry (site specific and non-specific), protein characterization (SDS-PAGE, HPLC, LCMS, WB, SEC, LAL), protein purification (IMAC, AKTA FPLC, endotoxin removal), protein expression (*E. coli*), synthetic organic chemistry, solid phase peptide synthesis, small molecule analysis (NMR, MS, TLC, HPLC), normal-phase purification, data analysis (GraphPad, PyMOL, ChemDraw, Microsoft office), *in vitro*

cellular assays (flow cytometry, ELISA), cell culture, *in vivo* experimental design (tissue collection, safety studies, vaccination)

AWARDS

NIH T32 Chemical and Structural Biology Training Grant Fellowship 2016
Chancellor's Fellowship in Chemistry 2014
Best 1st Year Teaching Assistant 2015
Phillips 66 Undergraduate Summer Research Fellowship 2013
Knapman Chemistry Scholarship 2012
Chemistry Department Merit Based Partial Tuition Waiver 2012

ADDITIONAL EXPERIENCES

Seed Consulting Group . 2018-present
Consultant (2018), Project Manager (2019)

- Volunteer for Seed Consulting Group, a non-profit that provides pro-bono consulting for other non-profits promoting missions of sustainability.
- Fall 2018 project cycle: project manager leading a diverse team to develop a marketing strategy for BioPower Enterprises, a startup company.
- Spring 2018 project cycle: consultant for the Wyland Foundation Mobile Learning Center to improve marketing efforts and operations.

SciPhD Business of Science for Scientists Workshop 2017

- Four-day workshop to develop communication, leadership, negotiation, team building, networking, and project management skills necessary for transitioning to industry.

Organic Chemistry Laboratory Teaching Assistant. 2014-2015

- Taught three quarters of undergraduate organic chemistry lab courses for honors/majors students.
- Awarded best 1st year TA award by the chemistry department

University of Washington Biomaterials Intensive Short Course 2013

- One-week course covering current state of biomaterials research topics.

PUBLICATIONS

1. **Albin, TJ***; Tom, JK*; Manna, S; Gilkes, AP; Stetkevich, SA; Katz, BB; Supnet, M; Felgner, J; Jain, A; Nakajima, R; Jasinskas, A; Zlotnik, A; Pearlman, E; Davies, DH; Felgner, PL; Burkhardt, AM; Esser-Kahn, AP. (2018) Covalently Linked Toll-Like Receptor Tri-agonists Stimulate Distinct, Combination Dependent Innate Immune Responses. Under Review. ***Co-first authors**
2. Gilkes, AP*; **Albin, TJ***; Manna, S; Supnet, M; Ruiz, S; Tom, JK; Jain, A; Nakajima, R; Felgner, J; Davies, DH; Stetkevich, SA; Zlotnik, A; Pearlman, E; Nalca, A; Felgner, PL; Esser-Kahn, AP; Burkhardt, AM. (2018) *Coxiella burnetti* Subunit Vaccines Adjuvanted with Covalently-Linked Toll-Like Receptor Agonists Elicit Unique Immune Responses to Immunization and Challenge. Under Review. ***Co-first authors.**

3. Tom, JK; **Albin, TJ**; Manna, S; Moser, BA; Steinhardt, R; Esser-Kahn, AP. (2018) Applications of Immunomodulatory Immune Synergies to Adjuvant Discovery and Vaccine Development. **Trends Biotechnol.**. *37* (4), 373-388.
4. Ignacio, BJ*; **Albin, TJ***; Esser-Kahn, AP; Verdoes, M. (2018) TLR Agonist Conjugation: A Chemical Perspective. **Bioconjug. Chem.**, *29* (3), 587-603. ***Co-first authors.**
5. Blatz, TJ; Fry, MM; James, EI; **Albin, TJ**; Pollard, Z; Kowalcyzk, T; Murphy, AR. (2017) Templating the 3D structure of Conducting Polymers with Self-Assembling Peptides. **J Mater. Chem. B**, *5* (24*)*, 4690-4696.
6. **Albin, TJ**; Fry, MM; Murphy, AR. (2014) Synthesis, Characterization, and Secondary Structure Determination of a Silk-Inspired, Self-Assembling Peptide: A Laboratory Exercise for Organic and Biochemistry Courses**. J. Chem. Educ.**, *91* (11), 1981-1984.

PRESENTATIONS

1. **Poster Presentation:** "Toll-like receptor agonist chemistries and protein microarray tools for development of a *Coxiella burnetii* subunit vaccine that protects against an aerosol challenge." *American Society of Tropical Medicine & Hygiene*, New Orleans, LA. October 31, **2018**.
2. **Poster Presentation:** "Distinct Immune Responses with Covalently-Linked TLR Agonist Combinations for a Q-Fever Vaccine." *World Vaccine & Immunotherapy Congress*, San Diego, CA. November 30, **2017**.
3. **Oral Presentation:** "Directed Immune Responses with Covalently-Linked TLR Agonist Combinations." *NIH Chemical and Structural Biology Training Grant Public Research in Progress Seminar,* Irvine, CA. May 8, **2017.**
4. **Poster Presentation:** "Directed Immune Responses via Covalently-Linked TLR Agonist Combinations for a Q-fever Vaccine." *253rd American Chemical Society National Meeting & Exposition,* San Francisco, CA. April 5, **2017.**
5. **Poster Presentation:** "Directed Immune Responses via Covalently-Linked TLR Agonist Combinations." 251st American Chemical Society National Meeting & Exposition San Diego, CA. March 15, **2016.**
6. **Oral Presentation:** "Functionalization of Conducting Polymers with Silk-Inspired Peptides." Honors Thesis Seminar Western Washington University, Bellingham, WA. May 16, **2014.**
7. **Oral Presentation:** "Functionalization of Conducting Polymers with Silk-Inspired Peptides." American Chemical Society Puget Sound Section Undergraduate Research Symposium Western Washington University, Bellingham, WA. May 3, **2014.**
    - Best Oral Presentation Award
8. **Poster Presentation:** "Functionalization of Conducting Polymers with Silk-Inspired Peptides to Develop Robust Materials for Biomedical Applications." Materials Research Society Spring Meeting & Exhibit San Francisco, CA. April 22, **2014.**

- Nominated: Best Poster Award

9. **Poster Presentation:** "Conducting Polymers Functionalized with Silk-Inspired Peptides to Develop Robust Materials for Biomedical Applications." Symposium of the Pacific Northwest Chapter of the American Vacuum Society, Edgefield, OR. September 19-20, **2013.**
    - Second Place Best Undergraduate Poster Award
10. **Poster Presentation:** "Investigation of Conducting Polymers Functionalized with Silk-Inspired Peptides to Create Robust Materials for Biomedical Applications." REU/Phillips Fellowship Summer Symposium Western Washington University, Bellingham, WA. August **2013.**
11. **Poster Presentation:** "Synthesis and Characterization of Silk-Peptide Functionalized Thiophene Derivatives for Use in Biomedical Applications." Scholar's Week, Western Washington University, Bellingham, WA. May 17, **2013.**
    - Sigma xi Outstanding Poster Award
12. **Poster Presentation:** "Synthesis and Characterization of Silk-Peptide Functionalized Thiophene Derivatives for Use in Biomedical Applications." American Chemical Society Puget Sound Section Undergraduate Research Symposium, Seattle Pacific University, Seattle, WA. April 27, **2013.**

AFFILIATIONS

American Chemical Society

ABSTRACT OF THE DISSERTATION

TLR Tri-Agonists and TLR-Antigen Conjugates as Modulators of Innate Immunity and as Adjuvants in a Q-Fever Vaccine

By

Tyler James Albin

Doctor of Philosophy in Organic Chemistry

University of California, Irvine, 2019

Professor Aaron Esser-Kahn, Advisor

Professor Jennifer Prescher, Chair

Although one of the greatest achievements of modern medicine, traditional vaccination strategies have failed to generate effective vaccines for many infections including global diseases, like tuberculosis, and regional diseases, like Q-Fever. New approaches are needed for each type of disease. The protective immunity and distinct responses of many successful vaccines come from activating multiple Toll-like Receptors (TLRs). Vaccines with multiple TLR agonists as adjuvants have proven effective in preclinical studies, but current research has not explored two important elements. First, few multi-TLR systems explore spatial organization – a critical feature of whole-cell vaccines. Secondly, no multi-TLR systems to date provide systematic analysis of the combinatorial space of three TLR agonists. This work describes the effects of conjugation between combinations of three TLR agonists and between TLR agonists and antigens on immunological activity. Here, we present the first examination of the combinatorial space of several spatially defined triple-TLR adjuvants, by synthesizing a series of five triple-TLR agonists and testing their innate activity both *in vitro* and *in vivo*. The combinations were evaluated by measuring activation of immune stimulatory genes (Nf-κB, ISGs), cytokine profiles (IL12-p70, TNF-α, IL-6, IL-10,

CCL2, IFN-γ, IFN-α, IFN-β) and *in vivo* cytokine serum levels (IL-6, TNF-α, IL12-p40, IFN-α, IFN-β). We demonstrate that linking TLR agonists substantially alters the resulting immune response compared to their unlinked counterparts and that each combination results in a distinct immune response, particularly between linked combinations. We show that combinations containing a TLR9 agonist produce more TH1 biasing immune response profiles, and that the effect is amplified upon conjugation. However, combinations containing TLR2/6 agonist are skewed toward TH2 biasing profiles despite the presence of a TLR9 agonist. To assess their efficacy in a vaccine, we formulated antigens from *C. burnetii,* the causative agent of Q-Fever, with TLR tri-agonists and evaluated the outcomes of vaccination *in vivo*. We found that the Tri-agonists elicited unique, antigen-specific immune responses *in vivo* which matched our initial *in vitro* analysis. We evaluated our top candidates in a live *C. burnetii* aerosol challenge model in mice and found two of our TLR tri-agonist containing formulations conferred partial protection to the challenged animals. Our findings characterize a novel adjuvant platform and offer an alternative approach to generating protective and effective vaccine candidates against *C. burnetii*. These results demonstrate the profound effects that conjugation and combinatorial administration of TLR agonists can have on immune responses, a critical element of vaccine development. In addition, numerous studies have shown that conjugation of TLR agonists to antigens can beneficially influence their potency, toxicity, pharmacokinetics, and function. Here, we present our work in developing site-specific conjugation approaches of TLR agonists to antigens.

CHAPTER 1

Introduction

1.1 Introduction

Immunotherapies are at the forefront of prophylactic and chronic disease treatments. Vaccines have drastically reduced the number of morbidities and infections, even eliminating many once devastating diseases, including smallpox and diphtheria.[1] This achievement demonstrates the need to develop new vaccines for diseases that continue to threaten public health, such as HIV and malaria, as well as emerging diseases such as Ebola and Zika, and persistent regional diseases like Q-Fever. However, most vaccines are empirically derived, with little understanding of their mechanism of action. This lack of understanding makes it difficult to rationally and rapidly develop new vaccines against prevalent diseases.

The effectiveness of a vaccine is influenced by its composition, where vaccines are composed of an antigen, the target of an immune response, and an adjuvant, an agent that activates the immune response.[2,3] Treatment with antigens alone can suffer from low immunogenicity, so an adjuvant is required to enhance the immune response toward the antigen of interest.[4] Adjuvants typically include a single immune agonist, aluminum salts, and/or in an oil-in-water emulsion. Recently, the development of adjuvants composed of multiple types of immune agonists has shown promise. This strategy aims to elicit an enhanced immune response, known as an immune synergy, potentially providing a more effective vaccine.[5,6]

In the Esser-Kahn lab, we aim to uncover the guiding principles in multi-valent, innate immune stimulation. With this knowledge we aim to develop novel immune stimulation strategies for therapeutic applications through chemistry. Activation of multiple innate immune response pathways can result in synergistic or inhibitory stimulation, leading to unique immune response

profiles.[7] This phenomenon is responsible for generating robust immunity to pathogens following natural infection and successful vaccines often mimic this model (**Fig. 1.1**).[8] Conjugation of multiple immunostimulants or immunostimulants with antigens more closely mimics natural encounters of host immune cells with pathogens. By evaluating the immunological activity of these conjugates, we can uncover guiding principles in stimulating distinct immune responses, leading to more rational design of adjuvants for vaccines and immunotherapies.

1.2 The Immune System

The immune system is comprised of two major components – the innate and adaptive immune systems. Both systems encompass a complex network of cells and biochemical processes evolved to protect the host from pathogens, mainly viruses, bacteria, and fungi.[9] The innate immune system is responsible for rapidly responding to infection, mounting a preliminary defense. The major effector cells in this role include neutrophils, natural killer cells, basophils, eosinophils, macrophages, and dendritic cells (DCs).[9] These cells fight infection through a variety of non-specific mechanisms including phagocytosis, release of toxic compounds, and killing of infected cells. [9]

Most pathogens succumb to the innate immune system and the host is never made aware of the prevented infection.[10] However, sometimes a particular infection is difficult to quench, requiring reinforcements. DCs are especially important at this juncture as they function to alert and train the adaptive immune system to specifically target the pathogen through a process called antigen presentation.[11] During the innate response at the site of infection, dendritic cells engulf and digest pathogens in lysosomes. The DCs then load peptides derived from the digested proteins, antigens, of the pathogen onto major histocompatibility complex (MHC) proteins.[11] These antigen-

MHC complexes are then presented on the cell surface to naïve helper ($CD4^+$) and killer ($CD8^+$) T cells, inducing activation.[12] Among other immunomodulatory functions, the activated T cells aid in activating B cells, resulting in the production of antibodies toward the pathogen. Generation of these adaptive immune responses are considered the hallmark of immunity toward future infection. Immunity through vaccination engages these same processes. However, the immune responses originate through exposure to antigens and immunostimulants in the vaccine formulation, traditionally from inactivated whole-cell pathogens, generating immunity without infection (**Fig 1.1 B**).[8]

Although exposure to antigen is necessary to confer T and B cell specificity toward the pathogen, it is not sufficient for the development of an effective immune response.[3] In addition to encountering antigen, dendritic cells must also encounter pathogen associated molecular patterns (PAMPs) which are ligated by pattern recognition receptors (PRRs), the main class of them being Toll-Like Receptors (TLRs).[13] PAMPs act as adjuvants for the immune system, as their recognition results in activation of the dendritic cell and the successful development of the immune response.[14] Thus, stimulation of these receptors is essential to generating protection.

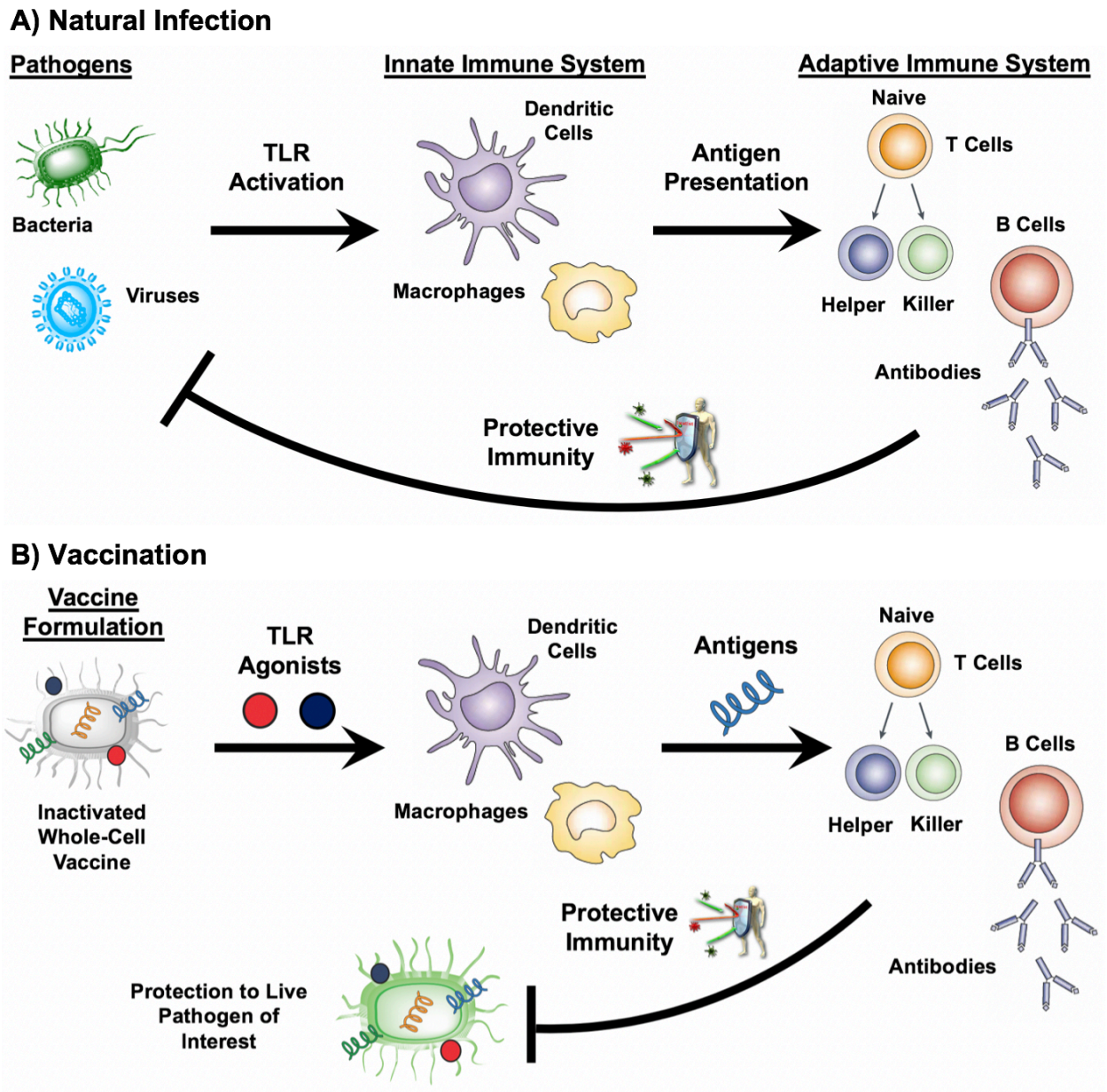

Figure 1.1 Generation of Protective Immunity from Natural Infection and Vaccination. A) Upon infection, pathogens first activate the innate immune system through pattern recognition receptor stimulation, including TLR stimulation. This leads to antigen presentation and activation of the adaptive immune system, ultimately generating long-lasting protective immune responses against the infecting pathogen. B) Vaccines generate protective immunity through the same processes, but often through exposure to inactivated pathogens. By inactivating the organism, the immune system is exposed to TLR agonists and antigen, but without the consequences of infection.

1.3 Toll Like-Receptor Activation

TLRs are a class of transmembrane PRRs. Their role is to recognize conserved molecular components of pathogens, PAMPs, as well as cellular damage-associated molecular patterns (DAMPs).[15] The receptors are predominantly expressed in immune cells and show distinct expression patterns across different cell types.[16]

The human TLR family comprises 10 functional TLRs that are expressed both on the cell surface (TLR1, 2, 4, 5, and 6) and intracellularly in endosomal compartments (TLR 3, 4, 7, 8, and 9).[17,18] The cellular localization of TLRs reflects the origin of the ligand it is responsible for detecting (**Fig 1.2**). TLRs found at the cell surface respond to extracellular components of pathogens, including lipoproteins (TLR1, 2, and 6), lipopolysaccharides (TLR4), and bacterial flagellin (TLR5). Endosomal TLRs recognize components from the intracellular compartments of pathogens, such as double-stranded RNA (dsRNA, TLR3), single-stranded RNA (ssRNA, TLR7 and 8), and unmethylated cytosine-phosphate-guanine (CpG) DNA (TLR9).[19] Although the role and natural ligand for human TLR10 is not yet fully understood, it is thought to be a negative regulator of TLR signaling.[20–22] Binding of ligands to TLRs induces homo- or heterodimerization of TLR receptors and subsequent downstream signaling through two distinct pathways, the MyD88-dependent (TLRs 1, 2, and 4–9) and TRIF-dependent pathway (TLR3 and 4), generally mediating inflammatory and antiviral responses, respectively.[23,24]

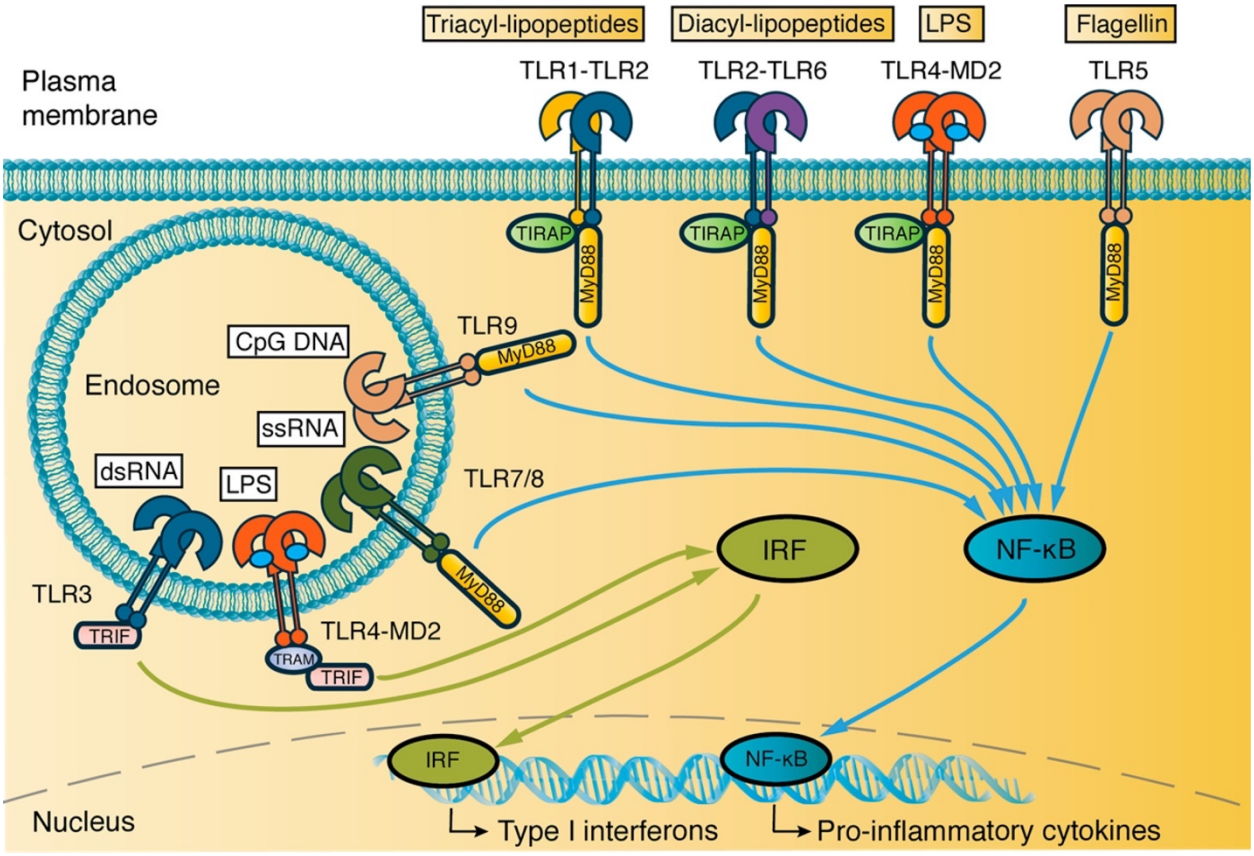

Figure 1.2 TLR Ligands, Localization, and Transcription Pathways. Cellular location of TLRs, their ligands, and signal transduction pathways. TLRs 1, 2, 6, 4 and 5 are located on the plasma membrane and signal, together with endosomal TLRs 7, 8, and 9, in a MyD88-dependent manner. The MyD88 pathway leads to NF-κB translocation to the nucleus and, ultimately, production of inflammatory cytokines. Activated TLR4 is endocytosed and, together with endosomal TLR3, signals through the IRF pathway, leading to Type I interferon production. MD2, TRAM and TIRAP are adaptor proteins.

TLRs are crucial in the innate immune system for their role in fighting infection. They are responsible for the initial response to pathogens and their activity drives the generation of innate and adaptive immune responses.[16,17] Upon stimulation, DCs up-regulate expression of cytokines (mainly TNF-α, IL-6, and IL-12), up-regulate expression of costimulatory molecules (CD40, CD80, and CD86), increase antigen-presenting capacity, and migrate from the peripheral tissues

to draining lymph nodes.[17] There, antigen presenting DCs stimulate naïve T-cells which begins the adaptive immune response. B-cells also express TLRs and present antigen upon activation, resulting in antibody production specific for the encountered antigen.[25] Since T- and B-cell maturation is influenced by TLR, costimulatory, and cytokine signaling, TLR agonists play an important role in establishing the magnitude and type of adaptive immune response that is generated.

1.4 Toll-Like Receptor Synergy

Many adjuvant formulations consist of a single type of PAMP. Unfortunately, a single immune agonist is not always as effective as a whole pathogen at eliciting an efficacious immune response. Activation from natural pathogens and their PAMP profile results in unique, highly effective immune responses that is well suited for clearing the pathogen responsible for activation.[7] This process was demonstrated with the yellow fever virus vaccine which activates TLRs 2, 7, 8 and 9 in a spatially confined manner, with a single dose conferring lifelong immunity.[26] The authors showed that removal of any TLR from this system dramatically reduced the effectiveness of the vaccine in generating protection. Owing to this inherent efficacy, there has been greater use of multiple ligands to synergistically enhance the immune response in therapeutic development.

Recent discoveries have prompted collaboration between different scientific disciplines, leading to the development of new methods to improve the adjuvanticity of native and synthetic PRR agonists as well as the delivery of synergistic adjuvants. Innovative chemical, biological, and engineering methods are being utilized to rapidly screen and analyze synergistic immune responses for adjuvant discovery, determine dosing, localize delivery of multi-agonist adjuvants, and deliver vaccine cargo to specific immune cell subtypes and cellular compartments.

High-throughput screening (HTS) has recently been utilized as a method to analyze multiple cytokines when screening different immune synergy combinations and choosing the best adjuvant for a vaccine.[27,28] HTS is widely used in drug discovery to rapidly screen compound libraries for biologically active molecules. Several TLR small-molecule immune potentiators (SMIPs; e.g., TLR2 and TLR7 small molecule agonists) have recently been discovered by HTS, which can screen millions of compounds for adjuvanticity, and these SMIPs have been used as vaccine adjuvants.[29,30] The efficiency of HTS allows rapid determination of potential adjuvant hits, making this platform a powerful tool for adjuvant discovery.

Because not all TLRs have small molecule agonists (e.g., TLRs 3, 5, and 9), HTS can quickly determine what types of chemical structures activate specific TLRs. A multiplexed high-throughput method was used to screen several compound libraries (>100000 compounds) for specific PRR activity with the aim to discover new small molecule adjuvants.[28] From the molecule screen, amphotericin B (AmpB) was discovered to elicit TLR2 and TLR4 immune activity, with an immune response profile similar to MPLA, suggesting the potential of AmpB as a new adjuvant. Zhang and colleagues also used HTS technology to screen a library of compounds for activity against TLR3.[31] With one hit compound, they performed structure–activity relationship (SAR) studies leading to one molecule that activates TLRs 3, 8, and 9. All three TLRs are activated by virus-derived nucleic acids, which may explain how this one molecule can activate all three TLRs. The HTS platform provided analysis of 59 different compounds and subsequent derivatives of the hit small molecule. These processes would be laborious and time-consuming without high-throughput technology. Applying medicinal chemistry approaches and HTS to adjuvant discovery can lead to other synergistic small molecule adjuvants, where pharmacokinetics, pharmacodynamics, and biodistribution properties can all be optimized.

In addition, HTS has been applied to the analysis and characterization of synergistic immune responses from specific agonist combinations. Immune synergies typically have been studied using standard cytokine readouts, such as ELISA.[32] However, ELISA is not the most efficient method to analyze multiple cytokines because only one cytokine can be measured at a time. The invention of multiplexed screens, such as Luminex assays, improved the screening process, allowing analysis of a larger number of samples or multiple cytokines in a single sample. Unfortunately, this type of technology still suffers from a detection limit of pg/ml, resulting in the requirement for high volumes of supernatant or sera.[28,33] To circumvent these challenges, Garcia-Cordero and colleagues developed a nanoscale high-throughput immunoassay chip using soft lithography techniques to analyze synergistic activity between PRR agonist combinations.[27] Their data provided results comparable to those obtained by traditional ELISAs. Their microfluidic device can detect four different biomarkers using only nanoliters of sera in a 384-well plate format. They can also reach a lower detection limit of 100 fM with in vitro cell media and in vivo sera. Using their technology, they identified agonist combinations from 10 different TLR agonists that resulted in synergistic or inhibitory cytokine production. They validated their synergistic in vitro observations in an in vivo model system. The ability to screen a large quantity of PRR agonist combinations in a dose-dependent manner provides a faster and more cost-efficient readout to determine effective immune responses from distinct agonist combinations for adjuvant discovery. Multiplex assays still face challenges with non-specific binding and cross-reactivity when analyzing complex biological samples, but this technology is a step toward developing platforms that solve analytical challenges, providing the ability to screen for compounds that elicit desired immune responses.

These improved responses can provide reduced adjuvant and antigen dosing, also known as dose sparing.[5,6] In addition, response amplification through immune synergies aids in differentiating foreign antigens from self-antigens, thus working to prevent autoimmune responses. Immune synergies can also dictate the type of response generated, which depends on the specific combination of PRRs targeted, ensuring that the protective immune responses produced are tailored to the pathogen of interest.[27,32] The use of multiple classes of PAMPs as adjuvants in clinical models has demonstrated positive vaccination results, suggesting considerable potential for these molecules as new adjuvants.

1.5 Modulating Immune Stimulation Through TLR Agonist Conjugation

The discovery of synergistic interactions between multiple types of PRRs has led to the covalent conjugation of PAMPs to develop new multi-agonist adjuvants that improve vaccine immunogenicity. PAMPs are spatially associated with one another owing to the natural structure of pathogens. Although unconjugated mixtures of multiple PRR agonists elicit synergistic immune activity, this approach does not mimic the spatial component of PRR activation by a pathogen. Adjuvants that are mixtures of unconjugated agonists can diffuse through the immune system and may be cleared more readily.

Developing more potent and effective immunostimulants *via* covalent conjugation has led to the application of these tools as adjuvants in vaccination models. The first example of this was CL429, a chimeric molecule containing the agonists Pam2C (2,3-dipalmitoyl-S-glyceryl cysteine) and murabutide (muramyl dipeptide (MDP) derivative), which stimulate TLR2 and NOD2, respectively.[34] CL429 was used as an adjuvant in a HIV-1 subunit vaccine and increased HIV-1 p-24 antigen specific IgG and IgA antibody titers compared to either the individual agonists or a

mixture of the unconjugated TLR2 and NOD2 agonists. The ability to induce specific and high antibody titers of different subtypes further demonstrated the utility of PRR agonist conjugation in modulating the immune response and improving adjuvant potency.

In addition to covalent localization of multi-agonist adjuvants, particulate vaccine delivery systems have been synthesized that mimic pathogens in size and spatial organization.[35,36] Particulate systems, including nanoparticles, nanodiscs, and liposomes, that range in diameter from sub- to low-micron size provide cargo delivery at sizes similar to that of a virus or bacteria.[37,38] These delivery systems have shown enhanced antigen uptake by antigen-presenting cells (APCs), which can lead to increased antigen presentation and immune activation.[39,40] Biodegradable PLGA [poly(lactic-co-glycolic acid)] particles (~300nm in diameter) have been developed to encapsulate or adsorb dual or triple combinations of TLR agonists, imitating the size and composition of a pathogen.[41,42] Mice immunized with multi-TLR agonist adjuvant formulations have demonstrated distinct changes in the immune response compared to the use of one agonist or antigen alone. These immune responses include the production of the highest avidity antibody titers against the target antigen and balanced TH1/TH2 responses via increased IgG1 and IgG2c levels.[41] Although targeting the antigen and adjuvant to the same endosome is known to increase antigen presentation, stronger humoral responses were observed when the antigen and adjuvant were in separate nanoparticles, requiring more mechanistic investigation.[42] Even so, delivering antigen and adjuvant in different particles would provide a platform system for vaccine formulation development. Nanodiscs are another novel adjuvant delivery system developed to encapsulate dual TLR agonist combinations.[38] Immunizations with this scaffold led to a reduction in plasma cholesterol levels and potent antitumor activity in two different model systems, presenting another efficacious platform that can easily combine synergistic adjuvants with a range of antigens. In

addition, synergistic TLR agonist combinations have been conjugated to whole tumor cells and exhibited enhanced activation marker and cytokine responses upon incubation with immune cells.[43] This study demonstrates that TLR synergy can also be useful for cancer immunotherapy applications.

Other techniques, such as mesoporous silica templating and agonist adsorption to particles via electrostatic and non-covalent interactions, have also been used to synthesize multi-PRR adjuvant delivery systems. Mesoporous silica templating provides uniform particles with high surface area for agonist loading. In an *in vivo* ovalbumin (OVA) immunization model, NOD2 and TLR9 agonist-loaded mesoporous silica particles exhibited synergistic increases in cytokine production and enhanced $CD4^+$ and humoral TH1 responses compared to either NOD2 or TLR9 agonist-loaded particles.[44] Tukhvatulin and colleagues also studied NOD/TLR synergies by adsorbing TLR4 (MPLA) and NOD2 (MDP) agonists to alum particles.[45] By activating TLR4 instead of TLR9, both TH1 and TH2 responses were enhanced as well as OVA-specific IgG antibodies across multiple subsets (IgG1, IgG2, and IgG3), demonstrating an increased breadth in the immune response. These results show how activating multiple PRRs can tune the immune response depending on the PRRs that are activated and how the role of an agonist can change depending on the agonist pairing.

An advantage of particle delivery systems is that their physiochemical properties can be tuned to target cargo delivery, alter release kinetics, and direct the immune response. Particulate delivery vehicles that traffic to specific locations in vivo and create a depot in tissues to provide slow drug release have had a significant impact on vaccine efficacy. Lynn and colleagues synthesized a nanoparticulate adjuvant that exemplified targeted biodistribution.[40] A TLR7/8 agonist was conjugated to a polymer scaffold at different densities and with varying polymer

attributes, such as linker length and composition. Increased density of the TLR agonist on the polymer scaffold resulted in particle formation (~700nm). The particulate form of the adjuvant led to higher cytokine production in the lymph nodes, promoted local lymph node retention and APC uptake, limited systemic toxicity, and enhanced protective T cell responses. They have since shown the broad applicability of this idea to several proteins and adjuvants.[46,47] Applying this technology to multiple PRR agonists and immune synergy studies may provide targeted delivery, specific biodistribution, and mechanistic insight into immune activation.

The few examples of multi-TLR agonist systems in polymer particles and whole-cell vaccines, show great promise, but most studies are done in solution and only with two agonists. In summary, others have shown that; (1) spatial organization of TLR agonists with antigens enhances the immune response, (2) the signaling architecture of TLRs is multimeric, (3) particles with multiple TLR agonists improve immune responses in vaccine applications, and (4) single molecules which activate multiple TLRs provide a unique response (**Fig. 1B**). In our work, we have shown that linked multi-TLR agonists alter immune responses. Covalently linked agonists exhibited more potent activation compared to a solution of unlinked agonists and is dependent on the conjugation method. A panel of dimeric TLR agonists was synthesized, containing combinations of TLR2, TLR4, and TLR9 agonists, which were separated by polyethylene glycol linkers – PEG_6, PEG_{12}, and PEG_{24} linkers.[48,49] These single molecular entities aimed to mimic the spatial proximity of immunostimulatory components in natural pathogens with initial inspiration from herpes simplex virus.[50] Evaluation of the immunostimulatory activity of these compounds provided evidence that the immunogenicity was dependent on the linker length, the specific combination of conjugated TLR agonists, and the sizes of the agonists due to possible steric interactions, all important considerations for adjuvant development.

Recently, we further explored covalently linked PRR agonist research in the development of a trimeric agonist adjuvant because many pathogens contain agonists for three to five different PRRs.[26,43,51] The trimeric molecule is composed of TLR4, 7, and 9 agonists linked to a triazine core. The tri-agonist increased antibody breadth and depth against vaccinia virus antigens in a vaccinia model vaccination study, and elicited a more balanced TH1/TH2 immune response compared to its unconjugated counterparts or the corresponding conjugated di-agonists. This balanced and enhanced antigen-specific response may elicit unique and potentially protective cellular and antibody immune responses compared to solely a TH1 or TH2 response. The covalently linked PRR agonists demonstrate that spatial components play an important role in effective immune system activation. Despite these promising results, this was only one of over 300 potential hetero-trimeric TLR combinations. The synthetic systems discussed are modular, so PRR agonists can be exchanged to test different immune synergies. The specific combination of covalently linked agonists is crucial to obtain the desired immune response because each agonist stimulates characteristic immune signaling pathways and cytokine production. To date, no study has created a systematic comparison of even a small set of covalent multi-TLR combinations.

Here, Chapters 2 and 3 discuss the synthesis of five distinct TLR tri-agonist combinations and compare their immunological response for both spatially organized and unorganized systems (**Fig. 1.3**). The combinations were evaluated by measuring activation of immune stimulatory genes, cytokine profiles from stimulated primary cells, serum cytokine levels, and weight loss after model vaccinations *in vivo*. The linked TLR tri-agonists elicit distinct innate immune responses compared to their unlinked counterparts and led us to further explore their efficacy as adjuvants.

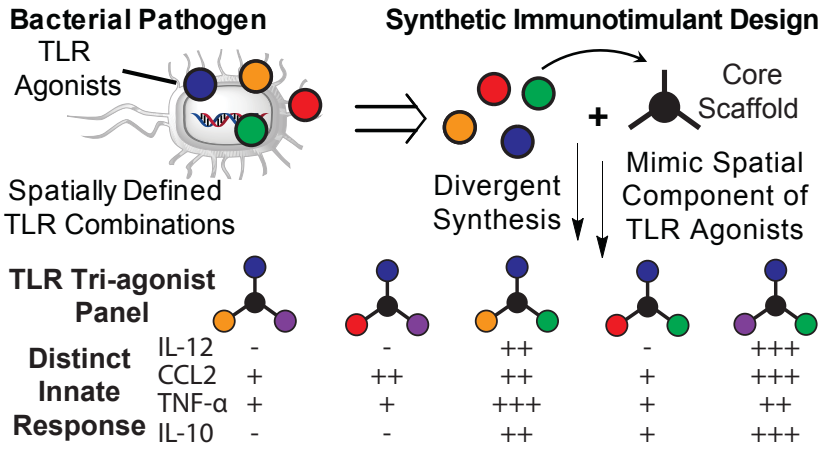

Figure 1.3 Conceptual Illustration of TLR Tri-Agonist Design Inspired by Native, Multi-TLR Agonist Stimulation and our Evaluation of Their *In Vitro* Activity

Chapter 4 discusses our work to evaluate the *in vivo* activity of the five tri-agonists as adjuvants in a subunit vaccine for Q-Fever. In these studies, we evaluated the adjuvant activity of a library of TLR tri-agonists in subunit vaccines formulated with recombinant *C. burnetii* antigens (**Fig. 1.4**). We characterized the ability of our TLR tri-agonists to stimulate robust, antigen specific adaptive immune responses in *in vivo* immunogenicity studies and evaluated the functional efficacy of these responses in a live *C. burnetii* aerosol challenge model in mice. Given the reactogenicity, safety, and implementation issues associated with Q-Vax®, we chose to take a subunit vaccine approach to develop our vaccine candidates against *C. burnetii*. From these studies, we identified multiple vaccine candidates, formulated with specific TLR tri-agonist combinations, that conferred signs of protection against a live *C. burnetii* challenge.

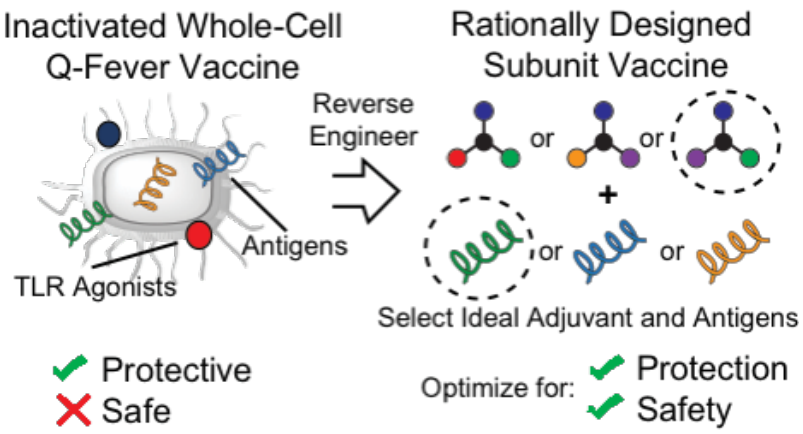

Figure 1.4 Conceptual Illustration of *C. burnetii* Subunit Vaccine Design Where TLR Tri-Agonists are Used as Adjuvants and Paired with Immunogenic *C. burnetii* Antigens

Chapter 5 discusses our initial work investigating site-specific methods for TLR agonist-antigen conjugates. Numerous studies have shown that conjugation of TLR agonists to antigens can dramatically improve the magnitude of the immune response, particularly T cell responses, toward the antigen. This phenomenon is likely the result of co-delivery of the adjuvant and antigen to the same endosome (**Fig. 1.5**) However, recent studies have shown that the enhancement in the response depends on how many TLR agonists are conjugated to the antigen. In addition, B cell epitopes on antigens are comprised following conjugation, preventing the production of antibodies. These studies all utilized non-specific chemistry for conjugation, and no study to date has demonstrated site-specific conjugation to full length protein antigens, which could address both of these issues. Thus, we attempted site-specific conjugation of TLR agonists to *C. burnetii* antigens and we present our initial results in developing these techniques.

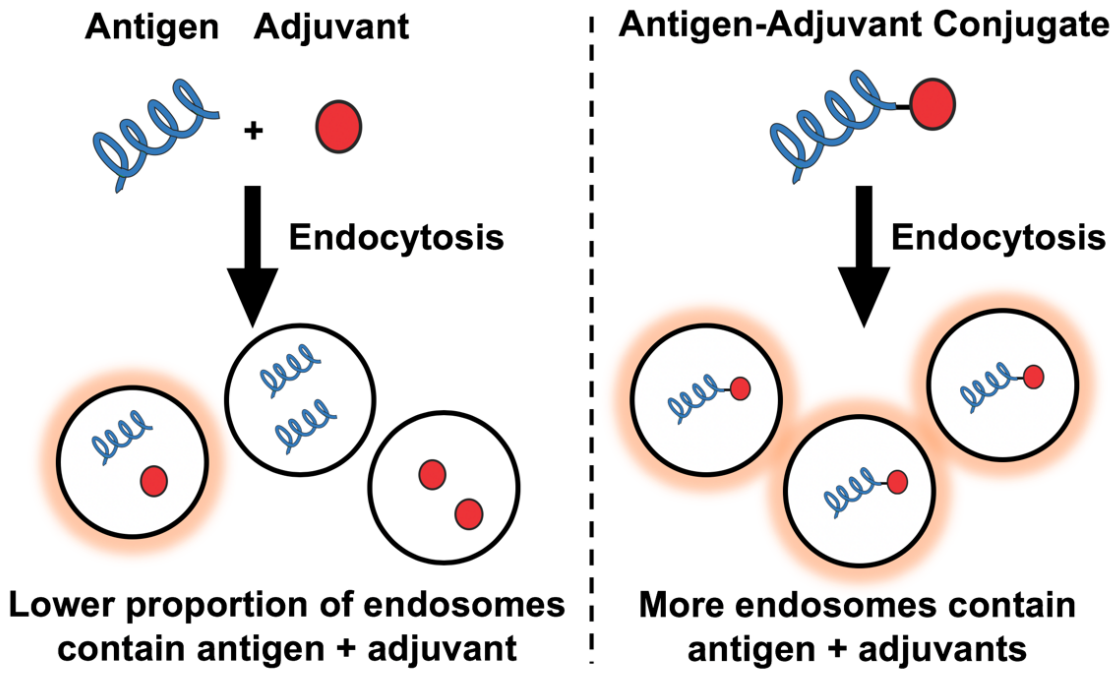

Figure 1.5 Conceptual Illustration of Admixed TLR Agonists and Antigens vs TLR Agonist-Antigen Conjugates.

1.6 Conclusions

Stimulation of the innate immune system is critical for the generation of robust immune responses. Studies utilizing TLR synergy have demonstrated exciting results and conjugation of TLR agonists is promising. Here, we report our work exploring the effects of conjugating different combinations of three TLR agonists has on the resulting immune response. We also investigate methods to site-specifically conjugate TLR agonists to antigens. This work demonstrates the ability to modulate immune responses with the aim of improving the rational design of vaccines and immunotherapies.

1.7 References

(1) Brian, G. The contribution of vaccination to global health: past, present and future. *Philos. Trans. R. Soc. B Biol. Sci.* **2014**, *369* (1645), 20130433.

(2) Orr, M. T.; Fox, C. B.; Baldwin, S. L.; Sivananthan, S. J.; Lucas, E.; Lin, S.; Phan, T.; Moon, J. J.; Vedvick, T. S.; Reed, S. G.; et al. Adjuvant formulation structure and composition are critical for the development of an effective vaccine against tuberculosis. *J. Control. Release* **2013**, *172* (1), 190–200.

(3) Moyer, T. J.; Zmolek, A. C.; Irvine, D. J. Beyond antigens and adjuvants: formulating future vaccines. *J. Clin. Invest.* **2016**, *126* (3), 799–808.

(4) Reed, S. G.; Orr, M. T.; Fox, C. B. Key roles of adjuvants in modern vaccines. *Nat. Med.* **2013**, *19*, 1597.

(5) Cao, X. Self-regulation and cross-regulation of pattern-recognition receptor signalling in health and disease. *Nat. Rev. Immunol.* **2015**, *16*, 35.

(6) Tan, R. S. T.; Ho, B.; Leung, B. P.; Ding, J. L. TLR cross-talk confers specificity to innate immunity. *Int. Rev. Immunol.* **2014**, *33* (6), 443–453.

(7) Mogensen, T. H. Pathogen recognition and inflammatory signaling in innate immune defenses. *Clin. Microbiol. Rev.* **2009**, *22* (2), 240–273.

(8) Pulendran, B. Learning immunology from the yellow fever vaccine: innate immunity to systems vaccinology. *Nat. Rev. Immunol.* **2009**, *9*, 741–747.

(9) Chaplin, D. D. Overview of the immune response. *J. Allergy Clin. Immunol.* **2010**, *125* (2, Supplement 2), S3–S23.

(10) Elliott, D. E.; Siddique, S. S.; Weinstock, J. V. Innate immunity in disease. *Clin. Gastroenterol. Hepatol.* **2014**, *12* (5), 749–755.

(11) Blum, J. S.; Wearsch, P. A.; Cresswell, P. Pathways of antigen processing. *Annu. Rev. Immunol.* **2013**, *31* (1), 443–473.

(12) W., P. N.; Ruslan, M. Pattern recognition receptors and control of adaptive immunity. *Immunol. Rev.* **2008**, *227* (1), 221–233.

(13) Kawai, T.; Akira, S. The role of pattern-recognition receptors in innate immunity: update on toll-like receptors. *Nat. Immunol.* **2010**, *11* (5), 373–384.

(14) Dowling, J. K.; Mansell, A. Toll-like receptors: the swiss army knife of immunity and vaccine development. *Clin Trans Immunol*. Australasian Society for Immunology Inc. May 20, 2016, p e85.

(15) O'Neill, L. A. J.; Golenbock, D.; Bowie, A. G. The history of toll-like receptors-redefining innate immunity. *Nat. Rev. Immunol.* **2013**, *13* (6), 453–460.

(16) Iwasaki, A.; Medzhitov, R. Control of adaptive immunity by the innate immune system. *Nat. Immunol.* **2015**, *16*, 343.

(17) Iwasaki, A.; Medzhitov, R. Toll-like receptor control of the adaptive immune responses. *Nat Immunol* **2004**, *5* (10), 987–995.

(18) Barton, G. M.; Kagan, J. C. A cell biological view of toll-like receptor function: regulation through compartmentalization. *Nat. Rev. Immunol.* **2009**, *9*, 535.

(19) Medzhitov, R. Toll-like receptors and innate immunity. *Nat. Rev. Immunol.* **2001**, *1* (2), 135.

(20) Oosting, M.; Cheng, S.-C.; Bolscher, J. M.; Vestering-Stenger, R.; Plantinga, T. S.; Verschueren, I. C.; Arts, P.; Garritsen, A.; van Eenennaam, H.; Sturm, P.; et al. Human TLR10 is an anti-inflammatory pattern-recognition receptor. *Proc. Natl. Acad. Sci. U. S. A.*

2014, *111* (42), E4478--84.
(21) Jiang, S.; Li, X.; Hess, N. J.; Guan, Y.; Tapping, R. I. TLR10 is a negative regulator of both Myd88-dependent and independent TLR signaling. *J. Immunol.* **2016**, *196* (9), 3834–3841.
(22) Hess, N. J.; Felicelli, C.; Grage, J.; Tapping, R. I. TLR10 suppresses the activation and differentiation of monocytes with effects on DC-mediated adaptive immune responses. *J. Leukoc. Biol.* **2017**, *101* (5), 1245–1252.
(23) Yamamoto, M.; Sato, S.; Hemmi, H.; Hoshino, K.; Kaisho, T.; Sanjo, H.; Takeuchi, O.; Sugiyama, M.; Okabe, M.; Takeda, K.; et al. Role of adaptor TRIF in the Myd88-independent toll-like receptor signaling pathway. *Science,* **2003**, *301* (5633), 640–643.
(24) Akira, S.; Takeda, K. Toll-like receptor signalling. *Nat. Rev. Immunol.* **2004**, *4* (7), 499–511.
(25) Hua, Z.; Hou, B. TLR signaling in B-cell development and activation. *Cell. Mol. Immunol.* **2013**, *10* (2), 103–106.
(26) Querec, T.; Bennouna, S.; Alkan, S.; Laouar, Y.; Gorden, K.; Flavell, R.; Akira, S.; Ahmed, R.; Pulendran, B. Yellow fever vaccine yf-17d activates multiple dendritic cell subsets via TLR2, 7, 8, and 9 to stimulate polyvalent immunity. *J. Exp. Med.* **2006**, *203* (2), 413–424.
(27) Garcia-Cordero, J. L.; Nembrini, C.; Stano, A.; Hubbell, J. A.; Maerkl, S. J. A high-throughput nanoimmunoassay chip applied to large-scale vaccine adjuvant screening. *Integr. Biol.* **2013**, *5* (4), 650–658.
(28) Salyer, A. C. D.; Caruso, G.; Khetani, K. K.; Fox, L. M.; Malladi, S. S.; David, S. A. Identification of adjuvantic activity of amphotericin b in a novel, multiplexed, poly-TLR/NLR high-throughput screen. *PLoS One* **2016**, *11* (2), e0149848–e0149848.
(29) Wu, T. Y.-H.; Singh, M.; Miller, A. T.; De Gregorio, E.; Doro, F.; D'Oro, U.; Skibinski, D. A. G.; Mbow, M. L.; Bufali, S.; Herman, A. E.; et al. Rational design of small molecules as vaccine adjuvants. *Sci. Transl. Med.* **2014**, *6* (263), 263ra160.
(30) Santone, M.; Aprea, S.; Wu, T. Y. H.; Cooke, M. P.; Mbow, M. L.; Valiante, N. M.; Rush, J. S.; Dougan, S.; Avalos, A.; Ploegh, H.; et al. A new TLR2 agonist promotes cross-presentation by mouse and human antigen presenting cells. *Hum. Vaccin. Immunother.* **2015**, *11* (8), 2038–2050.
(31) Zhang, L.; Dewan, V.; Yin, H. Discovery of small molecules as multi-toll-like receptor agonists with proinflammatory and anticancer activities. *J. Med. Chem.* **2017**, *60* (12), 5029–5044.
(32) Timmermans, K.; Plantinga, T. S.; Kox, M.; Vaneker, M.; Scheffer, G. J.; Adema, G. J.; Joosten, L. A. B.; Netea, M. G. Blueprints of signaling interactions between pattern recognition receptors: implications for the design of vaccine adjuvants. *Clin. Vaccine Immunol.* **2013**, *20* (3), 427–432.
(33) Fischetti, L.; Zhong, Z.; Pinder, C. L.; Tregoning, J. S.; Shattock, R. J. The synergistic effects of combining TLR ligand based adjuvants on the cytokine response are dependent upon p38/jnk signalling. *Cytokine* **2017**, *99*, 287–296.
(34) Pavot, V.; Rochereau, N.; Rességuier, J.; Gutjahr, A.; Genin, C.; Tiraby, G.; Perouzel, E.; Lioux, T.; Vernejoul, F.; Verrier, B.; et al. Cutting edge: new chimeric NOD2/TLE2 adjuvant drastically increases vaccine immunogenicity. *J. Immunol.* **2014**, *193* (12), 5781–5785.
(35) Ali, O. A.; Verbeke, C.; Johnson, C.; Sands, R. W.; Lewin, S. A.; White, D.; Doherty, E.; Dranoff, G.; Mooney, D. J. Identification of immune factors regulating antitumor immunity using polymeric vaccines with multiple adjuvants. *Cancer Res.* **2014**, *74* (6), 1670–1681.

(36) Gutjahr, A.; Phelip, C.; Coolen, A.-L.; Monge, C.; Boisgard, A.-S.; Paul, S.; Verrier, B. Biodegradable polymeric nanoparticles-based vaccine adjuvants for lymph nodes targeting. *Vaccines* . 2016.
(37) Fox, C. B.; Sivananthan, S. J.; Duthie, M. S.; Vergara, J.; Guderian, J. A.; Moon, E.; Coblentz, D.; Reed, S. G.; Carter, D. A nanoliposome delivery system to synergistically trigger TLR4 and TLR7. *J. Nanobiotechnology* **2014**, *12* (1), 17.
(38) Kuai, R.; Sun, X.; Yuan, W.; Ochyl, L. J.; Xu, Y.; Hassani Najafabadi, A.; Scheetz, L.; Yu, M.-Z.; Balwani, I.; Schwendeman, A.; et al. Dual TLR agonist nanodiscs as a strong adjuvant system for vaccines and immunotherapy. *J. Control. Release* **2018**, *282*, 131–139.
(39) Junkins, R. D.; Gallovic, M. D.; Johnson, B. M.; Collier, M. A.; Watkins-Schulz, R.; Cheng, N.; David, C. N.; McGee, C. E.; Sempowski, G. D.; Shterev, I.; et al. A robust microparticle platform for a sting-targeted adjuvant that enhances both humoral and cellular immunity during vaccination. *J. Control. Release* **2018**, *270*, 1–13.
(40) Lynn, G. M.; Laga, R.; Darrah, P. A.; Ishizuka, A. S.; Balaci, A. J.; Dulcey, A. E.; Pechar, M.; Pola, R.; Gerner, M. Y.; Yamamoto, A. In vivo characterization of the physicochemical properties of polymer-linked TLR agonists that enhance vaccine immunogenicity. *Nat. Biotechnol.* **2015**, *33*, 1201–1210.
(41) Madan-Lala, R.; Pradhan, P.; Roy, K. Combinatorial delivery of dual and triple TLR agonists via polymeric pathogen-like particles synergistically enhances innate and adaptive immune responses. *Sci. Rep.* **2017**, *7* (1), 2530.
(42) Kasturi, S. P.; Skountzou, I.; Albrecht, R. A.; Koutsonanos, D.; Hua, T.; Nakaya, H. I.; Ravindran, R.; Stewart, S.; Alam, M.; Kwissa, M.; et al. Programming the magnitude and persistence of antibody responses with innate immunity. *Nature* **2011**, *470*, 543–547.
(43) Tom, J. K.; Dotsey, E. Y.; Wong, H. Y.; Stutts, L.; Moore, T.; Davies, D. H.; Felgner, P. L.; Esser-Kahn, A. P. Modulation of innate immune responses via covalently linked TLR agonists. *ACS Cent. Sci.* **2015**, *1* (8), 439–448.
(44) Gause, K. T.; Yan, Y.; O'Brien-Simpson, N. M.; Cui, J.; Lenzo, J. C.; Reynolds, E. C.; Caruso, F. Codelivery of NOD2 and TLR9 ligands via nanoengineered protein antigen particles for improving and tuning immune responses. *Adv. Funct. Mater.* **2016**, *26* (41), 7526–7536.
(45) Tukhvatulin, A. I.; Dzharullaeva, A. S.; Tukhvatulina, N. M.; Shcheblyakov, D. V; Shmarov, M. M.; Dolzhikova, I. V; Stanhope-Baker, P.; Naroditsky, B. S.; Gudkov, A. V; Logunov, D. Y.; et al. Powerful complex immunoadjuvant based on synergistic effect of combined tlr4 and nod2 activation significantly enhances magnitude of humoral and cellular adaptive immune responses. *PLoS One* **2016**, *11* (5), e0155650.
(46) Zhu, G.; Lynn, G. M.; Jacobson, O.; Chen, K.; Liu, Y.; Zhang, H.; Ma, Y.; Zhang, F.; Tian, R.; Ni, Q.; et al. Albumin/vaccine nanocomplexes that assemble in vivo for combination cancer immunotherapy. *Nat. Commun.* **2017**, *8* (1), 1954.
(47) Francica, J. R.; Lynn, G. M.; Laga, R.; Joyce, M. G.; Ruckwardt, T. J.; Morabito, K. M.; Chen, M.; Chaudhuri, R.; Zhang, B.; Sastry, M.; et al. Thermoresponsive polymer nanoparticles co-deliver RSV f trimers with a TLR-7/8 adjuvant. *Bioconjug. Chem.* **2016**, *27* (10), 2372–2385.
(48) Mancini, R. J.; Tom, J. K.; Esser-Kahn, A. P. Covalently coupled immunostimulant heterodimers. *Angew. Chemie Int. Ed.* **2014**, *53* (1), 189–192.
(49) Ryu, K. A.; Slowinska, K.; Moore, T.; Esser-Kahn, A. Immune response modulation of conjugated agonists with changing linker length. *ACS Chem. Biol.* **2016**, *11* (12), 3347–

3352.
(50) Sato, A.; Linehan, M. M.; Iwasaki, A. Dual recognition of herpes simplex viruses by TLR2 and TLR9 in dendritic cells. *Proc. Natl. Acad. Sci.* **2006**, *103* (46), 17343–17348.
(51) Mogensen, T. H.; Paludan, S. R.; Kilian, M.; Østergaard, L. Live streptococcus pneumoniae, haemophilus influenzae, and neisseria meningitidis activate the inflammatory response through toll-like receptors 2, 4, and 9 in species-specific patterns. *J. Leukoc. Biol.* **2006**, *80* (2), 267–277.

CHAPTER 2

Synthesis and Characterization of a TLR Tri-agonist Panel

2.1 Introduction

To explore the potential of unique TLR combinations, we needed to synthesize a series of TLR tri-agonists. This represents a major synthetic challenge as agonists encompass a diverse range of molecular structures, including lipopolysaccharides, peptidoglycans, flagellin protein, single-stranded DNA, and RNA.[1] To undertake this task, we designed a novel, divergent set of bioconjugation reactions. Each agonist was functionalized with an amine, carboxylic acid, thiol, or azide and linked to a triazine core functionalized with an amine or carboxylic acid, a maleimide, and an alkyne (**Fig. 2.1**). We previously reported a TLR4_7_9 tri-agonist synthesis using this core.[2] In this study, we expanded the design of the triazine core scaffold to access multiple TLR agonist combinations by interchanging TLR agonists functionalized with the appropriate chemical handle – creating a panel of linked TLR agonists.

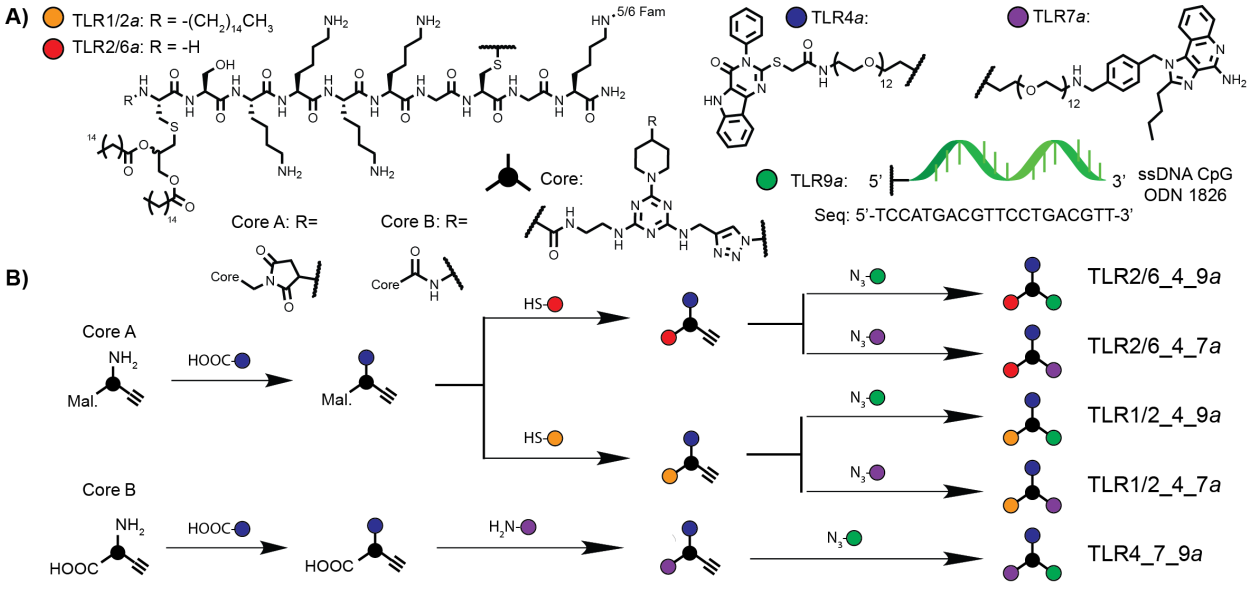

Figure 2.1 Synthetic Strategy to Develop TLR Tri-Agonists. A) Chemical structure of linkable TLR Agonists. B) Divergent synthetic strategy scheme of various TLR tri-agonists combinations.

TLR tri-agonists were synthesized containing different combinations of three of the following TLR agonists (TLR*a*): TLR1/2*a* (Pam3CSK4), TLR2/6*a* (Pam2CSK4), TLR4a (pyrimido-indole derivative)[3], TLR7*a* (imidazoquinoline derivative)[4,5], and TLR9*a* (ODN 1826 CpG DNA containing a phosphorothioate backbone), (Fig. 2.1A). These agonists were chosen for their synthetic accessibility and synergistic effects. The pyrimido-indole TLR4*a* is less potent than the conventional MPLA agonists for TLR4, but is more well suited for conjugation.[3] Similarly, the TLR7*a* imidazoquinoline was selected for its free amino moiety for conjugation, although its activity compared to the conventional R848 molecule is similar.[6] The five combinations synthesized were TLR1/2_4_7*a*, TLR2/6_4_7*a*, TLR1/2_4_9*a*, TLR2/6_4_9*a*, and TLR4_7_9*a* (**Fig. 2.2**). In our design, we incorporated PEG linkers to improve tri-agonist solubility and reduce potential steric effects between the agonist and TLR*a* during binding. Each tri-agonist was purified by either HPLC or gel extraction and confirmed by MALDI-TOF or ESI-MS.

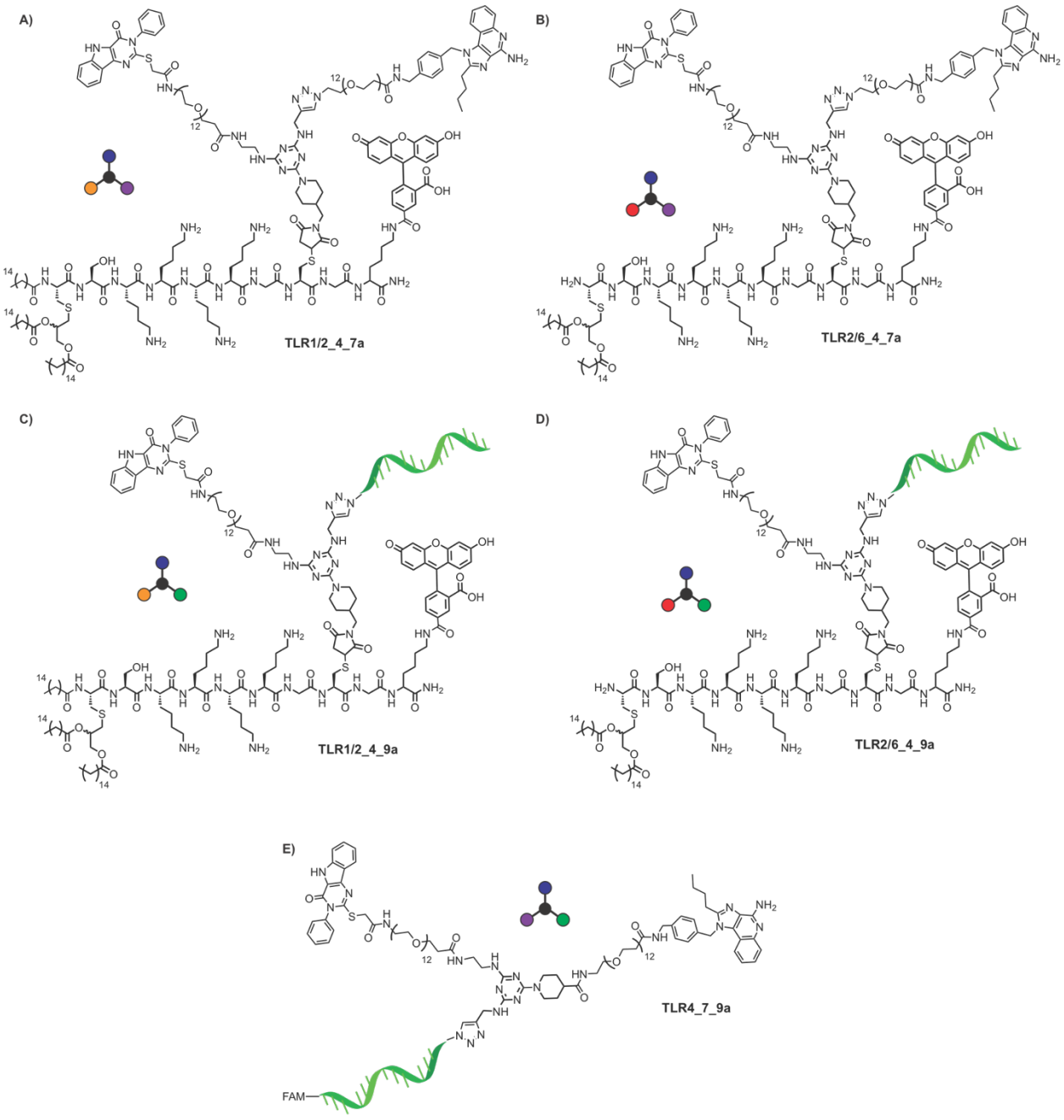

Figure 2.2 Chemical Structures of Tri-Agonists. A) TLR1/2_4_7a, B) TLR2/6_4_7a, C) TLR1/2_4_9a, D) TLR2/6_4_9a, and E) TLR4_7_9a. CpG ODN 1826 (20 bp ss DNA) depicted as green cartoon.

2.2 Synthesis of a TLR1/2_4_7 Tri-Agonist

In our previous work, a triazine core bearing an amine, maleimide, and alkyne (Core A) was used as the scaffold for TLR agonist conjugation in a TLR4_7_9*a*.[2] TLR1/2_4_7*a* is quite different in chemical structure to our first TLR4_7_9*a* tri-agonist, as the hydrophilic, single-stranded DNA (TLR9*a*) is replaced with the hydrophobic peptide, Pam_3CSK_4 (TLR1/2*a*), resulting in vastly different biophysical characteristics. In addition, the original TLR7*a*, azido-loxoribine, was replaced with a more potent, scalable, and conjugation-amenable imidazoquinoline TLR7*a* derivative.[4,5] We also decided to incorporate PEG linkers for the small molecule agonists (TLR4*a* and TLR7*a*) in an attempt to improve receptor-agonist interactions upon conjugation and improve solubility. We choose PEG_{12} as the linker length (4.6 nm) because, based on the crystal structure, the TLR agonist binding site is approximately 2-3 nm from the protein surface, in addition to previous TLR agonist-PEG linker length studies in our lab.[3,7,8] Thus, we had to redesign the synthetic strategy to accommodate the new TLR agonists and linkers.

We started with the Core A scaffold due to our previous experience and its versatility in bioconjugation. Synthesis of TLR1/2_4_7*a* began with boc-deprotection of Core A using TFA and, following work up, conjugation *via* HBTU-mediated amide bond formation with Fmoc-NH-PEG_{12}-COOH with 81% yield over two steps (**Scheme 2.1**). Next, the Core A-PEG_{12}-Fmoc was Fmoc-deprotected using diethylamine (DEA). Following work up, Core A-PEG_{12}-NH_2 was conjugated to TLR4*a*-COOH *via* HBTU-mediated amide bond formation resulting in Core A-PEG_{12}-TLR4*a* (TLR4*a*-Core) in 41 % yield, over two steps. Despite several attempts to optimize reaction conditions, we found this reaction generally gave low yields. We observed that upon TLR4*a* activation with HBTU and DIPEA, a dark-purple precipitate would immediately begin to form in the absence of Core A-PEG_{12}-NH_2. Although this side product was insoluble in most

solvents, making it difficult to analyze, we speculate that it was a product of either an inter- or intra- molecular amide bond formation of TLR4*a*, with the secondary amine potentially acting as the nucleophile. We found that formation of this side product could be reduced, as indicated by less coloration during the reaction, when HBTU was added last, in the presence of Core A-PEG_{12}-NH_2. Following purification, TLR4a-Core was heated in DMSO to expose the active maleimide, yielding TLR4a-Core-Mal ,for conjugation to TLR1/2*a via* Michael addition.

Scheme 2.1 Synthesis of TLR4*a*-Core-Mal

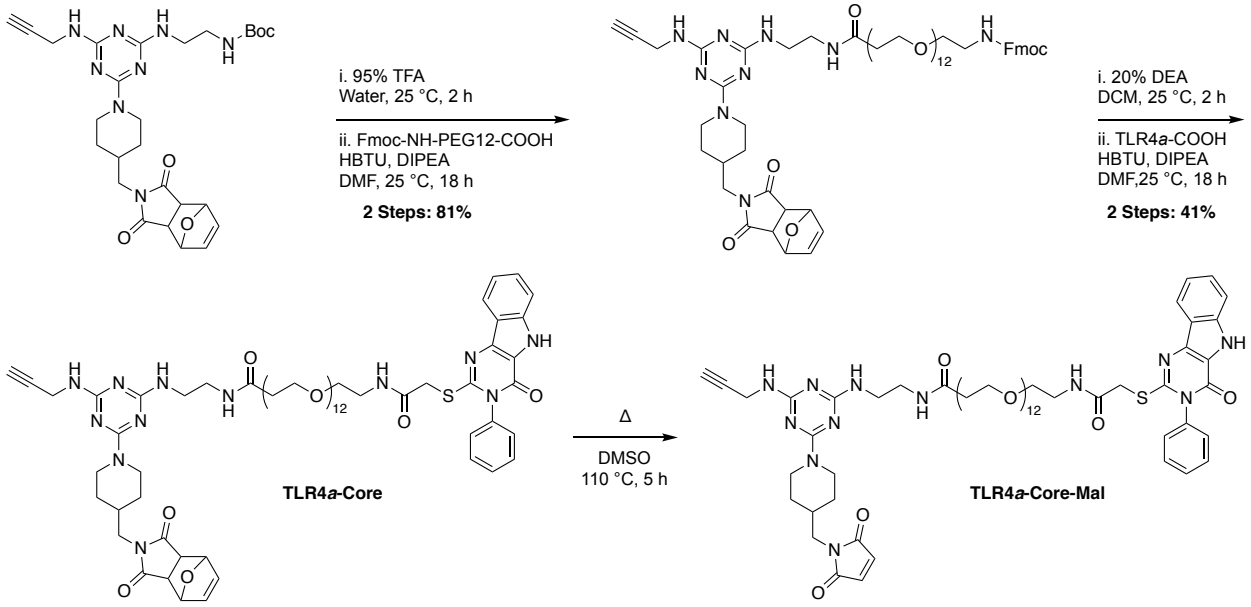

The functional groups present on Pam_3CSK_4 (TLR1/2*a*), including primary amines and a carboxylic acid, can compete for conjugation, making selective attachment of the peptide to the triazine core difficult. Thus, we designed a TLR1/2*a* conjugation strategy to selectively conjugate TLR4*a*-Core-Mal *via* Michael addition to a resin bound, Pam_3CSK_4 derivative bearing a thiol (**Scheme 2.2**). To facilitate conjugation, a cysteine was incorporated into the peptide sequence. Glycine was included on either side of the cysteine to provide additional flexibility. In addition,

an amine-reactive carboxy fluorescein (5/6-Fam) functionalized lysine was included at the C-terminus of the peptide to simplify purification, quantification, and future microscope experiments. The peptide Pam_3CS(OtBu)K(Boc)4GC(Mmt)GK(5/6FAM) was synthesized by solid phase peptide synthesis (SPPS) on MBHA rink amide resin. We selected the cysteine monomethoxytrityl (Mmt) protecting group for its acid lability and MBHA rink amide resin for its relatively high acid stability, a strategy used for selectively exposing thiols on resin bound peptides using low acid concentrations.[9] We found that standard Fmoc deprotection with 20% piperidine in DMF during SPPS resulted in significant side product formation with a mass of +66 m/z from the expected exact mass and an altered absorbance profile above 495 nm, suggesting modification to the fluorophore. Previous work suggests that peptides synthesized containing 5/6-FAM can undergo piperidine addition (+84 amu) resulting in loss of water (-18 amu), which accounts for the shift in mass.[10] Following literature suggestion, we substituted piperidine with piperazine for fmoc deprotection and found that this change prevented formation of the functionalized 5/6-FAM side product. This change also has the advantage that piperazine is not a controlled substance, unlike piperidine, although longer time is needed for full Fmoc deprotection. With optimal conditions for SPPS determined, TLR4*a*_Core-Mal was then conjugated to the resin bound peptide *via* Michael addition. Resin cleavage and purification afforded the $TLR4_a$-Core A-TLR1/2*a* conjugate (TLR1/2_4*a*).

Scheme 2.2 Synthesis of TLR1/2_4_7*a*

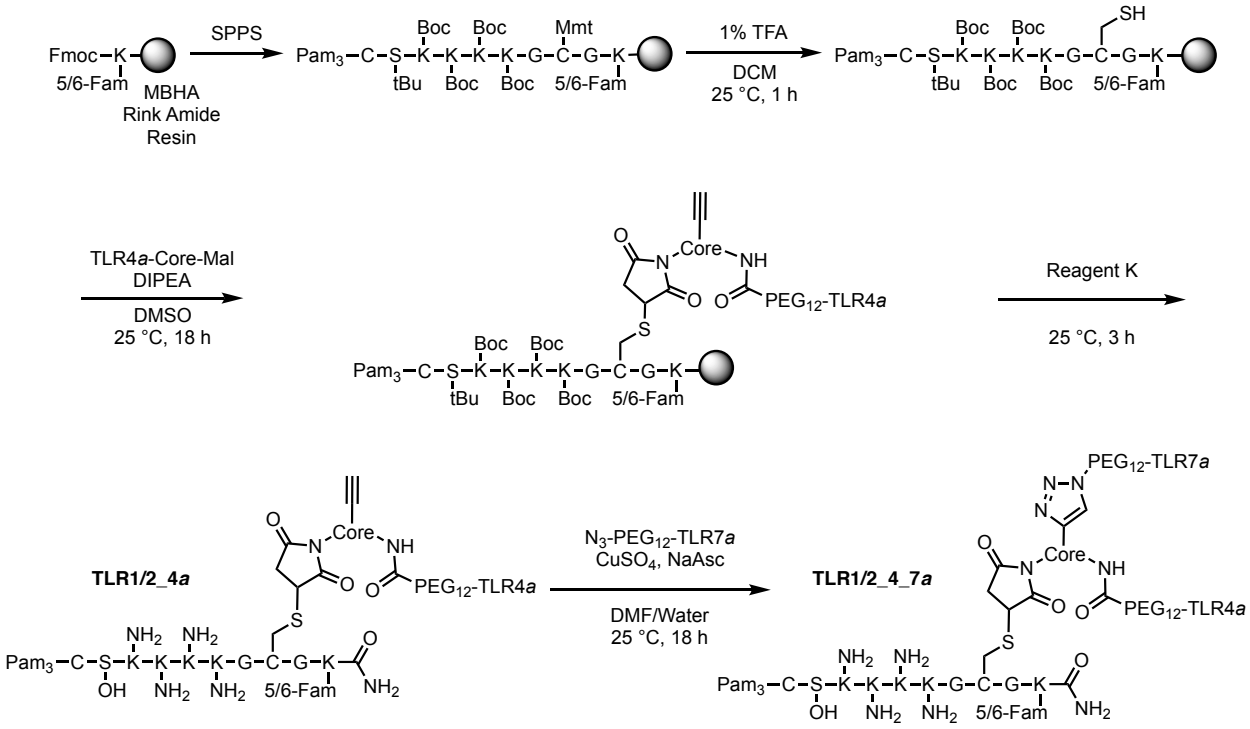

TLR1/2_4*a* contains a terminal alkyne amenable to copper-catalyzed azide-alkyne cycloaddition (CuAAC) click chemistry. This intermediate serves as a common precursor to both TLR1/2_4_7*a* and TLR1/2_4_9*a*. For TLR1/2_4_7*a*, we synthesized an azido-PEG_{12} functionalized TLR7*a via* amide bond formation between Azido-PEG_{12}-NHS and the TLR7*a*. The resulting N_3-PEG_{12}-TLR7*a* was reacted with TLR1/2_4*a via* CuAAC to yield TLR1/2_4_7*a*. We found this compound to have poor water solubility, which made initial analysis of the compound difficult. However, we found that the tri-agonist could be purified by preparatory HPLC and the compound confirmed by MALDI-TOF. Although only 2.5 mg (550 nmol) of TLR1/2_4_7*a* was recovered from this reaction, we found in later experiments that the tri-agonists were very potent immunostimulants. Only 1 nmol compound was needed per mouse injection, sufficient to vaccinate 275 mice with boost.

2.3 Synthesis of a TLR2/6_4_7 Tri-Agonist

TLR1/2 and TLR2/6 both signal with TLR2 responsible for binding a majority of the agonist. Upon agonist binding to TLR2, the complex heterodimerizes with either TLR1 or TLR6 for activation, depending on the agonist chemical structure.[11,12] Although TLR1/2 and TLR2/6 activation results in similar signaling pathway activation, TLR1 and TLR2 show unique expression patterns across different cell types, which can result in the generation of different immune responses *in vivo*.[13,14] The only difference between the chemical structures of their agonists is that Pam_2CSK_4 (TLR2/6*a*) has a free N terminus while that of Pam_3CSK_4 (TLR1/2*a*) is palmitoylated. Thus, TLR2/6_4_7*a* was synthesized, purified, and characterized similar to TLR1/2_4_7*a*. To accommodate the difference in chemical structure, the N-terminus of the peptide was left fmoc-protected during the Michael addition of TLR4*a*_Core_Mal and was deprotected with 6% piperazine in DMF prior to peptide cleavage (**Scheme 2.3**).

Scheme 2.3 Synthesis of TLR2/6_4_7*a*

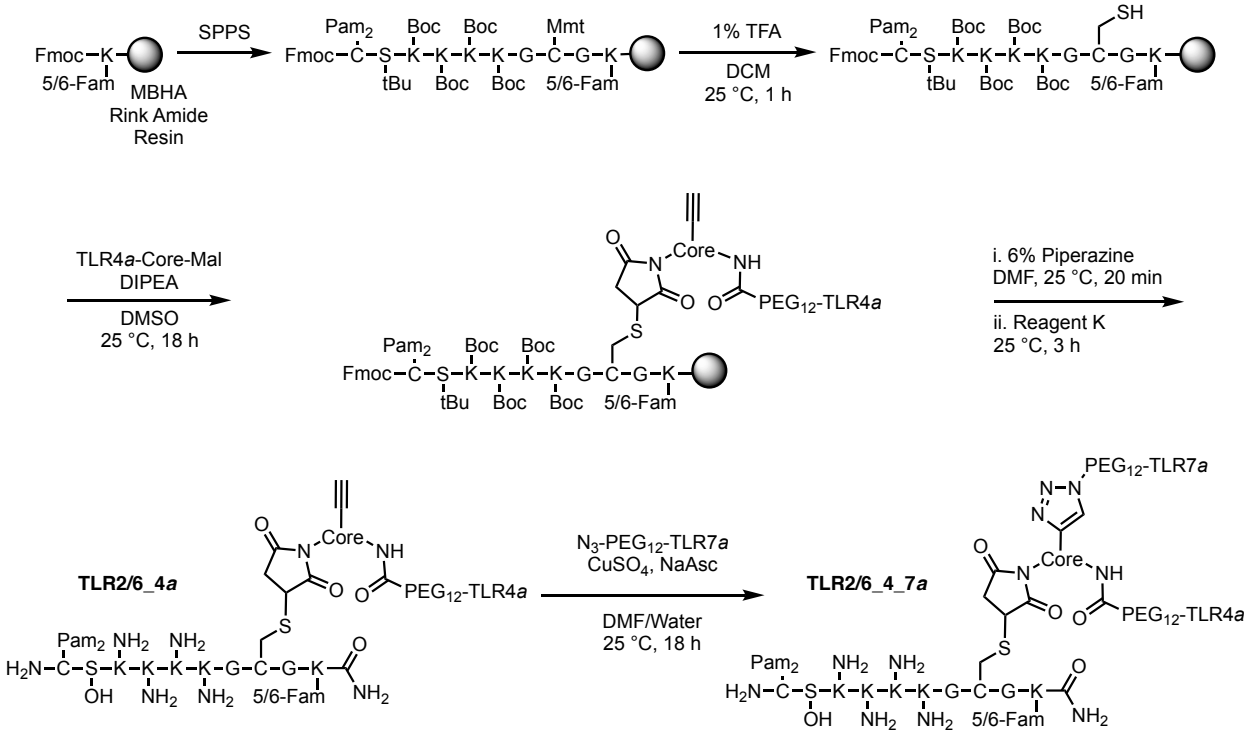

2.4 Synthesis a TLR1/2_4_9 Tri-Agonist

The design TLR1/2_4_9*a* is different from the TLR1/2_4_7*a* in that the small molecule, pegylated TLR7a is replaced with a single stranded DNA (TLR9*a*). This drastically changes the biophysical properties, making this molecule have particularly eclectic chemical moieties – three lipid chains, cationic amino acids, single stranded DNS, PEG, and small heterocyclic molecules. The tri-agonist was synthesized using the same TLR1/2_4*a* precursor as for TLR1/2_4_7*a* (**Scheme 2.4**). In this case, TLR1/2_4*a* was conjugated to azido-TLR9*a* *via* CuAAC. Owing to the unique combination of chemical moieties in the molecule, we found it was difficult to analyze and purify the tri-agonist. Ultimately, we found we could purify the compound by SDS-PAGE, followed by gel extraction, washing with ultrapure water, and spin filtration. We confirmed the product by SDS-PAGE and by ESI-MS.

Scheme 2.4 Synthesis of TLR1/2_4_9*a*

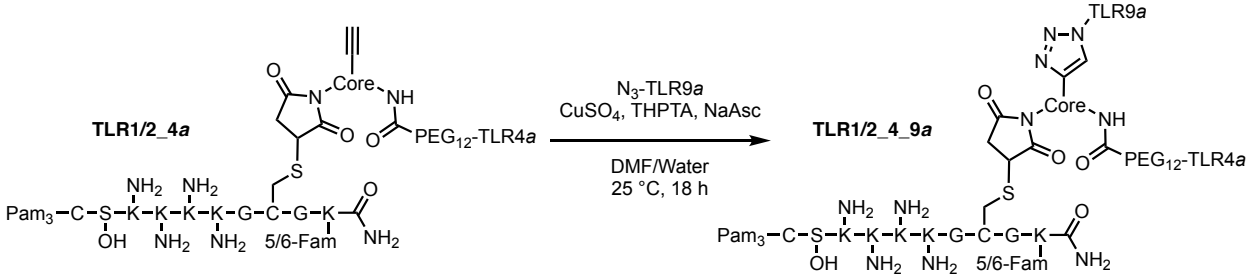

2.5 Synthesis of a TLR2/6_4_9 Tri-Agonist

The design TLR1/2_4_9*a* is slightly different from TLR2/6_4_7a in that the N-terminus of the peptide is free, instead of palmitoylated. The tri-agonist was synthesized using the TLR2/6_4*a* precursor instead of TLR1/2_4*a* (**Scheme 2.5**). TLR2/6_4*a* was conjugated to azido-TLR9*a* *via* CuAAC by the same conditions. We found this molecule could be purified by SDS-

PAGE, followed by gel extraction, washing, and spin filtration similar to TLR1/2_4_9*a*. We confirmed the product by SDS-PAGE and by ESI-MS.

Scheme 2.5 Synthesis of TLR2/6_4_9*a*

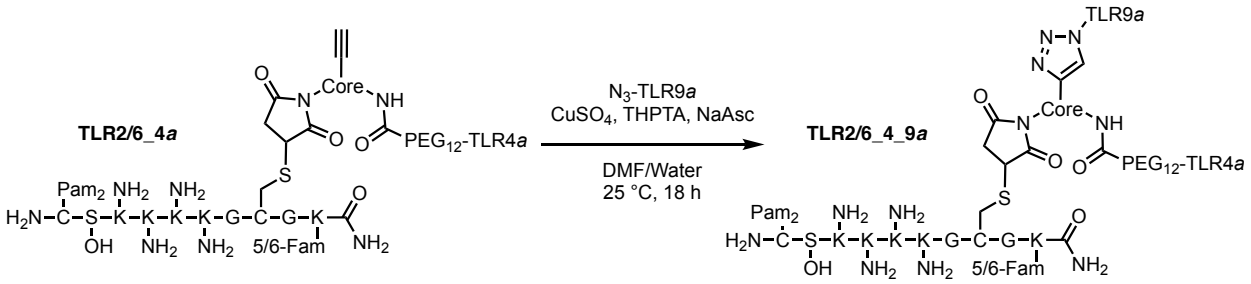

2.6 Synthesis of a TLR4_7_9 Tri-Agonist (with Dr. Janine Tom)

TLR4_7_9*a* amongst the panel of tri-agonists as it was the only one that did not contain either TLR1/2*a* or TLR2/6*a*. This combination was different from our previously reported TLR4_7_9*a* in that the TLR4*a* and TLR7*a* were conjugated to the core *via* PEG_{12} linkers and the less potent loxoribine TLR7*a* was replaced with the more potent imidazoquinoline derivative TLR7*a*. These changes required a new synthetic route be developed to accommodate the agonists (**Scheme 2.6**). Thus, we designed a new carboxylic acid-functionalized triazine core (Core B) in place of the maleimide handle.

TLR7*a* was first functionalized with Fmoc-NH-PEG_{12}-COOH *via* amide bond formation mediated by HBTU to afford the product, Fmoc-NH-PEG_{12}-TLR7*a*, in 94% yield. Following fmoc deprotection with diethylamine, the H_2N-PEG_{12}-TLR7*a* was conjugated to Core B using HBTU to afford the product, TLR7*a*-Core B, in 57% yield. Next, TLR7*a*-Core B was boc deprotected and then coupled to Fmoc-NH-PEG_{12}-NHS to afford the product, TLR7*a*-Core B-PEG_{12}-NH-Fmoc, in 41% yield. Following a final fmoc deprotection, TLR7*a*-Core B-PEG_{12}-NH_2 was conjugated to $TLR4_a$-COOH via HBTU coupling to afford TLR4*a*-PEG_{12}-Core C-PEG_{12}-TLR7*a* (TLR4_7*a*) in

20% yield. Finally, TLR4_7*a* was conjugated to azido-TLR9*a*-FAM via CuAAC by the same procedure for TLR1/2_4_9*a* and TLR2/6_4_9*a*. The product, TLR4_7_9*a* was also purified by gel extraction, however, TBE-Urea PAGE was used instead of SDS.

Scheme 2.6 Synthesis of TLR4_7_9*a*

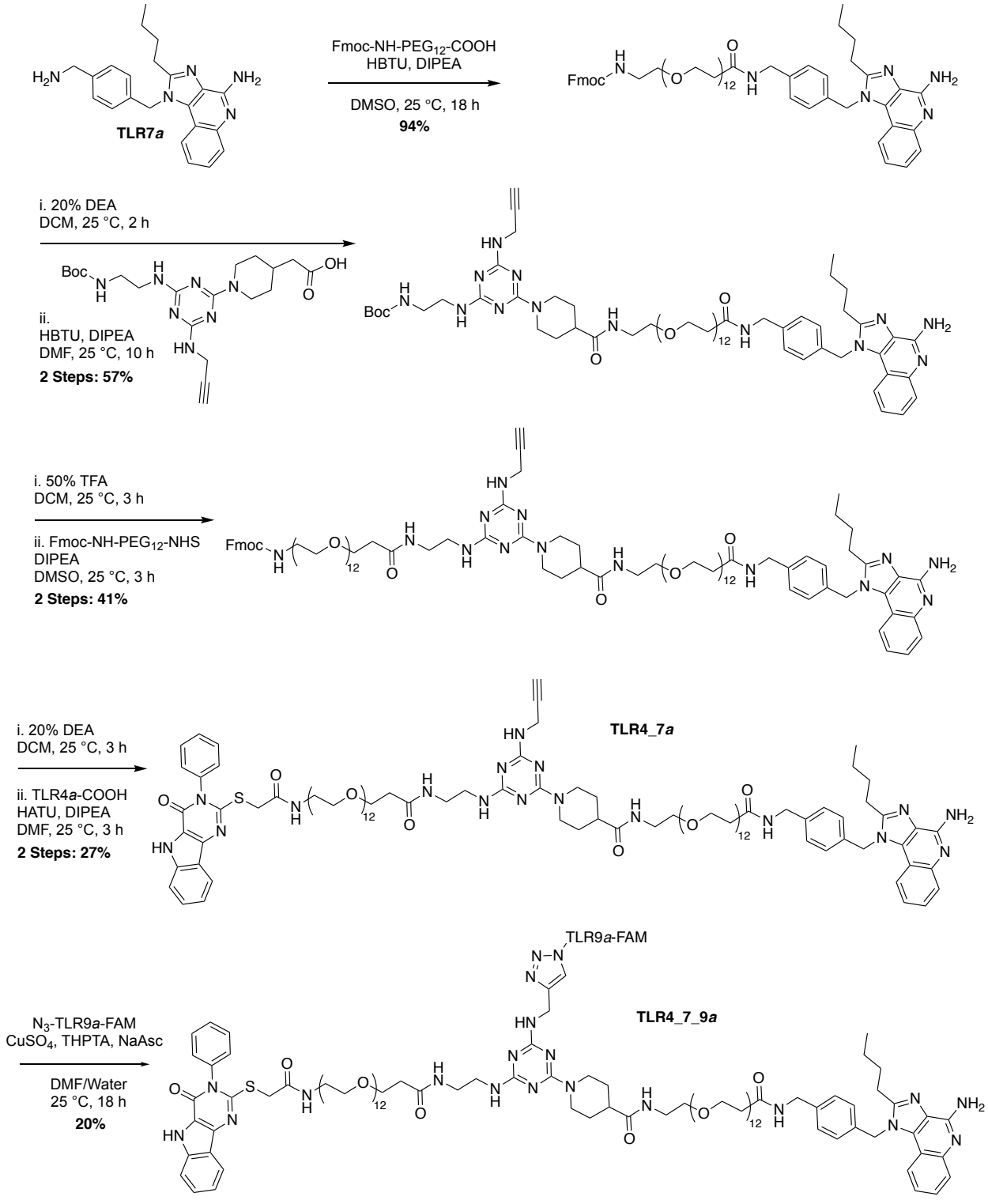

2.7 Conclusions

To evaluate the effects of different covalently linked TLR tri-agonist combinations on immunological activity, we needed to design a synthetic strategy to rapidly access several TLR tri-agonist combinations. The divergent synthetic approach we developed resulted in the generation of a panel of five TLR tri-agonists. These unique molecules are comprised of complex chemical moieties, which made purification and analysis challenging. However, we developed analytical techniques and purification stratagies that allows us to recover enough materials for subsequent *in vitro* and *in vivo* experiments.

2.8 Experimental Methods and Materials

Materials and Instrumentation

Reagents were purchased from Sigma-Aldrich, ThermoFisher, Quanta Biodesign, Anaspec, or Acros Organics and used as is unless otherwise noted. Single stranded CpG-ODN1826, Azide-C6-5′-TCCATGACGTTCCTGACGTT-3′-6-FAM or Azide-C6-5′-TCCATGACGTTCCTGACGTT-3′-OH, with a phosphorothioated backbone was purchased from IDT. TLR4*a* and furan-protected maleimide/boc-protected amine/alkyne functionalized triazine core (Tri-agonist Core) were made as previously described.[2] Buffers and media for cell culture were purchased from Fisher Life Technologies. Centrifugal Filter Devices (3k) were purchased from Millipore. Compounds were filtered using 0.22 μM syringe filters (Restek). Tri-agonists were quantified using either a NanoDrop 2000c spectrophotometer or a Promega Quantus Fluorimeter E6150. Gel images were obtained using a GE Typhoon scanner. ^{1}H and ^{13}C NMR spectra were taken on a Bruker CRYO500 NMR spectrometer (500 MHz) and analyzed using MestreNova software. Spectra are referenced to solvent peak for ^{1}H NMR (CD_3OD = 3.33 ppm, $(CD_3)_2SO$ = 2.50 ppm, $CDCl_3$ = 7.26 ppm) and

^{13}C NMR (CD_3OD = 49.00 ppm, $(CD_3)_2SO$ = 39.52 ppm, CDCl3 = 77.16 ppm). Analytical high-performance liquid chromatography (HPLC) was performed using an Agilent 1260 Infinity HPLC with a Phenomenex Luna 5 μm C8 100 Å 150X 4.6 mm LC column. Preparative HPLC was performed on a Gilson Preperative HPLC System with 333 HPLC Pumps and GX-271 liquid handler using a Phenomenex Luna 5 μm C8(2) 100 Å 150X 21.2 mm LC column. High resolution mass spectrometry (HRMS) was performed by the University of California, Irvine Mass Spectrometry Center. Electrospray ionization – mass spectrometry (ESI-MS) was performed on an ESI LC – TOF Micromass LCT 3 instrument. MALDI TOF was performed on an AB SCIEX TOF/TOF 5800 System instrument. Silica Gel Chromatography was performed using RediSep Rf normal silica columns on a Teledyne-Isco CombiFlash Rf auto column instrument. Gel electrophoresis was carried out using 10% Mini-PROTEAN TBE-urea gels or 12% Mini-PROTEAN TGX precast protein gels in a MiniPROTEAN tetra cell (BIO-RAD).

ESI-MS Technical Note for Oligonucleotide Containing Compounds

Negative mode analysis of oligonucleotide conjugates was performed on a Waters UPLC-QDA single quad mass analyzer (Waters, Milford, MA, USA). A 5 min gradient, 18%B to 80%B, was used to elute each sample off a C18 stationary phase. Mobile buffers were prepared gravimetrically; phase A consisted of 0.2% triethylamine (TEA) with 0.2% hexafluoro-2-propanol (HFIP) in water while phase B was 0.2% HFIPA in methanol. The addition of HFIP as a counter ion in both phases was essential for ionization of the oligo conjugates in the QDA mass analyzer. Waters masslynx MaxEnt1 software was used to deconvolute the charge-state ladder into an accurate MS1 mass.

Fmoc-PEG$_{12}$-Core Synthesis.

Scheme 2.7. Fmoc-NH-PEG Functionalization of Tri-agonist Core Synthetic Scheme

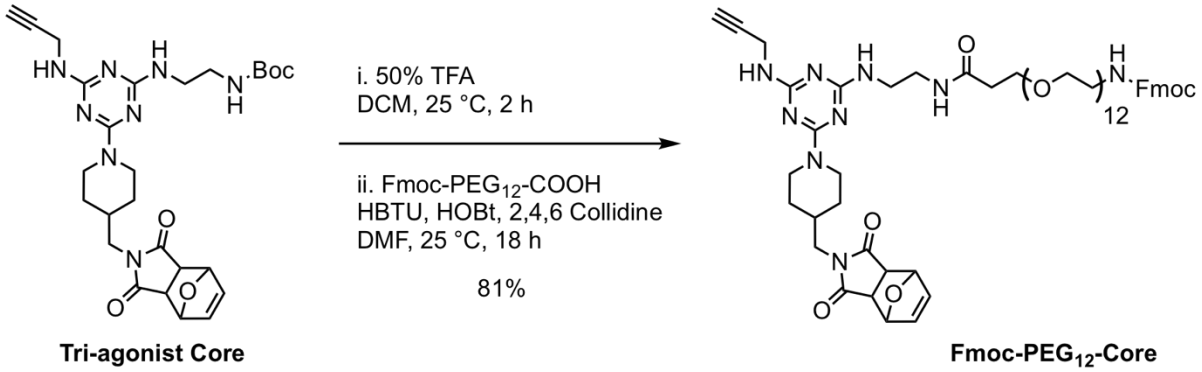

Triazine Core Boc-deprotection: Tri-agonist Core A[2] (160 mg, 0.286 mmol, 1.2 equiv.) was dissolved in 50% TFA/DCM (5 mL) and stirred for 2 h. The solvent was removed by rotary evaporation.

Fmoc-PEG$_{12}$-COOH coupling: Fmoc-PEG$_{12}$-COOH (200 mg, 0.238 mmol, 1 equiv.), Boc-deprotected tri-agonist core (described above), HBTU (109 mg, 0.286 mmol, 1.2 equiv.), and HOBt (44 mg, 0.29 mmol, 1.2 equiv.) were dissolved in 25% 2,4,6-collidine/DMF (0.5 mL) and stirred for 18 h. The reaction mixture was diluted to 200 mL with DCM and the organic layer washed with 0.1 M HCl (3X 200 mL), 10% saturated $NaHCO_3$ (aq.) in water (3X 200mL), and DI water (3X 200 mL). The organic layer was dried over anhydrous sodium sulfate, filtered, and evaporated to dryness. The crude product was purified by flash chromatography to obtain the final product as a viscous, tan oil (248 mg, 81% yield). The product was characterized by ^{1}H NMR, ^{13}C NMR, and ESI-MS. Rf 0.44 (10% MeOH/DCM); ^{1}H NMR (500 MHz,$CDCl_3$) δ 7.75 (d, *J* = 7.6 Hz, 2H), 7.60 (d, *J* = 7.5 Hz, 2H), 7.39 (t, *J* = 7.3 Hz, 2H), 7.30 (td, *J* = 7.5, 1.1 Hz, 2H), 6.51 (s, 2H), 5.27 (s, 2H), 4.70 (s, 2H), 4.39 (d, *J* = 6.9 Hz, 2H), 4.21 (t, *J* = 6.7 Hz, 2H), 4.14 (s, 2H), 3.69 (t, *J* = 5.7 Hz, 2H), 3.62 (m, 42H), 3.56 (t, *J* = 5.0, 2H), 3.48 (s, 2H), 3.43 – 3.33 (m, 6H), 2.84 (s, 2H), 2.69 (t, *J* = 11.7 Hz, 2H), 2.42 (t, *J* = 5.8 Hz, 2H), 2.19 (s, 1H), 2.09 (s, 1H), 1.95 (s, 1H),

1.61 (d, *J* = 11.8 Hz, 2H), 1.13 (m, 2H). ^{13}C NMR (126 MHz, $CDCl_3$) δ 176.49, 171.97, 144.06, 141.35, 136.58, 127.71, 127.09, 125.14, 120.00, 81.10, 81.10, 77.30, 70.78, 70.55, 70.49, 70.37, 70.35, 70.25, 70.12, 67.32, 66.59, 47.39, 47.32, 44.21, 42.81, 40.98, 40.24, 37.09, 34.98, 30.40 , 29.57. ESI-MS m/z calc'd for $C_{64}H_{91}N_9O_{18}$ $[M+H]^+$: 1274.66; Observed $[M+H]^+$: 1274.46.

TLR4a-PEG$_{12}$-Core Synthesis

Scheme 2.8 TLR4*a* Conjugation to PEG-Functionalized Tri-agonist Core.

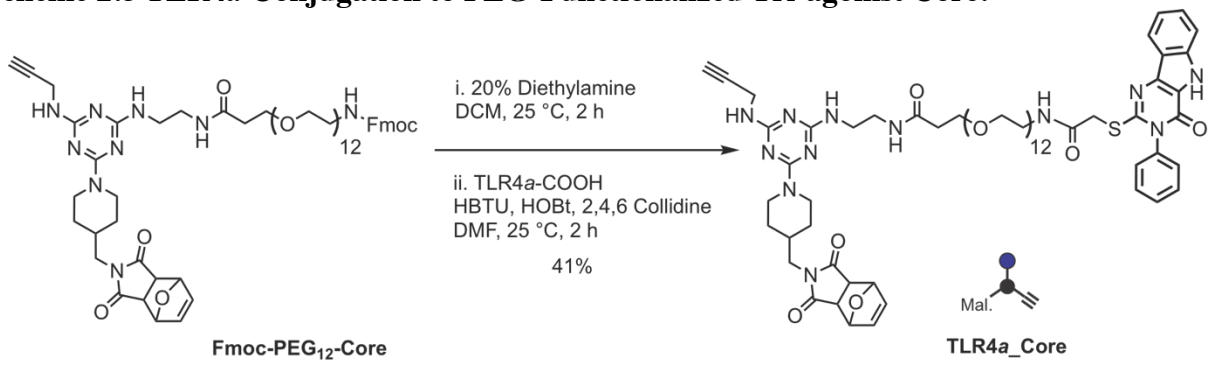

Fmoc Deprotection: Fmoc-PEG$_{12}$-Core (248 mg, 0.193 mmol, 1 equiv.) was dissolved in 20% diethylamine/DCM and stirred for 2 h. The solution was evaporated to dryness by rotary evaporation. The product was suspended in diethyl ether (10 mL), centrifuged, and decanted 3X. The product was dried under high vacuum and obtained as a white solid.

TLR4*a* coupling: TLR4*a* (82 mg, 0.23 mmol, 1.2 equiv.) and H_2N-PEG$_{12}$-Core (0.193 mmol, 1 equiv.) were dissolved in 25% 2,4,6-collidine (2 mL). HBTU (88 mg, 0.23 mmol, 1.2 equiv.) and HOBt (36 mg, 0.23 mmol, 1.2 equiv.) were then added to the reaction solution and the solution stirred for 18 h. The reaction was concentrated by rotary evaporation and the crude purified by flash chromatography. The product was further purified with a silica plug by washing with ethyl acetate and subsequently eluted with 10% MeOH/DCM to afford the pure product. The solvent was evaporated, the solid lyophilized, and the product obtained as a white powder (110 mg, 41%

yield). The product was characterized by ^{1}H NMR, ^{13}C NMR, HPLC and ESI-MS. Rf 0.37 (10% MeOH/DCM); 1H NMR (500 MHz,CD_3OD) δ 8.14 (d, *J* = 7.9 Hz, 1H), 7.63-7.58 (m, 3H), 7.56 (m, 1H), 7.50 (ddd, *J* = 8.4, 7.0, 1.2 Hz, 1H), 7.47 – 7.40 (m, 2H), 7.28 (ddd, *J* = 8.0, 7.0, 1.0 Hz, 1H), 6.53 (s, 2H), 5.15 (s, 2H), 4.72 (s, 1H), 4.13 (s, 2H), 3.94 (s, 2H), 3.68 (t, *J* = 5.9 Hz, 2H), 3.62 – 3.32 (m, 52H), 2.90 (s, 2H), 2.77 (m, 2H), 2.61 (s, 1H), 2.41 (t, *J* = 5.9 Hz, 2H), 1.95 (s, 1H), 1.66 (s, 2H), 1.11 (s, 2H). ^{13}C NMR (126 MHz, CD_3OD) δ 177.3, 173.1, 169.6, 155.9, 152.5, 139.6, 138.5, 136.2, 135.9, 130.0, 129.5, 129.3, 127.7, 120.8, 120.6, 120.5, 119.1, 112.4, 80.9, 70.12, 70.06, 70.02, 69.9, 69.1, 66.8, 43.3, 39.6, 36.4, 35.8, 34.8, 29.6, 29.3. ESI-MS m/z calc'd for $C_{64}H_{91}N_9O_{18}$ $[M+Na]^+$: 1407.60; Observed $[M+Na]^+$: 1407.56**.**

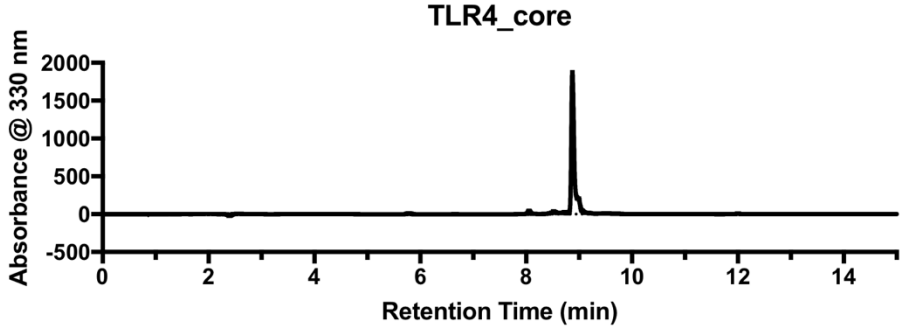

Figure 2.3 HPLC Trace of TLR4*a*_Core Measured at 330 nm on a C8 analytical column. Solvent A: 0.1 % TFA in HPLC grade water, Solvent B: 0.1% TFA in HPLC grade acetonitrile. Gradient: t 0-1 min hold 50% B, t 1-11 min ramp to 90% B, t 11-15 min hold 90% B.

$Pam_2CSK_4GC(Core)GK(5/6\ FAM)$ (TLR2/6a _Core) Synthesis.

Scheme 2.9 Synthetic Scheme of TLR2/6*a*_Core by Modified SPPS.

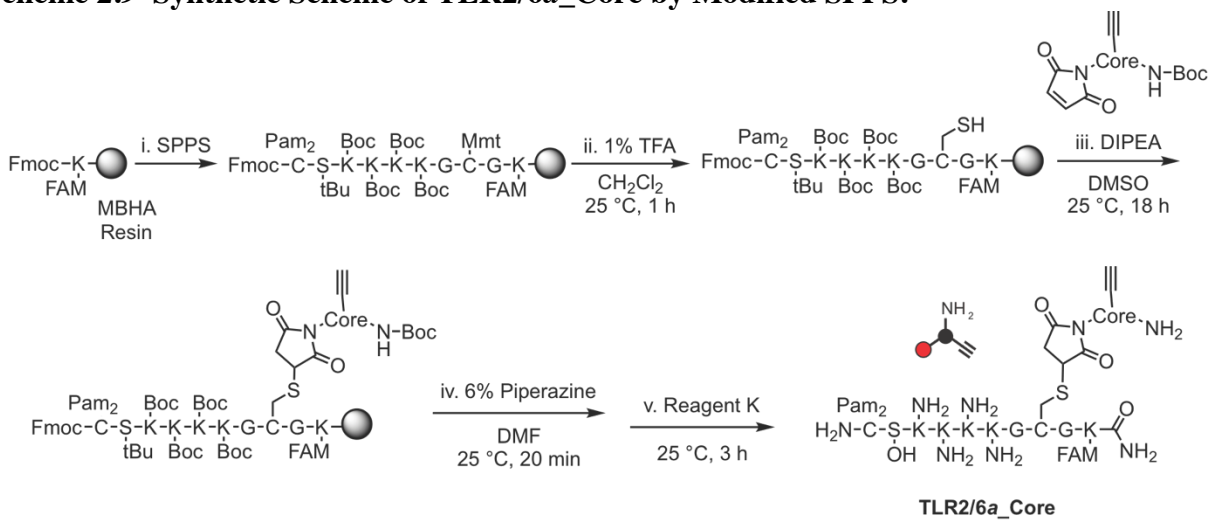

i.) Fmoc-based SPPS. ii.) Mmt deprotection. iii.) Michael addition to tri-agonist core. iv.) Fmoc deprotection. v.) Resin cleavage.

Resin Loading: MBHA rink amide resin (300 mg, 0.78 mmol/g) was added to a Bio-Rad Poly Prep column. The resin was suspended in DCM (10 mL) and agitated for 30 min. The resin was drained of the solution and suspended in DMF (10 mL) for 10 min. Fmoc deprotection was performed by suspending the resin in 6% piperazine/DMF (10 mL) for 10 min (2X). The resin was then washed with DMF (3X 10 mL). The DMF was drained and the resin suspended in a solution of Fmoc-Lys(5/6 FAM)-OH (187 mg, 0.255 mmol, 1.1 equiv.) and HATU (100 mg, 0.255 mmol 1.1 equiv.) in 25% 2,4,6-collidine/DMF (3 mL) for 1 h. The resin was drained of the solution, washed with DMF (3X 10 mL), and capped by suspending in a solution of acetic anhydride (478 mg, 4.68 mmol, 20 equiv.) in 25% DIPEA/DMF (3 mL) for 20 min. The solution was drained and the resin washed with DMF (3X 10 mL).

Solid Phase Peptide Synthesis: The following steps were followed to synthesize the sequence Fmoc-S(OtBu)-K(Boc)$_4$-G-C(Mmt)-G-K(5,6 FAM)-Resin: i. Fmoc deprotection with 6% piperazine/DMF (10 mL) for 10 min (2X) ii. DMF wash (3X 10 mL) iii. Coupling of the amino acid (0.936 mmol, 4 equiv.) in the presence of HBTU (355 mg, 0.936 mmol, 4 equiv.) dissolved in 25% 2,4,6-collidine/DMF (3 mL) for 30 min, and iv. DMF wash (3X 10 mL). The same four steps were followed for Fmoc-C(Pam$_2$)-OH (322 mg, 0.351 mmol, 1.5 equiv.) coupling, but the amino acid was coupled to the resin in a solution of 25% 2,4,6-collidine/DMF (3 mL), HBTU (178 mg, 0.468 mmol, 2 equiv.), and HOBt (191 mg, 0.468 mmol, 2 equiv.) and shaken for 18 h.

Coupling of Triazine Core to Resin bound TLR2/6*a*. Furan protected tri-agonist Core (65 mg, 1.8 mmol, 3.0 equiv.) was dissolved in DMSO (3 mL) and stirred for 5 h at 110 °C to expose the maleimide. The Fmoc-Pam$_2$CS(OtBu)K(Boc)$_4$GC(Mmt)GK(5/6 FAM)-Resin (1/6th of batch, 0.039 mmol peptide) described above was swollen in DCM (10 mL) for 30 min and then the DCM drained. Cys(Mmt) was deprotected by washing the resin several times with 1% TFA/DCM (5 mL each wash) over 1 h. The resin was washed 3X with DCM (10 mL) and 3X with DMF (10 mL). The furan deprotected triagonist core solution and DIPEA (1 mL) was then added to the peptide bound resin and the reaction mixture shaken for 18 h. The solution was drained from the resin and the resin washed 3X with DMF (10 mL) and 3X with DCM (10 mL). The peptide was Fmoc deprotected with 6% piperazine/DMF (2X 10 mL, 10 min) washed with DMF (3X 10 mL) and DCM (3X 10 mL). The peptide was cleaved from the resin with Reagent K (TFA/phenol/water/EDT/thioanisole 34:2:2:2:1, 2 mL) for 4 h, and the resin washed 2X with Reagent K (2 mL). The cleavage solutions were combined and the peptide was precipitated in ice cold diethyl ether (20 mL), and centrifuged (2,400X g, 10 min, 4 °C). The peptide pellet was

washed 2X with ice cold diethyl ether (20 mL). The resulting crude product was dried and purified by HPLC. The pure isolated product was quantified by fluorescence spectroscopy (0.8 mg recovered, 340 nmol) and analyzed by MALDI-TOF. MALDI-TOF: m/z calc'd for $C_{117}H_{184}N_{24}O_{23}S_2$ $[M+H]^+$ 2358.3; Observed $[M+H]^+$ 2358.6.

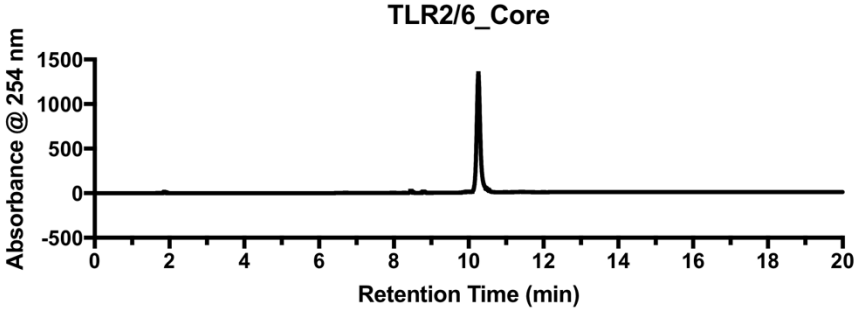

Figure 2.4 HPLC Trace of TLR2/6*a*_Core. Measured at 254 nm on a C8 analytical column. Solvent A: 0.1 % TFA in HPLC grade water, Solvent B: 0.1% TFA in HPLC grade acetonitrile. Gradient: t 0-1 min hold 10% B, t 1-11 min ramp to 90% B, t 11-20 min hold 90% B.

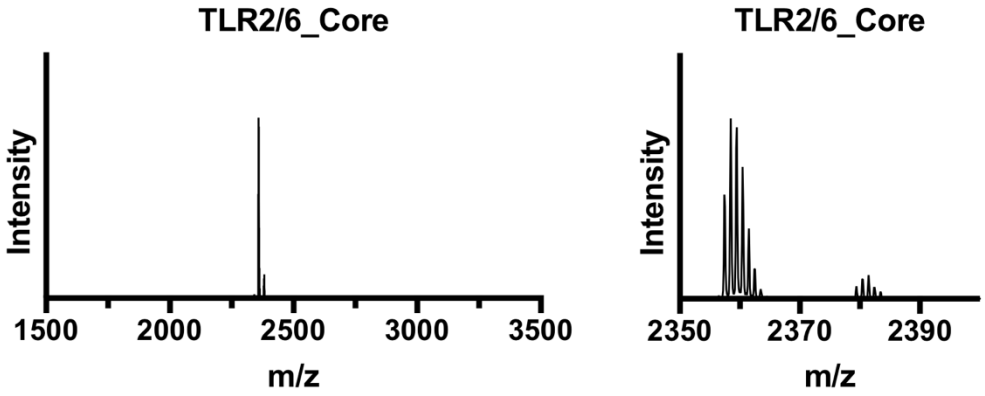

Figure 2.5 MALDI Trace of TLR2/6a_Core . Broad view (left) and close up view of peak (right). Sample acquired in positive reflector mode using dihydroxybenzoic acid matrix.

Pam_3CSK_4GC(Core)GK(5/6 FAM) (TLR1/2a _Core) Synthesis.

Scheme 2.10 Synthetic Scheme of TLR1/2*a*_Core by Modified SPPS.

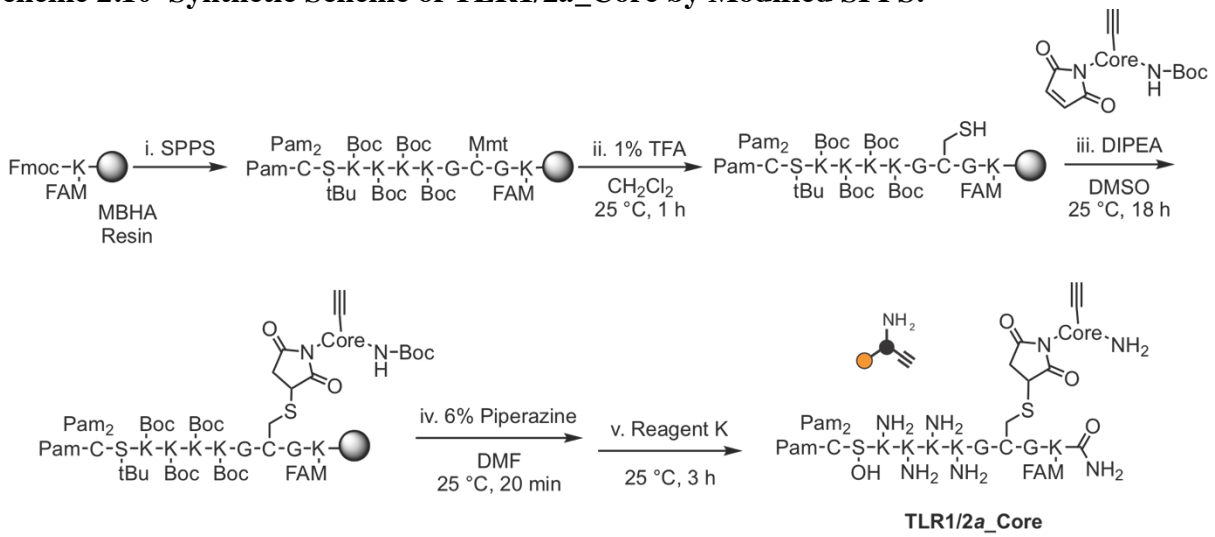

i.) Fmoc-based SPPS. ii.) Mmt deprotection. iii.) Michael addition to tri-agonist core. iv.) Resin cleavage.

Fmoc-Pam_2CSK_4GC(Mmt)GK(5/6 FAM)-Resin was synthesized as described above. The resin was suspended in DCM (10 mL) and agitated for 30 min. The resin was drained of the solution and suspended in DMF (10 mL) for 10 min. Fmoc deprotection was performed by suspending the resin in 6% piperazine/DMF (10 mL) for 10 min (2X). The resin was then washed with DMF (3X 10 mL). The DMF was drained and the resin suspended in a solution of palmitic acid (41 mg, 0.16 mmol, 4 equiv.) and HBTU (61 mg, 0.16 mmol 4 equiv.) in 25% 2,4,6 collidine/DMF (3 mL) for 3 h. The solution was drained from the resin, the resin washed 3X with DMF (10 mL), and 3X with DCM (10 mL). The peptide was then conjugated to furan deprotected tri-agonist core analogously as described above. The resin-bound peptide was cleaved in Reagent K (TFA/phenol/water/EDT/thioanisole 34:2:2:2:1, 2 mL) for 2 h, and the resin washed 2X with Reagent K (2 mL). The cleavage solutions were combined and the peptide was precipitated in ice

1:1 cold hexanes/diethyl ether (20 mL), and centrifuged (2,400X g, 10 min, 4 °C). The peptide pellet was washed 2X with ice cold diethyl ether (20 mL). The resulting crude product was dried and purified by HPLC. The pure isolated product was quantified by fluorescence microscopy (1.1 mg, 424 nmol recovered) and analyzed by MALDI-TOF. MALDI-TOF: m/z calc'd for $C_{133}H_{214}N_{24}O_{24}S_2$ $[M+H]^+$ 2596.6; Observed $[M+H]^+$ 2596.6.

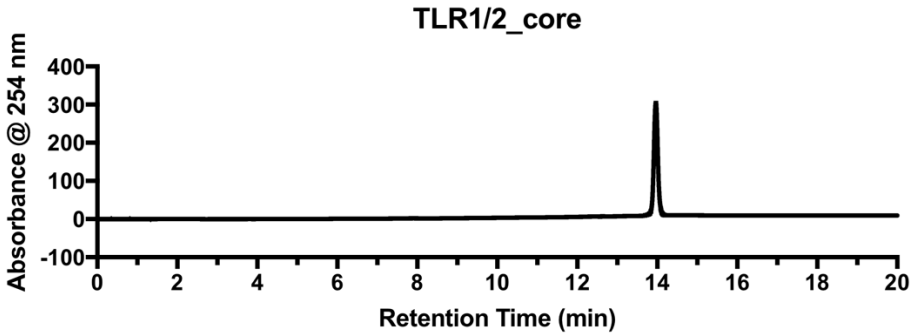

Figure 2.6 HPLC Trace of TLR2/6a_Core. Measured at 254 nm on a C8 analytical column. Solvent A: 0.1 % TFA in HPLC grade water, Solvent B: 0.1% TFA in HPLC grade acetonitrile. Gradient: t 0-1 min hold 50% B, t 1-11 min ramp to 90% B, t 11-20 min hold 90% B.

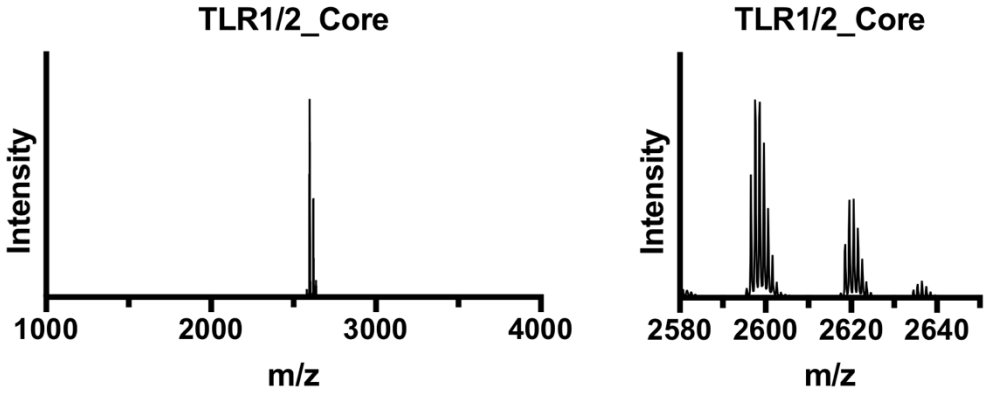

Figure 2.7 MALDI Trace of TLR1/2a_Core. Broad view (left) and enlarged view of the major peak (right). Sample acquired in positive reflector mode using dihydroxybenzoic acid matrix.

Pam_2CSK_4GC(Core-TLR4a)GK(5,6 FAM) (TLR2/6_4*a*) Synthesis.

Scheme 2.11 Synthetic Scheme of TLR2/6_4*a* by Modified SPPS.

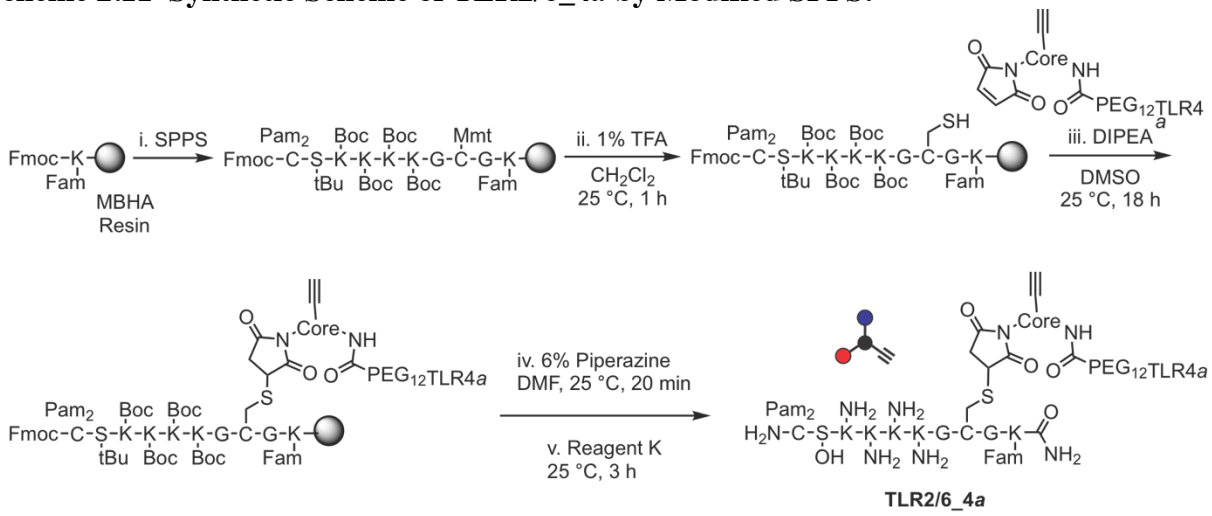

i.) Fmoc-based SPPS. ii.) Mmt deprotection. iii.) Michael addition to TLR4*a*_Core. iv.) Fmoc deprotection v.) Resin cleavage.

Pam_2CSK_4GC(Core)GK(5/6 FAM)-Resin Synthesis: Pam_2CSK_4GC(Core)GK(5,6 FAM)-Resin Synthesis was synthesized as described above.

Coupling of TLR4*a*_Core to Resin bound TLR2/6*a*. Furan protected TLR4*a*_Core (283 mg, 0.204 mmol, 1.3 equiv.) was conjugated to the resin bound peptide (200 mg resin) and the product obtained analogously as TLR2/6*a*_Core described above. The isolated product was quantified by fluorescence spectroscopy analyzed by HPLC and MALDI-TOF (11.7 mg, 3.5 □mol recovered). MALDI-TOF: m/z calc'd for $C_{162}H_{248}N_{28}O_{38}S_3$ $[M+H]^+$: 3290.8; Observed $[M+H]^+$: 3290.3.

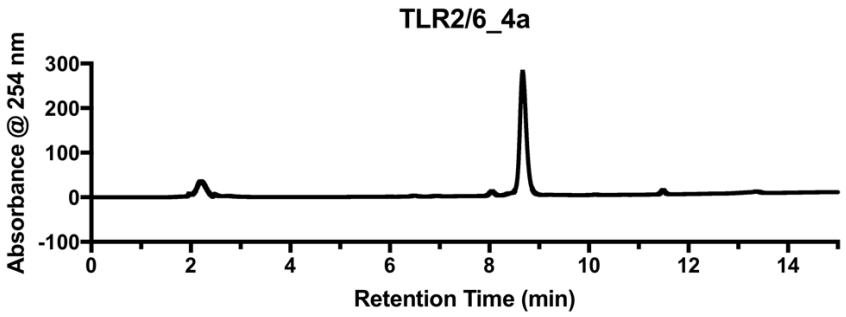

Figure 2.8 HPLC Trace of TLR4*a*_Core. Measured at 254 nm on a C8 analytical column. Solvent A: 0.1 % TFA in HPLC grade water, Solvent B: 0.1% TFA in HPLC grade acetonitrile. Gradient: t 0-1 min hold 50% B, t 1-11 min ramp to 90% B, t 11-15 min hold 90% B.

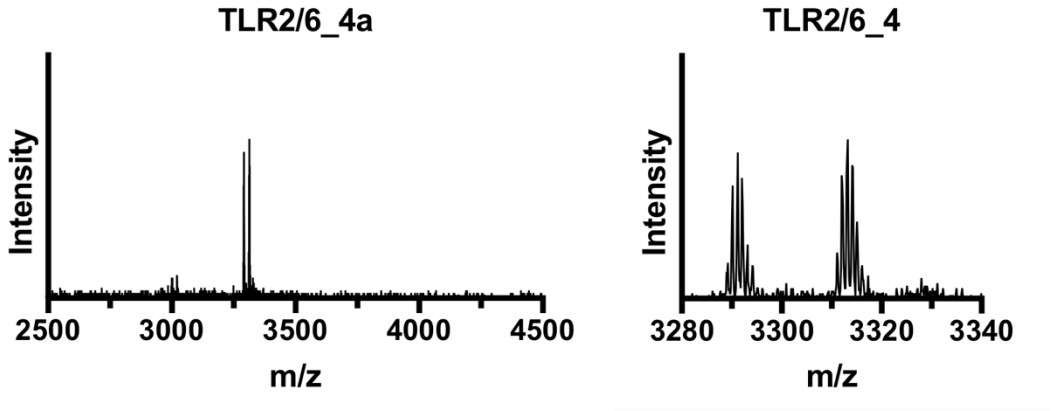

Figure 2.9 MALDI Trace of TLR2/6_4*a*. Broad view (left) and enlarged view of the major peak (right). Sample acquired in positive reflector mode using dihydroxybenzoic acid matrix.

Pam_3CSK_4GC(Core-TLR4a)GK(5,6_FAM) (TLR1/2_4*a*) Synthesis.

Scheme 2.12 Synthetic Scheme of TLR1/2_4*a* by modified SPPS.

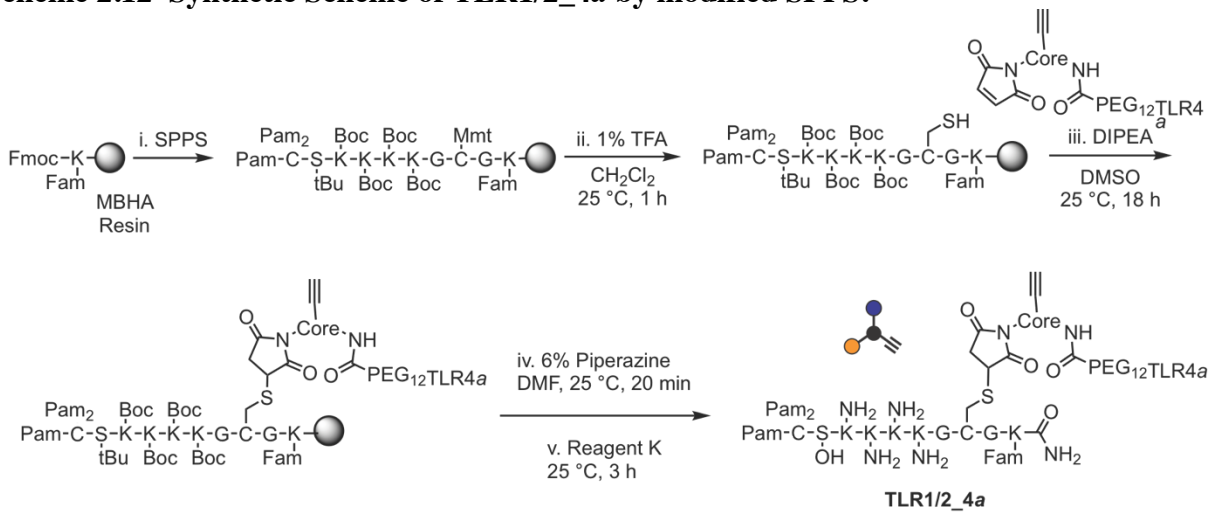

i.) Fmoc-based SPPS. ii.) Mmt deprotection. iii.) Michael addition to TLR4*a*_Core. iv.) Resin cleavage.

Pam_3CSK_4GC(Mmt)GK(5,6 FAM)-Resin (100 mg starting resin) was prepared as described above. TLR4*a*_Core (110 mg, 0.08 mmols, 1.1 equiv.) was then conjugated by Michael addition, analogously to that of Fmoc-Pam_2CS(OtBu)K$(Boc)_4$GC(Mmt)GK(5/6 FAM)-Resin described above. The pure isolated product was quantified by fluorescence spectroscopy and analyzed by MALDI-TOF and HPLC (6 mg recovered, 1.7 μmol). MALDI-TOF: m/z calc'd for $C_{178}H_{278}N_{28}O_{39}S_3$ $[M+H]^+$:3529.0; Observed $[M+H]^+$: 3528.9.

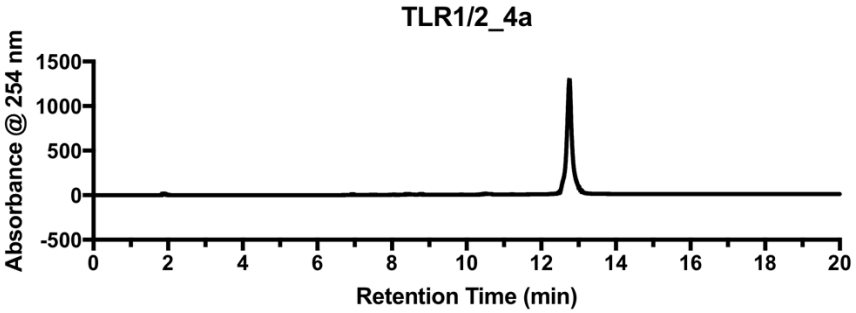

Figure 2.10 HPLC Trace of TLR4*a*_Core. Measured at 254 nm on a C8 analytical column. Solvent A: 0.1 % TFA in HPLC grade water, Solvent B: 0.1% TFA in HPLC grade acetonitrile. Gradient: t 0-1 min hold 10% B, t 1-11 min ramp to 90% B, t 11-20 min hold 90% B.

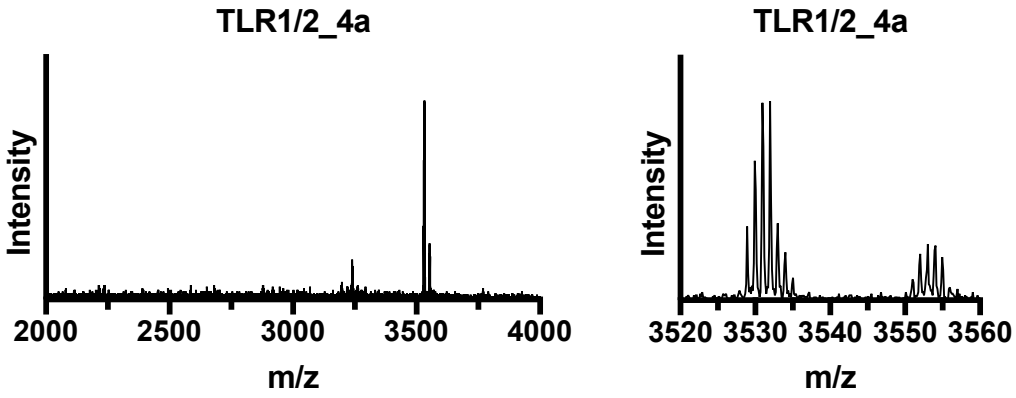

Figure 2.11 MALDI Trace of TLR1/2_4*a*. Broad view (left) and enlarged view of the major peak (right). Sample acquired in positive reflector mode using dihydroxybenzoic acid matrix.

TLR7*a* Synthesis (By Dr. Janine Tom):

Scheme 2.13 TLR7*a* Synthesis

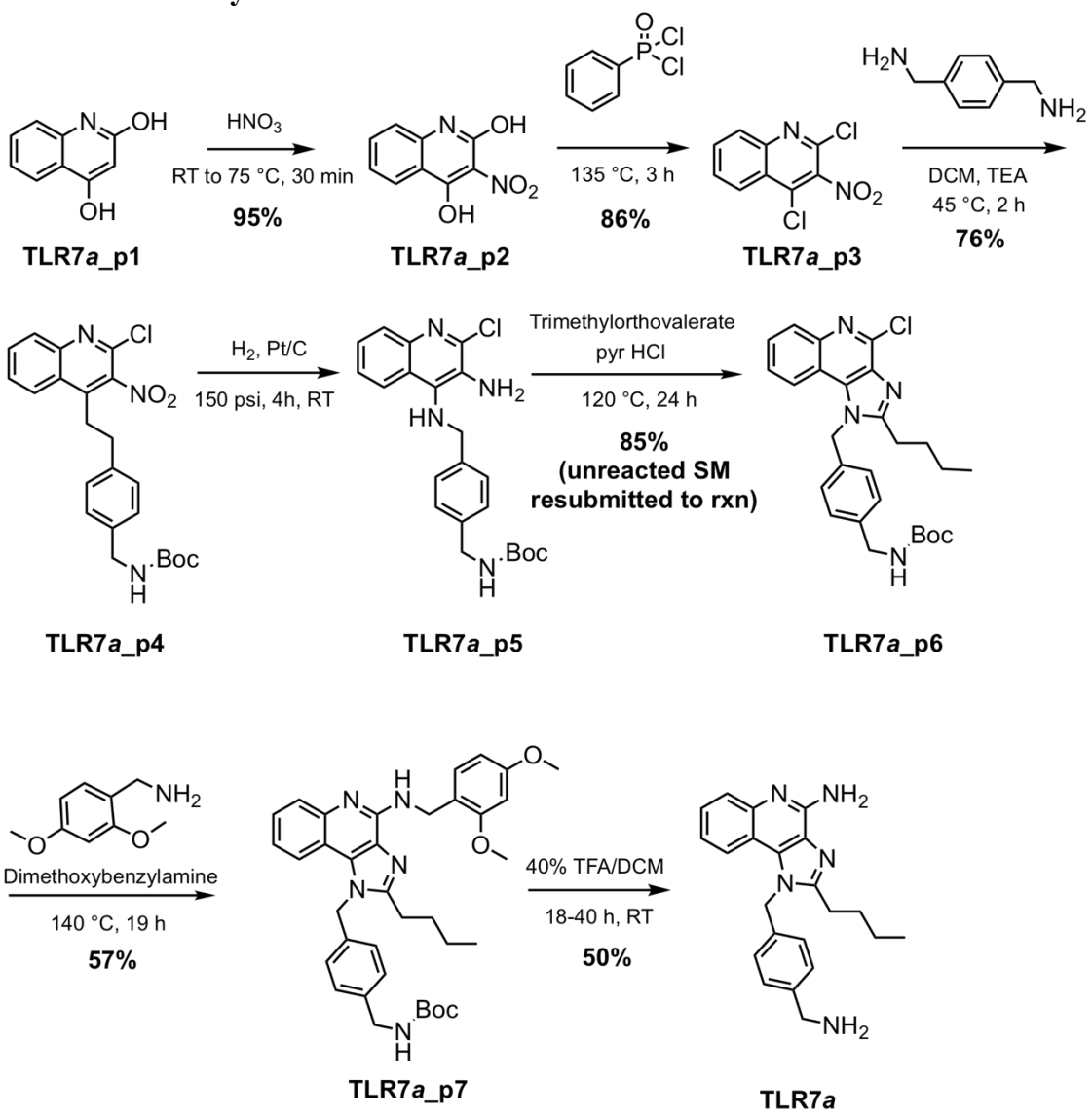

Compounds TLR7*a*-precursor 1 (TLR7*a*-p1) – TLR7*a*-p2 were synthesized according to literature procedures reported by Shukla, *et al*.[5,15] Compounds TLR7*a*-p5-TLR7*a* were synthesized according to the modified procedure[6] below to increase yield for scale up purposes (Scheme 1).

TLR7*a*-p5:

The nitro-substrate (TLR7*a*-p4) (5.0 g, 11 mmol) and sodium sulfate (0.050 g) were dissolved in ethyl acetate (0.040 L) that was purged with argon in a Parr Reactor (Parr Instrument Company). 10% Pt/C (0.050 g) was added to the reaction mixture and the reactor was filled with hydrogen gas at 350 psi. The reaction was allowed to stir at room temperature until hydrogen gas was consumed and the pressure remained constaint (overnight, ~ 24 hours). The reaction was filtered through Celite and concentrated by rotary evaporation. A yellow solid was obtained (4.5 g, 98% yield). ^{1}H NMR (500 MHz, DMSO-d_6) δ 7.98 (d, J = 6.5 Hz, 1H), 7.65 (d, J = 7.5 Hz, 1H), 7.40-7.35 (m, 2H), 7.30 (d, J = 6.5 Hz, 3H), 7.13 (d, J =6.5 Hz, 2H), 5.81 (s, 1H), 5.07 (s, 2H), 4.42 (d, J = 6 Hz, 2H), 4.06 (d, J =5.5 Hz, 2H), 1.38 (s, 9H). HRMS: m/z calc'd for $C_{22}H_{25}ClN_4O_2$ $[M+Na]^+$ 435.17, observed 435.1566.

TLR7*a*-p6:

The reduced substrate (TLR7*a*-p5) (0.15 g, 0.36 mmol) was suspended in toluene (2.0 mL). Trimethylorthovalerate (0.13 mL, 0.73 mmol) and pyridine hydrochloride (5.0 mg, 36 μmol) were added to the solution. The reaction was allowed to stir and heated at 120 ºC for 20 h. The crude reaction was then concentrated and purified by column chromatography (50% EtOAc/Hex) to obtain the product as a white solid (70 mg, 41%).

The uncyclized intermediate was resubmitted to the reaction according to the following procedure. The uncyclized substrate (0.11 g, 0.22 mmol) was dissolved in xylenes (2.0 mL). Pyridine hydrochloride (5.1 mg, 44 μmol) was added to the reaction mixture, which was heated at 130 ºC for 24 h. The reaction was allowed to cool, was concentrated, and purified by column chromatography (50% EtOAc/Hex) to obtain the product (77 mg, 73%).

Combined total yield (147 mg, 85% yield).

^{1}H NMR (500 MHz, CD_3OD) δ 8.08-8.04 (dd, *J* = 14, 7.3 Hz, 2H), 7.65 (t, *J* = 5.8 Hz, 1H), 7.48 (t, *J* = 7 Hz, 1H), 7.25 (d, *J* = 7 Hz, 2H), 7.02 (d, 2H), 5.98 (s, 1H), 4.18 (s, 2H), 3.06 (t, *J* = 6.3 Hz, 2H), 1.79-1.74 (m, 2H), 1.41 (s, 9H), 1.29 (br s, 2H), 0.92 (t, *J* = 6 Hz, 3H). HRMS: *m/z* calc'd for $C_{27}H_{31}ClN_4O_2$ $[M+Na]^+$ 501.21, observed 501.2023.

TLR7*a*-p7:

Cyclized compound TLR7*a*-p6 (44 mg, 0.090 mmol) was suspended in dimethoxybenzylamine (1.6 mL, 0.010 mol). The reaction was run neat and heated at 140 ºC for 19 h. The crude reaction mixture was poured into methylene chloride (0.10 L) and washed with 1 M HCl (4X 100 mL). The organic layer was dried with sodium sulfate, filtered, and concentrated. The crude product was purified by column chromatography (5% MeOH/methylene chloride) to provide the product as a white powder (31 mg, 57%).

^{1}H NMR (500 MHz, CD_3OD) δ 7.86 (t, *J* = 6.5 Hz, 2H), 7.50 (t, *J* = 6.5 Hz, 1H), 7.33 (d, *J* = 7.3 Hz, 1H), 7.25 (d, *J* = 6.5 Hz, 2H), 7.20 (br s, 1H), 7.03 (d, *J* = 6.5 Hz, 2H), 6.61 (s, 1H), 6.53-6.52 (dd, *J* = 6.5, 2 Hz, 1H), 5.87 (s, 2H), 4.18 (br s, 2H), 3.87 (s, 3H), 3.80 (s, 3H), 2.94 (t, *J* = 6.3 Hz, 2H), 1.79-1.74 (m, 2H), 1.42 (s, 9H), 1.29 (br s, 2H), 0.91 (t, *J* = 6.3 Hz, 3H). HRMS: *m/z* calc'd for $C_{36}H_{43}N_5O_4$ $[M+H]^+$ 610.34, observed 610.3387.

TLR7*a*:

Protected imidazoquinoline TLR7*a*-p7 (0.20 g, 0.50 mmol) was dissolved in methylene chloride (15 mL). Trifluoroacetic acid (0.010 L) was added to the solution to provide a 40% TFA/methylene chloride solution. The reaction was allowed to stir at RT for 38 h. The reaction mixture was

concentrated and 1 M HCl (100 mL) was added to the crude solid. The solid was filtered off and the filtrate was adjusted to pH 10 using 10 M NaOH. The aqueous solution was extracted with methylene chloride (6X 200 mL). The organic layer was then dried with sodium sulfate, filtered, and concentrated to provide the product as a white solid (180 mg, 50% yield).

^{1}H NMR (500 MHz, DMSO-d_6) δ 7.79 (d, J = 7.5 Hz, 1H), 7.56 (t, J = 8.5 Hz, 1H), 7.32 (t, J = 7 Hz, 1H), 7.26 (d, J = 8.5 Hz, 2H), 7.02 (t, J = 7 Hz, 1H), 6.95 (d, J = 8 Hz, 2H), 6.53 (s, 1H), 5.82 (s, 2H), 3.64 (s, 2H), 2.90 (t, J = 7.5 Hz, 2H), 1.74-1.68 (m, 2H), 1.42-1.34 (m, 2H), 0.87 (t, J = 7.5 Hz, 3H). HRMS: m/z calc'd for $C_{22}H_{25}N_5$ $[M+H]^+$ 360.22, observed 360.2183.

TLR7a-PEG$_{12}$-N$_3$ Synthesis

Scheme 2.14 PEG$_{12}$-N$_3$ Functionalization of TLR7*a*.

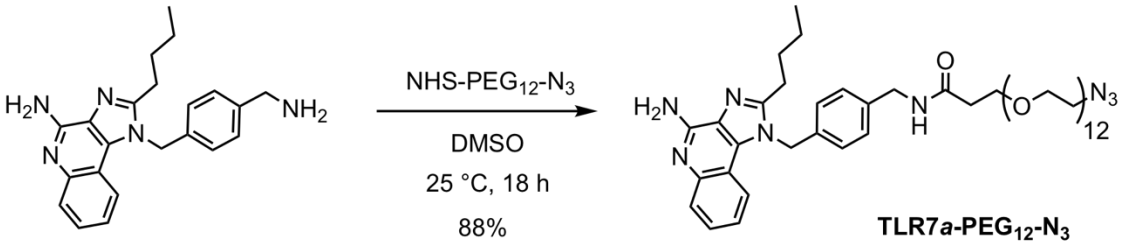

TLR7a (6.0 mg, 16.7 μmol, 1 equiv.) and NHS-PEG$_{12}$-N$_3$ (12.4 mg, 16.7 μmol, 1 equiv.) were dissolved in anhydrous DMSO (250 μL) and stirred for 18 h. The reaction solution was added to ethyl acetate and washed with basified water 1X (pH 8.5 with $NaHCO_3$). The organic layer was dried over $NaSO_4$, filtered, and dried by rotary evaporation to afford the product (14.4 mg, 88%). ESI-MS: m/z calc'd for $C_{49}H_{76}N_8O_{13}$ $[M+H]^+$: 985.56; Observed $[M+H]^+$: 985.50.

TLR7a-PEG$_{12}$-N$_3$ Conjugation to Tri-agonist Core *via* CuAAC (TLR7*a*_Core).

Scheme 2.15 CuAAC reaction of TLR7*a*-PEG$_{12}$-N$_3$ and Tri-agonist Core

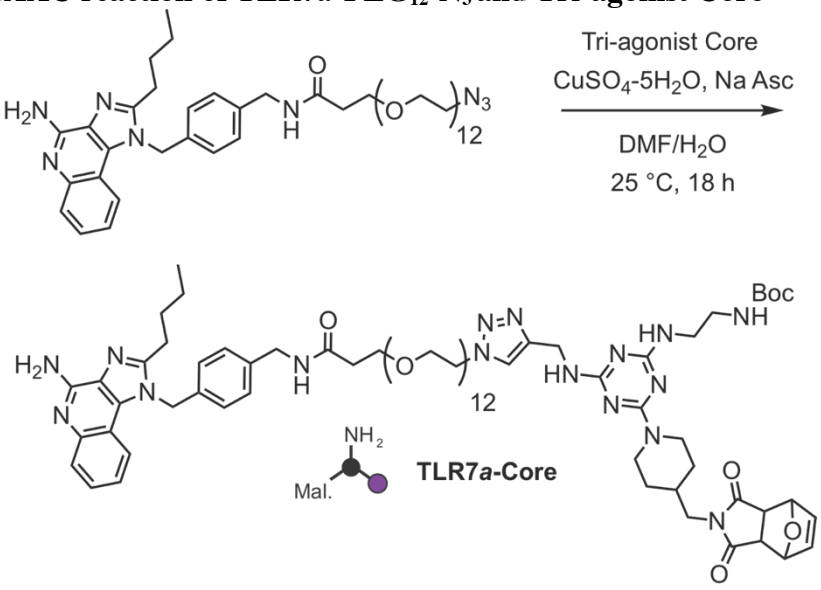

TLR7*a*-PEG$_{12}$-N$_3$ (2.0 mg, 2 μmol, 1 equiv.) was dissolved in DMF (167 μL). Tri-agonist Core (1.7 mg, 3 μmol, 1.5 equiv.) was added to the solution. $CuSO_4$•$5H_2O$ (5.0 mg, 20 μmol, 10 equiv.) and sodium ascorbate (7.9 mg, 40 μmol, 20 equiv.) were pre-dissolved in degassed water (15 μL for each reagent) and then added to the reaction mixture. The reaction was placed on a shaker at room temperature for 24 h. The reaction mixture was centrifuged and supernatant was removed. The supernatant was diluted in acetonitrile (final concentration in 1:1 v/v DMF/acetonitrile) and purified by HPLC, and lyophilized to obtain TLR7*a*_Core. The product was quantified by UV absorbance and characterized by HPLC and MALDI-TOF. MALDI-TOF: m/z calc'd for $C_{72}H_{109}N_{16}O_{17}$ $[M\text{-Furan+H}]^+$: 1469.8; Observed $[M\text{-Furan+H}]^+$: 1469.6.

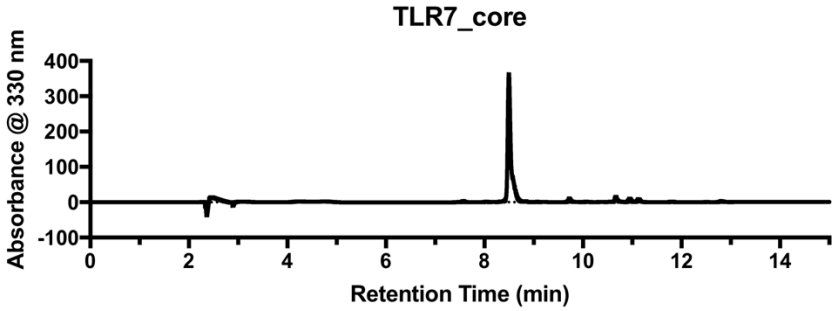

Figure 2.12 HPLC Trace of TLR7*a*_Core. Measured at 330 nm on a C8 analytical column. Solvent A: 0.1 % TFA in HPLC grade water, Solvent B: 0.1% TFA in HPLC grade acetonitrile. Gradient: t 0-1 min hold 10% B, t 1-11 min ramp to 90% B, t 11-15 min hold 90% B.

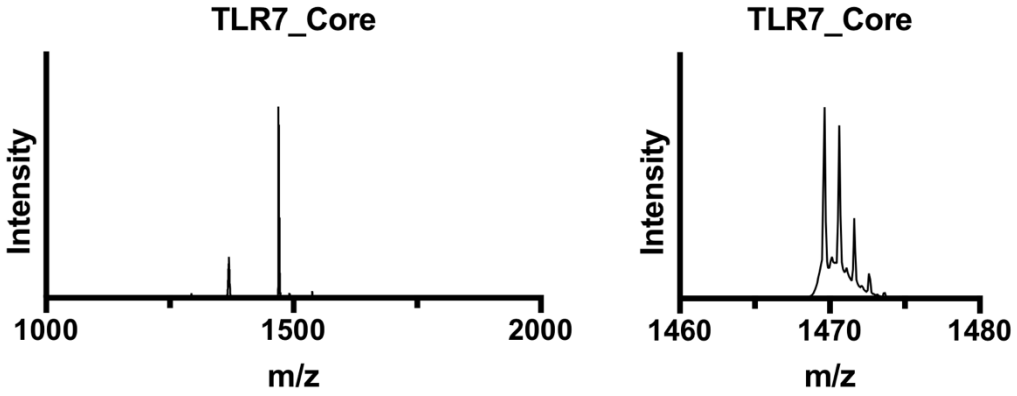

Figure 2.13 MALDI Trace of TLR7*a*_Core. Broad view (left) and enlarged view of the major peak (right). Sample acquired in positive reflector mode using dihydroxybenzoic acid matrix.

TLR7a-PEG$_{12}$-N$_3$ conjugation to TLR2/6a_Core *via* CuAAC (TLR2/6_7*a*).

Scheme 2.16 CuAAC Reaction of TLR7*a*-PEG$_{12}$-N$_3$ and TLR2/6*a*_Core

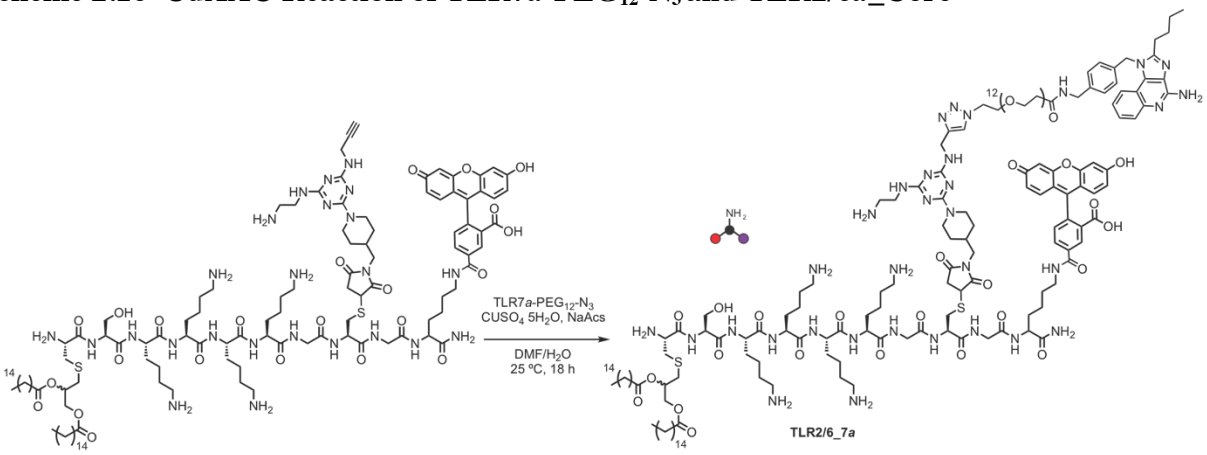

TLR2/6*a*_Core (0.56 mg, 0.24 μmol, 1 equiv.) was dissolved in water (65 μL). DMF (266 μL) and then TLR7*a*-PEG$_{12}$-N$_3$ (2.4 mg, 2.4 μmol, 10 equiv.) in DMF (185 μL) were added to the solution. $CuSO_4$•$5H_2O$ (1.2 mg, 4.8 μmol, 20 equiv.) and sodium ascorbate (1.4 mg, 7.2 μmol, 30 equiv.) were pre-dissolved in degassed water (17 μL for each reagent) and then added to the reaction mixture. The reaction was placed on a shaker at room temperature for 24 h. The reaction mixture was centrifuged and supernatant was removed to obtain a pellet. The pellet was washed with 0.1 M EDTA (2X 400 μL). The resulting pellet was dissolved in DMSO/acetonitrile (1:1 v/v) and purified by HPLC, and lyophilized to obtain TLR2/6_7*a*. The product was quantified by fluorescence spectroscopy and characterized by MALDI-TOF and HPLC (19 nmol, 64 μg recovered). MALDI-TOF: m/z calc'd for $C_{166}H_{260}N_{32}O_{36}S_2$ $[M+H]^+$: 3342.9; Observed $[M+H]^+$: 3342.8.

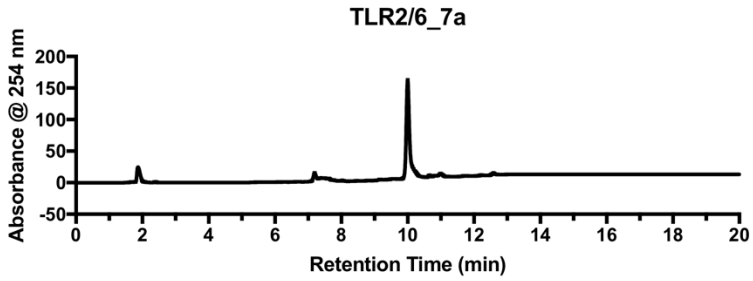

Figure 2.14 HPLC Trace of TLR2/6_7*a*. Measured at 254 nm on a C8 analytical column. Solvent A: 0.1 % TFA in HPLC grade water, Solvent B: 0.1% TFA in HPLC grade acetonitrile. Gradient: t 0-1 min hold 10% B, t 1-11 min ramp to 90% B, t 11-20 min hold 90% B.

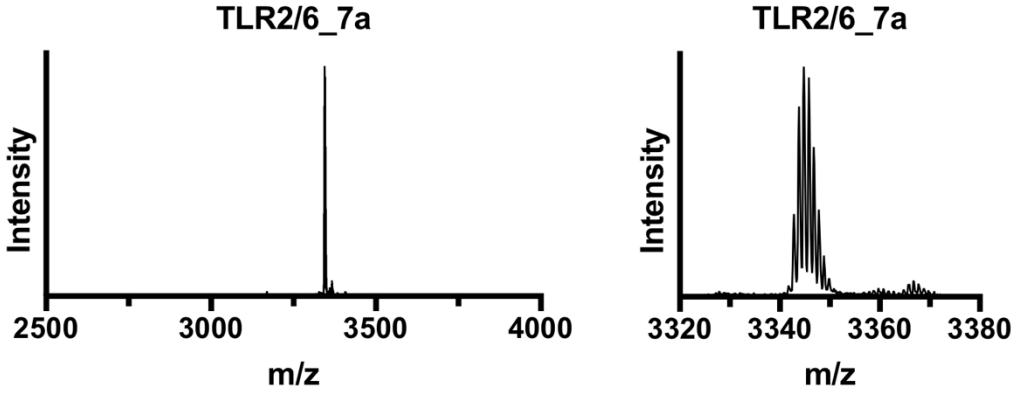

Figure 2.15 MALDI trace of TLR2/6_7*a*. Broad view (left) and enlarged view of the major peak (right). Sample acquired in positive reflector mode using dihydroxybenzoic acid matrix.

TLR7a-PEG$_{12}$-N$_3$ conjugation to TLR1/2*a*_Core *via* CuAAC (TLR1/2_7*a*).

Scheme 2.17 CuAAC reaction of TLR7*a*-PEG$_{12}$-N$_3$ and TLR1/2*a*_Core.

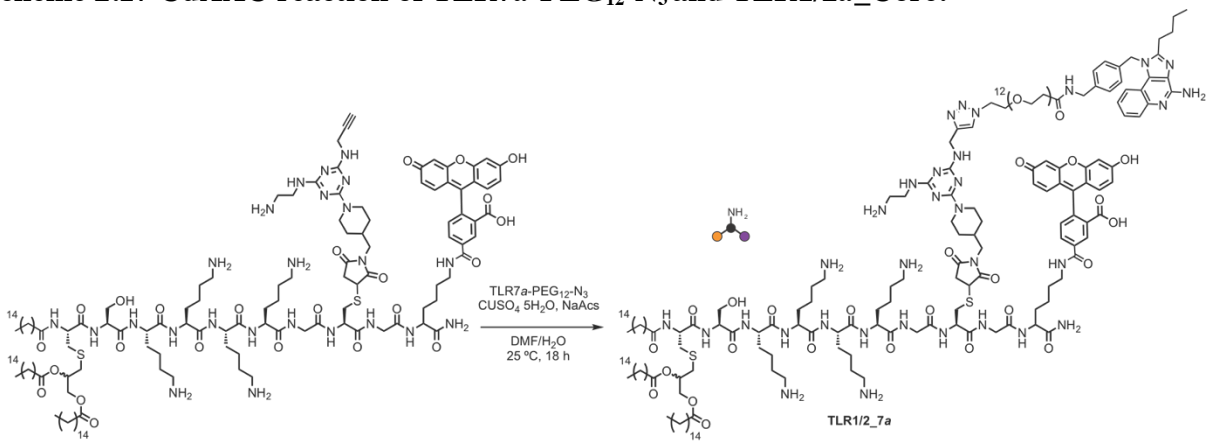

$CuSO_4$•$5H_2O$ (1.1 mg, 4.6 μmol, 20 equiv.) was pre-dissolved in degassed water (55 μL) and added to a solution of TLR1/2a_Core (0.60 mg, 0.23 μmol, 1 equiv.) dissolved in DMF (130 μL). TLR7a-PEG$_{12}$-N$_3$ (1.1 mg, 1.2 μmol, 5 equiv.) and sodium ascorbate (1.4 mg, 6.9 μmol, 30 equiv.) were then added to the reaction mixture. The reaction was placed on a shaker at room temperature for 24 h. The reaction mixture was centrifuged and supernatant was removed to obtain a pellet. The pellet was washed with 0.1 M EDTA (2X 400 μL). The resulting pellet was dissolved in DMSO/acetonitrile (1:1 v/v) and purified by HPLC, and lyophilized to obtain TLR1/2_7*a*. The product was quantified by fluorescence spectroscopy and characterized by MALDI-TOF and HPLC (160 nmol, 0.57 mg recovered). MALDI-TOF: m/z calc'd for $C_{182}H_{290}N_{32}O_{37}S_2$ $[M+H]^+$:3581.1; Observed $[M+H]^+$: 3580.8.

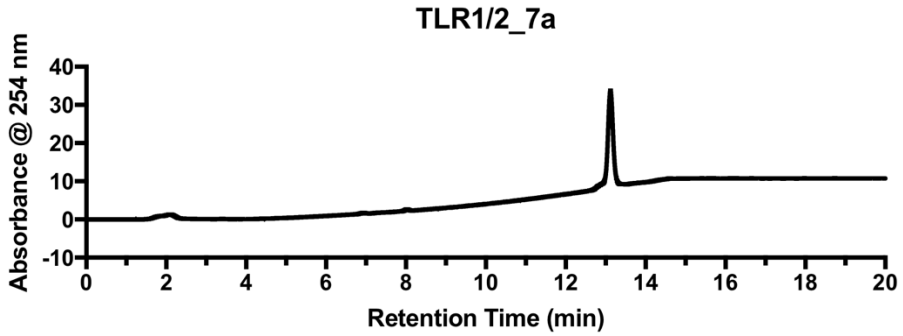

Figure 2.16 HPLC trace of TLR1/2_7*a*. Measured at 254 nm on a C8 analytical column. Solvent A: 0.1 % TFA in HPLC grade water, Solvent B: 0.1% TFA in HPLC grade acetonitrile. Gradient: t 0-1 min hold 50% B, t 1-11 min ramp to 90% B, t 11-20 min hold 90% B.

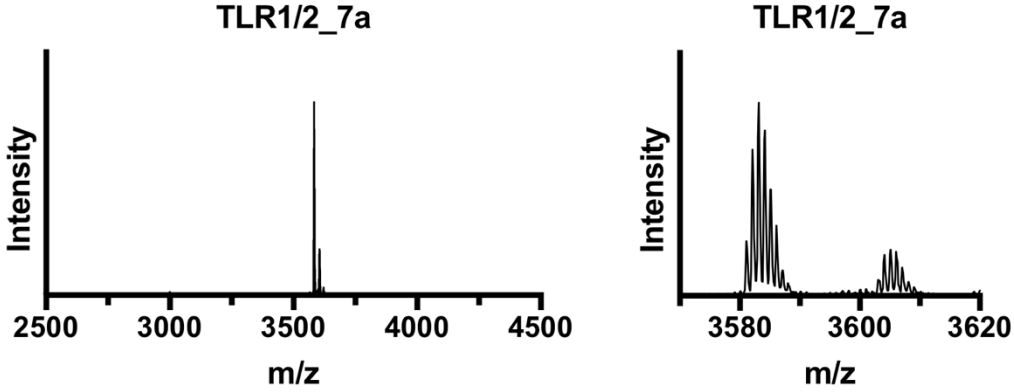

Figure 2.17 MALDI trace of TLR1/2_7*a*. Full (left) and enlarged view of the major peak (right). Sample acquired in positive reflector mode using dihydroxybenzoic acid matrix.

TLR9*a*-N_3 conjugation to Triazine Core *via* CuAAC (TLR9*a*_Core).

Scheme 2.18 CuAAC reaction of Tri-agonist Core and TLR9*a* to afford TLR9*a*_Core.

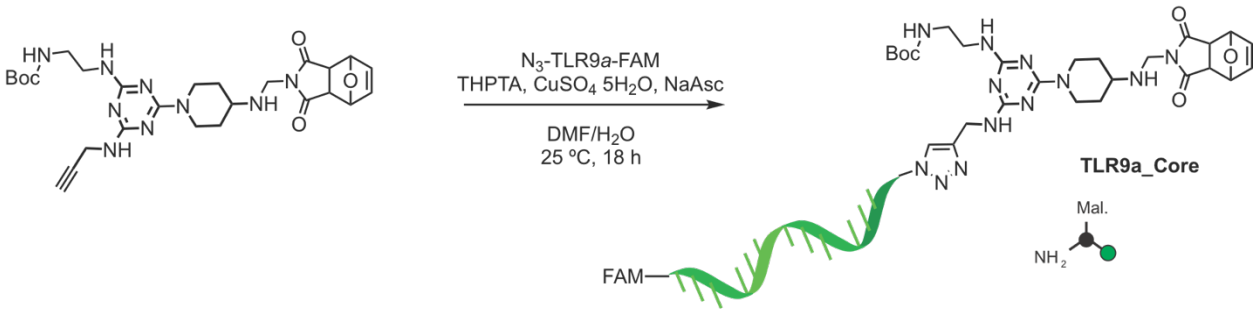

Triazine Core A (83 μg, 150 nmol) in DMF (83 μL) and CpG-ODN1826-N_3 (363 μg, 50 nmol) in water (50 μL) were mixed with DMF (215 μL). Copper sulfate pentahydrate (250 μg, 1 μmol) pre-dissolved in degassed water (5 μL) and THPTA (425 μg, 1 μmol) in degassed water (14 μL) were mixed and then added to the reaction vial. Lastly, sodium ascorbate (297 μg, 1.5 μmol) dissolved in water (5 uL) was added to the reaction mixture to give a final ratio of DMF: H_2O (4:1). The reaction mixture was placed on a shaker at RT for 18 h. The crude reaction was purified via SDS-PAGE and gel extraction. The product band was excised and eluted into endotoxin free water overnight at RT. The solution was concentrated and desalted using a 3k centrifugal filter unit (EMD Millipore) to provide the desired product and quantified by fluorescence spectroscopy (14 nmol, 0.11 mg recovered). ESI: Calculated MW: 7821 Observed $[M-H]^-$: 7821.

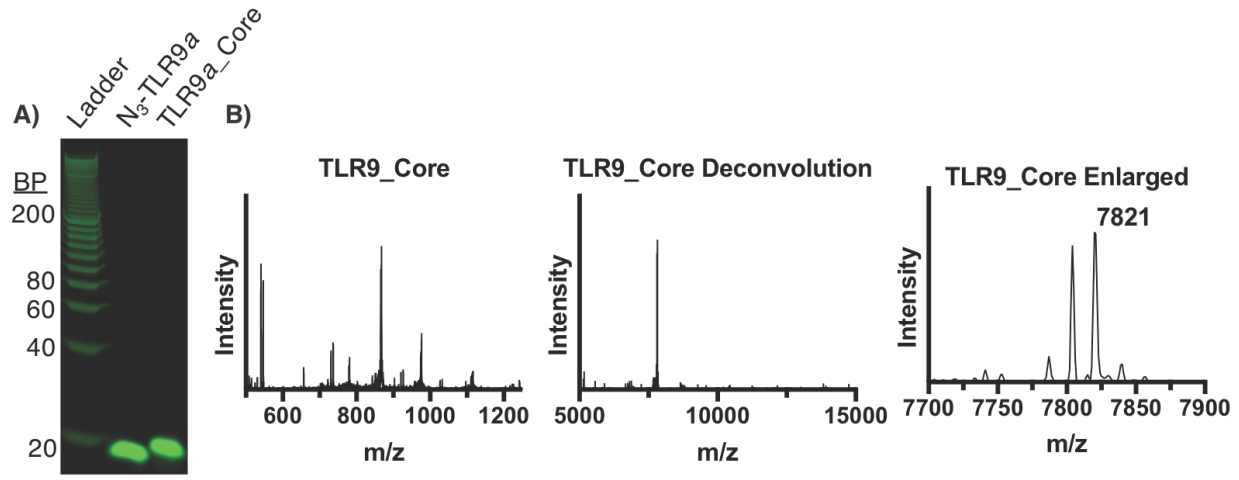

Figure 2.18 SDS-PAGE and Mass Spectrometry of TLR9*a*_Core . A) Fluorescence gel image of N_3-TLR9*a*-FAM and TLR9*a*_Core compared to 20 bp molecular weight ladder ran on a 10% Mini-PROTEAN TBE-UREA gel and stained with SYBR Safe DNA gel stain. B) ESI-MS data of TLR9*a*_Core. Left, raw mass spectrum. Middle, deconvolution of raw data mass spectrum. Right, enlarged view of major peak in deconvolution data.

TLR9a-N_3 conjugation to TLR2/6a_Core *via* CuAAC (TLR2/6_9a).

Scheme 2.19 CuAAC reaction of TLR2/6*a*_Core and TL9*a* to afford TLR2/6_9*a*.

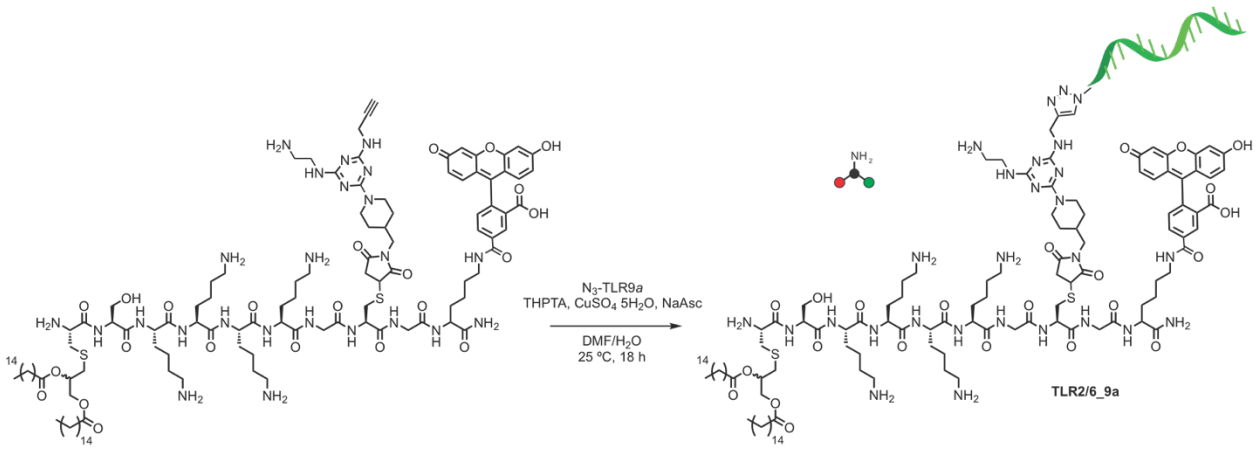

TLR2/6*a*_Core (0.18 mg, 78 nmol) in DMF (116 μL) and CpG-ODN1826-N_3 (0.17 μg, 26 nmol) in water (26 μL) were mixed with DMF (58 mL). Copper sulfate pentahydrate (0.13 mg, 520 nmol) pre-dissolved in degassed water (1.8 μL) and THPTA (0.23 mg, 520 nmol) in degassed water (12 μL) were mixed and then added to the reaction vial. Lastly, sodium ascorbate (0.15 mg, 780 nmol) in degassed water (3.7 μL) was added to the reaction mixture to give a final ratio of DMF: H_2O (4:1). The reaction mixture was placed on a shaker at RT for 18 h. The crude reaction was purified via SDS-PAGE and gel extraction. The product band was excised and eluted into endotoxin free water overnight at RT. The solution was concentrated and desalted using a 3k centrifugal filter unit (EMD Millipore) to provide the desired product which was quantified by fluorescence spectroscopy (recovered 0.13 mg, 14 nmol). ESI: Calculated MW: 9040 Observed $[M-H]^-$: 9039.

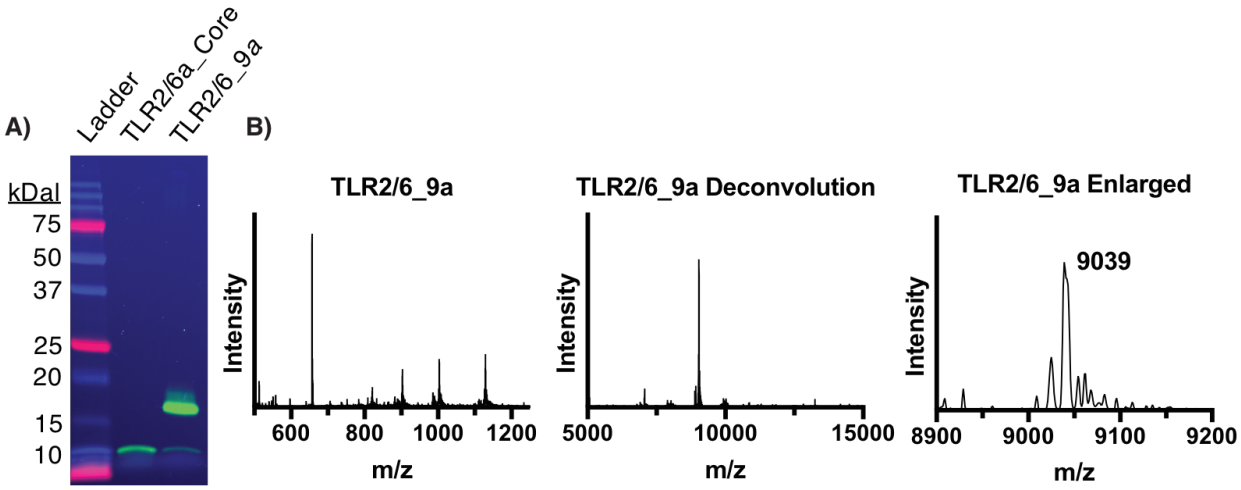

Figure 2.19 SDS-PAGE and Mass Spectrometry of TLR2/6_9*a*. A) Fluorescence gel image of TLR2/6*a*_Core and TLR2/6_9*a* compared to Precision Plus Protein Dual Xtra Prestained Protein Standards Ladder ran on a 12% Mini-PROTEAN TGX SDS-PAGE gel. B) ESI-MS data of TLR2/6_9*a*. Left, raw mass spectrum. Middle, deconvolution of raw data mass spectrum. Right, enlarged view of major peak in deconvolution data.

TLR9a-N_3 conjugation to TLR1/2a_Core *via* CuAAC (TLR1/2_9a).

Scheme 2.20 CuAAC reaction of TLR1/2*a*_Core and TL9*a* to afford TLR1/2_9*a*.

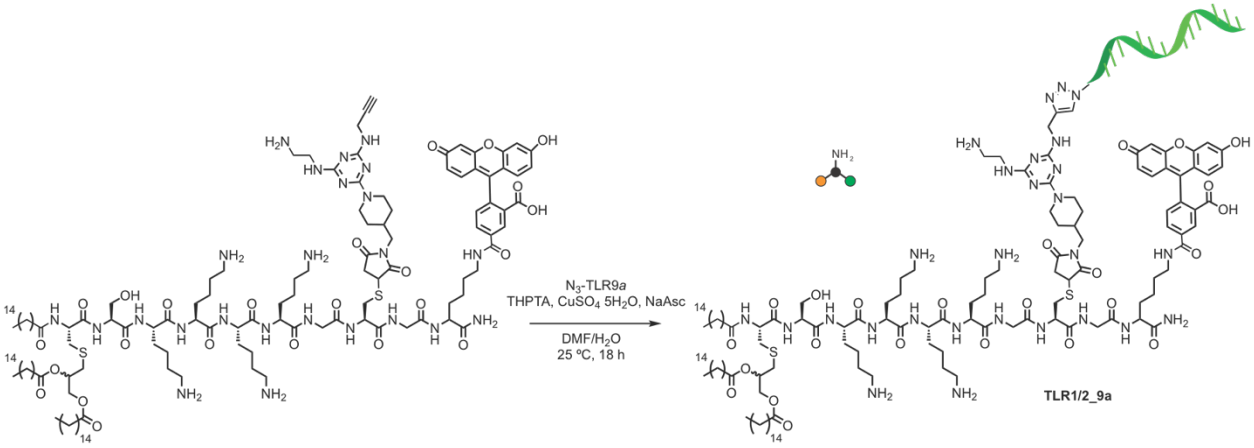

TLR1/2*a*_Core (0.39 mg, 150 nmol) in DMF (150 μL) and CpG-ODN1826-N_3 (0.33 mg, 50 nmol) in water (50 μL) were mixed with DMF (178 mL). Copper sulfate pentahydrate (0.25 mg, 1.0 □mol) pre-dissolved in degassed water (4.3 μL) and THPTA (0.65 mg, 1.5 μmol) in degassed water (16.7 μL) were mixed and then added to the reaction vial. Lastly, sodium ascorbate (0.59 μg, 3.0 μmol) was added to the reaction mixture to give a final ratio of DMF: H_2O (4:1). The reaction mixture was placed on a shaker at RT for 18 h. The crude reaction was purified via SDS-PAGE and gel extraction. The product band was excised and eluted into endotoxin free water overnight at RT. The solution was concentrated and desalted using a 3k centrifugal filter unit (EMD Millipore) to provide the desired product and quantified by fluorescence spectroscopy (recovered 0.32 mg, 34 nmol). ESI: Calculated MW: 9279, Observed $[M-H]^-$: 9279.

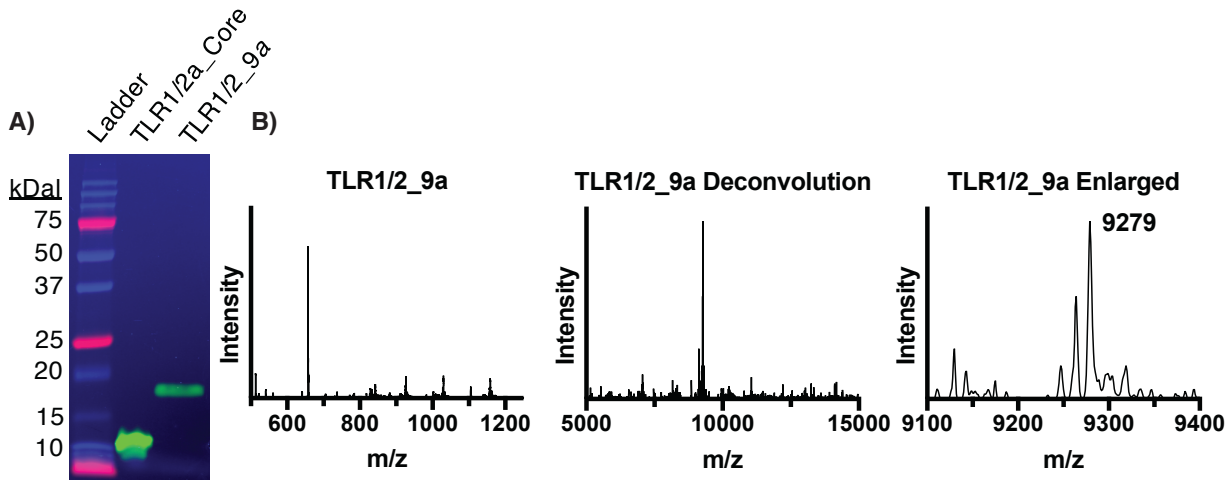

Figure 2.20 SDS-Page and Mass Spectrometry of TLR1/2_9*a*. A) Fluorescence gel image of TLR1/2*a*_Core and TLR1/2_9*a* compared to Precision Plus Protein Dual Xtra Prestained Protein Standards Ladder ran on a 12% Mini-PROTEAN TGX SDS-PAGE gel. B) ESI-MS data of TLR1/2_9*a*. Left, raw mass spectrum. Middle, deconvolution of raw data mass spectrum. Right, enlarged view of major peak in deconvolution data.

TLR7*a*-PEG$_{12}$-N$_3$ conjugation to TLR4a_Core *via* CuAAC (TLR4_7a).

Scheme 2.21 CuAAC reaction of TLR7*a*-PEG$_{12}$-N$_3$ and TLR4*a*_Core to afford TLR4_7*a*.

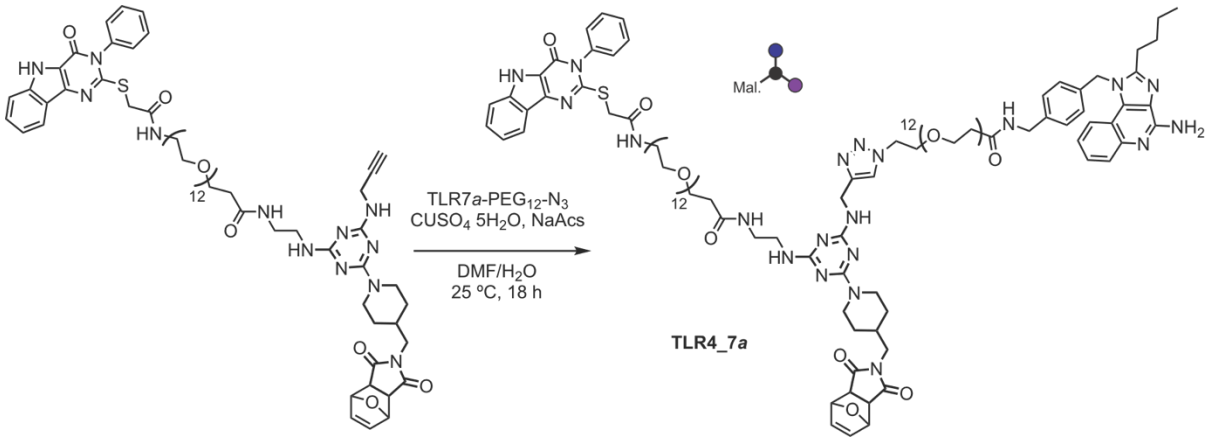

TLR4a_Core (1.8 mg, 1.5 μmol, 1 equiv.) and TLR7a-PEG$_{12}$-N$_3$ (5.9 mg, 6 μmol, 4 equiv.) were dissolved in DMF (400 μL) was added to the solution. $CuSO_4$•$5H_2O$ (3.7 mg, 15 μmol, 10 equiv.) and sodium ascorbate (5.9 mg, 30 μmol, 20 equiv.) were pre-dissolved in degassed water (37 μL

for each reagent) and then added to the reaction mixture. The reaction was placed on a shaker at room temperature for 24 h. The reaction mixture was centrifuged and supernatant was removed. The supernatant was diluted in acetonitrile (final concentration in 1:1 v/v DMF/acetonitrile) and purified by HPLC to obtain TLR4_7a. The product was quantified by UV absorbance and characterized by MALDI-TOF (171 μg recovered, 72 nmol). MALDI-TOF: m/z calc'd for $C_{116}H_{168}N_{20}O_{31}S$ $[M\text{-furan}+H]^+$: 2302.2; Observed $[M\text{-furan}+H]^+$: 2302.0.

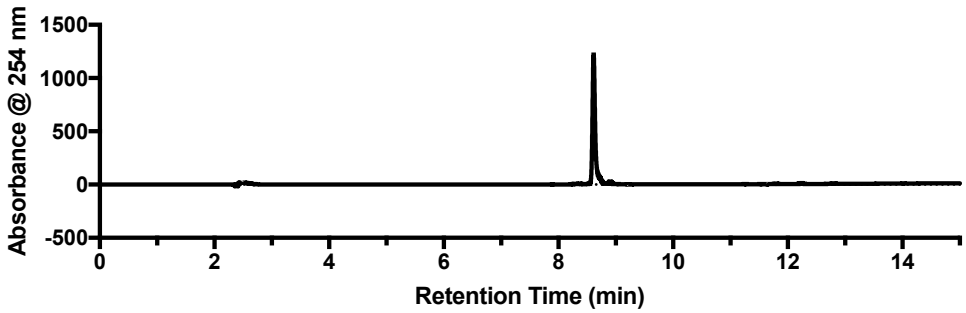

Figure 2.21 HPLC trace of TLR4_7*a*. Measured at 254 nm on a C8 analytical column. Solvent A: 0.1 % TFA in HPLC grade water, Solvent B: 0.1% TFA in HPLC grade acetonitrile. Gradient: t 0-1 min hold 50% B, t 1-11 min ramp to 90% B, t 11-15 min hold 90% B.

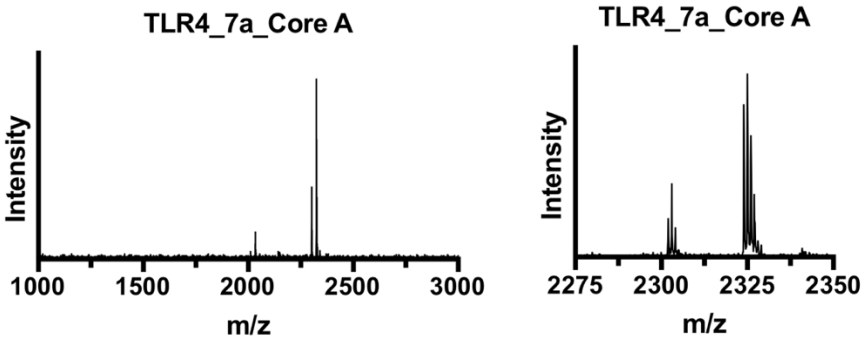

Figure 2.22 MALDI trace of TLR4_7*a*. Full (left) and enlarged view of the major peak (right). Sample acquired in positive reflector mode using dihydroxybenzoic acid matrix.

TLR7*a*-PEG$_{12}$-N$_3$ conjugation to TLR2/6_4*a* *via* CuAAC (TLR2/6_4_7*a*).

Scheme 2.22 CuAAC reaction of TLR7*a*-PEG$_{12}$-N$_3$ and TLR2/6_4*a* to afford TLR2/6_4_7*a*.

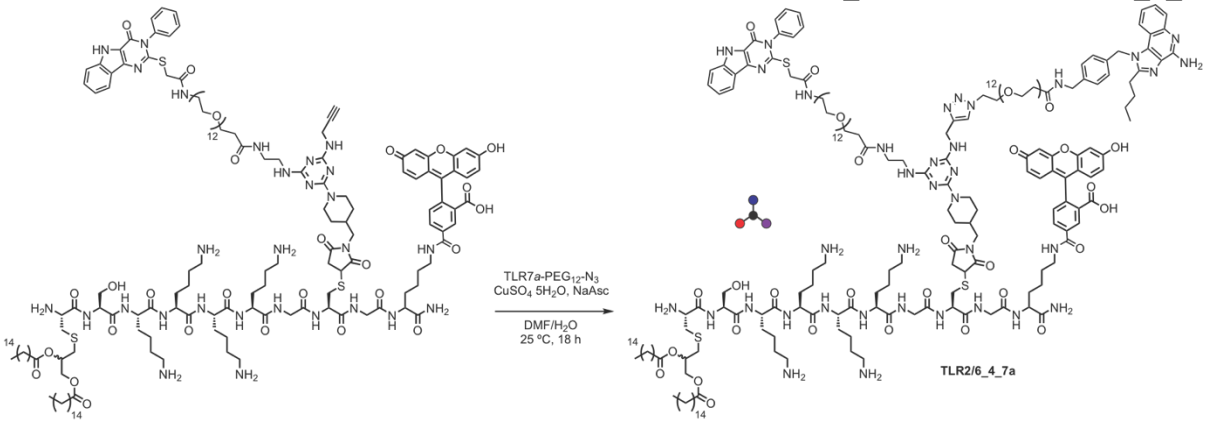

TLR2/6_4a (2.0 mg, 0.6 μmol, 1 equiv.) dissolved in DMF (290 μL) TLR7a-PEG$_{12}$-N$_3$ (4.8 mg, 4.9 μmol, 8 equiv.) in DMF (130 μL) was added to DMF (110 μL). $CuSO_4$•$5H_2O$ (3.8 mg, 15.2 μmol, 25 equiv.) and sodium ascorbate (4.8 mg, 24 μmol, 40 equiv.) were pre-dissolved in degassed water (50 μL for each reagent) and then added to the reaction mixture. The reaction was placed on a shaker at room temperature for 24 h. The reaction mixture was centrifuged and supernatant was removed to obtain a pellet. The pellet was washed with 0.1 M EDTA (2X 400 μL). The resulting pellet was dissolved in DMSO/acetonitrile (1:1 v/v) and purified by HPLC and lyophilized to obtain the TLR2/6_4_7*a*. The product was quantified by fluorescence spectroscopy and characterized by MALDI-TOF and HPLC (1.9 mg, 440 nmol recovered). MALDI-TOF: m/z calc'd for $C_{211}H_{325}N_{36}O_{51}S_3$ $[M+H]^+$: 4275.3; Observed $[M+H]^+$: 4275.9.

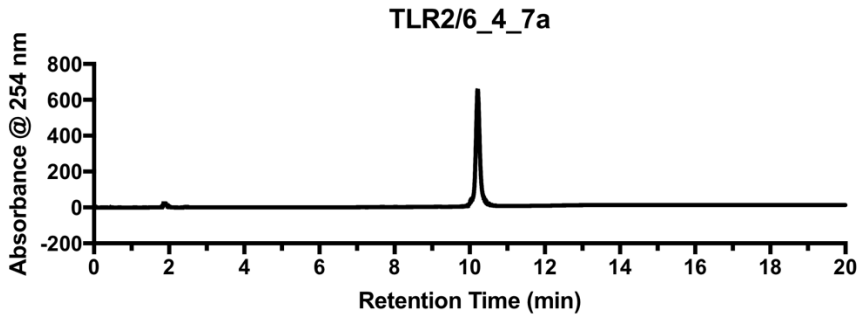

Figure 2.23 HPLC trace of TLR2/6_4_7*a*. Measured at 254 nm on a C8 analytical column. Solvent A: 0.1 % TFA in HPLC grade water, Solvent B: 0.1% TFA in HPLC grade acetonitrile. Gradient: t 0-1 min hold 10% B, t 1-11 min ramp to 90% B, t 11-20 min hold 90% B.

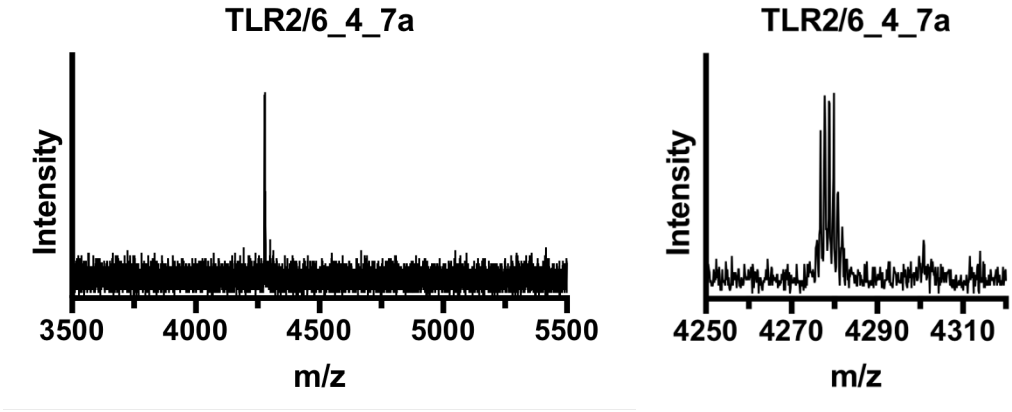

Figure 2.24 MALDI trace of TLR2/6_4_7*a*. Full (left) and enlarged view of the major peak (right). Sample acquired in positive reflector mode using dihydroxybenzoic acid matrix.

TLR7a-PEG$_{12}$-N$_3$ conjugation to TLR1/2_4*a* *via* CuAAC (TLR1/2_4_7*a*).

Scheme 2.23 CuAAC reaction of TLR7*a*-PEG$_{12}$-N$_3$ and TLR1/2_4*a* to afford TLR1/2_4_7*a*.

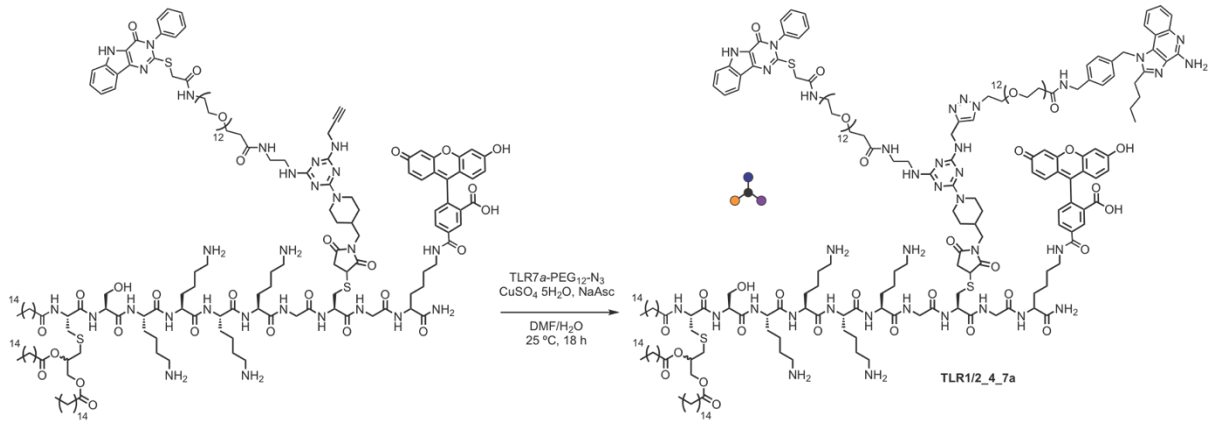

TLR1/2_4*a* (2.0 mg, 0.57 μmol, 1 equiv.) dissolved in DMF (343 μL). DMF (1.35 mL) and then TLR7*a*-PEG$_{12}$-N$_3$ (3.3 mg, 3.4 μmol, 6 equiv.) were added to the solution. $CuSO_4$•$5H_2O$ (2.8 mg, 11.3 μmol, 20 equiv.) and sodium ascorbate (3.4 mg, 17 μmol, 30 equiv.) were pre-dissolved in degassed water (230 μL) and then added to the reaction mixture. The reaction was placed on a shaker at room temperature for 24 h. The reaction mixture was centrifuged and supernatant was removed to obtain a pellet. The pellet was washed with 0.1 M EDTA (2X 400 μL). The resulting pellet was dissolved in DMSO/acetonitrile (1:1 v/v) and purified by HPLC and lyophilized to obtain TLR1/2_4_7*a*. The product was quantified by fluorescence spectroscopy and characterized by MALDI-TOF and HPLC (2.5 mg, 550 nmol recovered). MALDI-TOF: m/z calc'd for $C_{227}H_{354}N_{36}O_{52}S_3$ $[M+Na]^+$: 4535.5; Observed $[M+Na]^+$: 4536.2.

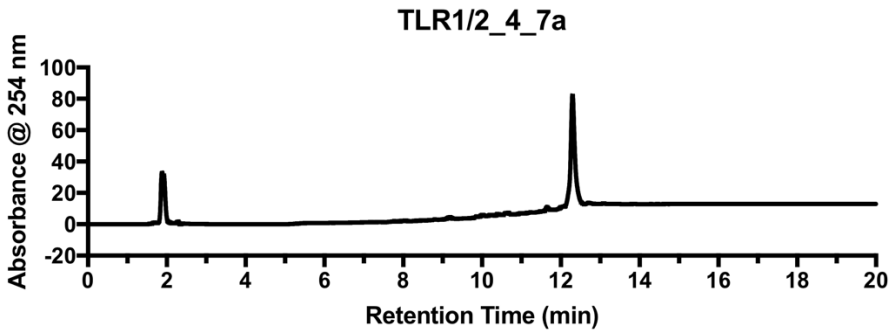

Figure 2.25 HPLC trace of TLR1/2_4_7*a*. Measured at 254 nm on a C8 analytical column. Solvent A: 0.1 % TFA in HPLC grade water, Solvent B: 0.1% TFA in HPLC grade acetonitrile. Gradient: t 0-1 min hold 50% B, t 1-11 min ramp to 90% B, t 11-20 min hold 90% B.

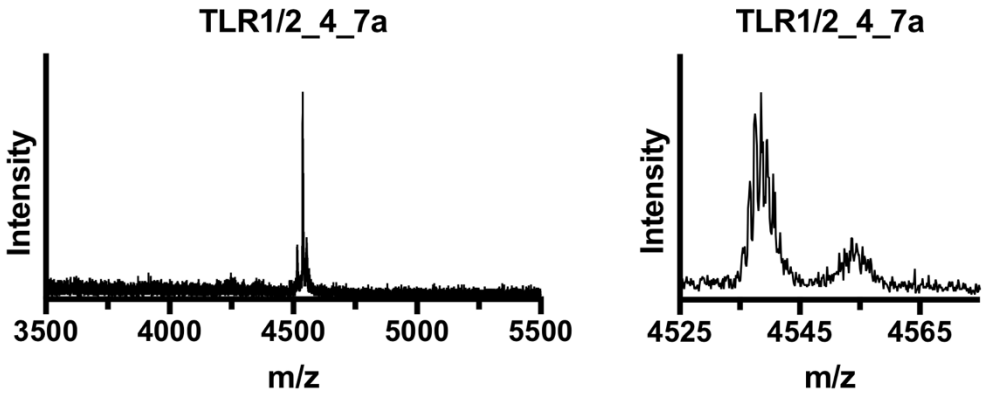

Figure 2.26 MALDI trace of TLR1/2_4_7*a* Full (left) and enlarged view of the major peak (right). Sample acquired in positive reflector mode using dihydroxybenzoic acid matrix.

TLR9a-N_3 conjugation to TLR1/2_4*a* *via* CuAAC (TLR1/2_4_*9a*)

Scheme 2.24 CuAAC reaction of N_3-TLR9*a* and TLR1/2_4*a* to afford TLR1/2_4_9*a*.

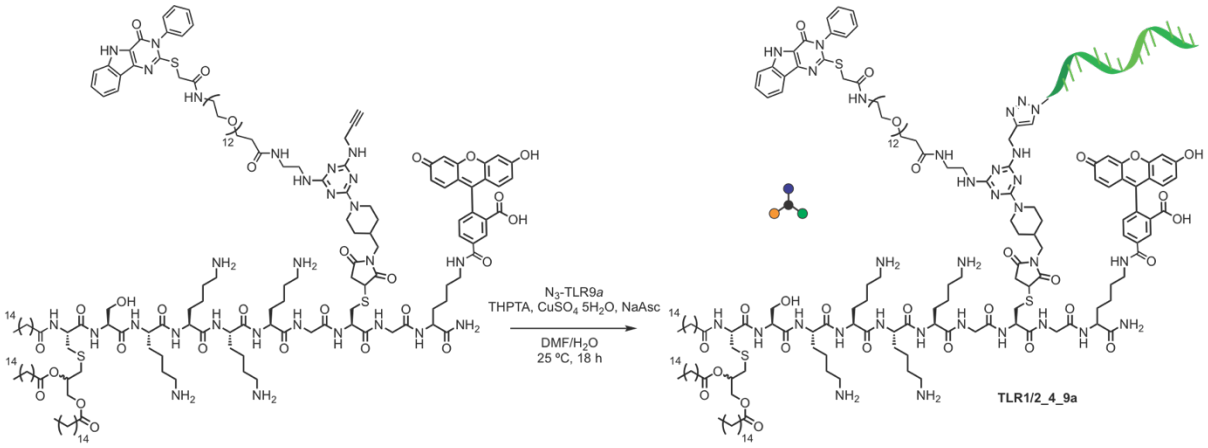

Copper sulfate pentahydrate (750 μg, 3 μmol) pre-dissolved in ultrapure water (10 μL) and THPTA (1.96 mg, 4.5 μmol) in ultrapure water (50 μL) were added to DMF (928 μL). TLR1/2_4*a* (1.6 mg, 450 nmol) in DMF (40 μL) and CpG-ODN1826-N_3 (1.0 mg, 150 nmol) in water (150 μL) were added to the reaction mixture. Lastly, sodium ascorbate (1.78 mg, 9 μmol) was added to the reaction mixture to give a final ratio of DMF: H_2O (4:1). The reaction mixture was placed on a shaker at RT for 24 h. The crude reaction was purified *via* SDS-PAGE and gel extraction. The product band was excised and eluted into endotoxin free water overnight at RT. The solution was concentrated and desalted using a 3k centrifugal filter unit (EMD Millipore) to provide the desired product which was quantified by fluorescence spectroscopy (Recovered 15.5 nmol, 158 μg). ESI: Calculated MW: 10212 Observed $[M-H]^-$: 10211

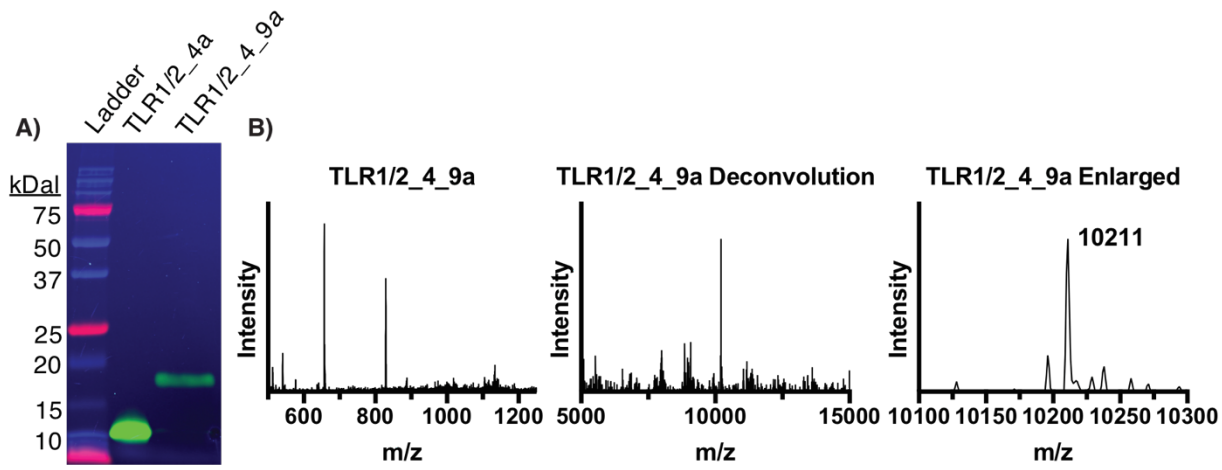

Figure 2.27 SDS-PAGE and Mass Spectrometry of TLR1/2_4_9*a*. A) Fluorescence gel image of TLR1/2*a*_Core and TLR1/2_4_9*a* compared to Precision Plus Protein Dual Xtra Prestained Protein Standards Ladder ran on a 12% Mini-PROTEAN TGX SDS-PAGE gel. B) ESI-MS data of TLR1/2_4_9*a*. Left, raw mass spectrum. Middle, deconvolution of raw data mass spectrum. Right, enlarged view of major peak in deconvolution data.

TLR9*a*-N_3 conjugation to TLR2/6_4a *via* CuAAC (TLR2/6_4_9*a*).

Scheme 2.25 CuAAC reaction of N_3-TLR9*a* and TLR2/6_4*a* to afford TLR2/6_4_9*a*.

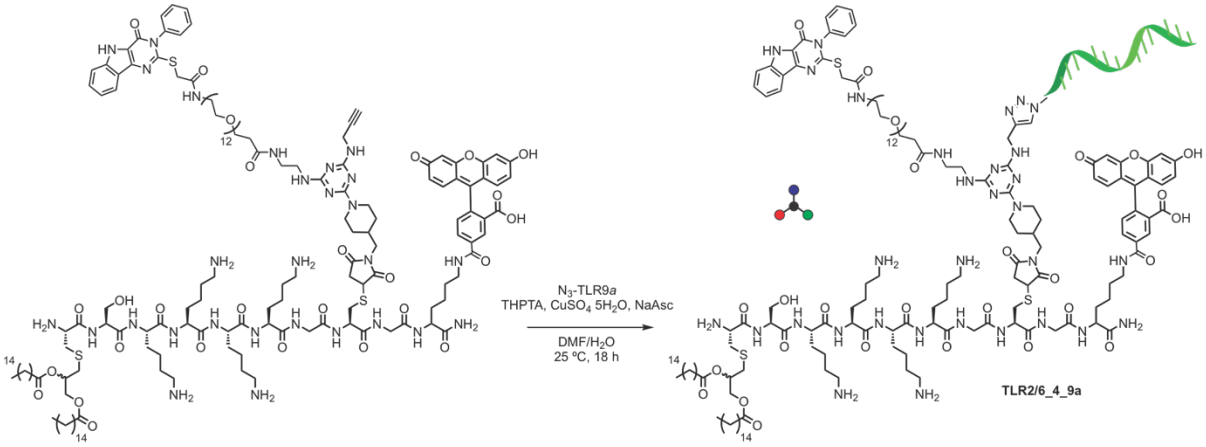

Copper sulfate pentahydrate (470 μg, 1.9 μmol) pre-dissolved in ultrapure water (104 μL) and THPTA (1.2 mg, 2.9 μmol) in ultrapure water (166 μL) were added to DMF (1.5 mL). TLR2/6_4*a* (0.95 mg, 292 nmol) in DMF (305 μL) and CpG-ODN1826-N_3 (0.65 mg, 97 nmol) in

water (97 μL) were added to the reaction mixture. Lastly, sodium ascorbate (1.1 mg, 5.8 μmol) in ultrapure water (79 μL) was added to the reaction mixture to give a final ratio of DMF: H_2O (4:1). The reaction mixture was placed on a shaker at RT for 24 h. The crude reaction was purified via SDS-PAGE and gel extraction. The product band was excised and eluted into endotoxin free water overnight at RT. The solution was concentrated and desalted using a 3k centrifugal filter unit (EMD Millipore) to provide the desired product which was quantified by fluorescence spectroscopy (Recovered 56.6 nmols, 563 μg). ESI: Calculated MW: 9973 Observed $[M-H]^-$: 9974

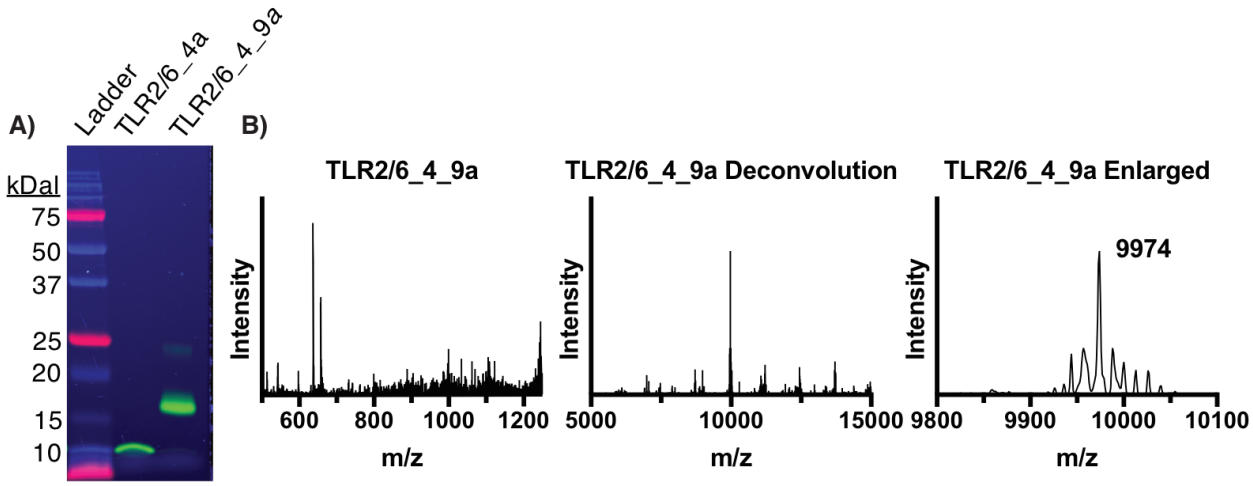

Figure 2.28 SDS-PAGE and Mass Spectrometry of TLR2/6_4_9*a*. A) Fluorescence gel image of TLR2/6_4*a* and TLR2/6_4_9*a* compared to Precision Plus Protein Dual Xtra Prestained Protein Standards Ladder ran on a 12% Mini-PROTEAN TGX SDS-PAGE gel. B) ESI-MS data of TLR2/6_4_9*a*. Left, raw mass spectrum. Middle, deconvolution of raw data mass spectrum. Right, enlarged view of major peak in deconvolution data

Tri-agonist Core B.

Scheme 2.26 Synthesis of Tri-Agonist Core B

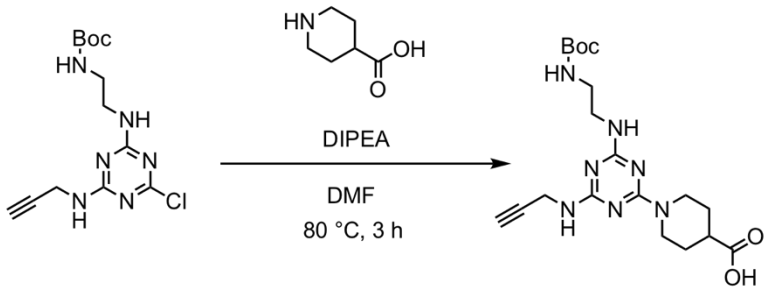

Core precursor[2] (0.20 g, 0.61 mmol) was dissolved in DMF (2.0 mL). DIPEA (0.12 mL) and isonipecotic acid (87 mg, 0.67 mmol) were subsequently added. The reaction was heated at 80 °C and stirred for 3 h. The reaction was then concentrated and purified by column chromatography (1% MeOH/EtOAc with 1% NH_4OH). The product was a white powder (170 mg, 67%). ^{1}H NMR (600 MHz, DMSO-d_6) δ 12.24 (br s, 1H), 7.04-6.44 (br m, 3 H), 4.50 (br s, 2H), 3.96 (s, 2H), 3.22 (br s, 2H), 3.04 (br s, 2H), 2.99 (s, 1H), 2.89 (br s, 2H), 2.48 (br s, 1H), 1.80 (br s, 2H), 1.40 (br s, 2H), 1.36 (s, 9H). ^{13}C NMR (600 MHz, DMSO-d_6) δ 175.84, 165.80, 165.79, 164.42, 159.60, 82.52, 77.55, 71.99, 41.95, 4th0.57, 40.00, 29.38, 28.24, 27.73. HRMS: m/z calc'd for $C_{19}H_{29}N_7O_4$ $[M+Na]^+$ 442.2179, observed 442.2162.

TLR7*a* conjugation to Fmoc-PEG$_{12}$-COOH (TLR7*a*-PEG$_{12}$-NH-Fmoc)

Scheme 2.27 TLR7*a* coupling to Fmoc-PEG$_{12}$-NHS to afford Fmoc-PEG$_{12}$-TLR7*a*.

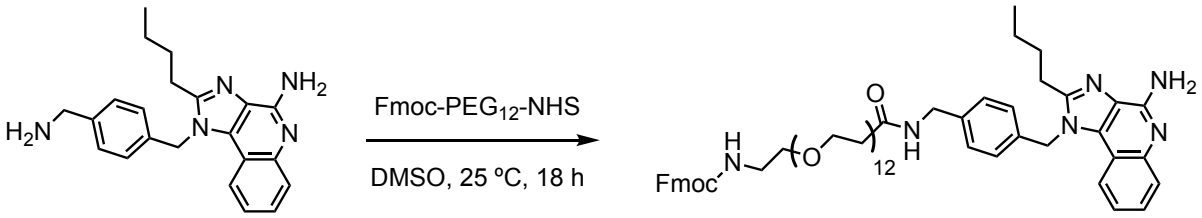

TLR7*a* (75 mg, 0.21 mmol) and NHS-PEG_{12}-NH-Fmoc (0.20 g, 0.21 mmol) were dissolved in DMSO (2.1 mL). The reaction was allowed to stir at RT overnight (18 h). The crude solution was purified by reverse phase HPLC using a C8 preparatory column, where the solvent system was A: water + 0.1% TFA, B: acetonitrile + 0.1% TFA (10-90% acetonitrile/water + 0.1% TFA gradient, 0-19 minutes). The HPLC fractions were lyophilized to afford the desired product as a clear gel (230 mg, 94% yield). ^{1}H NMR (600 MHz, $CDCl_3$) δ 10.1 (br s, 1H), 7.90 (d, *J* = 9.6 Hz, 1H), 7.75 (d, *J* = 9 Hz, 2H), 7.70 (d, *J* = 10.2 Hz, 1H), 7.59 (d, *J* = 8.4 Hz, 2H), 7.56-7.51 (br m, 3H), 7.39 (t, *J* = 9 Hz, 2H), 7.30 (t, *J* = 8.4 Hz, 2H), 7.28 (d, *J* = 9.6 Hz, 3H), 6.97 (d, *J* = 9.6 Hz, 2H), 5.73 (s, 2H), 5.52 (br s, 1H), 4.43 (d, *J* = 7.2 Hz, 2H), 4.39 (d, *J* = 8.4 Hz, 2H), 4.22 (t, *J* = 8.1 Hz, 1H), 3.73 (t, *J* = 6.6 Hz, 2H), 3.63-3.55 (br m, 38H), 3.53-3.51 (br m, 4H), 3.48 (br d, *J* = 4.8 Hz, 4H), 3.39 (br s, 2H), 2.90 (t, *J* = 9.3 Hz, 2H), 2.56 (t, *J* = 6.9 Hz, 2H), 1.80 (quintet, *J* = 9.6 Hz, 2H), 1.44 (sextet, *J* = 9 Hz, 2H), 0.934 (t, *J* = 8.7 Hz, 3H). ^{13}C NMR (600 MHz, $CDCl_3$) δ 173.6, 157.2, 149.4, 144.1, 141.4, 139.2, 135.8, 134.6, 132.7, 130.1, 128.8, 127.8, 127.2, 125.6, 125.2, 120.8, 120.1, 119.9, 112.5, 70.6, 70.5, 70.4, 70.2, 67.0, 66.8, 49.2, 47.4, 43.0, 41.0, 36.4, 29.6, 26.9, 22.5, 13.8. MALDI-TOF: m/z calc'd for $C_{64}H_{88}N_6O_{15}$ [M+H]+ 1181.6, observed 1181.4.

TLR7*a*-PEG$_{12}$_NH$_2$ conjugation to Tri-agonist Core B *via* amide bond formation. (TLR7*a*-Core B)

Scheme 2.28 TLR7*a*-PEG$_{12}$-NH-Fmoc coupling to Core B to afford TLR7*a*-Core B.

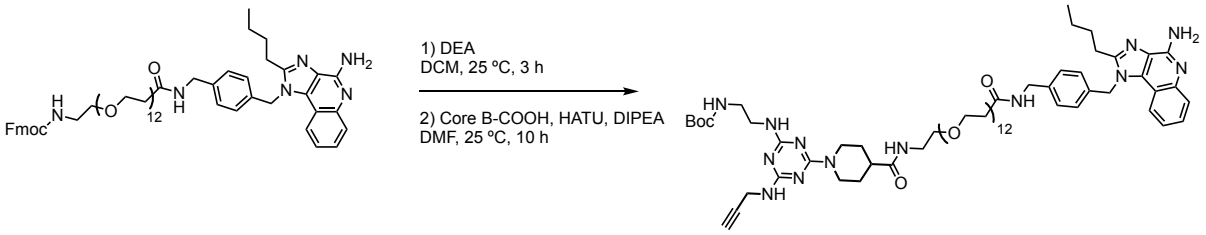

TLR7*a*-PEG$_{12}$-NH.Fmoc (230 mg, 0.19 mmol) was dissolved in anhydrous methylene chloride (1.8 mL). Diethylamine (10% v/v, 0.19 mL) was then added to the solution. The reaction was allowed to stir at RT for 10 h. The reaction mixture was concentrated and re-dissolved in minimal methylene chloride, which was then precipitated in diethyl ether (2x). The product was spun down, removed of diethyl ether, and dried on high-vacuum. The resulting free amine was used in the following procedure to synthesize TLR7*a*-CoreB. MALDI-TOF: m/z calc'd for $C_{49}H_{78}N_6O_{13}$ $[M+H]^+$ 959.6, observed 959.3.

Carboxylic acid core (88 mg, 0.21 mmol) was suspended in DMF (1.8 mL). DIPEA (66 μL, 0.38 mmol) and subsequently HATU (0.080 g, 0.21 mmol) were added to the carboxylic acid. The cloudy solution was allowed to stir for 15 min until cleared. In another round bottom flask, the free amine substrate (180 mg, 0.19 mmol) was dissolved in DMF (2.1 mL). The activated carboxylic acid was slowly added to the reaction mixture (over 1 h). The reaction was allowed to stir at RT for 3 h. The reaction mixture was concentrated, re-dissolved in DMSO, and purified by reverse phase HPLC using a C8 preparatory column, where the solvent system was A: water + 0.1% TFA, B: acetonitrile + 0.1% TFA (10-90% acetonitrile/water + 0.1% TFA gradient, 0-19

minutes). The HPLC fractions were lyophilized to afford the desired product as a clear gel (150 mg, 57% yield). ^{1}H NMR (500 MHz, $CDCl_3$) δ 10.6 (br s, 1H), 7.87 (br s, 1H), 7.82 (d, *J* = 8.5 Hz, 1H), 7.77 (br t, *J* = 4.8 Hz, 1H), 7.67 (d, *J* = 8.5 Hz, 1H), 7.46 (t, *J* = 7.8 Hz, 1H), 7.29-7.23 (m, 3H), 6.94 (d, *J* = 8, 2H), 6.88 (br s, 1H), 6.51 (br s, 1H), 5.71 (s, 2H), 5.19 (br s, 1H), 4.73 (br t, *J* = 12.5 Hz, 2H), 4.39 (d, *J* = 6 Hz, 2H), 4.11 (br s, 2H), 3.70 (t, *J* = 5.8 Hz, 2H), 3.63-3.57 (m, 32H), 3.54-3.50 (m, 10H), 3.47 (br d, *J* = 2.5, 6H), 3.42 (br q, *J* = 5 Hz, 2H), 3.32-3.29 (br m, 2H), 3.19 (d, *J* = 8.5 Hz, 1H), 3.04-2.98 (m, 2H), 2.86 (t, *J* = 7.8 Hz, 2H), 2.50 (t, *J* = 5.5 Hz, 2H), 2.43 (br t, *J* = 11 Hz, 1H), 2.22 (s, 1H), 1.89 (br d, *J* = 13 Hz, 2H), 1.78 (quintet, *J* = 8 Hz, 2H), 1.70 (br q, *J* = 11.5 Hz, 2H), 1.43-1.39 (m, 2H), 1.39 (s, 9H), 0.91 (t, *J* = 7 Hz, 3H). ^{13}C NMR (500 MHz, $CDCl_3$) δ 174.3, 172.4, 162.6, 161.4, 157.0, 156.0, 155.5, 149.7, 139.4, 135.6, 134.6, 132.7, 129.6, 128.6, 125.5, 125.2, 124.7, 120.7, 119.6, 117.3, 115.0, 112.5, 79.6, 78.5, 77.4, 71.9, 70.3, 70.2, 70.1, 69.8, 67.1, 49.0, 43.8, 42.7, 41.2, 39.7, 39.3, 36.6, 30.3, 29.4, 28.4, 27.0, 22.4, 13.8. MALDI-TOF: m/z calc'd for $C_{68}H_{105}N_{13}O_{16}$ $[M+H]^+$ 1360.8, observed 1360.7.

TLR7*a*_Core B conjugation to HOOC-PEG$_{12}$-NH-Fmoc *via* amide bond formation.

Scheme 2.29 TLR7*a*-Core B coupling to Fmoc-PEG$_{12}$-COOH to afford TLR4_7*a*.

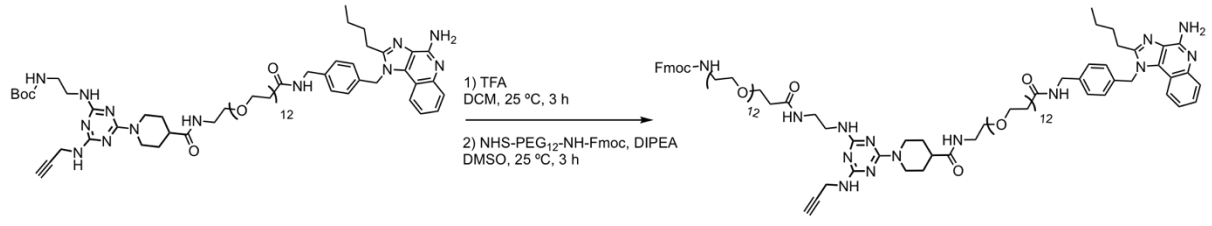

TLR7*a*_Core B (0.080 g, 59 μmol) was dissolved in TFA/methylene chloride (1:1 v/v) (0.60 mL). The reaction was allowed to stir at RT for 3 h. The solution was concentrated and re-

dissolved in minimal methylene chloride, which was then precipitated in diethyl ether (2X). The product was spun down, removed of diethyl ether, and dried on high-vacuum.

The free amine substrate (74 mg, 59 μmol) and NHS-PEG_{12}-NH-Fmoc (58 mg, 62 μmol) were dissolved in DMSO (0.60 mL). DIPEA (21 μL, 120 μmol) was then added to the reaction mixture, which was allowed to stir at RT for 16 h. The reaction mixture was purified by reverse phase HPLC using a C8 preparatory column, where the solvent system is A: water + 0.1% TFA, B: acetonitrile + 0.1% TFA (40-60% acetonitrile/water + 0.1% TFA gradient, 0-15 minutes). The HPLC fractions were lyophilized to afford the desired product as a light brown gel (51 mg, 41% yield). ^{1}H NMR (500 MHz, $CDCl_3$) δ 10.63 (br s, 1H), 8.16 (br s, 1H), 7.87 (d, *J* = 7.8 Hz, 2H), 7.73 (d, *J* = 7.8 Hz, 2H), 7.68 (d, *J* = 8.4 Hz, 1H), 7.58 (d, *J* = 7.2 Hz, 2H), 7.49 (t, *J* = 7.5 Hz, 1H), 7.37 (t, *J* = 7.2 Hz, 2H), 7.30-7.24 (m, 6H), 6.94 (d, *J* = 7.8 Hz, 2H), 6.85 (br s, 1H), 6.57 (br s, 1H), 5.70 (s, 2H), 5.52 (br s, 1H), 4.74 (br t, *J* = 12.6 Hz, 2H), 4.39 (d, *J* = 6 Hz, 2H), 4.37 (d, *J* = 6.6 Hz, 2H), 4.19 (t, *J* = 6.9 Hz, 1H), 4.12 (br d, *J* = 3 Hz, 2H), 3.71 (t, *J* = 5.7 Hz, 2H), 3.69-3.66 (m, 1H), 3.63-3.59 (m, 72H), 3.57-3.51 (m, 18H), 3.48 (br d, *J* = 3 Hz, 6H), 3.43-3.41 (br m, 4H), 3.38-3.36 (br m, 2H), 3.00 (br q, *J* = 10.8 Hz, 2H), 2.86 (t, *J* = 7.8 Hz, 2H), 2.50 (t, *J* = 5.7 Hz, 2H), 2.46 (br t, *J* = 5.1 Hz, 2H), 2.44 (br s, 1H), 2.22 (t, *J* = 2.4 Hz, 1H), 1.89 (br d, *J* = 12 Hz, 2H), 1.79 (quintet, *J* = 7.8 Hz, 2H), 1.70 (br t, *J* = 10.5 Hz, 2H), 1.42 (sextet, *J* = 7.2 Hz, 2H), 0.92 (t, *J* = 7.5 Hz, 3H). ^{13}C NMR (600 MHz, $CDCl_3$) δ 174.4, 172.9, 172.2, 162.3, 162.0, 161.4, 156.9, 156.7, 155.9, 155.6, 149.8, 144.1, 141.5, 139.5, 135.6, 134.7, 132.7, 129.7, 128.6, 127.7, 127.1, 125.5, 125.1, 124.9, 120.7, 120.0, 119.8, 117.2, 115.2, 112.6, 78.7, 71.8, 70.5, 70.4, 70.3, 70.2, 70.1, 69.9, 67.2, 67.0, 66.6, 49.0, 47.3, 43.8, 42.7, 41.0, 40.4, 39.3, 38.5, 36.7, 36.5, 30.3, 29.4, 28.6, 27.0, 22.4, 13.8. MALDI-TOF: m/z calc'd for $C_{105}H_{160}N_{14}O_{29}$ $[M+H]^+$ 2082.2, observed 2082.2.

TLR4*a*-COOH conjugation to TLR7a-Core B-NH Fmoc *via* amide bond formation. (TLR4_7*a*-Core B).

Scheme 2.30 TLR7*a*-Core B-NH-Fmoc coupling to TLR4-COOH to afford TLR4_7*a*.

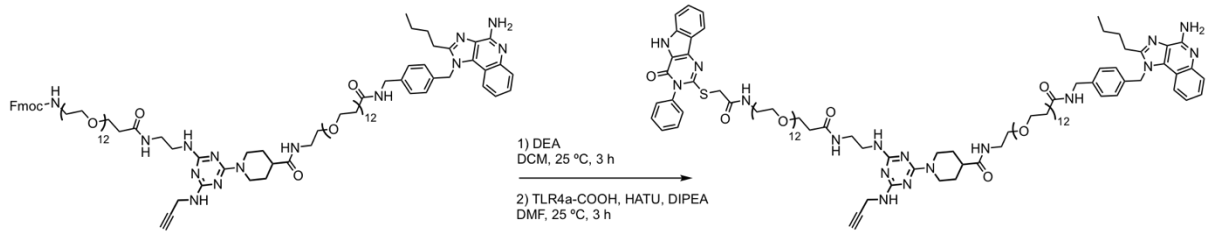

TLR7*a*-Core B-NH-Fmoc (0.050 g, 24 μmol) was dissolved in anhydrous methylene chloride (0.90 mL). Diethylamine (10% v/v, 0.10 mL) was then added to the solution. The reaction was allowed to stir at RT for 3 h. The reaction mixture was concentrated and re-dissolved in minimal methylene chloride, which was then precipitated in diethyl ether (2X). The product was spun down, removed of diethyl ether, and dried on high-vacuum.

TLR4a-COOH (2.4 mg, 6.9 μmol) was dissolved in DMF (0.25 mL). DIPEA (3.3 μL, 19 μmol) and HATU (2.6 mg, 6.9 μmol) were then added to the solution in this order to give a blue colored solution. The free amine substrate (12 mg, 6.3 μmol) was dissolved in DMF in a separate vial. The preactivated indole carboxylic acid solution was slowly added to the solution of free amine and the reaction was allowed to stir at RT for 22 h. The reaction mixture was concentrated, re-dissolved in DMSO, and purified by reverse phase HPLC using a C8 preparatory column, where the solvent system was A: water + 0.1% TFA, B: acetonitrile + 0.1% TFA (10-90%

acetonitrile/water + 0.1% TFA gradient, 0-19 minutes, $t_{retention}$: 12.25 min). The HPLC fractions were lyophilized to afford the desired product as a clear gel (3.7 mg, 27% yield). ^{1}H NMR (600 MHz, $CDCl_3$) δ 10.16 (br s, 1H), 8.22 (br s, 1H), 8.11 (d, *J* = 9.6 Hz, 1H), 7.96 (d, *J* = 10.2 Hz, 2H), 7.72 (d, *J* = 11.4 Hz, 1H), 7.58-7.44 (m, 7H), 7.38-7.36 (m, 2H), 7.29 (br d, *J* = 9.6 Hz, 3H), 6.97 (d, *J* = 9 Hz, 2H), 6.78 (br s, 1H), 5.73 (s, 2H), 4.74 (br m, 2H), 4.42 (d, *J* = 6.6 Hz, 2H), 4.09 (br s, 2H), 3.90 (s, 2H), 3.73 (t, *J* =6.6 Hz, 2H), 3.69-3.53 (m, 84H), 3.49-3.45 (m, 16H), 3.40-3.38 (m, 2H), 3.32-3.30 (br m, 2H), 3.21-3.19 (br m, 2H), 2.99 (br s, 2H), 2.87 (t, *J* = 9.3 Hz, 3H), 2.53 (t, *J* = 6.9 Hz, 2H), 2.49 (br s, 3H), 2.23 (br s, 1H), 1.91 (br d, *J* = 13.2 Hz, 2H), 1.82 (quintet, *J* = 9 Hz, 2H), 1.74-1.69 (br s, 2H), 1.44 (sextet, *J* = 9 Hz, 2H), 0.94 (t, *J* = 8.7 Hz, 3H). Analysis for purity checked by analytical HPLC C8, A: water + 0.1% TFA, B: acetonitrile + 0.1% TFA (10-90% acetonitrile/water + 0.1% TFA gradient, 0-11 minutes, $t_{retention}$: 8.46 min). MALDI-TOF: m/z calc'd for $C_{108}H_{161}N_{17}O_{29}S$ $[M+H]^+$ 2193.2, observed 2194.0.

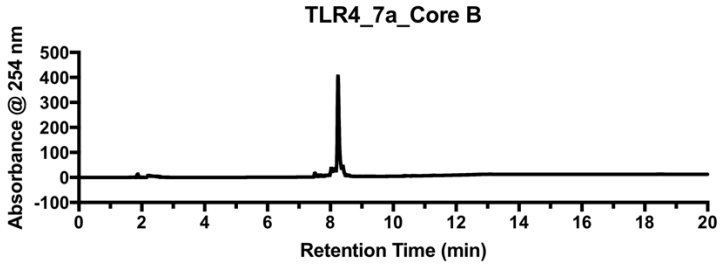

Figure 2.29 HPLC trace of TLR4_7*a* (Core B). Measured at 254 nm on a C8 analytical column. Solvent A: 0.1 % TFA in HPLC grade water, Solvent B: 0.1% TFA in HPLC grade acetonitrile. Gradient: t 0-1 min hold 10% B, t 1-11 min ramp to 90% B, t 11-20 min hold 90% B.

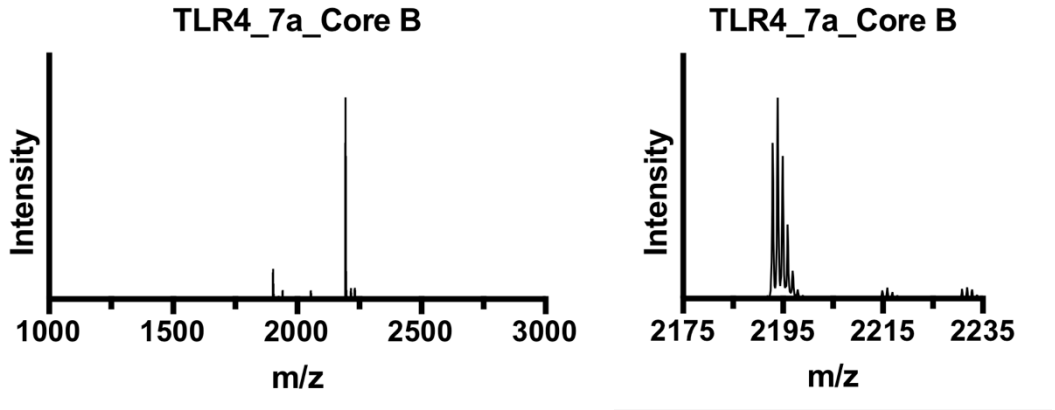

Figure 2.30 MALDI trace of TLR4_7*a*_Core B. Full (left) and enlarged view of the major peak (right). Sample acquired in positive reflector mode using dihydroxybenzoic acid matrix.

TLR9*a*-N_3 conjugation to TLR7*a*_Core *via* CuAAC (TLR4_9*a*).

Scheme 2.31 CuAAC reaction of N_3-TLR9*a* and TLR4*a*_Core B to afford TLR4_9*a*.

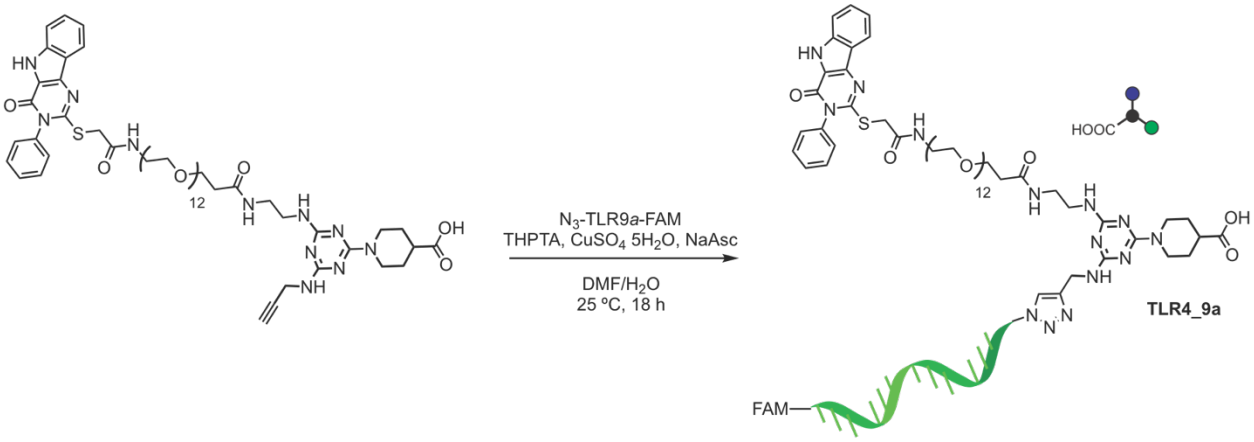

TLR7*a*_Core B (72 μg, 58 nmol) in anhydrous DMF (80 μL) and CpG (70 μg, 10 nmol) in degassed water (9.6 μL) were mixed in a vial. Copper sulfate pentahydrate (48 μg, 190 nmol) pre-dissolved in degassed water (3.4 μL) and THPTA (130 μg, 290 nmol) in degassed water (4.2 μL) were mixed and then added to the reaction vial. Lastly, sodium ascorbate (57 μg, 290 nmol) in

degassed water (2.4 μL) was added to the reaction mixture to give a final volume (DMF: H_2O 4:1). The reaction mixture was placed on a shaker at RT for 18 h. The crude reaction was purified via TBE-urea gel electrophoresis and gel extraction. The product band was excised and eluted into endotoxin free water overnight at RT. The solution was concentrated and desalted using a 3k centrifugal filter unit (EMD Millipore) to provide the desired product and quantified by fluorescence spectroscopy (Recovered 48 μg, 5.6 nmol). ESI: Calculated MW: 8521, Observed $[M-H]^-$: 8521

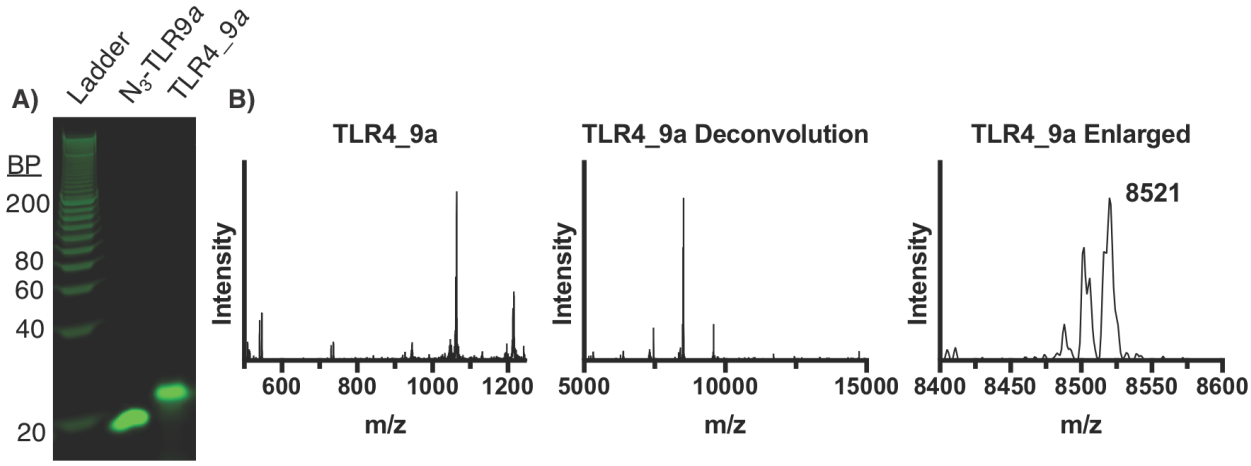

Figure 2.31 TBE-Urea-PAGE and Mass Spectrometry of TLR4_9*a*. A) Fluorescence gel image of N_3-TLR9*a*-FAM and TLR4_9*a* compared to 20 bp molecular weight ladder ran on a 10% Mini-PROTEAN TBE-UREA gel and stained with SYBR Safe DNA gel stain. B) ESI-MS data of TLR4_9*a*. Left, raw mass spectrum. Middle, deconvolution of raw data mass spectrum. Right, enlarged view of major peak in deconvolution data.

TLR9*a*-N_3 conjugation to TLR7*a*_Core *via* CuAAC (TLR7_9*a*).

Scheme 2.32 CuAAC reaction of N_3-TLR9*a* and TLR7*a*_Core B to afford TLR7_9*a*.

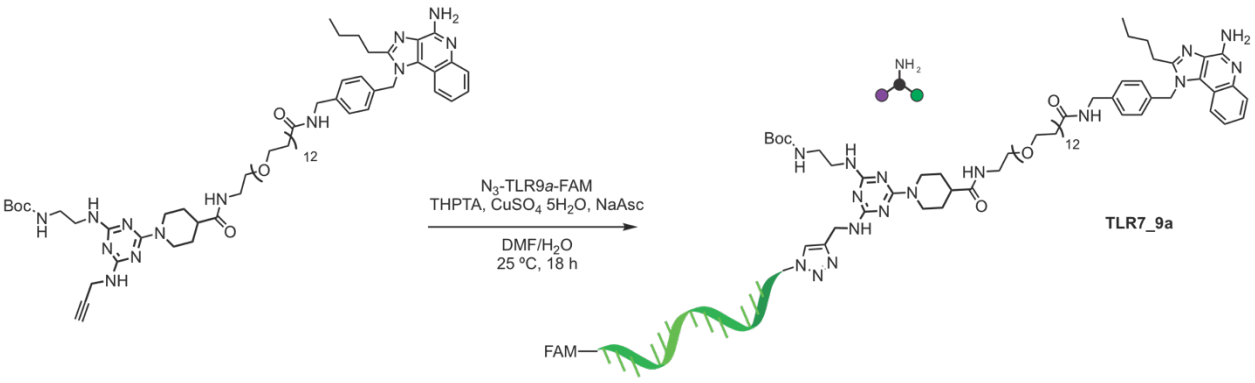

TLR7*a*_Core B (52 μg, 39 nmol) in anhydrous DMF (69 μL) and CpG (70 μg, 9.6 nmol) in degassed water (9.6 μL) were mixed in a vial. Copper sulfate pentahydrate (48 μg, 190 nmol) pre-dissolved in degassed water (3.4 μL) and THPTA (0.13 mg, 290 nmol) in degassed water (4.2 μL) were mixed and then added to the reaction vial. Lastly, sodium ascorbate (57 μg, 290 nmol) in degassed water (2.4 μL) was added to the reaction mixture to give a final volume (DMF: H_2O 4:1). The reaction mixture was placed on a shaker at RT for 18 h. The crude reaction was purified via TBE-urea gel electrophoresis and gel extraction. The product band was excised and eluted into endotoxin free water overnight at RT. The solution was concentrated and desalted using a 3k centrifugal filter unit (EMD Millipore) to provide the desired product and quantified by fluorescence spectroscopy (recovered 19 μg, 2.2 nmol). ESI: Calculated MW: 8629, Observed [M-H]$^-$: 8628

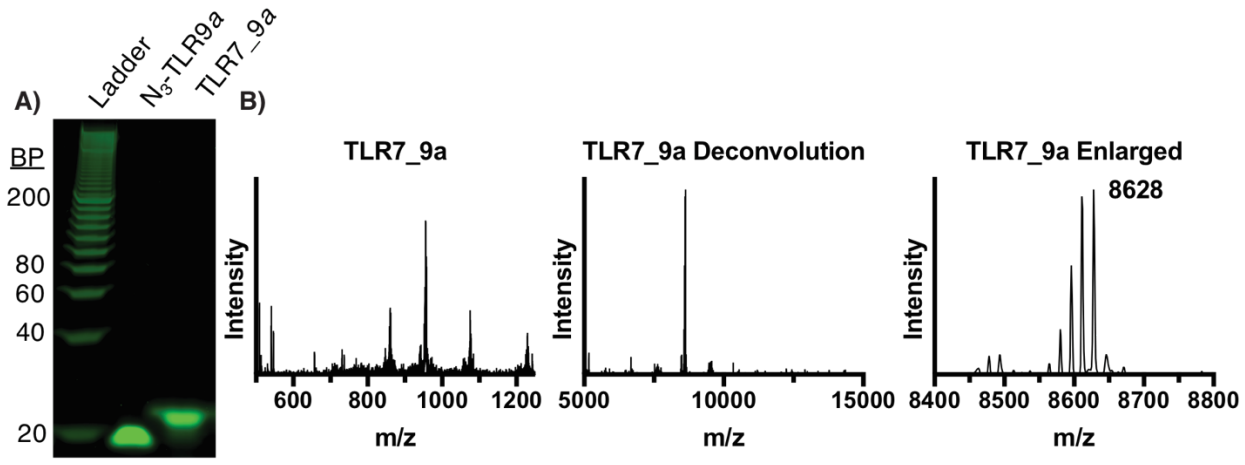

Figure 2.32 TBE Urea-Page and Mass Spectrometry of TLR7_9*a*. A) Fluorescence gel image of N_3-TLR9*a*-FAM and TLR7_9*a* compared to 20 bp molecular weight ladder ran on a 10% Mini-PROTEAN TBE-UREA gel and stained with SYBR Safe DNA gel stain. B) ESI-MS data of TLR7_9*a*. Left, raw mass spectrum. Middle, deconvolution of raw data mass spectrum. Right, enlarged view of major peak in deconvolution data.

TLR9*a*-N_3 conjugation to TLR4_7*a* *via* CuAAC (TLR4_7_9*a*)

Scheme 2.33 CuAAC reaction of N_3-TLR9*a*-FAM and TLR4_7*a* to afford TLR4_7_9*a*.

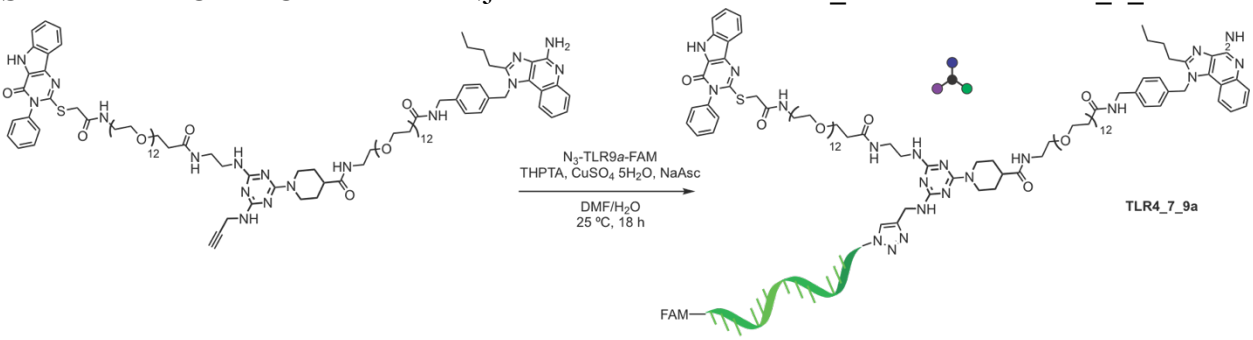

TLR4_7*a*_Core B (0.14 mg, 66 nmol) in anhydrous DMF (73 μL) and CpG (0.080 mg, 11 nmol) in degassed water (11 μL) were mixed in a vial. Copper sulfate pentahydrate (55 μg, 220 nmol) pre-dissolved in degassed water (4.0 μL) and THPTA (0.14 mg, 330 nmol) in degassed water (4.8 μL) were mixed and then added to the reaction vial. Lastly, sodium ascorbate (65 μg,

330 nmol) in degassed water (2.7 μL) was added to the reaction mixture to give a final volume (DMF: H_2O 4:1). The reaction mixture was placed on a shaker at RT for 18 h. The crude reaction was purified via TBE-urea gel electrophoresis and gel extraction. The product band was excised and eluted into endotoxin free water overnight at RT. The solution was concentrated and desalted using a 3k centrifugal filter unit (EMD Millipore) to provide the desired product and quantified by fluorescence spectroscopy (recovered 19 μg, 2.2 nmol). ESI: Calculated MW: 9462, Observed [M-H]$^-$: 9462.

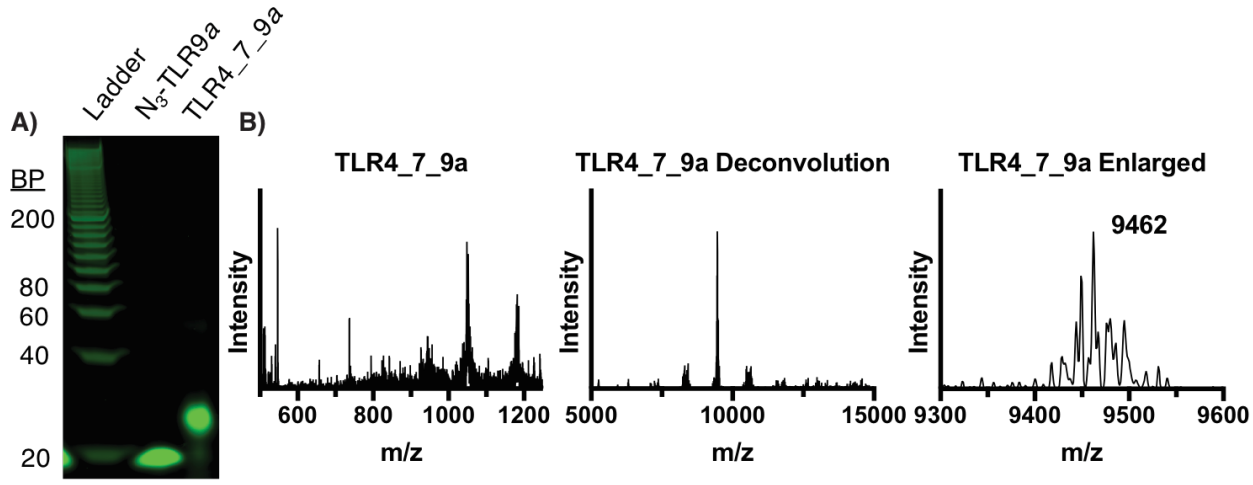

Figure 2.33 TBE-Urea PAGE and Mass Spectrometry of TLR4_7_9*a*. A) Fluorescence gel image of N_3-TLR9*a*-FAM and TLR4_7_9*a* compared to 20 bp molecular weight ladder ran on a 10% TBE-UREA Mini-PROTEAN gel and stained with SYBR Safe DNA gel stain. B) ESI-MS data of TLR4_7_9*a*. Left, raw mass spectrum. Middle, deconvolution of raw data mass spectrum. Right, enlarged view of major peak in deconvolution data.

Table 2.1 Percentage of free agonist in purified product of Tri-agonists.

Tri-agonist	% Free Agonist
TLR1/2_4_7*a*	Non detected[a]
TLR2/6_4_7*a*	Non detected[a]
TLR1/2_4_9*a*	3.3 %[b]
TLR2/6_4_9*a*	4.1 %[b]
TLR4_7_9*a*	6.4 %[b]

[a] Determined by HPLC
[b] Determined by gel analysis

2.8 References

(1) Beutler, B. A. TLRs and innate immunity. *Blood* **2009**, *113* (7), 1399–1407.
(2) Tom, J. K.; Dotsey, E. Y.; Wong, H. Y.; Stutts, L.; Moore, T.; Davies, D. H.; Felgner, P. L.; Esser-Kahn, A. P. Modulation of innate immune responses via covalently linked TLR agonists. *ACS Cent. Sci.* **2015**, *1* (8), 439–448.
(3) Chan, M.; Hayashi, T.; Mathewson, R. D.; Nour, A.; Hayashi, Y.; Yao, S.; Tawatao, R. I.; Crain, B.; Tsigelny, I. F.; Kouznetsova, V. L. Identification of substituted pyrimido [5, 4-b] indoles as selective toll-like receptor 4 ligands. *J. Med. Chem.* **2013**, *56* (11), 4206–4223.
(4) Shukla, N. M.; Malladi, S. S.; Mutz, C. A.; Balakrishna, R.; David, S. A. Structure– activity relationships in human toll-like receptor 7-active imidazoquinoline analogues. *J. Med. Chem.* **2010**, *53* (11), 4450–4465.
(5) Shukla, N. M.; Malladi, S. S.; Mutz, C. A.; Balakrishna, R.; David, A. Structure-activity relationships in human toll-like receptor 7- active imidazoquinoline analogues. *J. Med. Chem* **2011**, *53* (11), 4450–4465.
(6) Lynn, G. M.; Laga, R.; Darrah, P. A.; Ishizuka, A. S.; Balaci, A. J.; Dulcey, A. E.; Pechar, M.; Pola, R.; Gerner, M. Y.; Yamamoto, A. In vivo characterization of the physicochemical properties of polymer-linked TLR agonists that enhance vaccine immunogenicity. *Nat. Biotechnol.* **2015**, *33*, 1201–1210.
(7) Zhang, Z.; Ohto, U.; Shibata, T.; Krayukhina, E.; Taoka, M.; Yamauchi, Y.; Tanji, H.; Isobe, T.; Uchiyama, S.; Miyake, K.; et al. Structural analysis reveals that toll-like receptor 7 is a dual receptor for guanosine and single-stranded rna. *Immunity* **2016**, *45* (4), 737–748.
(8) Ryu, K. A.; Slowinska, K.; Moore, T.; Esser-Kahn, A. Immune response modulation of conjugated agonists with changing linker length.
(9) Aimetti, A. A.; Shoemaker, R. K.; Lin, C.-C.; Anseth, K. S. On-resin peptide macrocyclization using thiol–ene click chemistry. *Chem. Commun.* **2010**, *46* (23), 4061–4063.
(10) Tokmina-Roszyk, M.; Tokmina-Roszyk, D.; Fields, G. B. The synthesis and application of

fmoc-lys(5-fam) building blocks. *Biopolymers* **2013**, *100* (4), 347–355.
(11) Kang, J. Y.; Nan, X.; Jin, M. S.; Youn, S.-J.; Ryu, Y. H.; Mah, S.; Han, S. H.; Lee, H.; Paik, S.-G.; Lee, J.-O. Recognition of lipopeptide patterns by toll-like receptor 2-toll-like receptor 6 heterodimer. *Immunity* **2009**, *31* (6), 873–884.
(12) Jin, M. S.; Kim, S. E.; Heo, J. Y.; Lee, M. E.; Kim, H. M.; Paik, S.-G.; Lee, H.; Lee, J.-O. Crystal structure of the TLR1-TLR2 heterodimer induced by binding of a tri-acylated lipopeptide. *Cell* **2007**, *130* (6), 1071–1082.
(13) Zarember, K. A.; Godowski, P. J. Tissue expression of human toll-like receptors and differential regulation of toll-like receptor mrnas in leukocytes in response to microbes, their products, and cytokines. *J. Immunol.* **2002**, *168* (2), 554–561.
(14) Katja, F.; Sabine, R.; Holger, H.; Jennifer, D.; Roland, L.; Jörg, M.; Ute, B.; Kristina, R.; Günther, J.; Karl-Heinz, W.; et al. Heterodimerization of TLR2 with TLR1 or TLR6 expands the ligand spectrum but does not lead to differential signaling. *J. Leukoc. Biol.* **2007**, *83* (3), 692–701.
(15) Shukla, N. M.; Mutz, C. A.; Ukani, R.; Warshakoon, H. J.; Moore, D. S.; David, S. A. Syntheses of fluorescent imidazoquinoline conjugates as probes of toll-like receptor 7. *Bioorg. Med. Chem. Lett.* **2010**, *20* (22), 6384–6386.

CHAPTER 3

In Vitro Activity of TLR Tri-agonist Panel

3.1 Introduction

Developing novel vaccines that generate appropriate effector responses and protection against a pathogen remains a challenge. The process of generating a desired response is complicated by a lack of understanding between innate immune signaling and their long-term effect on protective adaptive responses. Innate immune system activation with individual TLR agonists has been studied. However, most pathogens and effective vaccines stimulate multiple TLRs, and the understanding of how these combinations of agonists affect the immune response is less clear. In addition, the TLR agonists in these natural systems are organized in a structural manner, which influences activity and necessitates consideration in vaccine formulation development.[1] Here, we evaluated the activity of a panel of five TLR tri-agonist combinations on immunologically relevant cells to gain understanding to how linkage and different combinations effect the resulting immune response.

3.2 Evaluation of Toxicity

To first understand the activity of our TLR agonists, we had to ensure that the compounds were not toxic to cells. Ensuring the compounds are non-toxic is essential, as cell death can also cause activation of innate immune pathways in neighboring cells, which would influence our results.[2] Thus, the compounds, and their deconstructed components were incubated on cells and the cell viability *via* MTT assay measured following incubation. We found that none of the compounds tested caused considerable cell death (**Fig. 3.1**)

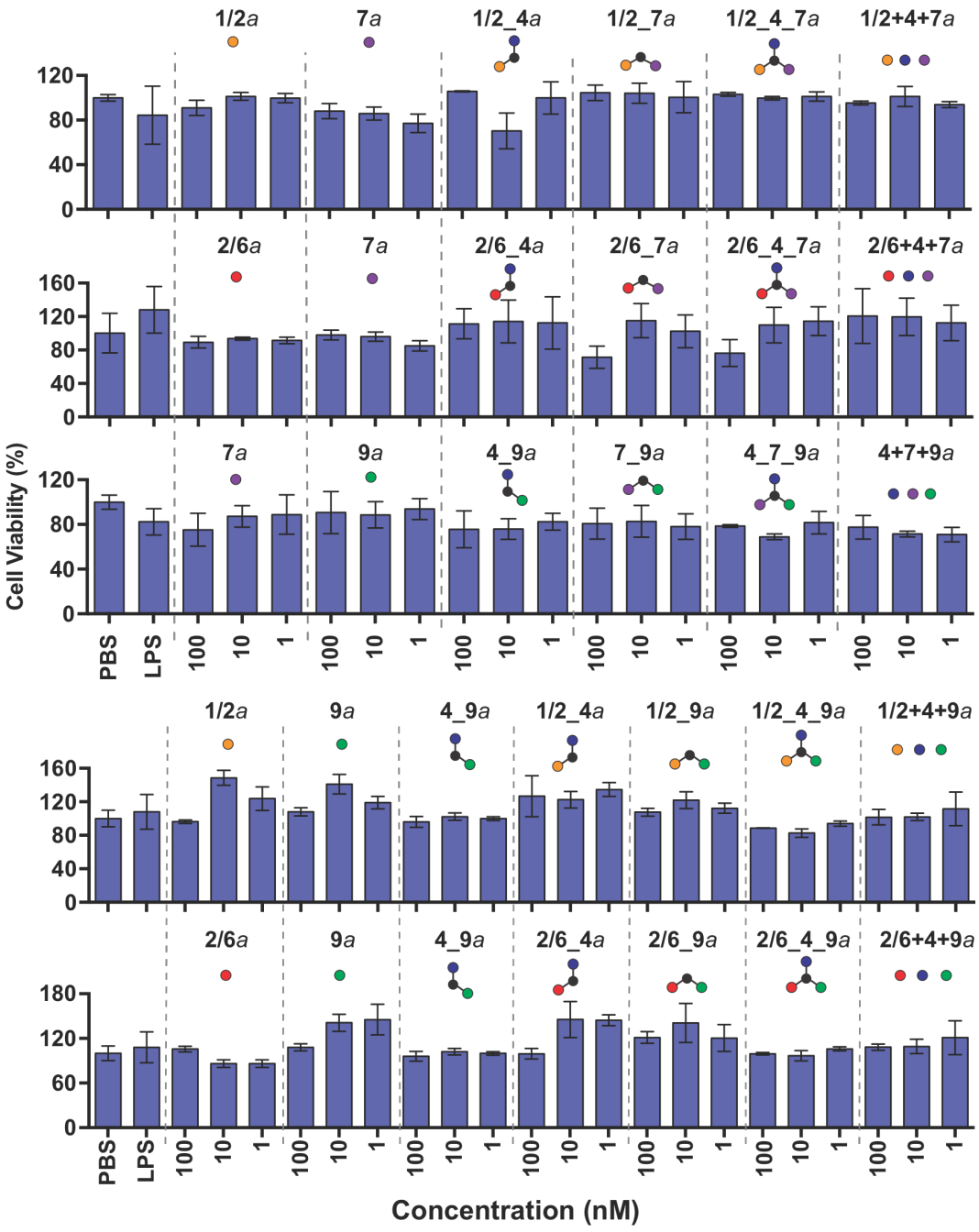

Figure 3.1 Cell Viability of TLR Tri-Agonists and Their Components. Cell viability as measured by MTT activity in RAW-Blue 264.7 macrophage cell assay treating with various linked or unlinked TLR agonists. Cells were incubated with each compound (100 nM) for 18 h at 37 °C. Supernatant was removed, the cells incubated with MTT for 30 min, the supernatant removed, the MTT crystals dissolved in DMSO, and the absorbance at 540 nm measured. Error bars represent SD. Samples were run in triplicate.

3.3 Effects of Conjugation on Individual Agonist Activity

Conjugating individual TLR agonists to a triazine scaffold could potentially affect their biological activity by disrupting binding to the receptor. Thus, we compared the activity of the triazine core conjugated to single agonists with that of the individual agonist without any linkers or core. All TLR agonists, except TLR9a (which was unaffected), had decreased activity upon conjugation to the triazine core as follows: TLR1/2*a* (2-fold decrease), TLR2/6*a* (20-fold decrease), TLR4*a* (10-fold decrease), and TLR7*a* (50-fold decrease, **Fig. 3.2**). One might assume that this loss in activity would lead to drastically lower activity of the tri-agonists compared to the additive effect of mixing the unlinked agonists, which were not attached to the core. However, apart from TLR1/2_4_7*a*, the compounds stimulated similar activity to the unlinked mixture. Because all of the individual agonists lost activity when linked to the core, we hypothesized that the activity is partially restored due to amplified synergistic effects from conjugation compared to the mixed, unlinked agonists.

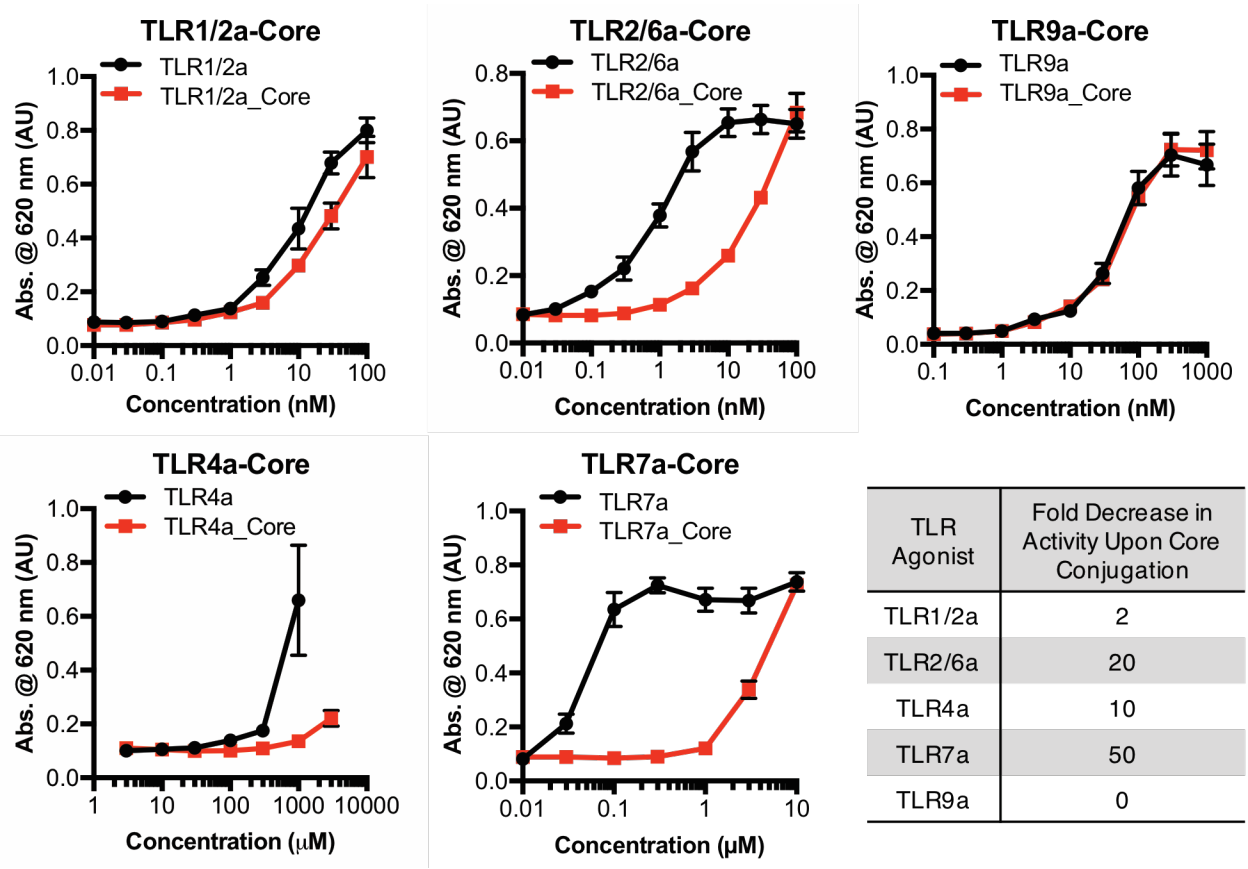

TLR Agonist	Fold Decrease in Activity Upon Core Conjugation
TLR1/2a	2
TLR2/6a	20
TLR4a	10
TLR7a	50
TLR9a	0

Figure 3.2 Individual and Core-linked TLR Agonists NF-κB Concentration Curves. NF-κB activity concentration curves of individual TLR agonists linked and unlinked (without linkers or Core) to the triazine core on a RAW-Blue 264.7 macrophage cell assay. Cells were incubated with each compound for 18 h at 37 °C. Supernatant was removed, incubated with QUANTI-Blue for 1 h and the absorbance at 620 nm measured. Estimates on fold decrease of activation shown in table. Error bars represent SD. Samples were run in hexaplet (TLR7, TLR2/6, TLR1/2) or triplicate (TLR4, TLR9).

3.4 Stimulation of Transcription Factors

One element of synergistic activity from TLR combinations is the activation of transcription factor activity. We initially examined stimulation of the transcription factor Nuclear Factor kappa-light-chain-enhancer of activated B cells (NF-κB). NF-κB responses are a broad measure of TLR agonist adjuvanticity which is correlated, but not directly related, to overall adjuvanticity.[3] NF-κB activity was compared in RAW-Blue NF-κB macrophage reporter cells stimulated either with the

synthesized TLR tri-agonists or with analogous unlinked combinations. At the highest concentration tested (100 nM), TLR2/6_4_7*a*, TLR1/2_4_9*a*, and TLR2/6_4_9*a* stimulated the highest NF-κB activity of the five, linked tri-agonists and were not statistically significant from one another ($p > 0.05$, **Fig. 3.3A**). TLR4_7_9*a* showed an intermediate level of NF-κB activity, and TLR1/2_4_7*a* stimulated the least NF-κB activity. The trend in NF-κB activity generally followed the order of potency of individual agonists alone, where TLR2/6*a* was the most potent, followed by TLR1/2*a* and TLR9*a* (**Fig. 3.2**). With the exception of TLR1/2_4_7*a*, all of the linked compounds stimulated similar levels of NF-κB activity compared to their unlinked counterparts.

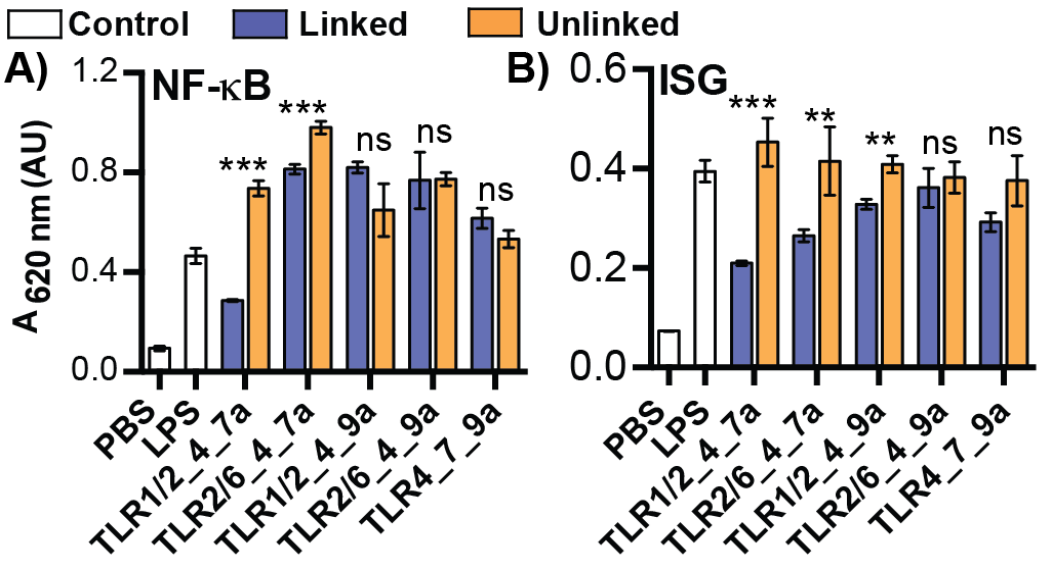

Fig. 3.3 Transcription Factor Activity of Linked and Unlinked TLR Tri-Agonists. NF-κB (A) and ISG (B) activity in RAW-Blue 264.7 macrophage cell assay treated with TLR tri-agonists or a 1:1:1 mixture of the analogous unlinked agonists. Cells were incubated with each compound (100 nM) for 18 h at 37 °C. Supernatant was removed, incubated with QUANTI-Blue for 1 h (NF-κB) or 4 h (ISG), and the absorbance at 620 nm measured. Error bars represent SD. Samples were run in triplicate, where **: $p < 0.01$, ***: $p < 0.001$, ns: not significant as determined by a two-tailed student's t test. All noted statistical analysis represent the asterisked compound compared to the analogous unlinked compounds. See SI for full data set. AU = Absorbance units.

To further assess the contributions of specific TLR agonists when linked to the core, we evaluated the deconstructed components of each tri-agonist combination (**Fig. 3.4**). Overall, we found that the activity of each tri-agonist typically followed that of the most potent individual TLR agonist in the combination. For example, TLR2/6_4_7*a* demonstrated high NF-κB activity similar to that of the potent individual TLR2/6*a*. However, linkage-dependent, synergistic effects were observed. In one case, TLR2/6_7*a* had 41% higher activity, despite the negative effects of being linked, than the unlinked combination of TLR2/6*a* and TLR7*a*. In other cases, inhibitory effects were observed. For example, the unlinked TLR1/2+4+7*a* and linked TLR1/2_4_7*a* both resulted in lower NF-κB activity than the predicted additive activity of the three individual agonists.

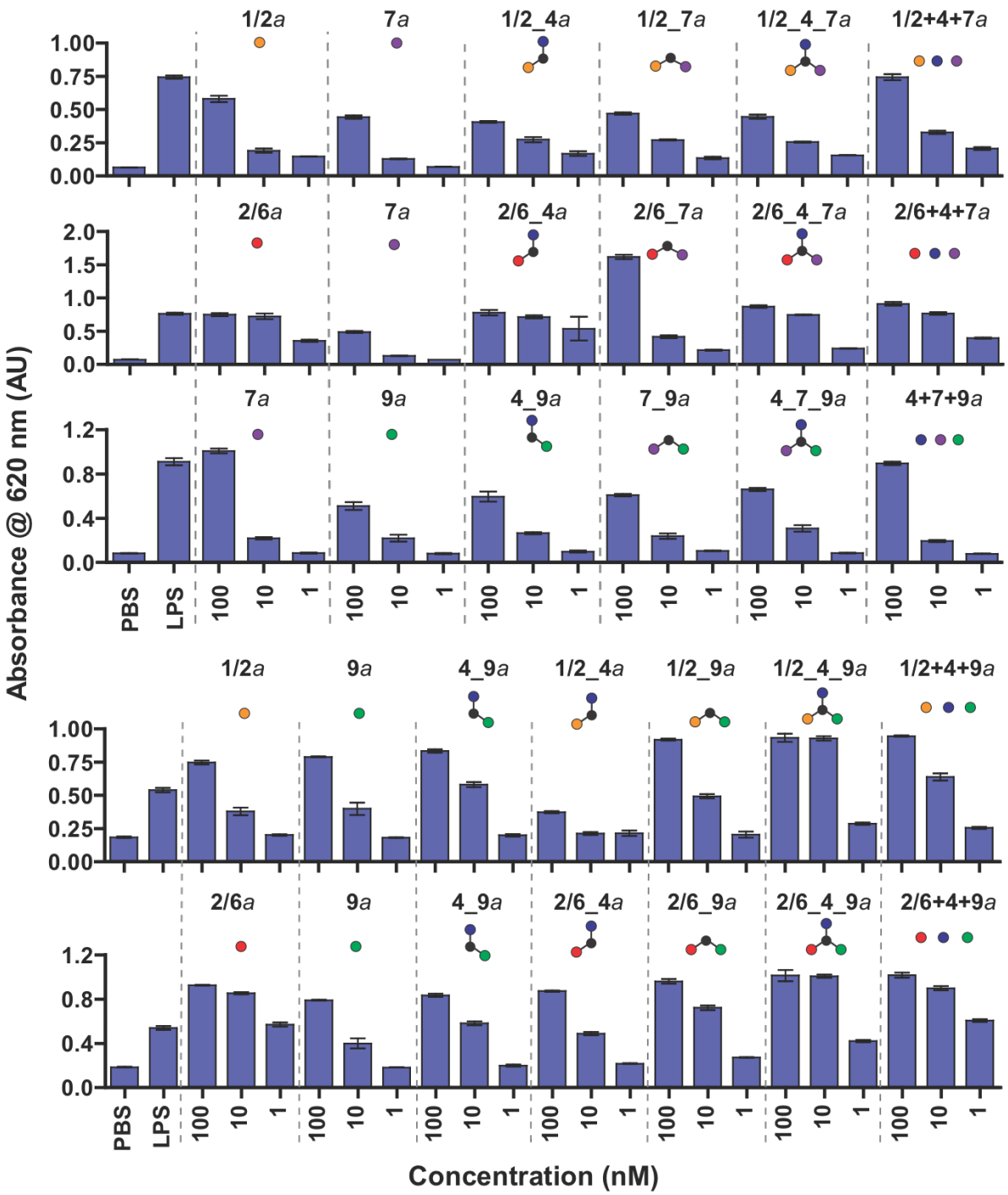

Figure 3.4 NF-κB Activity Elicited by Linked or Unlinked TLR Agonists. RAW-Blue cells were incubated with each compound (100 nM) for 18 h at 37 °C. Supernatant was removed, incubated with QUANTI-Blue for 1 h and the absorbance at 620 nm measured. Error bars represent SD. Samples were run in triplicate. Note: TLR4a and TLR4_7a did not show any appreciable activity at the tested concentrations.

Evaluation of TLR activation of ISGs by TLR Tri-agonists. Beyond activating NF-κB and subsequent inflammatory cytokines, the activation of interferons can be critical for a successful adjuvant, particularly in stimulating the differentiation of antigen specific $CD4^+$ and $CD8^+$ T cells.[4] We investigated interferon stimulatory genes (ISG) activity following TLR tri-agonist activation using an ISG-Blue RAW macrophage reporter cell line.

Generally, the unlinked tri-agonist combinations stimulated higher ISG activity, measured by the absorbance at 620 nm (absorbance units, AU), than the linked tri-agonists (**Fig. 3.3B**). The tri-agonists lacking TLR9*a*, TLR1/2_4_7*a* (0.21 AU) and TLR2/6_4_7*a* (0.27 AU), induced 50% less ISG stimulatory activity compared with their unlinked counterparts, TLR1/2+4+7*a* (0.46 AU) and TLR2/6+4+7*a* (0.42 AU). The tri-agonists containing TLR9*a* (TLR1/2_4_9a (0.33 AU), TLR2/6_4_9*a* (0.37 AU), and TLR4_7_9*a* (0.30 AU)) stimulated similar levels of ISG activity compared to unlinked counterparts. Thus, ISG activity was enhanced with the addition of TLR9*a* in the linked compounds but did not change when unlinked.

In addition, we assessed compound stability *in vitro* following incubation in FBS. We found that in general compounds retained most of their NF-κB activity following 24 h FBS incubation, where TLR1/2_4_7*a* had the lowest drop in activity, 77% of the non-FBS treated Tri-agonist activity (**Fig. 3.5**). From this we concluded that conjugation changes the activity of NF-κB partially between a balance of decreasing potency and increasing activation.

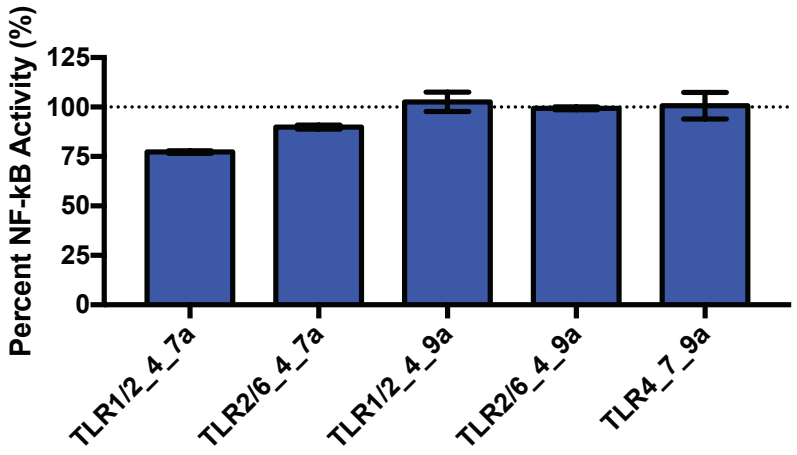

Figure 3.5 Tri-agonist Stability by Retention of Activity Following FBS Incubation. Compounds were incubated in 50% FBS at 37 °C for 24 h. Samples were diluted onto NF-κB RAW-Blue 264.7 macrophage cells and were incubated with each compound (final concentration 100 nM except for TLR1/2_4_9a which was at 10 nM) for 18 h at 37 °C. Supernatant was removed, incubated with QUANTI-Blue for 1 h and the absorbance at 620 nm measured. The percentage of activity of the FBS incubated samples relative to unincubated samples is plotted. Error bars represent SD. Samples were run in triplicate.

3.5 Stimulation of Cytokines

Although the tri-agonists induced NF-κB and ISG activity, the largest difference we observed was the tri-agonist's ability to elicit distinct cytokine profiles, consistent with our initial study of tri-agonist acitivty.[5] Synergistic or inhibited secretion of specific cytokines is another element of stimulation from multi-TLR systems. These distinct cytokine profiles can potentially define the type of immune response generated.[6] Thus, we analyzed the cytokine profiles elicited by TLR tri-agonist stimulation of murine bone marrow-derived dendritic cells (BMDCs) *in vitro* (**Fig. 3.6**). BMDCs were stimulated with linked or unlinked TLR agonists for 6 h. The supernatant was analyzed by cytometric bead array (CBA) for IL-12p70, TNF-α, IFN-γ (TH1 promoting) and IL-6, IL-10, CCL2 (TH2 promoting) cytokine and chemokine concentrations, or by ELISA if the detected cytokines were near the limit of CBA detection (IL-6, IL-12p70, IFN-α, IFN-β).

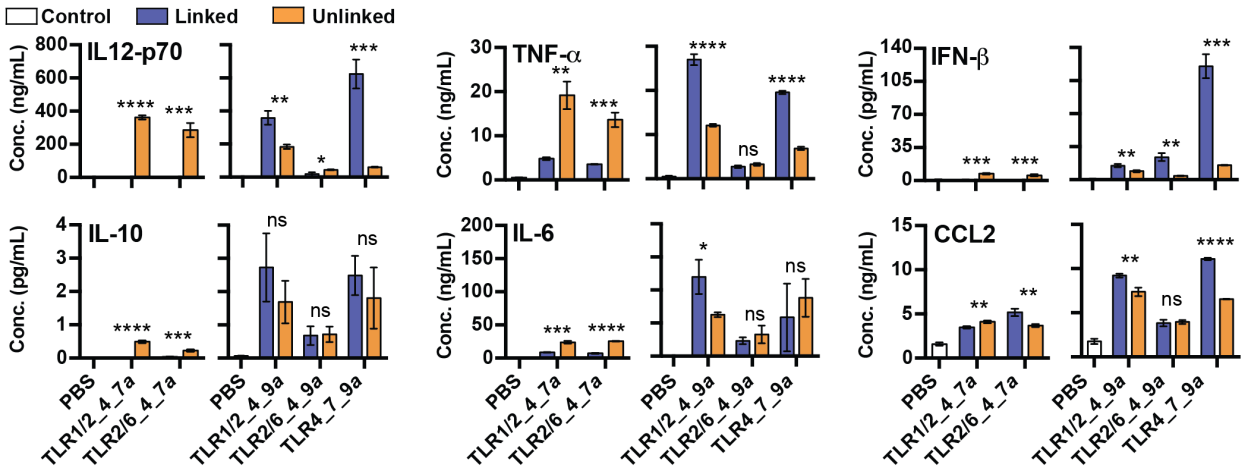

Figure 3.6 *In Vitro* Cytokine Expression from BMDCs as Measured by CBA and ELISA. *In vitro* cytokine expression from BMDCs as measured by CBA (TNF-α, IL-10, and CCL2) and ELISA (IL-12p70, IL-6, and IFN-β). Cells were incubated with each TLR tri-agonist (100 nM) or a 1:1:1 (molar ratio) mixture of the analogous unlinked TLR agonists (100 nM each) for 6 h at 37 °C. Error bars represent standard deviation of the mean. Samples were run in triplicate, where *: $p < 0.05$, **: $p < 0.01$, ***: $p < 0.001$, ****: $p < 0.0001$, ns: not significant. Statistical analysis is between the linked vs unlinked agonists, performed by two-tailed student's t-test. TLR1/2_4_7*a* and TLR2/6_4_7*a* were tested separately from TLR1/2_4_9*a*, TLR2/6_4_9*a*, and TLR4_7_9*a* due to assay size constraints. No measurable levels of IFN-γ or IFN-α were detected.

TLR1/2_4_9*a* and TLR4_7_9*a*, elicited high levels of IL-12p70 (TLR1/2_4_9a: 358 pg/mL, TLR4_7_9*a*: 624 pg/mL) and TNF-α (TLR1/2_4_9*a*: 27.0 ng/mL, TLR4_7_9*a*: 19.6 ng/mL), which is consistent with the reported role for TLR9*a* in selectively inducing TH1 cells.[7] For these two compounds, the linked agonists stimulated significantly higher levels of IL-12p70 (TLR1/2_4_9*a*: 95% increase, TLR4_7_9*a*: 900% increase) and TNF-α (TLR1/2_4_9*a*: 123% increase, TLR4_7_9*a*: 184% increase) than the analogous unlinked mixtures. In addition, the linked TLR4_7_9*a* produced relatively high levels of IFN-β (120 pg/mL) compared to the unlinked mixture (15 pg/mL). In contrast, compounds containing TLR2/6*a*, including TLR2/6_4_7*a* and TLR2/6_4_9*a*, stimulated relatively more IL-10, IL-6, and CCL2. Thus, TLR2/6*a* shifted the cytokine profile toward a TH2 type response, overcoming the TH1 biasing effect of TLR9*a*, as observed when comparing TLR1/2_4_9*a* (IL12-p70: 358 pg/mL) and

TLR2/6_4_9*a* (IL12-p70: 18 pg/mL). The cells stimulated by TLR2/6_4_7*a* also displayed a more TH2 biasing cytokine profile. TLR1/2_4_7*a* produced relatively low levels of all cytokines compared to the other tri-agonist combinations and the unlinked agonists – suggesting this linked combination suppresses agonist activity. While we observed changes in cytokine expression for both the linked and unlinked combinations, we did not see statistically significant, reproducible changes in cell surface activation markers (data not shown). From these results, we conclude that both the trimeric combination and its spatial ordering can drastically alter the activity of stimulated cells with the greatest increases/decreases being changes of over 900%. These results point to the significant opportunities provided by these compounds to elicit unique responses in cell culture and potentially *in vivo*.

To further analyze the origin of characteristic cytokine profiles generated by the different tri-agonists, we compared how individual TLR agonists contributed to the response. We determined that the cytokine profile of a TLR agonist could be dramatically altered by being linked with another agonist. For example, TLR2/6*a* linked to TLR9*a* (TLR2/6_9*a*) resulted in a reduction of IL-12p70 (100% decrease), TNF-α (81% decrease), CCL2 (58% decrease), IL-6 (44% decrease), and IL-10 (60% decrease) levels compared to TLR9*a* alone. This result shows that the cytokine profile observed for TLR2/6_4_9*a* more closely resembled that of TLR2/6*a* than TLR9*a* (**Fig. 3.7**). In another case, conjugation of TLR1/2*a* with TLR9*a* (TLR1/2_9*a*) induced a similar effect as TLR2/6*a* conjugation. However, linking TLR4*a*, a very weak agonist on its own, to the tri-agonist TLR1/2_4_9*a* resulted in a restored TLR9*a*-like cytokine profile, unlike TLR2/6_4_9*a* (**Fig. 3.7**). We found that TLR4a, and TLR4_7a were too weak to stimulate notable levels of cytokine on their own (**Fig 3.8**)

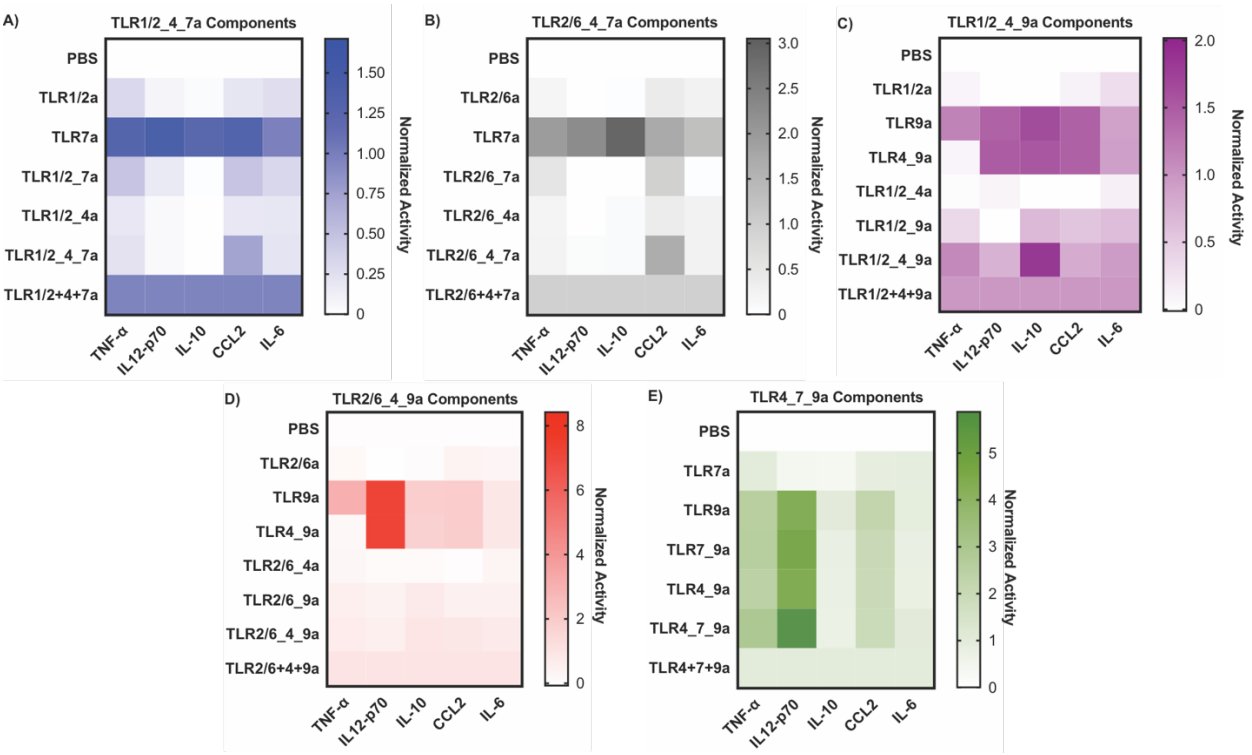

Figure 3.7 Heat Map of *In Vitro* Cytokine Expression from BMDCs as Measured by CBA Following Incubation with Tri-Agonists or Their Components. A) TLR1/2_4_7*a*, B) TLR2/6_4_7*a*, C) TLR1/2_4_9*a*, D) TLR2/6_4_9*a*, E) TLR4_7_9*a*. Cells were incubated with each compound (100 nM) or a 1:1:1 (molar ratio) mixture of the analogous unlinked TLR agonists (100 nM each) for 6 h at 37 °C. In each set, the data was normalized for each cytokine readout, where the level stimulated by the unlinked tri-agonist mixture was set to 1. Samples were run in triplicate. Note: TLR4*a* and TLR4_7*a* did not show any appreciable activity at the tested concentration.

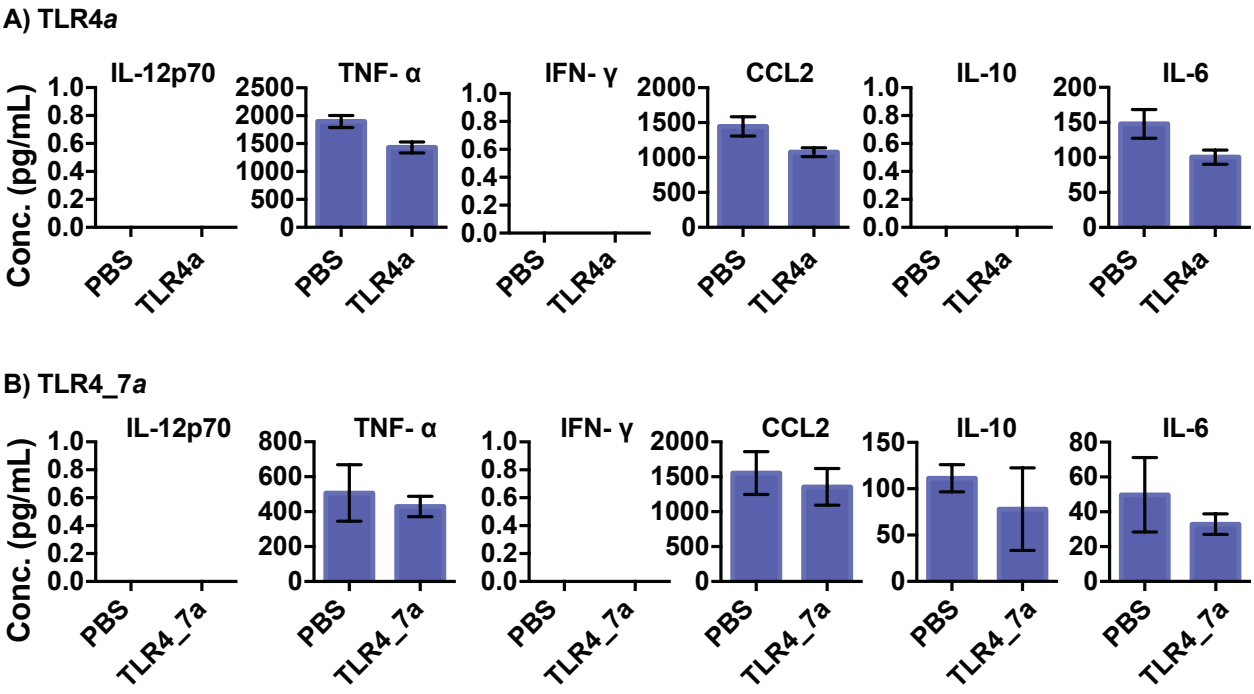

Figure 3.8 *In Vitro* Cytokine Expression from BMDCs as Measured by CBA Following Incubation with TLR4*a* and TLR4_7*a*. BMDCs were incubated with TLR4a (A) or TLR4_7a (B) (100 nM) for 6 h at 37 °C. Error bars represent standard deviation of the mean. Samples were run in triplicate. Note: the concentration curve for all cytokines ranged from 100-25000 pg/mL.In bars not shown, no signal was detected.

TLR1/2_4_7*a* Components. The linked TLR1/2_4_7 tri-agonist stimulated low levels of cytokines compared to the unlinked and individual agonists (**Fig. 3.9**). The only exception observed was that the linked agonists stimulated high expression levels of CCL2 (3493 pg/mL). TLR7*a* was the only other component that stimulated high levels of TH1 type cytokines, like IL12-p70 (336 pg/mL). Mixing TLR7*a* with both TLR1/2*a* and TLR4*a* resulted in 41% lower IL12-p70 expression compared to TLR7*a* alone (TLR1/2+4+7*a*: 197 pg/mL). Conjugating TLR1/2_4*a* with TLR7*a* reduced various cytokine levels drastically from TLR7*a* levels alone, but was slightly higher than TLR1/2*a* levels. For example, conjugation of TLR4*a* with TLR7*a* (TLR4_7*a*) completely diminished IL-12p70 and IL-10 expression. Conjugation of TLR1/2*a* with TLR4*a* (TLR1/2_4*a*) reduced cytokine levels of TNF-α (42% decrease), CCL2 (11% decrease), and IL-6

(28% decrease). When linked, the tri-agonist behaved more similarly to TLR1/2*a*, in that it elicited low levels of IL-12p70 (<100 pg/mL) and IL-10 (<100 pg/mL), moderate levels of TNF-α (4.8 ng/mL) and IL-6 (19.2 ng/mL), and high levels of CCL2 (3.5 ng/mL). This suggests that the tri-agonist follows the activity trends of TLR1/2*a* and not that of the TLR7*a* agonist.

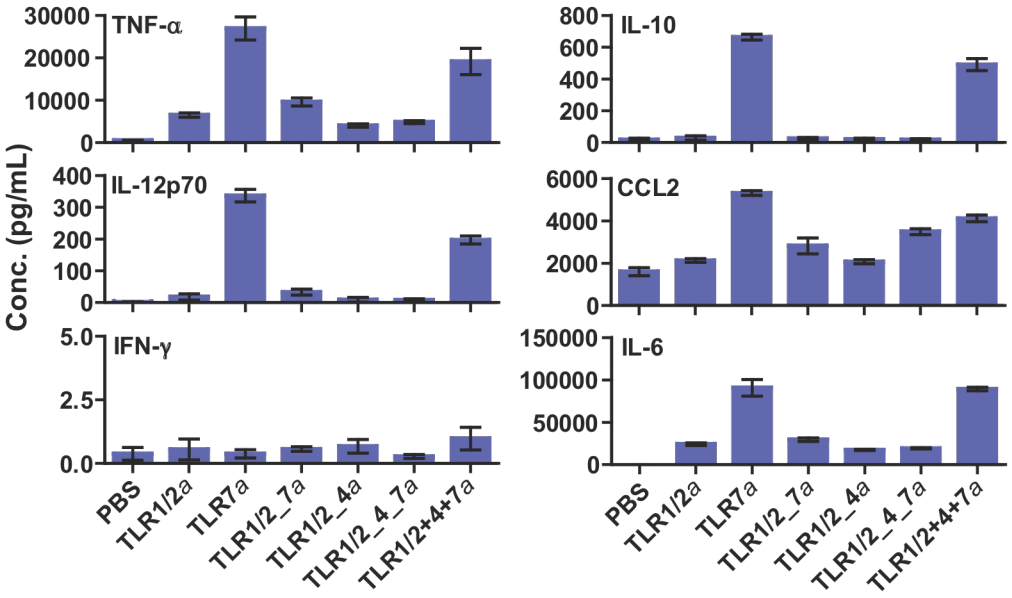

Figure 3.9 *In Vitro* Cytokine Expression from BMDCs as Measured by CBA Following Incubation with TLR1/2_4_7*a* or its Components. BMDCs were incubated with TLR1/2_4_7*a* (100 nM), a deconstructed component of the tri-agonist (100 nM), or a 1:1:1 mixture of the analogous unlinked TLR agonists (100 nM each) for 6 h at 37 °C. Error bars represent standard deviation of the mean. Samples were run in triplicate. Note: the concentration curve for all cytokines ranged from 100-25000 pg/mL. Note: TLR4*a* and TLR4_7*a* did not show any appreciable activity at the tested concentration.

TLR2/6_4_7*a* Components. TLR2/6_4_7*a* behaved similarly to TLR1/2_4_7*a* (**Fig 3.10**). It stimulated relatively low levels of all cytokines other than CCL2 (5187 pg/mL). The tri-agonist appeared to follow the activity of TLR2/6*a* and not TLR7*a* or TLR4*a*. This differs from the analogous unlinked agonists, which stimulated relatively high levels of all cytokines. Similar to the results with TLR1/2*a* and TLR7*a*, mixing TLR2/6*a* and TLR7*a* in the unlinked mixture (TLR2/6+4+7*a*) or linking them as a di-agonist (TLR2/6_7*a*) drastically reduced the levels of IL-

12p70 (compared to TLR2/6+4+7*a* 57%, TLR2/6_7*a* 100% decrease), TNF-α (TLR2/6+4+7*a* 50%, TLR2/6_7*a* 74% decrease), CCL2 (TLR2/6+4+7*a* 43%, TLR2/6_7*a* 44% decrease), IL-6 (TLR2/6+4+7*a* 25%, TLR2/6_7*a* 96% decrease), and IL-10 (TLR2/6+4+7*a* 67%, TLR2/6_7*a* 100% decrease).

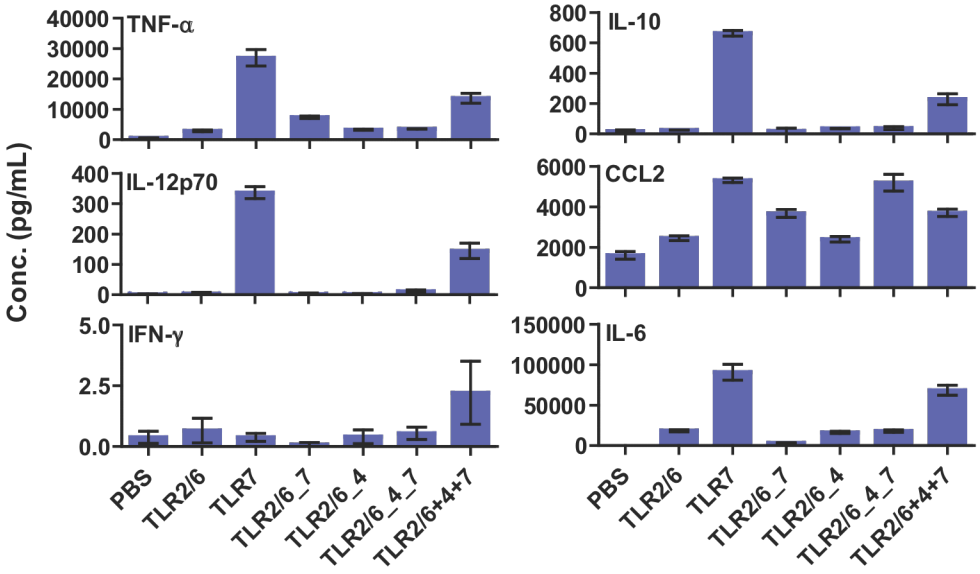

Figure 3.10 *In Vitro* Cytokine Expression from BMDCs as Measured by CBA Following Incubation with TLR2/6_4_7*a* or its Components. BMDCs were incubated with TLR2/6_4_7*a* (100 nM), a deconstructed component of the tri-agonist (100 nM), or a 1:1:1 mixture of the analogous unlinked TLR agonists (100 nM each) for 6 h at 37 °C. Error bars represent standard deviation of the mean. Samples were run in triplicate. Note: the concentration curve for all cytokines ranged from 100-25000 pg/mL. Note: TLR4*a* and TLR4_7*a* did not show any appreciable activity at the tested concentration.

TLR1/2_4_9*a* Components. TLR1/2_4_9*a* stimulated the highest observed levels of cytokines and was higher than the analogous unlinked compounds for TH1 type cytokines (99% higher IL-12p70, 123% higher TNF-α, **Fig. 3.11**). Most of the cytokine production elicited by the tri-agonist appeared to be due to TLR9*a*. The cytokine profile of TLR9*a* was not affected by conjugation of TLR4*a*, except in the case of TNF-α (93% decrease). However, when conjugating

TLR1/2*a* and TLR9*a* (TLR1/2_9*a*), there was an inhibitory effect as the cytokine levels of IL-12p70 (100% decrease), TNF-α (70% decrease), CCL2 (62% decrease), IL-6 (29% decrease), and IL-10 (61% decrease) were all reduced compared to TLR9*a*. Incorporation of TLR4*a* to form the tri-agonist (TLR1/2_4_9*a*) restored the TNF-α, IL-10, and IL-6 levels to that of TLR9*a* alone.

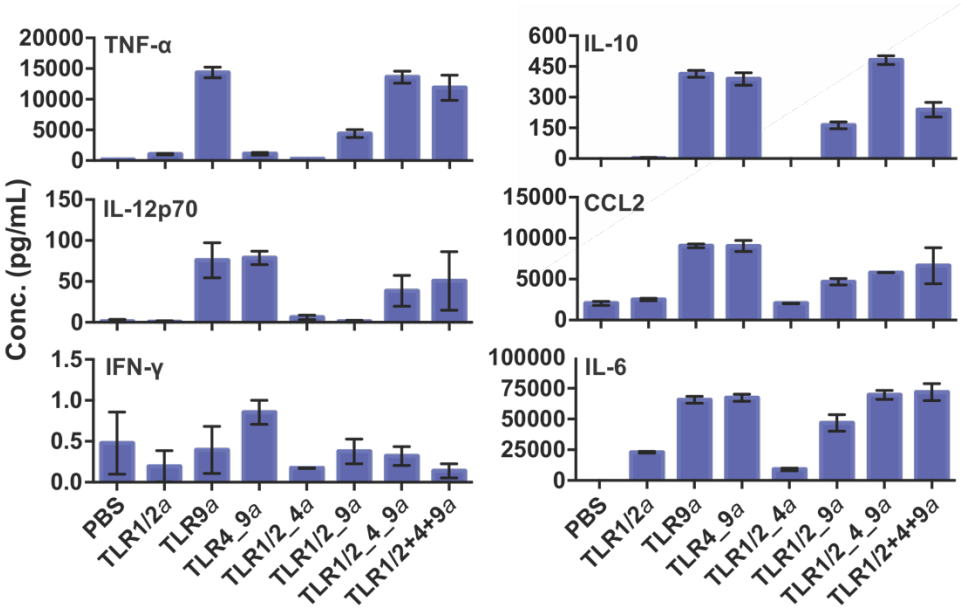

Figure 3.11 *In Vitro* Cytokine Expression from BMDCs as Measured by CBA Following Incubation with TLR1/2_4_9*a* or its Components. BMDCs were incubated with TLR1/2_4_9*a* (100 nM), a deconstructed component of the tri-agonist (100 nM), or a 1:1:1 mixture of the analogous unlinked TLR agonists (100 nM each) for 6 h at 37 °C. Error bars represent standard deviation of the mean. Samples were run in triplicate. Note: the concentration curve for all cytokines ranged from 100-25000 pg/mL.

TLR2/6_4_9*a* Components. Unlike TLR1/2_4_9*a*, the TLR2/6_4_9*a* stimulated low levels of TH1-biasing cytokine expression (IL-12p70: 18 pg/mL, TNF-α 2.8 ng/mL, **Fig. 3.12**). This observation is particularly interesting, as the only difference between TLR2/6_4_9*a* and TLR1/2_4_9*a* is a single palmitoyl chain. This structural difference distinguishes the target receptor between the TLR1/2 and TLR2/6 heterodimers, which are thought to share the same signaling pathway.[8–10] TLR2/6*a* conjugation to TLR9*a* (TLR2/6_9*a*) resulted in a reduction of IL-

12p70 (100% decrease), TNF-α (81% decrease), CCL2 (58% decrease), IL-6 (44% decrease), and IL-10 (60% decrease) levels compared to TLR9*a*. Thus, conjugation of TLR9*a* with TLR2/6*a* (TLR2/6_9*a*) inhibited cytokine levels compared to conjugation with TLR1/2*a*. However, additional conjugation with TLR4*a* (TLR2/6_4_9*a*) partially restored TNF-α, IL-10, CCL2, and IL-6 levels compared to TLR9*a* alone.

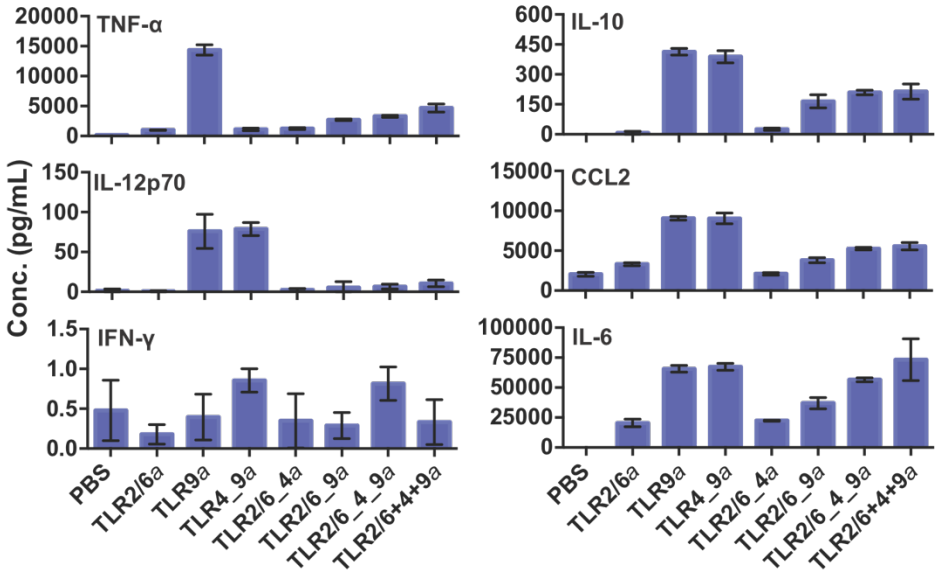

Figure 3.12 *In Vitro* Cytokine Expression from BMDCs as Measured by CBA Following Incubation with TLR2/6_4_9*a* or its Components. BMDCs were incubated with TLR2/6_4_9*a* (100 nM), a deconstructed component of the tri-agonist (100 nM), or a 1:1:1 mixture of the analogous unlinked TLR agonists (100 nM each) for 6 h at 37 °C. Error bars represent standard deviation of the mean. Samples were run in triplicate. Note: the concentration curve for all cytokines ranged from 100-25000 pg/mL.

TLR4_7_9*a* Components. TLR4_7_9*a* stimulated a similar cytokine profile to the TLR1/2_4_9*a* in that there were relatively high levels of TH1 cytokines generated (IL-12p70: 624 pg/mL, TNF-α 19.6 ng/mL, **Fig. 3.13**). The IL-12p70 levels appeared to mainly originate from TLR9*a* activity. Conjugating either TLR7*a* or TLR4*a* to TLR9*a* (TLR7_9*a* and TLR4_9*a*) did not have a significant effect on any of the measured cytokines. The tri-agonist (TLR4_7_9*a*) had slightly improved cytokine levels compared to TLR9*a* alone, suggesting that unlike TLR1/2*a* and TLR2/6*a*, TLR4*a* and TLR7*a* did not have an inhibitory effect upon conjugation with TLR9*a* (TLR4_9*a*, TLR 7_9*a*). However, the unlinked TLR4+7+9*a* combination did cause reduction of cytokine levels compared to TLR9*a* alone, suggesting that linking the TLR agonists, in this case, preserves activity from TLR9*a*.

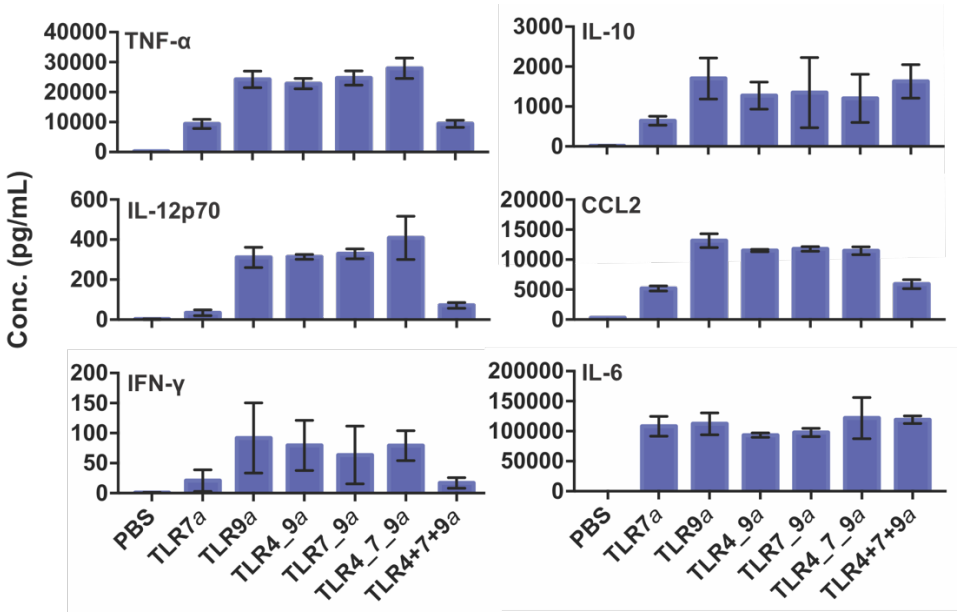

Figure 3.13 *In Vitro* Cytokine Expression from BMDCs as Measured by CBA Following Incubation with TLR4_7_9*a* or its Components. BMDCs were incubated with TLR4_7_9*a* (100 nM), a deconstructed component of the tri-agonist (100 nM), or a 1:1:1 mixture of the analogous unlinked TLR agonists (100 nM each) for 6 h at 37 °C. Error bars represent standard deviation of the mean. Samples were run in triplicate. Note: the concentration curve for all cytokines ranged from 100-25000 pg/mL. Note: TLR4*a* and TLR4_7*a* did not show any appreciable activity at the tested concentration.

3.6 Serum Cytokine Expression and Toxicity Upon Tri-agonist Injection

After finding that spatial arrangement alters *in vitro* cytokine activity, we sought to determine how this changed *in vivo* activity. We measured systemic cytokines (IL-6, TNF-α, IL12-p40, IFN-α, IFN-β) levels in the blood of C57BL/6 mice *via* ELISA (**Fig. 3.14**). We also monitored the mouse weight shortly after IM injection of the compounds (**Fig. 3.14F**). Injection of individual TLR agonists often results in high levels of systemic cytokines, which can have adverse health effects as indicated by weight loss in the animals.[11] We hypothesized that the linked tri-agonists might cause less systemic cytokine production due to their distinct immune responses as well as the changes in biophysical properties.

The differences observed in systemic cytokines varied between linked and unlinked compounds and between different combinations (**Fig. 3.14**). We observed that TNF-α, IFN- α, and IFN-β expression reached its maximum 1 h post injection, while IL-6 and IL-12p40 expression continued to increase at 3 h post injection, consistent with previous reports of systemic cytokine detection following TLR stimulation.[12] We observed that many compounds elicited modest concentrations of serum cytokines. (**Fig. 3.14A-E**). Only unlinked TLR2/6+4+7*a* produced high levels of IL-6 (2215 pg/mL), IFN-α (90 pg/mL), IFN-β (66 pg/mL) while both unlinked TLR2/6+4+7*a* and linked TLR2/6_4_9*a* resulted in high TNF-α serum levels (582 pg/mL and 385 pg/mL, respectively). Several combinations stimulated high levels of IL-12p40 (**Fig. 3.14C**). Generally, the unlinked compounds stimulated similar levels of IL-12p40, where unlinked TLR2/6_4_7*a* stimulated the highest (1949 pg/mL). Of the linked combinations, only the TLR9*a* containing combinations showed appreciable levels of IL12p40. Interestingly, TLR2/6_4_9*a* stimulated the highest amounts of IL12-p40 (1637 pg/mL) of the linked combinations, the opposite trend observed *in vitro* for the expression of the functional IL12-p70.

Where we saw the biggest correlation, was in weight loss. TLR2/6+4+7*a* resulted in the most dramatic weight loss (8.3% loss) in mice 24 h post injection (**Fig. 3.14F**) correlating well with its large increase in serum cytokines. Therefore, the weight increase observed with TLR2/6_4_7*a* (2.2% increase) confirmed our hypothesis that agonist linkage can dampen systemic effects upon adjuvant administration and alter systemic responses. However, not all of the differences between compounds were as stark. For example, there was notable weight loss in mice following TLR2/6_4_9*a* or TLR4_7_9*a* injection, regardless of linkage, despite low levels of systemic cytokines for both.

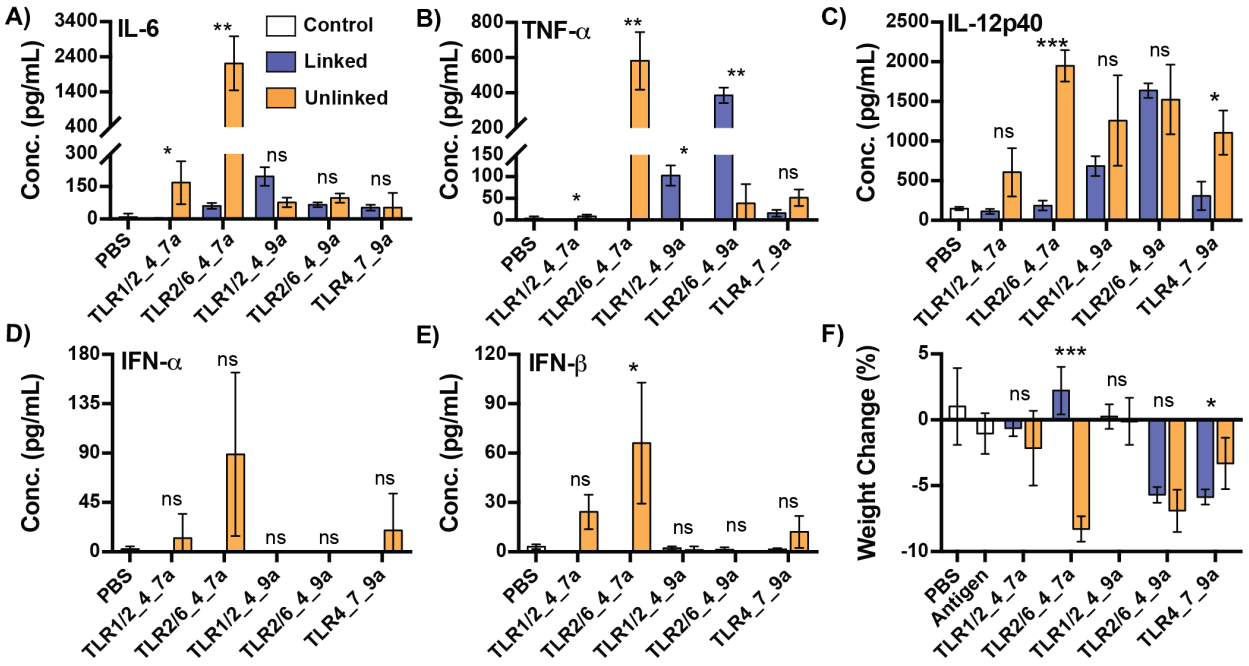

Figure 3.14 *In Vivo* Cytokine Serum Levels and Weight Loss in Mice Following Tri-Agonist Injection. *In vivo* IL-6 (**A**), TNF-α (**B**), IL-12p40 (**C**), IFN-α (**D**), IFN-β (**E**) serum levels in C57BL/6 mice 3 h (IL-6 and IL-12p40) and 1 h (TNF- α, IFN-α, and IFN-β) post injection as measured by ELISA. Mice were injected *via* IM with TLR tri-agonists (1 nmol) or a 1:1:1 molar ratio mixture of the analogous unlinked TLR agonists (1 nmol each). (**F**) Percent weight change 24 h post tri-agonist injection mixed with 0.5 nmol CBU_1910 antigen. Samples were run in triplicate for ELISA experiments, and in n=8 for percent weight experiment (except PBS and TLR2/6_4_7*a* where n=5), where *: $p < 0.05$, **: $p < 0.01$, ***: $p < 0.001$, ns: not significant. Statistical analysis is between the linked versus unlinked agonist for the indicated compound, performed using a two-tailed student's t-test.

TLR1/2_4_7*a*. TLR1/2_4_7*a* did not elicit significant amounts of any cytokines in the serum (**Fig. 3.14**). However, the unlinked combination stimulated relatively low levels of IL-6 (168 pg/mL at 3 h), TNF-α (8 pg/mL at 1 h, 39 pg/mL 3h), and IL12p40 (606 pg/mL at 3 h). Interestingly, this was the only compound where TNF-α levels were higher at 3 h post injection than at 1 h post injection. In addition, no weight loss was observed following injection (**Fig. 3.14F**)

TLR2/6_4_7*a*. The TLR2/6_4_7*a* matched our hypothesis, that the linked compounds would produce fewer systemic cytokines than the unlinked combination *in vivo* (TNF-α: 100% decrease at 1 h, IL-6: 98% decrease at 3 h, IL12p40: 90% decrease at 3 h, IFN-α: 100% decrease

at 1 h, IFN-β: 100% decrease at 1 h, Fig. 5). However, this may be in part due to the agonists' weaker ability to stimulate these cytokines as determined *in vitro* (**Fig. 3.6**). Mice receiving linked TLR2/6_4_7*a* did not show any signs of weight loss, as expected from the low levels of systemic cytokines detected (**Fig. 3.14F**). However, mice receiving unlinked TLR2/6_4_7*a* showed the most weight loss (8.3% loss) of any of the agonists tested, consistent with the highest observed systemic cytokine levels.

TLR1/2_4_9*a*. Unlike the TLR2/6_4_7*a*, the linked TLR1/2_4_9*a* stimulated higher serum concentrations of IL-6 (197 pg/mL, 155% higher than the unlinked agonists), TNF-α (103 pg/mL, none detected for the unlinked agonists) than the unlinked combination (**Fig. 3.14**). This result was consistent with the *in vitro* cytokine results, where TLR1/2_4_9*a* stimulated higher levels of IL-6 and TNF-α than its unlinked counterpart (**Fig. 3.6**). However, it also suggests that linking the agonists does not always reduce the generation of systemic cytokines, although the levels of cytokines detected were low relative to TLR2/6_4_7*a*. Conversely, linked TLR1/2_4_9*a* stimulated less (684 pg/mL, 54% of unlinked activity) IL12p40 than the unlinked combination. Although this is more in line with our linkage hypothesis, it is contradictory to the in vitro cytokine results which showed that linked TLR1/2_4_9*a* stimulated high levels of IL12p70. Thus, the unlinked might stimulate higher levels of the non-functional IL12-p40, while the linked combination results in higher amounts of the functional Il12p70. Neither the linked and unlinked TLR1/2_4_9*a* caused mice to lose weight 24 h post injection.

TLR2/6_4_9*a*. The linked and unlinked TLR2/6, 4, 9 agonist combinations did not result in high IL-6 concentrations, in the serum (Linked: 66 pg/mL, 97 pg/mL unlinked, **Fig. 3.14A**). However, linked TLR2/6_4_9*a* stimulated relatively high levels of TNF-α in the serum (385 pg/mL, **Fig. 3.14B**). Interestingly, TLR2/6_4_9*a* did not induce notable TNF-α *in vitro* (**Fig. 3.6**).

Both the linked an unlinked combinations stimulated similar, but relatively high levels of IL12p40 (1637 pg/mL linked, 1524 pg/mL unlinked). In addition, both the linked and unlinked TLR2/6_4_9*a* combinations resulted in >5% weight loss in mice, suggesting that the weight loss is not entirely due to serum cytokine levels.

TLR4_7_9*a*. Both the linked and unlinked TLR4_7_9*a* produced relatively low levels of IL-6 (<75 pg/mL) and TNF-α (<50 pg/mL, **Fig. 3.14**). In addition, the tri-agonist showed 70% lower TNF-α levels than the unlinked combination after 1 h, although the difference was not statistically significant. However, the linked combination did stimulate significantly less IL12p40 in the serum (308 pg/mL linked vs 1105 pg/mL unlinked, 28% of unlinked) These results were surprising as linked TLR4_7_9*a* elicited some of the highest TNF-α and IL-6 levels among the tri-agonists *in vitro*, suggesting that this combination could potentially result in higher local tissue immune activation (**Fig. 3.6**). However, both the linked and unlinked combinations caused the mice to lose some weight 24 h post injection (**Fig. 3.14F**).

3.7 Conclusions

TLR Combinations. In this study, we presented an initial evaluation of combinations of three different TLR agonists and their influence on innate immune response. We found that the combination of TLR agonists in the linked tri-agonists drastically affected the immune response profile generated. Although most of the tri-agonists stimulated similar levels of NF-ϰB and ISG activity, the specific tri-agonist combinations stimulated distinct cytokine profiles, which can lead to discrete adaptive immune responses (**Table 1**).

Overall, the presence of TLR9*a* in a trimeric combination had the greatest effect on the resulting immune response. Two of the three TLR9*a* containing tri-agonists (TLR1/2_4_9*a* and

TLR4_7_9*a*) showed a TH1-biasing cytokine response, characterized by higher levels of IL-12p70, and TNF-α.[6] In addition, the linked TLR4_7_9*a* elicited relatively high levels of IFN-β. This is perhaps not surprising as TLR9*a* is reported to elicit a biased TH1, cellular response compared to other TLR agonists in its use in clinical vaccines.[7] However, the presence of TLR2/6*a* diminished production of TH1-inducing cytokines, even when TLR9*a* was present (TLR2/6_4_9*a*). This observation was consistent with previous reports that TLR2 stimulation exhibits inhibitory effects on IL-12 originating from CpG stimulation.[13] TLR1/2*a* also demonstrated this effect when conjugated with TLR9*a* (TLR1/2_9*a*). TLR1/2*a* is also known to display an inhibitory effect on TH1-inducing cytokine secretion upon co-administration with CpG DNA.[13,14] However, further conjugation with TLR4*a* to afford the tri-agonist, TLR1/2_4_9*a*, restored cytokine profile activity similar to that of TLR9*a* alone. We speculate this could be a result of the relatively high potency of TLR2/6*a* compared to TLR1/2*a,* which further biases the immune response toward a TH2 response (**Fig. 3.6**).

This TH1/TH2 biasing property can be useful in designing adjuvants for vaccines. In further studies we have observed that adjuvanting a subunit vaccine with TLR2/6_4_7*a* generated a robust TH2 antigen specific antibody response, while TLR4_7_9*a* elicited the most potent antigen specific TH1 T cell responses of all the tri-agonists, but low antibody titers (**Chapter 4**). These results are consistent with the cytokine profiles observed in this study. Interestingly, when TLR1/2_4_9*a* is used as an adjuvant, a balanced TH1/TH2 response is observed. We hypothesize that in this case, the TLR1/2*a* TH2 biasing properties are sufficient to generate large antibody titers, while the TLR9*a* still influences generation of a TH1 response.

Tri-agonists lacking TLR9*a* (TLR1/2_4_7*a* and TLR2/6_4_7*a*) generally elicited a TH2 biased immune response, characterized by higher proportions of IL-6 and CCL2 compared to other

cytokines (**Fig. 3.6**). Following this result, these compounds generated larger proportions of IgG1 to IgG2c antibodies in a subunit vaccine (**Chapter 4**). However, these tri-agonists were relatively weak at stimulating indicators of immune responses *in vitro* (**Fig. 3.6**). The weaker potency of these compounds may be due to differences in biophysical properties upon linkage. Another possibility is that when linked, this particular combination does not behave in a synergistic manner. For example, TLR1/2, TLR4, and TLR7 agonists all exhibit inhibitory effects on IL-6 expression when co-administered *in vitro*, which is supported by both the linked and unlinked TLR1/2_4_7*a* combination studied in this work (**Fig. 3.7A**).[13]

These observations are particularly pertinent for vaccine development because they give insight into how linking particular TLR agonists in combination determines their immunological activity. In the case of TLR9*a* containing tri-agonists, the TLR9*a* guided the immune response, unless influenced by TLR2/6*a*, whereas TLR tri-agonists lacking TLR9*a* stimulated relatively fewer markers of immune activation.

In addition, the linked compounds varied greatly in their cytokine profiles, both *in vitro* and *in vivo*, from their unlinked counterparts, demonstrating that the linking of the agonists played a role in their activity (**Table 3.1**). Interestingly, there was less variation in the immune response profile between the unlinked agonists, regardless of TLR combination. This difference demonstrates that a wider range of innate immune responses are accessible by linking the agonists.

Table 3.1 Summary of Results Comparing TLR Tri-agonist Combinations, Linked (L) or Unlinked (U).

Measurement		TLR1/2_4_7*a*		TLR2/6_4_7*a*		TLR1/2_4_9*a*		TLR2/6_4_9*a*		TLR4_7_9*a*	
		L	U	L	U	L	U	L	U	L	U
***In-Vitro* Transcription Factors**	NF-κB	+	++	+++	+++	+++	++	+++	+++	++	++
	ISGs	+	++	+	++	++	++	++	++	+	++
***In-Vitro* BMDC Cytokines**	TNF-α	+	++	+	++	+++	++	+	+	++	+
	IL-12p70	-	++	-	++	++	+	-	-	+++	+
	IFN-β	-	-	-	-	+	-	+	-	++	+
	IL-10	-	+	-	-	+++	++	+	+	+++	++
	CCL2	+	+	++	+	++	++	+	+	+++	++
	IL-6	-	+	-	+	+++	++	+	+	++	++
***In-Vivo* Serum Cytokines**	TNF-α	-	-	-	+++	++	-	+++	+	-	+
	IL-6	-	++	+	+++	++	+	+	+	+	+
	IL12-p40	-	++	-	+++	++	++	+++	+++	+	++
	IFN-α	-	-	-	+	-	-	-	-	-	-
	IFN-β	-	-	-	+	-	-	-	-	-	-
	Weight Loss	-	-	-	+++	-	-	++	++	++	+

***In-Vitro* Transcription Factors:** <2x increase: -, 2-4x increase: +, 4-8x increase: ++, >8x increase: +++
Fold over negative control (if statistically significant from control)

***In-Vitro* BMDC Cytokines:**

TNF-α: 2-10 ng/mL: +, 10-20 ng/mL: ++, >20 ng/mL: +++
IL-12p70: <50 pg/mL: -, 50-200 pg/mL: +, 200-400 pg/mL: ++, >400 pg/mL: +++
IFN-β: 10-25 ng/mL: +, >25 ng/mL: ++
IL-10: <0.3 ng/mL: -, 0.3-1 ng/mL: +, 1-2 ng/mL: ++, >2 ng/mL: +++
CCL2: <2.5 ng/mL: -, 2.5-5 ng/mL: +, 5-10 ng/mL: ++, <10 ng/mL: +++
IL-6: <20 ng/mL: -, 20-50 ng/mL: +, 50-100 ng/mL: ++, >100 ng/mL: +++

***In-Vivo* Serum Cytokines:**

TNF-α & IL-6:<25 pg/mL: -, 25-100 pg/mL: +, 100-300 pg/mL: ++, >300 pg/mL: +++
IL12-p70: <200 pg/mL: -, 200-500 pg/mL: +, 200-1500 pg/mL: ++, >1500 pg/mL: +++
IFN-α & IFN-β: <60 pg/mL: -, >300 pg/mL: +

Weight loss 24 h after injection: 0-2.5% loss: -, 2.5-5.0% loss: +, 5.0-7.5% loss: ++, >7.5% loss: +++

Linked vs Unlinked Tri-agonists. Under normal physiological conditions, TLR agonists interact with immune cells while structurally organized in the pathogen's cellular architecture.[15] Although stimulating cells with soluble mixtures of TLR agonists has been demonstrated, this approach lacks the spatial association of the agonists as they are displayed on the surface and within the pathogens. Administering TLR agonist combinations that are spatially confined to a particle has shown promise in vaccine applications.[16,17] To more accurately examine the role of spatial arrangement of TLR agonists, we linked combinations of three TLR agonists and evaluated the effects of linked versus unlinked TLR agonist combinations on immune system activation.

Covalently linking TLR agonists to the tri-agonist scaffold decreases the activity of an individual TLR agonist, most likely through steric interactions with the receptor. Most agonists displayed a 10- to 50-fold decrease in NF-κB activity, which should result in drastically lower activity of the linked combination. We found that although linking three TLR agonists in some cases resulted in slightly lower activity, generally linkage had little effect (within 20% of activity in more cases). We found this result surprising as single agonists linked to the core showed dramatic decreases in activity. Therefore, linking the combination of multiple TLR agonists compensated for the loss in activity of each individual agonist.

One of the major differences we noted regarding *in vivo* administration of linked tri-agonists was their effect on systemic cytokine levels in mice. We originally hypothesized that the larger molecular weight of the tri-agonists and change in biophysical properties compared to the individual agonists would result in higher local retention of the compound, and thus lower systemic cytokines. For example, Lynn, *et al*. demonstrated that by linking TLR7*a* to a polymer, the compounds remain localized near the lymph nodes rather than in the bloodstream.[18] However, this hypothesis was not fully supported, as the linked combination resulted in higher serum cytokine levels, while in other instances those elicited by the unlinked agonists were higher. We now postulate that the level of systemic cytokines can vary between the specific combinations of tri-agonists. For example, all tri-agonists bearing TLR7*a* had higher systemic cytokines when unlinked than when linked (**Table 3.1**). TLR7*a* is known to quickly diffuse into the blood stream, causing high levels of systemic cytokines.[11,18] By linking it to a larger molecule, its systemic diffusion may be hindered. However, the only case where linkage made a notable impact on mouse weight 24 h post injection was for TLR2/6_4_7*a*. We speculate that the inflammatory properties

of free TLR7*a* and TLR2/6*a* are synergistic in this case, but this activity is suppressed when the agonists are linked.

Linked TLR tri-agonists containing TLR9*a* generally showed an increase in immune stimulatory capabilities compared to unlinked combinations. The largest difference was observed with TLR1/2_4_9*a* and TLR2/6_4_9*a,* which had drastically higher TH1-inducing cytokines compared to their unlinked counterparts (IL12p70: TLR1/2_4_9*a*: 95% increase, TLR4_7_9*a*: 900% increase). This result surprised us as many of the compounds did not show much difference in transcription factor activation. This result suggests that the increased cytokine levels may not stem from activating TLRs on the same cell (overall activity of NF-kB was similar), but perhaps helps activate distinct cell types *via* one of the attached agonists. The other two agonists might then alter the resulting cytokine profile generated by that cell type as we observed *in vitro*.

As difficult and emerging diseases continue to threaten global health, there is a pressing need for new and effective vaccine strategies. In developing these vaccine strategies, eliciting a targeted immune response tailored for the pathogen of interest is of paramount importance. TLR agonists play a major role in this development as they can direct the type of host effector responses generated during vaccination. Thus, understanding the effects of TLR agonist combinations, both linked and unlinked, is vital to furthering vaccine technologies. We presented an initial set of results showing that spatial organization can controllably, if not predictably, shape immune responses toward desired outcomes. In Chapter 4, we describe how these compounds can be used in a target subunit vaccine for Q-Fever and find that agonist conjugation helps improve immune responses in many cases, supporting this central idea. Methods to predictably tune immune responses are needed for reverse vaccinology approaches in the development of next-generation

vaccines.[19] This work provides a roadmap to the design and immune response outcome upon chemical manipulation of TLR agonist combinations to expedite vaccine development.

3.8 Experimental Methods and Materials

Reagents and Instrumentation. Buffers and media for cell culture were purchased from Fisher Life Technologies. Centrifugal Filter Devices (3k) were purchased from Millipore. Compounds were filtered using 0.22 μM nylon syringe filters (Restek). Tri-agonists were quantified using either a NanoDrop 2000c spectrophotometer or a Promega Quantus Fluorimeter E6150. RAW-Blue absorbance was measured on a Fisher Scientific MultiSkan FC. Cytometric bead array data was acquired on a ACEA Novocyte flow cytometer. Gel images were obtained using a GE Typhoon scanner. Data was analyzed using student's T test or one-way ANOVA in Graph Pad Prisim software. All values were reported as mean ± SD, where error bars represent biological replicates.

Cell Culture. RAW-Blue NF-κB and RAW-Blue ISG reporter cells were purchased from Invivogen and were cultured in D-MEM High Glucose medium (Life Technologies), 10% FBS, 2 mM L-glutamine, 200 μg/mL Zeocin (InvivoGen), and antibiotic-antimycotic (1×). Experiments were run in D-MEM High Glucose medium (Life Technologies), 10% heat inactivated FBS, 2 mM L-glutamine, and antibiotic-antimycotic (1×). Sterile phosphate buffered saline (PBS) buffer was obtained from Life Technologies.

Bone marrow derived dendritic cells (BMDCs) were harvested from the femurs of 6-week old C57BL/6 mice (Jackson Laboratory). BMDCs were cultured in BMDC primary medium: RPMI 1640 (Life Technologies), 10% heat inactivated fetal bovine serum (FBS), 20 ng/mL granulocyte-macrophage colony-stimulating factor (GM-CSF) (produced from "66" cell line), 2

mM L-glutamine (Life Technologies), antibioticantimycotic (1×) (Life Technologies), and 50 μM betamercaptoethanol (all components were 0.2 μM sterile filtered together before use).

RAW Blue NF-κB and Interferon Stimulatory Genes (ISG) Assay. RAW Blue NF-κB or ISG reporter cells were plated in 96-well plates ($1x10^5$ cells/well) in 180 μL of 10% HIFBS in DMEM. Samples at 10x concentration in 10% DMSO in water (20 μL) were added to each well. The cells were incubated with the compounds for 18 h at 37 °C. The supernatant (50 μL) was removed and combined with 150 μL of QuantiBlue solution in a new 96-well plate. The solution was incubated at 37 °C for 2 h (NF-κB) or 4 h (ISG). The absorbance of the solution at 620 nm was read by a Fisher Scientific MultiSkan FC and the data analyzed in Graph Pad Prism.

3-[4,5-dimethylthiazole-2-yl]-2,5-diphenyltetrazolium bromide (MTT) Cell Viability Assay. Cells from the RAW Blue assay after 18 h incubation were used for cell viability assay. The remaining supernatant was aspirated, and 10% HIFBS in FluoroBrite DMEM (Life Technologies, 100 μL) was added to the wells. MTT dye (10 μL at 10 mg/mL) was added to each well. The samples were left to incubate at 37 °C for 30 min. The supernatant was removed and 100 μL of DMSO was added to each well. The solution was incubated at 37 °C for 5 minutes to ensure the dye was fully dissolved. The absorbance at 440 nm was measured by a ThermoFisher Multi-Skan and the data analyzed in Graph Pad Prism.

***In vitro* cytokine analysis by cytometric bead array (CBA).** CBA mouse inflammation kit (IL-12p70, TNF-α, IFN-γ, IL-6, IL-10, and CCL2) was purchased from BD biosciences. BMDCs were plated in 48 well plates (4×10^5 cells in 400 μL) and stimulated with indicated sample for 6 h. The supernatant was transferred to Eppendorf tubes and centrifuged at 1000 x g for 10 minutes. The supernatant was removed, diluted by a factor of 5, and incubated with CBA

beads. The assay was then performed and analyzed by flow cytometry as described in the kit manual. All comparisons and conclusions are based on data from tests using the same kit.

***In vitro* cytokine analysis by ELISA.** The supernatants from the CBA study were also assessed by ELISA for IL-12p70 and IL-6. IL-12p70 and IL-6 ELISA kits were purchased from Biolegend and used according to instruction manual. Samples were undiluted for IL-12p70 or diluted by a factor of 1000 for IL-6 ELISA. Plotted values are dilution adjusted.

***In vivo* cytokine analysis by ELISA.** Groups (n=3) of 5-6 week old female C57BL/6 mice (purchased from Charles River) were injected *via* IM with indicated compounds (1 nmol adjuvants in 50 μL) while anesthetized under 2-2.5% isoflurane and 2L/min oxygen flow under standard atmospheric pressure. Mice were bled *via* facial vein 24 h prior to injection. Mice were then bled by cardiac puncture following termination with CO_2 asphyxiation and cervical dislocation 1 h or 3 h post injection. Sera samples were then analyzed by ELISA for IL-6, TNF-α, and IL-12p70 (Biolegend) according to manufacturer's instructions. All serum samples were assayed undiluted. Mice were housed in SPF facility with a 12 hour dark/light cycle with autoclaved bedding and irradiated food. All handling of mice was performed under an approved Institutional Animal Care and Use Committee protocol.

***In vivo* weight loss following tri-agonist injection.** Groups (n=5 or 8) of 5-6 week old female C57BL/6 mice (purchased from Charles River) were injected *via* IM with indicated compounds (1 nmol adjuvants in 50 μL) mixed with endotoxin free CBU_1910 (0.5 nmol, Genscript) while anesthetized under 2-2.5% isoflurane and 2L/min oxygen flow under standard atmospheric pressure. Mice were bled *via* facial vein 24 h prior to injection. Mice were weighed immediately prior to injection, and 24 h post injection. Mice were housed in SPF facility with a

12-hour dark/light cycle with autoclaved bedding and irradiated food. All handling of mice was performed under an approved Institutional Animal Care and Use Committee protocol.

3.9 References

(1) Moyer, T. J.; Zmolek, A. C.; Irvine, D. J. Beyond antigens and adjuvants: formulating future vaccines. *J. Clin. Invest.* **2016**, *126* (3), 799–808.

(2) Piccinini, A. M.; Midwood, K. S. DAMPening inflammation by modulating TLR signalling. *Mediators Inflamm.* **2010**, *2010*, 672395.

(3) Hayden, M. S.; West, A. P.; Ghosh, S. NF-κb and the immune response. *Oncogene* **2006**, *25*, 6758–6780.

(4) González-Navajas, J. M.; Lee, J.; David, M.; Raz, E. Immunomodulatory functions of type I interferons. *Nat. Rev. Immunol.* **2012**, *12*, 125–135.

(5) Tom, J. K.; Dotsey, E. Y.; Wong, H. Y.; Stutts, L.; Moore, T.; Davies, D. H.; Felgner, P. L.; Esser-Kahn, A. P. Modulation of innate immune responses via covalently linked TLR agonists. *ACS Cent. Sci.* **2015**, *1* (8), 439–448.

(6) Pulendran, B.; Ahmed, R. Translating innate immunity into immunological memory: implications for vaccine development. *Cell* **2006**, *124* (4), 849–863.

(7) Bode, C.; Zhao, G.; Steinhagen, F.; Kinjo, T.; Klinman, D. M. CpG dna as a vaccine adjuvant. *Expert Rev. Vaccines* **2011**, *10* (4), 499–511.

(8) Jin, M. S.; Kim, S. E.; Heo, J. Y.; Lee, M. E.; Kim, H. M.; Paik, S.-G.; Lee, H.; Lee, J.-O. Crystal structure of the TLR1-TLR2 heterodimer induced by binding of a tri-acylated lipopeptide. *Cell* **2007**, *130* (6), 1071–1082.

(9) Kang, J. Y.; Nan, X.; Jin, M. S.; Youn, S.-J.; Ryu, Y. H.; Mah, S.; Han, S. H.; Lee, H.; Paik, S.-G.; Lee, J.-O. Recognition of lipopeptide patterns by toll-like receptor 2-toll-like receptor 6 heterodimer. *Immunity* **2009**, *31* (6), 873–884.

(10) Katja, F.; Sabine, R.; Holger, H.; Jennifer, D.; Roland, L.; Jörg, M.; Ute, B.; Kristina, R.; Günther, J.; Karl-Heinz, W.; et al. Heterodimerization of TLR2 with TLR1 or TLR6 expands the ligand spectrum but does not lead to differential signaling. *J. Leukoc. Biol.* **2007**, *83* (3), 692–701.

(11) Wu, T. Y.-H.; Singh, M.; Miller, A. T.; De Gregorio, E.; Doro, F.; D'Oro, U.; Skibinski, D. A. G.; Mbow, M. L.; Bufali, S.; Herman, A. E.; et al. Rational design of small molecules as vaccine adjuvants. *Sci. Transl. Med.* **2014**, *6* (263), 263ra160.

(12) Longhi, M.; Trumpfheller, C.; Idoyaga, J.; Caskey, M.; Matos, I.; Kluger, C.; Salazar, A.; Colonna, M.; M Steinman, R. Dendritic cells require a systemic type I interferon response to mature and induce CD4+ TH1 immunity with poly ic as adjuvant. *J. Exp. Med.* **2009**, *206* (7), 1589–1602.

(13) Garcia-Cordero, J. L.; Nembrini, C.; Stano, A.; Hubbell, J. A.; Maerkl, S. J. A high-throughput nanoimmunoassay chip applied to large-scale vaccine adjuvant screening. *Integr. Biol.* **2013**, *5* (4), 650–658.

(14) Wenink, M. H.; Santegoets, K. C. M.; Broen, J. C. A.; van Bon, L.; Abdollahi-Roodsaz, S.; Popa, C.; Huijbens, R.; Remijn, T.; Lubberts, E.; van Riel, P. L. C. M.; et al. TLR2 promotes TH2/TH17 responses via TLR4 and TLR7/8 by abrogating the type I IFN amplification

loop. *J. Immunol.* **2009**, *183* (11), 6960 LP – 6970.
(15) Mogensen, T. H. Pathogen recognition and inflammatory signaling in innate immune defenses. *Clin. Microbiol. Rev.* **2009**, *22* (2), 240–273.
(16) Kasturi, S. P.; Skountzou, I.; Albrecht, R. A.; Koutsonanos, D.; Hua, T.; Nakaya, H. I.; Ravindran, R.; Stewart, S.; Alam, M.; Kwissa, M.; et al. Programming the magnitude and persistence of antibody responses with innate immunity. *Nature* **2011**, *470*, 543–547.
(17) Kuai, R.; Sun, X.; Yuan, W.; Ochyl, L. J.; Xu, Y.; Hassani Najafabadi, A.; Scheetz, L.; Yu, M.-Z.; Balwani, I.; Schwendeman, A.; et al. Dual TLR agonist nanodiscs as a strong adjuvant system for vaccines and immunotherapy. *J. Control. Release* **2018**, *282*, 131–139.
(18) Lynn, G. M.; Laga, R.; Darrah, P. A.; Ishizuka, A. S.; Balaci, A. J.; Dulcey, A. E.; Pechar, M.; Pola, R.; Gerner, M. Y.; Yamamoto, A. In vivo characterization of the physicochemical properties of polymer-linked TLR agonists that enhance vaccine immunogenicity. *Nat. Biotechnol.* **2015**, *33*, 1201–1210.
(19) Bonam, S. R.; Partidos, C. D.; Halmuthur, S. K. M.; Muller, S. An overview of novel adjuvants designed for improving vaccine efficacy. *Trends Pharmacol. Sci.* **2017**, *38* (9), 771–793.

CHAPTER 4

In Vivo Activity of TLR Tri-agonist Panel and Challenge Study Results

4.1 Introduction

Inactivated whole-organism vaccines stimulate both innate and adaptive immunity and do not require additional adjuvants to induce a robust and long-lasting immune memory. However, whole-organism vaccines for some diseases can cause adverse events in previously exposed or immunized individuals.[1–3] Subunit formulations based on recombinant proteins are a safer alternative for use in both immunocompetent and immunocompromised patients.[4–6] The antigens used in subunit vaccines do not induce adverse inflammatory responses, but they struggle to stimulate robust immune responses. The low immunogenicity of these antigens necessitates the use of adjuvants in subunit vaccine formulations. Selecting the appropriate antigens and adjuvants to induce a protective response toward a particular organism remains a challenge. Here, *Coxiella burnetii* was selected as the target pathogen to test the efficacy of the TLR tri-agonists as adjuvants in a subunit vaccine. Thus we hypothesized that an effective *C. burnetii* could be developed using the appropriate tri-agonists needed to generate the correct immune response to target appropriate *C. burnetii* antigens.

The addition of adjuvants, such as TLR agonists, to subunit vaccine formulations has many benefits as discussed in Chapter 1. TLR agonists are naturally present in heat-killed or attenuated whole-cell vaccines and are responsible for stimulating the innate immune system's response to the immunizing pathogen.[7] In fact, pathogens contain distinct TLR agonist combinations which stimulate tailored responses suited for combating the infection.[8] Including adjuvants in subunit vaccine formulations is necessary to generate immune responses against the antigen.[9] Different TLR agonists activate immune responses synergistically when administered simultaneously,

improving the efficacy of the vaccine.[10] However, small molecule TLR agonists may cause systemic toxicity due to rapid diffusion from the site of injection but can be overcome through conjugation to other chemical moieties or polymers.[11,12]

To circumvent these challenges, we linked different combinations of three TLR agonists to mimic their spatial organization on a pathogen to generate unique and distinct innate immune responses, as described in Chapters 2 and 3. Here, we evaluate the ability of these TLR tri-agonists to stimulate protective antigen-specific immune responses in subunit vaccine formulations *in vivo*. We chose *Coxiella burnetii* due to the lack of FDA approved vaccines and the need for improved responses in subunit formulations.

C. burnetii, the etiologic agent of Q-fever, is a category B bioterrorism agent that is easily aerosolized and has a single bacterium infectious dose.[13,14] The only licensed human vaccine against *C. burnetii* is Q-Vax®, a formalin-inactivated whole bacteria vaccine approved for use in Australia and some European countries (Fig. 1A). Individuals previously exposed or vaccinated against *C. burnetii* can have severe hypersensitivity reactions, necessitating pre-screening by serology and a skin test for previous sensitization to C. burnetii proteins prior to immunization with Q-Vax®.[3] The potential adverse response to immunization, general impracticalities presented by Q-Vax® immunization, and lack of FDA approval are major concerns given the potential of *C. burnetii*'s use as a bioterrorism agent. Thus, there is a critical need to develop a protective, but non-reactogenic, vaccine against this bacterium.

In these studies, we evaluated the adjuvant activity of a library of TLR tri-agonists in subunit vaccines formulated with recombinant *C. burnetii* antigens (**Fig. 4.1**). We characterized the ability of our novel adjuvant platform to stimulate robust, antigen specific adaptive immune responses in *in vivo* immunogenicity studies and evaluated the functional efficacy of these responses in a live

C. burnetii aerosol challenge model in mice. Given the reactogenicity, safety, and implementation issues associated with Q-Vax®, we chose to take a subunit vaccine approach to develop our vaccine candidates against *C. burnetii*. From these studies, we identified multiple vaccine candidates, formulated with specific TLR tri-agonist combinations, that conferred signs of protection against a live *C. burnetii* challenge. The experiments described in this chapter were performed in collaboration with the Felgner and Burkhardt Labs, as well as USAMRIID.

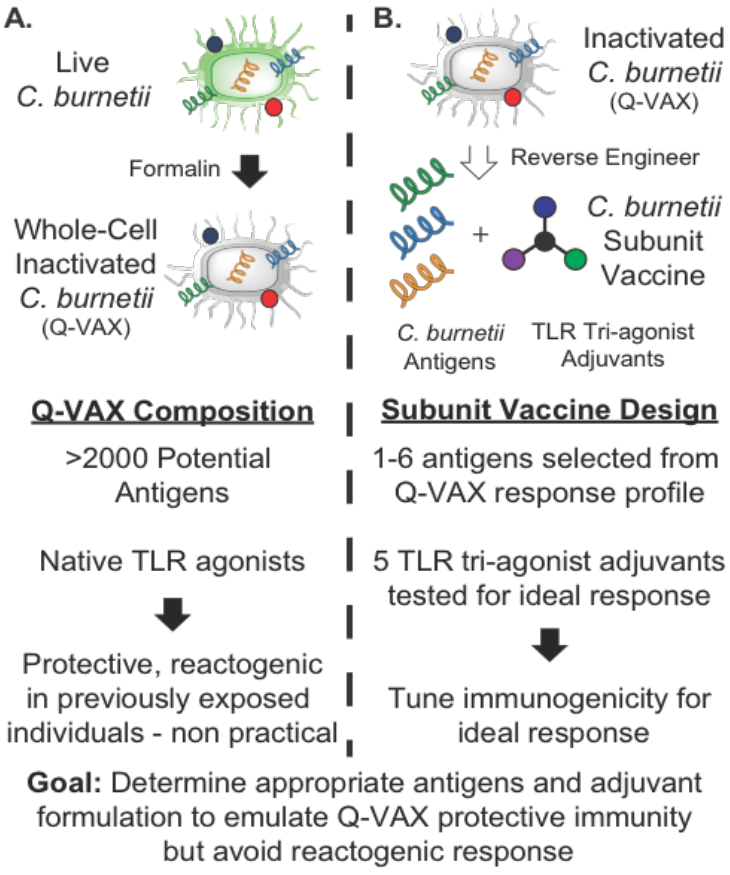

Figure 4.1 Comparison of Q-Vax and Our Subunit Vaccine Design. A) Q-Vax® is a formalin-inactivated *C. burnetii* whole-cell vaccine composed of thousands of proteins and several immunostimulants. B) Our goals are to emulate the protective response of the vaccine, while avoiding the reactogenicity associated with Q-Vax® with a subunit vaccine.

4.2 Subunit Vaccine Antigen Selection

The first goal was to identify immunogenic *C. burnetii* antigens that could be included in our vaccine formulations. Previously published literature identified several *C. burnetii* antigens that stimulate robust antigen specific humoral immune responses in a naturally infected human patient population.[15–17] The *C. burnetii* outer membrane protein CBU_1910, or COM1, was the dominant antigen identified many of these studies, including ours.[15–18] We also wanted to identify the antigen specific humoral response stimulated by immunization with Q-Vax®, since this vaccine is known to confer protection to immunized individuals and in mice. To accomplish this we immunized naive C57BL/6 mice with Q-Vax® and analyzed the antigen specific antibody response elicited 28 days post immunization (Fig. 2A) using a *C. burnetii* protein microarray. Despite immunization with a whole-cell vaccine containing over 2000 potential antigens, the antibody response was against few antigens (6 antigens >5000 signal intensity) from the *C. burnetii* proteome (**Fig. 4.2**). Furthermore, the only bacterial protein that generated robust and consistent antibody responses across all five immunized animals was CBU_1910, with an average signal intensity at least 3.4 fold higher than any other antigen (**Fig. 4.2**). In addition, the antibodies generated to CBU_1910 were completely IgG2c biased (**Fig. 4.2D and E**). Due to its relevance in human *C. burnetii* infections and the protective vaccine, we selected CBU_1910 as the antigen for immunogenicity testing in formulations with our novel TLR tri-agonist adjuvants.

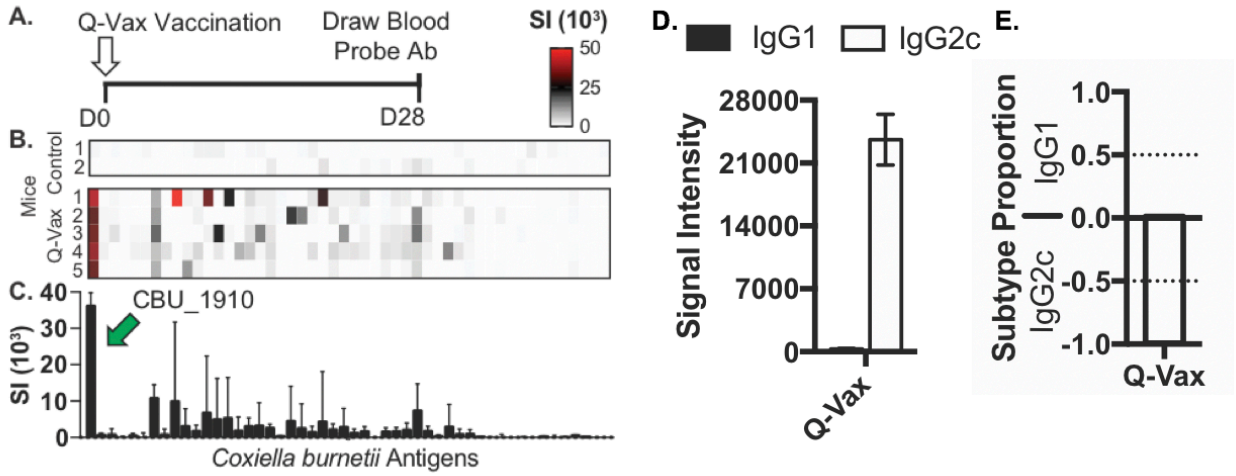

Figure 4.2 Q-VAX® Antigen Immunogenicity Analysis *via* Protein Microarray. A) Vaccination protocol of mice n = 5 B) Heat map of protein microarray antibody titers, antigens are along the x-axis. C) Graphical representation of antibody signal intensity (SI) on protein from Q-Vax® vaccination. D) Intensity and E) ratio of IgG1 and IgG2c CBU_1910 specific serum antibodies as measured by protein microarray from the serum of Q-Vax vaccinated mice 28 days post vaccination, n = 4. For the full data set, see **Fig. 4.10**.

4.3 Preliminary TLR Tri-Agonist Vaccine Candidate

In our first vaccine candidate, we formulated CBU_1910 with TLR2/6_4_7 tri-agonist (TLR2/6_4_7*a*). Our preliminary *in vitro* and *in vivo* studies indicated that this TLR tri-agonist activates dendritic cells and did not stimulate long lasting serum cytokines following immunization in the linked form (see **Chapter 3**), an indication of low systemic adjuvant-induced toxicity. We immunized cohorts of C57BL/6 mice intramuscularly (i.m.) on day 0 followed by a boost of the identical formulation on day 14. We then collected sera and draining lymph nodes at the completion of the experiment on day 21 post immunization (**Fig. 4.3A**). Experimental animals received either CBU_1910 with the TLR tri-agonist in either the linked (blue bars) or unlinked (orange bars) form to evaluate whether the physical linking of the three TLR agonists affected their immunomodulatory activity. Compared to PBS alone, the linked and unlinked TLR2/6_4_7*a* stimulated a significant expansion of $B220^{+}$ cells (2.5 fold and 3.1 fold increase, respectively) in

the draining lymph nodes (**Fig. 4.3B**). This expansion of B cells in the draining lymph nodes correlated with the increased production of IgG, which we detected in the sera on day 21 (**Fig. 4.3C**). We analyzed the CBU_1910 specific antibody response to immunization and detected both IgG1 and IgG2c antibody subtypes specific for the immunizing antigen in animals that received both the linked and unlinked forms of TLR2/6_4_7*a* (**Fig. 4.3C**). These two IgG subtypes provide insight into the type of T cell responses generated in response to immunization; IgG2c suggests a TH1-type, or inflammatory, T cell response and IgG1 suggests a TH2, or humoral biasing, T cell response.[19] CBU_1910 alone stimulated a low antigen specific IgG1 response and no IgG2c CBU_1910 specific antibodies following immunization. This suggests that this antigen is not inherently immunogenic and requires adjuvants to stimulate immune responses. Linked and unlinked TLR2/6_4_7*a* generated similar levels of CBU_1910 specific IgG1 antibody. However, the unlinked tri-agonist generated 2.1 fold higher IgG2c than the linked TLR tri-agonist, although the difference was not statistically significant **(Fig. 4.3C**). Previous studies suggest that T cell responses (TH1), in addition to B cell responses, are important for the protection against and clearance of *C. burnetii*.[20,21] Although the antibody response in this case skewed toward IgG1, vaccines adjuvanted with linked or unlinked TLR2/6_4_7*a* resulted in a significant increase in $CD4^+$ (1.6 fold and 1.7 fold increase, respectively) and $CD8^+$ (1.7 fold and 1.8 fold increase, respectively) T cells in the draining lymph node (**Fig. 4.3B**).

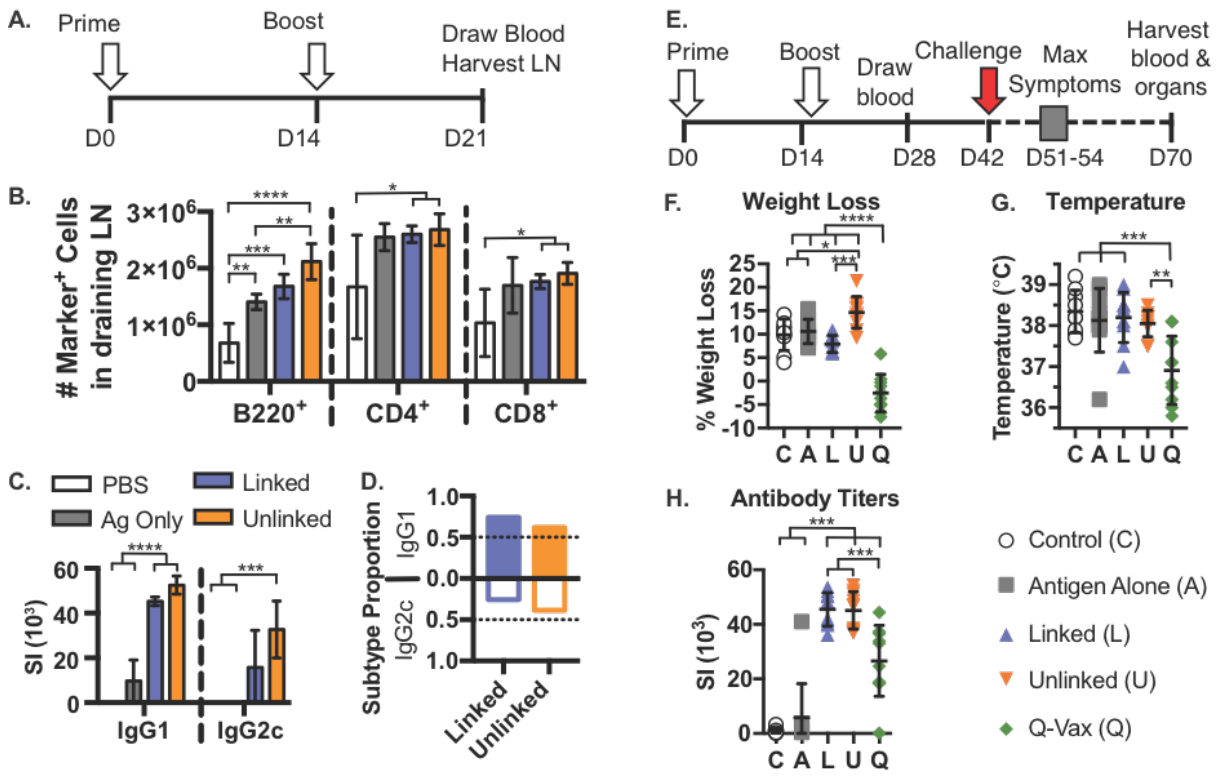

Figure 4.3 TLR2/6_4_7*a* Adjuvanted CBU_1910 Vaccine Efficacy. A) Vaccination schedule for immunogenicity assessment n = 5. B) Total counts of cells found in draining lymph node on d21 following vaccination. C) Signal intensity (SI) and D) calculated proportions of subtypes of antibodies upon vaccination with TLR2/6_4_7*a* and CBU_1910. E) Vaccination schedule for challenge study against aerosolized C. burnetii, n = 10. F) Percent weight loss and G) body temperature 10 days post vaccination. H) Total IgG signal intensity on d 28 post vaccination as measured by protein microarray. Statistical analysis: one-way ANOVA, *: $p < 0.05$, **: $p < 0.01$, ***: $p < 0.001$, ****: $p < 0.0001$.

We next evaluated the CBU_1910 vaccine candidates adjuvanted with linked or unlinked TLR2/6_4_7*a* in a live *C. burnetii* aerosol challenge model. For this experiment, we followed the same vaccination schedule used in our immunogenicity studies (**Fig. 4.3E**): cohorts of C57BL/6 mice received a prime immunization on day 0 followed by a boost on day 14. Blood was collected on day 28 for serum antibody analysis. On day 42, sera was collected before each cohort was challenged with aerosolized *C. burnetii*. In this model, animals should exhibit symptoms of infection between days 51 to 54 (9-12 days post-challenge). The experiment was terminated on day 70 (28 days post-challenge) and sera and tissue were collected to analyze the efficacy of our

vaccine candidates. A cohort of animals received Q-Vax® as a positive control for vaccine efficacy. The animals from each cohort were weighed and their temperature measured daily, as weight loss and fever can be used to monitor an animal's clinical response to a *C. burnetii* challenge (**Fig. 4.11 A and B**).[22–24] As expected, the animals that received PBS (C) or antigen only (A) immunizations lost weight in response to the C. burnetii challenge, especially on day 10 (9.9 % and 10.6 % loss, respectively) post-challenge (**Figs. 4.3F and G**). Q-Vax® immunized mice (Q) continued to gain weight throughout the study, as expected.[25,26] However, it was observed that mice immunized with the linked TLR2/6_4_7*a* (L) had minimal weight loss (d10: 7.9% loss) in comparison to the cohort that received the unlinked (U) TLR agonists (d10: 14.6% loss) (**Fig. 4.3F**) in response to *C. burnetii* challenge. Animals in both our TLR tri-agonist cohorts generated robust anti-CBU_1910 antibody responses to immunization prior to challenge, which were both significantly higher than the anti-CBU_1910 response generated by Q-Vax® immunization (**Fig. 4.3H**). This potentially indicated a better efficacy of the linked agonists compared to the unlinked agonists in the challenge model. We were unable to detect significantly lower levels of *C. burnetii* in the organs of any of the challenged cohorts by PCR (**Fig. 4.11C**). This is likely because the bacteria had been cleared at the time the tissues were collected 28 days post-challenge.[22,27] In addition, the only group that showed significantly lower organ weight following challenge was Q-Vax (**Fig. 4.11D**). These data indicate that the linked TLR2/6_4_7*a* tri-agonist is capable of generating antigen specific antibodies in response to immunization but does not confer protection in response to *C. burnetii* challenge. These data suggest the linked TLR2/6_4_7*a* is not the ideal adjuvant for use in vaccine candidates against *C. burnetii* when compared to Q-Vax® immunized mice that did not lose weight in response to challenge.

We hypothesized that in order to achieve better protection, we would need to emulate the

immune response type generated by Q-Vax®. One potential difference, noted above, was that mice immunized with TLR2/6_4_7*a* adjuvanted CBU_1910 vaccines generate predominately TH2 biased antibody responses, in contrast to Q-Vax® induced responses, which are predominantly TH1 biased (**Fig 4.2**). Therefore, we began characterizing the immunogenic activity of additional TLR tri-agonists with the goal of identifying a formulation that stimulated a more TH1 biased immune response.

4.4 Immunogenicity Screening of a TLR Tri-Agonist Panel

As detailed in Chapter 2, we synthesized four additional unique TLR tri-agonists to be evaluated for their immunogenic activity, specifically focusing on antigen specific IgG subtypes, and T cell responses elicited in response to immunization. CBU_1910 was the model immunizing antigen for all of these studies and we followed the same vaccination protocol as our prior experiments, with each cohort receiving a prime and boost immunization. The resulting immune responses were then evaluated at the termination of the experiment on day 21. All of the TLR tri-agonists generated CBU_1910 specific B and T cell responses to immunization (**Fig. 4.4**). As we observed in the TLR 2/6_4_7*a* immunogenicity studies, some of the linked and unlinked TLR tri-agonists generated distinct CBU_1910 specific humoral responses (**Fig. 4.4A**). Linked TLR1/2_4_7*a* generated relatively weak anti-CBU_1910 IgG1 (72% less) and IgG2c (79% less) antibodies compared to the unlinked form (**Fig. 4.4A**). Similar to TLR2/6_4_7*a*, the antibody profile was skewed toward TH2, IgG1 antibodies (26% IgG2c linked, 32% IgG2c unlinked) (**Fig. 4.4B**). Linked and unlinked TLR2/6_4_9*a* elicited the most IgG1 antibodies compared to the other combinations by at least a factor of 1.7. However, linked TLR2/6_4_9*a* elicited a 2.0 fold increase in IgG2c antibodies over the unlinked combination (**Fig. 4.4A**). This difference resulted in 46%

IgG2c-skewed profile with linked TLR2/6_4_9*a* compared to 31% IgG2c-skewed profile with the unlinked combination (**Fig. 4.4B**) Although lower in signal intensity, linked and unlinked TLR1/2_4_9*a* behaved similarly to TLR2/6_4_9*a* (52% IgG2c linked, 43% IgG2c unlinked). The linked and unlinked forms of the TLR4_7_9*a* generated some of the least robust antigen specific antibody responses out of all five TLR tri-agonist combinations we analyzed *in vivo* (**Fig. 4.4A**). However, both linked and unlinked TLR4_7_9*a* skewed the IgG1:IgG2c ratio the furthest towards IgG2c (60% and 64% IgG2c, respectively), suggesting this TLR tri-agonist preferentially stimulates TH1 responses to immunization (**Fig. 4.4B**). This was the only TLR tri-agonist of the five in our library that exhibited this property.

To directly analyze antigen specific T cell responses to immunization with these TLR tri-agonist adjuvanted vaccines, we evaluated IL-4 and IFN-γ production by splenocytes restimulated with CBU_1910, using ELISpot. IL-4 is a classical TH2 cytokine that stimulates humoral responses.[28] IFN-γ is produced by inflammatory T cells in response to stimulation with their cognate antigen and is indicative of TH1 CD4 T cell and CD8 T cell responses to immunization.[28,29] In line with the robust antibody responses observed in **Fig. 4.4A**, we found that T cells from cohorts immunized with each of the TLR tri-agonist combinations produced IL-4 in response to re-stimulation with CBU_1910 (**Fig. 4.4C**). However, only cohorts immunized with TLR4_7_9*a* generated IFN-γ producing T cells (**Fig. 4.4C**). In addition, the linked TLR4_7_9*a* elicited significantly more IFNy producing T cells (1.9 fold higher) compared to the unlinked combination (**Fig. 4.4C**).

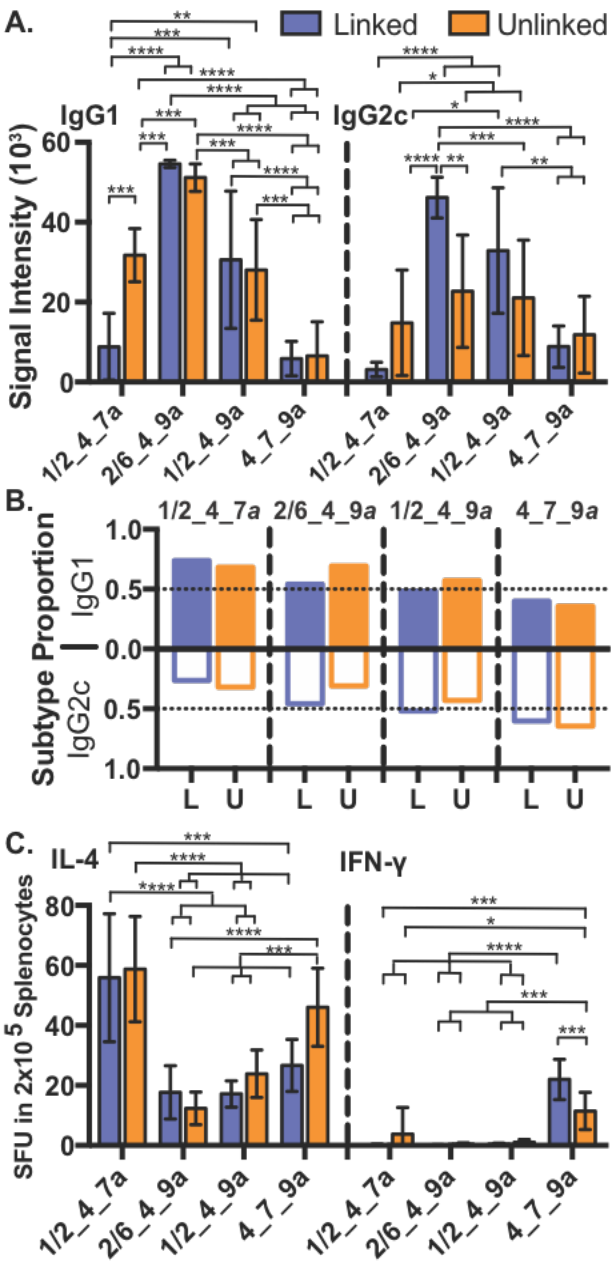

Fig. 4.4 Immunogenicity Screen of TLR Tri-Agonist Panel. A) Antibody signal intensity from protein microarray analysis. B) Calculated proportions of antibody subtypes. C) Spot forming units (SFU) of indicated cytokines upon antigen recall of splenocytes by ELISPOT. Statistical analysis: one-way ANOVA, *: $p < 0.05$, **: $p < 0.01$, ***: $p < 0.001$, ****: $p < 0.0001$.

4.5 Generating Vaccine Candidates with Additional Antigens and Emulsions

Based on the *in vivo* immunogenicity analysis of our expanded TLR tri-agonist library, we focused on optimizing the TLR tri-agonist TLR4_7_9*a* because of its TH1 skewing activity (**Fig.**

4.4). We adjusted two of our TLR tri-agonist formulations to include AddaVax™ to determine whether this could overcome the TH2 skewing activity of our adjuvants. We specifically chose TLR2/6_4_7*a* and TLR4_7_9*a* due to their opposing T cell skewing activity we observed in our previous experiments. AddaVax™ is an MF59-like squalene oil-in-water emulsion adjuvant with known TH1 and TH2-skewing properties.[30,31] We hypothesized that the inclusion of AddaVax™ in these two TLR tri-agonist adjuvanted vaccine formulations could aid in our efforts to further skew the resulting immune responses towards TH1 responses while maintaining the antigen specific antibody responses. Formulation of TLR2/6_4_7*a* with AddaVax™ increased the CBU_1910-specific IgG1 response by 38%, to match that of AddaVax™ alone (**Fig. 4.5A**). However, the antibody response was further skewed towards IgG2c when TLR2/6_4_7a was included with AddaVax™ compared to formulations with only AddaVax™ and CBU_1910 (**Fig. 4.5B**). The inclusion of AddaVax™ in TLR4_7_9*a* adjuvanted vaccines also resulted in IgG1 production similar to CBU_1910 formulated with only AddaVax™ (**Fig. 4.5C**), much higher than CBU_1910 adjuvanted with only TLR4_7_9*a* (**Fig. 4.5a**). However, including either linked TLR4_7_9*a* with AddaVax™ resulted in significantly higher production (92-114% increase) of IgG2c (**Fig. 4.5C**). As a result of the increased IgG2c, the ratio of IgG1:IgG2 became more balanced (57% IgG2c with linked TLR4_7_9a, **Fig. 4.5D**) compared to CBU_1910 formulated with only AddaVax™ .

As we observed that high, IgG1 biased antibody titers against CBU_1910 were insufficient for protection (**Fig. 4.3H**), we sought to include the other *C. burnetii* antigens that were immunogenic in Q-Vax®. We generated vaccine formulations including multiple *C. burnetii* antigens, an approach that has achieved better vaccine protection in other disease models compared to individual antigens alone (**Fig. 4.3F-H**).[32–35] We added three additional *C. burnetii* antigens to

our CBU_1910 vaccine formulations (CBU_0545, CBU_0630, and CBU_0370). These antigens were identified from our Q-Vax® immunized mice serum (**Fig. 4.2**) and from human patients that were either acutely or chronically infected with *C. burnetii* at the time their serum was collected.[15–17] We considered antigens that generated robust humoral immune responses to either vaccination or infection as candidates to be included in our vaccine formulations. In formulations adjuvanted with TLR2/6_4_7*a* and AddaVax™, IgG1 and IgG2c antigen-specific responses were detected against all four immunizing antigens (**Fig. 4.5E**). Importantly, the antibody responses detected in animals immunized with a single antigen was not significantly different when animals were immunized with all four antigens concurrently (**Fig. 4.5E**). This result suggests that the inclusion of multiple *C. burnetii* antigens in our vaccines should have an additive immune benefit and that a single antigen does not dominate or interfere with the immune response to the other antigens in the vaccine formulation. With the exception of CBU_0307, all of the antigen specific antibody responses generate a balanced IgG1:IgG2 response (**Fig. 4.5F**). These optimization studies indicated that a polyvalent vaccine would result in a broader immune response, potentially leading to a more efficacious vaccine formulation in challenge studies.

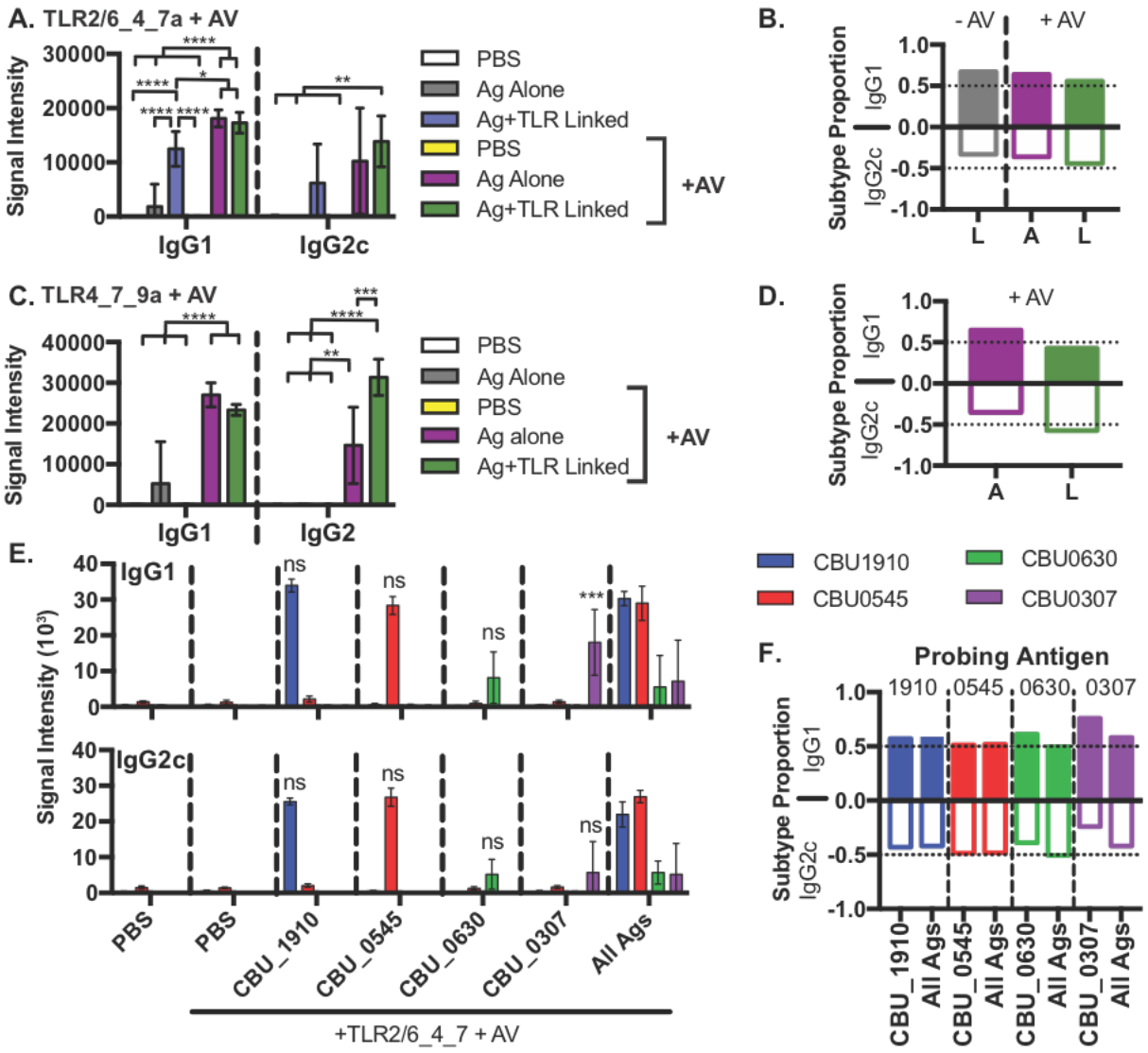

Figure 4.5 Immunogenicity Analysis Upon Addition of AddaVax™ Emulsion and of Multiple Antigens. A) Signal intensity and B) calculated proportions of subtypes of antibodies upon vaccination with TLR2/6_4_7*a*, CBU_1910, and AddaVax™. C) Signal intensity and D) calculated proportions of subtypes of antibodies upon vaccination with TLR4_7_9*a*, CBU_1910, and AddaVax™. E) Signal intensity and F) calculated proportions of antibody subtypes of antibodies upon vaccination with TLR2/6_4_7*a*, four antigens, and AddaVax™. Statistical analysis: one-way ANOVA, *: $p < 0.05$, **: $p < 0.01$, ***: $p < 0.001$, ****: $p < 0.0001$. A=Antigen alone, L=Linked TLR tri-agonist, U=Unlinked TLR tri-agonist.

4.6 Evaluation of Lead Vaccine Candidate Immunogenicity

Our immunogenicity studies (**Fig. 4.4**) and previous *in vitro* studies (**Chapter 3**) suggested that from the adjuvants in our library, the linked forms of TLR4_7_9*a* and TLR1/2_4_9*a* would elicit the strongest TH1 biased immune responses to immunization, while maintaining antigen specific antibody responses. We combined each of these TLR tri-agonists with AddaVax™ and six *C. burnetii* antigens (CBU_1910, CBU_0545, CBU_0630, CBU_0370, CBU_0612 and CBU_0891) and evaluated the antigen specific responses elicited in response to immunization to whether the responses were additive. Similar to what we had observed in our initial (4-plex) multi-antigen vaccine formulation (**Fig. 4.5E**), these 6-plex vaccines stimulated antigen-specific antibody responses to all 6 antigens (**Fig. 4.6A**), although CBU_0307 and CBU_0612 did not elicit robust antibody responses. We observed that the magnitude of the antibody response and the specific IgG subtype profile elicited in response to immunization was dependent on the TLR tri-agonist adjuvant in the formulation. The antibody response generated against CBU_0307 provided the clearest measure of the change mediated by our TLR tri-agonist adjuvants (Fig. 6A, purple column). With TLR4_7_9*a* we observed a statistically significant antigen-specific IgG2c humoral response against CBU_0307, but this response is significantly blunted in the vaccine formulation adjuvanted with TLR1/2_4_9*a*. When these antigens were formulated with TLR4_7_9*a*, the antibody response was skewed more strongly towards an IgG2c response (94%), compared to TLR1/2_4_9a (78%) (**Fig. 4.6A and B**). The humoral response to CBU_1910 and CBU_0891 was not influenced by our TLR tri-agonist adjuvant system (**Fig. 4.6A and B**). In addition, both of the tri-agonist formulations led to a significant expansion of $B220^+$ B cells (TLR4_7_9*a*: 5.5, TLR1/2_4_9*a*: 4.9 fold increase), $CD4^+$ (TLR4_7_9*a*: 2.8, TLR1/2_4_9*a*: 2.6 fold increase), and $CD8^+$ (TLR4_7_9*a*: 3.0, TLR1/2_4_9*a*: 2.9 fold increase) T cells in the draining lymph nodes in

response to immunization (**Fig. 4.6C**). Compared to each other, these TLR tri-agonists elicited similar numbers of immune cells in the draining lymph nodes (**Fig. 4.6C**). In summary, these two formulations elicit robust, TH1 biased immune responses toward several antigens, which we hypothesized would result in a more efficacious immune response in a live *C. burnetii* aerosol challenge model guiding us to use a multi-antigen approach for all vaccine candidates. We adjusted the antigen mixture, however, as CBU_0612 was non-immunogenic and CBU_0630 could not be produced on sufficient scale for all further experiments. We substituted CBU_1398 as it addressed both issues (data not shown).

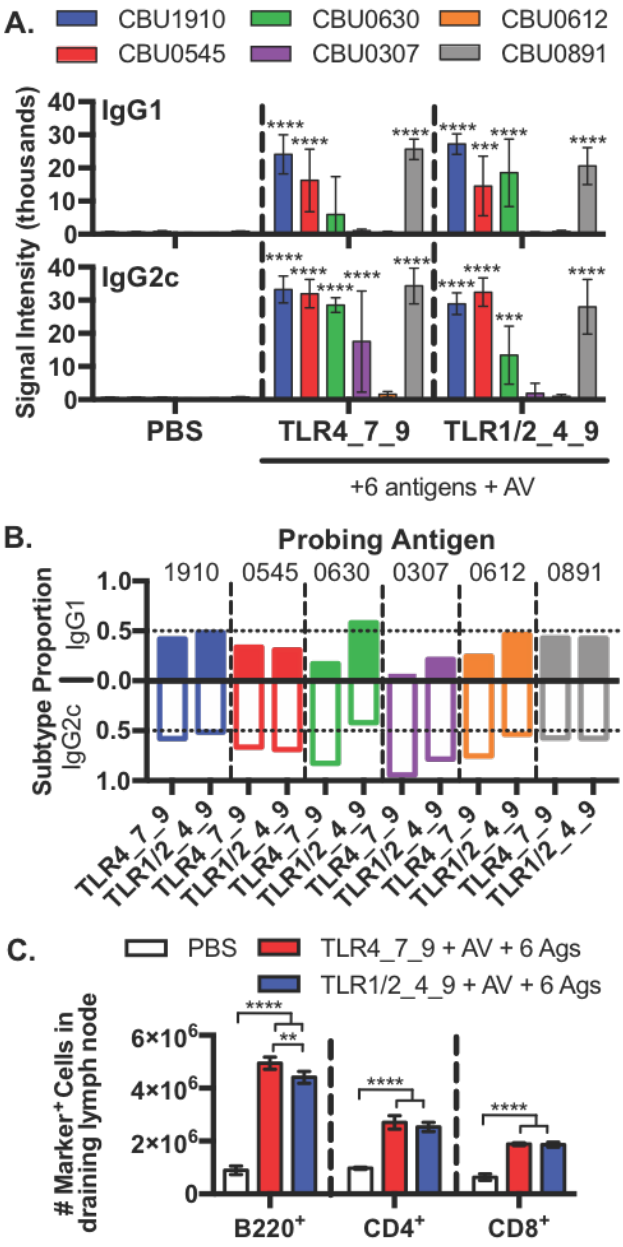

Figure 4.6 Immunogenicity Assessment of Optimized Vaccine Candidates. A) Signal intensity and B) calculated proportions of subtypes of antibodies upon vaccination with AddaVax™ (AV), six antigens and either TLR1/2_4_9*a* or TLR4_7_9*a*. C) Total counts of immune cells found in draining lymph node on d 17 following vaccination, n=5. Statistical analysis: one-way ANOVA, *: $p < 0.05$, **: $p < 0.01$, ***: $p < 0.001$, ****: $p < 0.0001$.

4.7 Efficacy Valuation of Lead Candidate Vaccines in Live *C. burnetii* Aerosol Challenge Model

Following the optimization of our two lead vaccine candidates (**Fig. 4.6**), we tested their protective efficacy in a live *C. burnetii* aerosol challenge model. We followed the same immunization protocol as our initial challenge model (**Fig. 4.3E**) and immunogenicity studies (**Fig. 4.3A**). For this experiment we split the cohort of 10 animals into two groups and terminated half the cohort on day 9 post-challenge, when the peak of infection should occur, in an attempt to evaluate changes in bacterial load due to immunization using PCR (**Fig. 4.7A**). The other half of each cohort was terminated 28 days post-challenge and similarly evaluated for changes in bacterial load (**Fig. 4.7A**). Following the challenge on day 42, animals from each cohort were monitored daily for changes in weight and body temperature. Similar to our previous challenge study (**Fig. 4.3E-H**), a Q-Vax® immunized cohort was the positive control for protective efficacy. On day 9 post-challenge (day 51 of the experiment) only the Q-Vax® immunized mice were fully protected from weight loss in response to the live *C. burnetii* challenge (**Fig. 4.7B**). However, the two tri-agonist vaccinated groups appeared to gain weight back faster than the PBS group (**Fig 4.12A**). In addition, animals immunized with the 5 antigen mix and TLR4_7_9*a* adjuvanted formulations exhibited significantly lower fever compared to the PBS immunization cohort (**Fig. 4.7C**).

PCR analysis revealed promising signs of protection with the TLR tri-agonist adjuvanted vaccine candidates. The day 9 bacterial load in spleens and lungs in animals that received our vaccine candidates was significantly reduced. However, TLR4_7_9*a* adjuvanted formulation conferred better protection (spleen: 8.3 fold less, lung: 4.3 fold less than PBS) as evidenced by the significant reduction in bacterial genomes detected compared to TLR1/2_4_9*a* adjuvanted formulation (spleen: 4.7 fold less, lung: 3.5 fold less than PBS) (**Fig. 4.7D and E**, blue diamonds

vs red inverted triangles). Although Q-Vax® results in more profound decreases in bacterial burden compared to PBS (spleen: 93.2 fold less, lung: 7.2 fold less), importantly, we could not detect significant differences between the bacterial burden in our TLR tri-agonist adjuvanted formulations compared to Q-Vax® (**Fig. 4.7D and E**, blue diamonds and red inverted triangles vs green triangles). By day 28, none of the vaccinated group showed statistically different levels of *C. burnetii* by PCR of organs (**Fig. 4.12D**) The TLR tri-agonist containing formulations generated robust antigen specific antibody responses to each antigen in the vaccine (**Fig. 4.7F**) and were either IgG1:IgG2c balanced or IgG2c biased (**Fig. 4.7G**). In line with our hypothesis that IgG2c responses are more protective in *C. burnetii* challenge, we observed that Q-Vax® immunization generated a strongly IgG2c biased (95% IgG2c) antibody response to CBU_1910 and almost no IgG1 (**Fig. 4.7F**). However, only the Q-Vax vaccinated group showed statistically lower spleen weight on day 9 and 28 following challenge (**Fig 4.12E**). Taken together, these data strongly support our findings that TLR4_7_9*a* and TLR1/2_4_9*a* adjuvanted formulations are capable of generating IgG2c skewing immune responses following immunization, and that these responses confer partial protection against a live *C. burnetii* challenge.

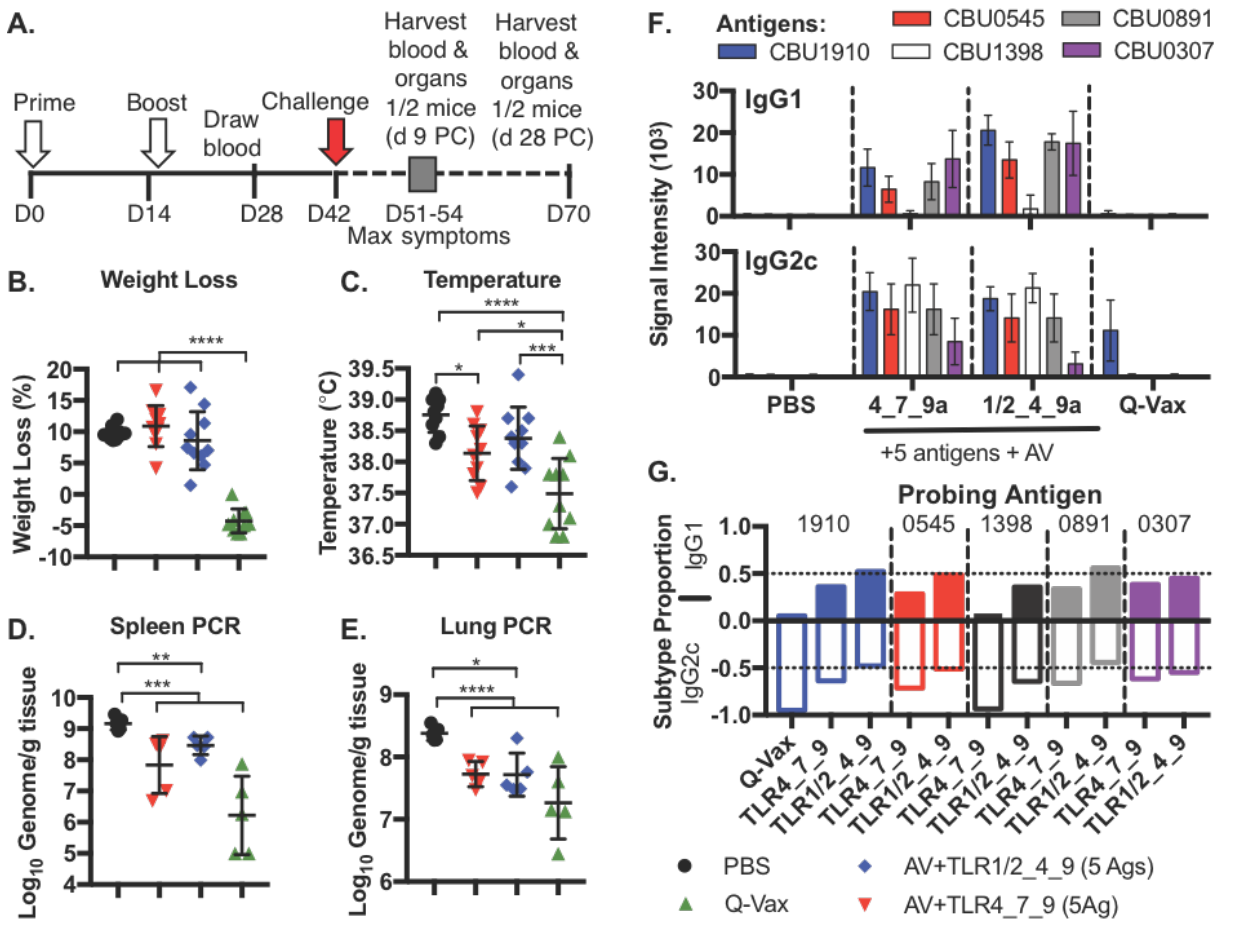

Figure 4.7 Challenge Study of TLR4_7_9*a* and TLR1/2_4_9*a* Adjuvanted Vaccines. A) Vaccination schedule for immunogenicity assessment n = 10. Percent weight loss compared to day of challenge B) and body temperature C) of mice on d 51 (d9 post-challenge). qPCR of *C. burnetii* gene marker from harvested spleens D) and lungs E) from mice on d 51, n = 5. Signal intensity of antibodies generated against immunizing *C. burnetii* antigens F) and corresponding subtype ratios G). Statistical analysis: one-way ANOVA, *: $p < 0.05$, **: $p < 0.01$, ***: $p < 0.001$, ****: $p < 0.0001$. AV=AddaVaxTM.

4.8 Future Directions: Human Compatible TLR4_7_9*a*

For our next steps, we are interested in testing the efficacy and reactogenic responses of our vaccine formulations in guinea pigs and non-human primates. However, one issue is that the TLR9*a* used in this study (CpG1826) is mouse specific. Thus, we have to substitute the TLR9a with a human specific sequence. Recently, HEPSILAV-B was approved which contains the human and mouse reactive TLR9a, CpG1018.[36] Since CpG1018 is FDA approved in a vaccine, has a

suitable safety profile, can activate human TLR9, we selected this TLR9*a* sequence for our human compatible TLR tri-agonists.

To date, we have successfully synthesized and purified a human compatible TLR4_7_9*a* while efforts to synthesize a human compatible TLR1/2_4_9*a* are ongoing. With the lessons learned in the work described in Chapter 2, the final synthetic step (CuAAC of azide-TLR9*a* and TLR4_7*a*) was improved. The optimization of reliable analytical techniques to monitor the reaction allowed us to ensure the azide-TLR9*a* was fully consumed to yield TLR4_7_9*a*. Following reaction completion, the tri-agonist could be purified using spin filtration. The final product was recovered, sterile filtered, and characterized.

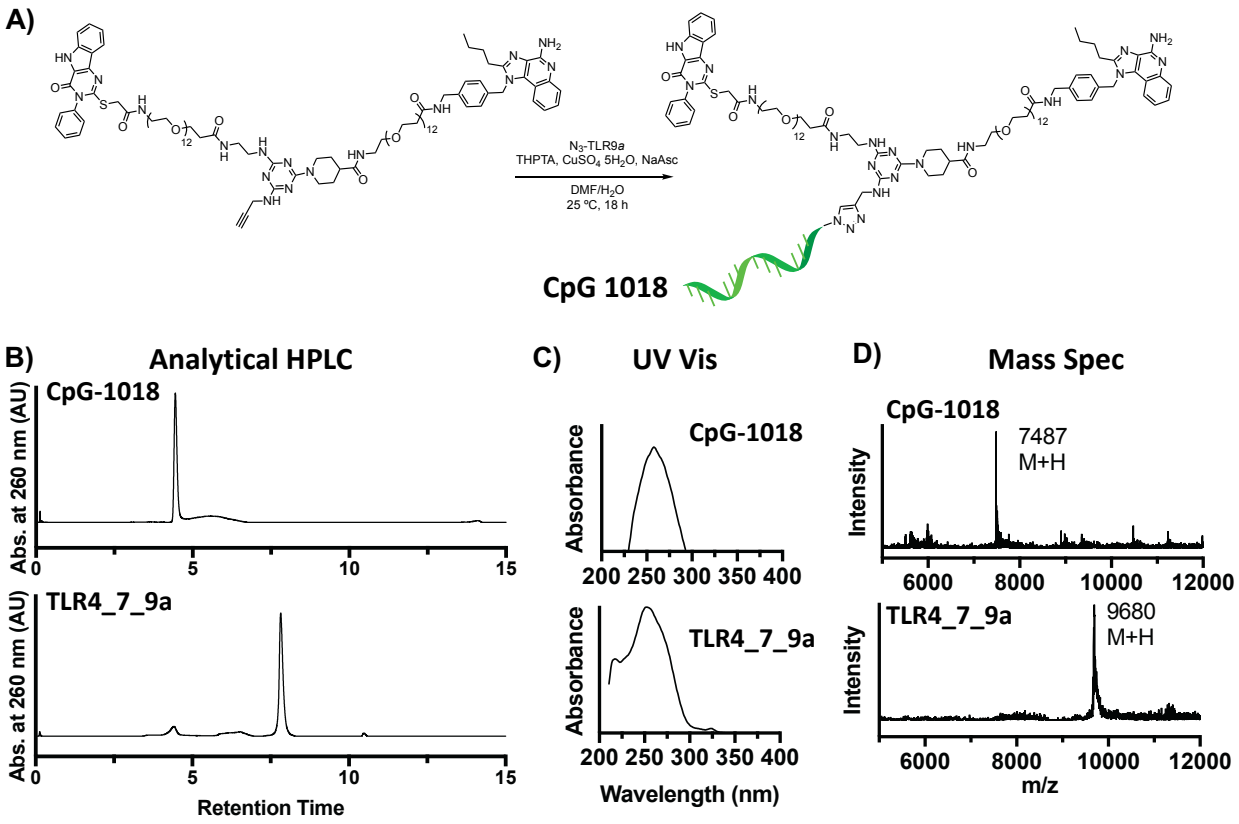

Figure 4.8 Synthesis and Characterization of Human Compatible TLR4_7_9*a*. A) Synthetic scheme of click reaction between TLR4_7*a* and TLR9*a* *via* CuAAC. Analytical HPLC trace with UV detection at 260 nm (B), UV absorption spectra (C), and mass spectra (D) of azide-TLR9*a* starting material and TLR4_7_9*a* purified product.

We performed a preliminary in vitro study of the human compatible TLR4_7_9*a* with Raw Blue NF-κB macrophages. Interestingly, the TLR7a shows much higher activity than the other compounds. However, the drop in activity upon conjugation appears to in part be due to the effects of PEGylation of the TLR7*a*. However, a major drop in activity from the TLR7a alone is also observed upon co-administration with TLR9*a* and TLR4*a*, although the activity is higher than TLR9*a* alone. Thus, there appears to be some type of inhibitory effect occurring from co-administration of TLR7*a* and TLR9*a* in this case, regardless of linkage. The TLR4_7_9*a* appeared to have similar activity to the unlinked combinations (with or without PEG). Importantly, none of the compounds showed signs of cytotoxicity as measured by LDH assay. Further studies will

include BMDC cytokine experiments and in *in vivo* immunogenicity experiments, where we saw the most significant differences in immune response profile. With validation of activity, we will more forward into guinea pig and non-human primate studies.

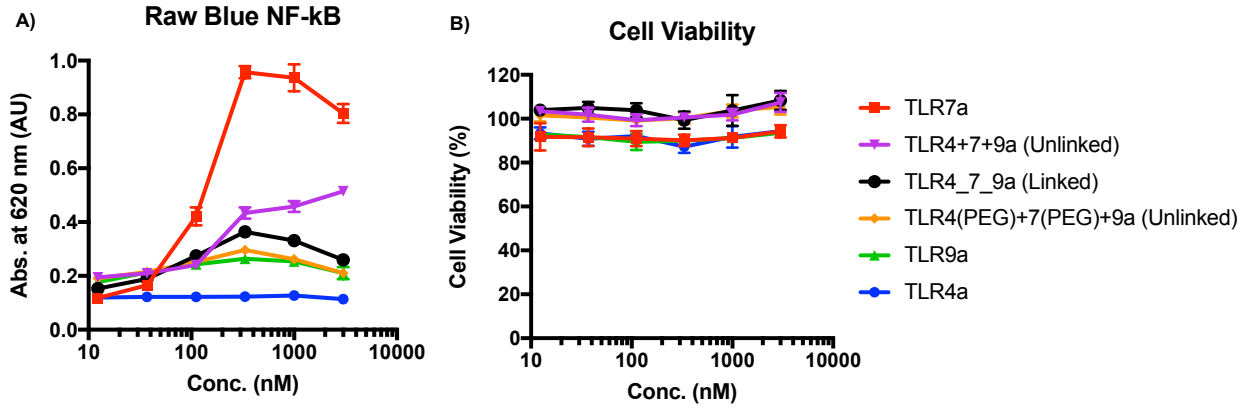

Figure 4.9 NF-kB Activity and Cell Viability of Raw Blue Cells Stimulated with Human Compatible TLR4_7_9*a*. A) NF-κB activity and cell viability (B) concentration curve as measured by Raw Blue assay or LDH assay following stimulation with human compatible TLR4_7_9*a* or its components, either alone or co-administered.

4.9 Conclusions

The current inactivated, whole-cell vaccine for Q-fever, Q-Vax®, although protective, causes reactogenicity in previous exposed individuals, limiting its practical application. This is a concern given *C. burnetii's* low infectious dose, durability in the environment, and its potential use as a biological weapon. It is necessary to develop an approved prophylactic vaccine against this bacterium. Due to reactogenicity limitations of the whole-cell vaccine, we believed formulating recombinant protein subunit vaccine candidates, composed of our novel TLR tri-agonists and immunogenic *C. burnetii* antigens, can generate vaccines that are as protective, but without the safety issues of a whole-cell vaccine.

Our initial *C. burnetii* vaccine candidate was composed of the antigen CBU_1910, identified as an ideal target through proteome microarray analysis of Q-Vax® vaccinated mice (**Fig 4.2A**) and in the literature[37–39], formulated with either linked or unlinked TLR2/6_4_7*a*. The origin of the reactogenic response generated from Q-Vax® is unknown, but we hypothesized that a recombinant protein-based subunit vaccine would be unlikely to produce a reactogenic response as it lacks the potentially reactogenic components found in Q-Vax®, specifically LPS.[40] Although our subunit vaccine candidate did not generate reactogenic responses, it did fail to produce a protective response compared to Q-Vax®. Our initial subunit vaccine formulation generated a TH2 biased response toward CBU_1910, while the Q-Vax® induced humoral response is heavily TH1 biased. We felt this was an important difference between our vaccine and Q-Vax® as inflammatory T cell responses are a critical component in Q-Vax® induced protection.[20,21,41] In other efforts to develop protective *C. burnetii* vaccines, adding multiple MHC-I epitopes from various *C. burnetii* antigens improved protection in other attempts to develop Q-fever vaccines[42–44], consistent with previously published studies suggesting that a cell-mediated response is important for protection against *C. burnetii*.[20] Finally, emulsions are commonly added to subunit vaccine formulations[30,31], but was not included in our initial vaccine. Thus, we investigated optimizing our vaccine formulation by evaluating the adjuvant, the inclusion of an emulsion, and finally multiplexing the number of antigens included in the vaccine.

In evaluating our adjuvants, we found that a more TH1 biased response could be achieved using different TLR tri-agonist combinations (**Fig. 4.3A**). TLR tri-agonists containing TLR2/6*a* showed to be more TH2 biasing (**Fig 4.2 and 4.4**). This result mirrored our *in vitro* studies (See Chapter 3) and previous studies showing that TLR2 agonists are potent TH2-inducing adjuvants. When TLR2/6*a* was replaced with TLR1/2*a*, we observed a slight shift toward a more TH1 biased

response, perhaps due to the lower potency of TLR1/2*a* compared to TLR2/6*a,* despite similar signaling pathways (**Fig. 4.4**). When TLR7*a* was exchanged for TLR9*a*, we observed a further shift in the immune response toward TH1 biasing (**Fig. 4.4**). We speculate that this is due to the higher potency of TLR9*a* when linked to the core than the TLR7*a*, which results in a stronger ability to overcome the TH2 biasing of the TLR1/2*a* and TLR2/6*a*. Although these TLR9*a* containing tri-agonists were more TH1 biased, they still generated high antibody titers when combined with a TLR2 agonist. When TLR2/6*a* was exchanged for a TLR7a (TLR4_7_9*a*), we observed the most TH1 biased immune response of the tri-agonist panel. However, the antibody response was significantly diminished. We speculate that the TLR2/6 agonist was essential for generating potent antibody responses from our compounds. Overall, we found that we could generate unique immune response profiles by changing the combination of TLR tri-agonist co-administered as the adjuvant. We envision this analysis will be impactful in vaccine development as particular TLR tri-agonists combinations, and their resulting immune response profiles, may be well suited for specific vaccine targets. For our Q-fever vaccine, we selected TLR1/2_4_9*a* and TLR4_7_9*a* as adjuvants in our *C. burnetii* vaccine candidates because they were the two most TH1 biasing combinations of the TLR tri-agonists evaluated in our studies.

Subunit vaccines often require an agent that increases antigen availability for presentation by antigen presenting cells[45–47] to improve vaccine efficacy. AddaVax™ is a commercially available vaccine adjuvant that is similar to an emulsion and has been licensed for use in influenza vaccines in Europe.[48–50] AddaVax™ has been shown to recruit and activate antigen presenting cells.[31,51] Squalene oil-in-water emulsions, including AddaVax™, elicit both B cell and T cell responses to immunization.[31] When AddaVax™ was added to our initial formulation (CBU_1910 and TLR2/6_4_7*a*), interestingly, the immune response was shifted to a more TH1 biased response

compared to either AddaVax™ alone or TLR2/6_4_7*a* alone. This result suggests there is some synergistic TH1 stimulating activity when the emulsion and TLR tri-agonist are mixed. The same was also true when our most TH1 biasing tri-agonist, TLR4_7_9*a*, was formulated with AddaVax™. In this formulation however, AddaVax™ significantly improved the amount of antibody generated compared to the tri-agonist alone, resulting in a TH1 biased response, without compromising antibody generation.

In addition to optimizing the adjuvant and emulsion, we included additional antigens to our formulation to increase the breadth of the immune response to immunization. We were concerned that the addition of multiple antigens to the formulation would increase the likelihood of our candidates to induce a reactogenic response, similar to Q-Vax®. However, other attempts at generating subunit vaccines for Q-fever have shown that including multiple T cell epitopes of *C. burnetii* antigens improved the efficacy of the vaccine.[20] Thus, we felt it was ideal to include additional *C. burnetii* antigens in the formulation. When adjuvanted with TLR2/6_4_7*a* and Addavax™, antibody responses could be generated to four antigens in the same vaccine, and that the responses were additive. This differs from Q-Vax®, where CBU_1910 appears to be the immunodominant antigen. Thus, multiple antigens could be incorporated into the vaccine with our adjuvant system, without compromising the individual antigen specific immune responses.

In our second challenge study, we developed two TH1-skewing candidate vaccine formulations incorporating what we learned from the optimization experiments: 1) TLR4_7_9*a* and TLR1/2_4_9*a* were more TH1 biasing adjuvants, 2) combining an oil-in-water emulsion (Addavax™) with our TLR tri-agonists generates a more TH1 biased immune response and significantly increases antibody titers, and 3) multiple antigens can be included in the formulation to expand the immune response breadth without generating any observed reactogenic responses.

The two formulations with these design principles were shown to elicit robust, TH1-biased antibody responses to four of the six antigens in the formulation. This result confirmed that we could use our formulation design principles to generate a vaccine with the desired type of immune response to selected antigens. When these formulations were tested in the challenge study, both were observed to reduce the bacterial burden in mice following a live *C. burnetii* aerosol challenge. In addition, the formulation adjuvanted with TLR4_7_9*a* resulted in a lower fever in mice challenge with the pathogen. However, the subunit vaccines did not decrease signs of infection to the same magnitude that Q-Vax did. We speculate that with further tuning of the vaccine formulation, similar levels of protection could be achieved. For example, the Q-Vax sample resulted in near complete IgG2c biasing of the antibody response, more so than the subunit vaccine groups, leaving room for further refinement of the a TH1 biased response. Conversely, the response generated in this experiment could account for partial protection, while Q-Vax elicits an additional, uncharacterized response that provides further protection, which is not present in our candidate vaccines. Thus, further evaluation of the protective nature of Q-Vax could guide further refinement of a subunit vaccine alternative.

In conclusion, we developed two promising Q-fever subunit vaccine candidates. The vaccines were developed through rational design using a novel TLR adjuvant platform that had not been previously evaluated for protective efficacy in an *in vivo* challenge model. By tuning the formulations' adjuvant, emulsion, and antigen composition, we generated an immune response that is specified for protection against *C. burnetii* challenge. Further efficacy experiments in more relevant animal models (non-human primates) and evaluations of reactogenicity in guinea pig models are underway and will further elucidate the potential utilization of these adjuvant systems in FDA approved subunit vaccine formulations. We envision this adjuvant platform and rational

vaccine design approaches could be used to generate subunit vaccine candidates against other human pathogens, resulting in more effective and safer vaccines specifically tailored to each human pathogen compared to traditional empirical approaches that utilize a single adjuvant system.

4.10 Experimental Methods and Materials

Mice

5-6 week old female C57BL/6 mice were purchased from Charles River Laboratories International, Inc. Mice were housed in SPF facility with a 12 hour dark/light cycle with autoclaved bedding and irradiated food. All handling of mice at both UCI and USAMRIID was performed under an approved Institutional Animal Care and Use Committee protocol. 5 or 8 mice were given a priming dose (day 0) and boosted 2 weeks later (day 14). Mice were administered 1 nmole of each TLR agonist linked to the inert core molecule or mixed in liquid formulations with 0.5 nmole of *C. burnetii* antigens. *C. burnetii* antigens were synthesized and purified by GenScript. In relevant vaccine formulations AddaVax™ (InvivoGen, San Diego, CA) was added at 50% of total vaccine volume. Fifty microliters of vaccine formulations were delivered intramuscularly in the thigh using a 31gauge needle (BD Insulin Syringes, Laguna Hills, CA, USA; 3/10cc). Animals were periodically weighed throughout the *in vivo* experiment protocol.

Ethics statement: All animal protocols were approved by the Institutional Animal Care and Use Committee of the University of California, Irvine. Animal research at the United States Army Medical Research Institute of Infectious Diseases (USAMRIID) was conducted under an animal use protocol approved by the USAMRIID Institutional Animal Care and Use Committee (IACUC)

in compliance with the Animal Welfare Act, PHS Policy, and other Federal statutes and regulations relating to animals and experiments involving animals. The facility where this research was conducted is accredited by the Association for Assessment and Accreditation of Laboratory Animal Care International (AAALACi) and adheres to principles stated in the Guide for the Care and Use of Laboratory Animals (National Research Council, 2011).

Q-Vax® immunogenicity evaluation

For Q-Vax® immunogenicity studies, groups of 5 female C57Bl/6 mice received 50µl Q-vax (CSL Ltd, Melbourne, Australia) administered either i.m. or. s.c. Mice were bled on day 0, 21, 28 and 67, and plasma used to probe *C. burnetii* proteome microarrays[15] to define reactive antigens.

***C. burnetii* protein microarray**

Custom-purified *C. burnetii* proteins (Genscript, Inc., Piscataway, NJ, USA) were diluted to 0.1 mg/mL in PBS-0.001% Tween-20 (T-PBS), and then printed in triplicate onto nitrocellulose-coated glass AVID slides (Grace Bio-Labs, Inc., Bend, OR, USA) using an Omni Grid 100 microarray printer (Genomic Solutions). Mouse serum samples were diluted 1:100 in protein array blocking buffer (GVS, Sanford, ME, USA) and then incubated on microarrays overnight at 4^{o}C with gentle agitation. Arrays were washed with TBS-0.05% Tween 20 (T-TBS) before incubation with biotinylated anti-mouse total IgG, IgG1, or IgG2c antibodies (Jackson Immunoresearch Labs, Inc., West Grove, PA, USA) diluted 1:200 in array blocking buffer. Bound anti-mouse antibodies were detected by incubation with streptavidin-conjugated Qdot®800 or streptavidin-Qdot® 585 (Thermo Fisher Scientific, Eugene, OR, USA) diluted 1:200 in array blocking buffer. Slides were washed and then air dried by brief centrifugation. Images were acquired using an ArrayCAM™

Imaging System (Grace Bio-Labs, Inc., Bend, OR, USA). Signal intensities were corrected for spot-specific background before further analysis.

Tissue Collection and Analysis

Plasma/Serum

Animals were anesthetized under 2-2.5% isoflurane and 2 L/min of oxygen flow under standard atmospheric pressure for these experiments. Plasma was collected on Days 0, 1, 14, 15 from isoflurane anesthesized mice via cheek bleed using a 25gauge needle (BD PrecisionGlide Needle). Blood was collected in Microvette CB 300 LH lithium heparin tubes (Sarstedt; Aktiengesellschaft & Co., Sparks, NV, USA) and plasma was separated at 2000xg for 5 minutes at 4°C. Serum was collected on termination day (day 17/21) via cardiac puncture of carbon dioxide euthanized mice using a 29 gauge needle (Insulin Syringe; Exelint International Co., Redondo Beach, CA, USA; 1mL), and separated at 2000xg for 10 minutes at 4°C. Plasma and serum samples were stored at -20°C for further analysis.

Flow cytometry analysis of immune cell populations

Spleen and draining inguinal LN samples were collected from mice on day 17 or 21. Whole spleens and LNs were passed through 40μm nylon mesh strainers (Fisherbrand®, Waltham, MA, USA) and rinsed with PBS to make single cell suspensions. Single cell suspensions of spleen cells were treated with ACK lysing buffer (ThermoFisher Scientific) for 5 minutes at room temperature to remove red blood cells. 1 x 10^6 cells, in FACS staining buffer (BioLegend), were transferred to a V-bottom plate (VWR, Radnor, PA). Fc receptors were blocked using anti-mouse CD16/32 (Biolegend) and B220 cells were stained using APC/Cy7 anti-mouse B220 (Biolegend). CD4 cells

were stained using FITC anti-mouse CD4 (Biolegend). CD8 cells were stained using PE/Cy7 anti-mouse CD8a (Biolegend). Samples were analyzed by flow cytometry using ACEA NovoCyte Flow Cytometer and analyzed using NovoExpress software and GraphPad Prism.

T cell Recall Response

1 x 10^6 splenocytes/mL were incubated in CytoOne (USA Scientific, Ocala, FL, USA) flat bottom tissue culture plates (USA Scientific). Cells were stimulated with 10μg/mL of *C. burnetii* antigen in RPMI supplemented with 10% FBS, 2% penicillin and streptomycin, and 0.2% 2-mercaptoethanol (complete RPMI) and incubated for 48 hours at 37°C at 5% CO_2. IFN-γ or IL-4 levels were analyzed in undiluted supernatants by ELISA (Biolegend) according to the manufacturer's instructions. For ELISpot Analysis, 2 x 10^5 splenocytes/well were incubated with 10μg/mL of *C. burnetii* antigen in complete RPMI in double color IL-4/IFN-γ ELISpot plates (Immunospot; CTL, Shaker Heights, OH, USA) for 48 hours at 37°C at 5% CO_2. Plates were processed using manufacturer's instructions and analyzed using CTL ImmunoSpot scanning services.

Vaccine Efficacy in Live *C. burnetii* Challenge Model

Vaccination and blood collection: Groups of 10 mice were given a priming dose (day 0) via intramuscular injection with either 3 recombinant protein vaccines (CBU_1910 alone, CBU_1910 and TLR tri-agonist 2/6_4_7a, or CBU_1910 and TLR agonists 2/6+4+7a), positive control Q-Vax, or saline control. Blood was collected from vaccinated mice on day 0 (baseline) and day 14 (just before boost except Q-Vax® vaccinated mice) and 70 (at the end of study).

Aerosol exposure: On the day of *C. burnetii* challenge (day 42), mice were moved to ABSL3 and housed there for the rest of the study. *C. burnetii* Nine Mile was propagated by the Diagnostic Systems Division in ACCM-2 (Sunrise Science Products) under micro-aerobic conditions for seven days. The bacteria were concentrated by centrifugation and brought up in ACCM-2. Mice were placed in wire mesh cages per their vaccination group and challenged via whole-body exposure chamber as described previously (Zumbrun et al.). Aerosols were performed using a 3-jet Collison nebulizer within a Class III Biosafety cabinet under control of the Automated Bioaerosol System. Starting concentrations and all glass impinger (AGI) samples were taken to enumerate bacteria concentration via PCR. All mice were exposed to a target dose of 10^{11} CFU/mL aerosolized *C. burnetii* Nine Mile strain 6 weeks following last vaccination.

Calculation of weight change: All of the mice, including negative saline control, survived the aerosol exposure with *C. burnetii*. Mice weighed once a day. The weight change was calculated as the percent difference between starting weight on the day of challenge (day 42 of the study) and weight on each subsequent day following challenge. All surviving mice were euthanized at the end of study on day 70 ± 2 days post-exposure via IP barbiturate overdose followed by cervical dislocation.

Statistical Analysis

All data was analyzed for statistical significance using one or two way ANOVA on GraphPad Prism 7 (GraphPad Software, Inc., La Jolla, CA, USA).

4.11 Additional Figures

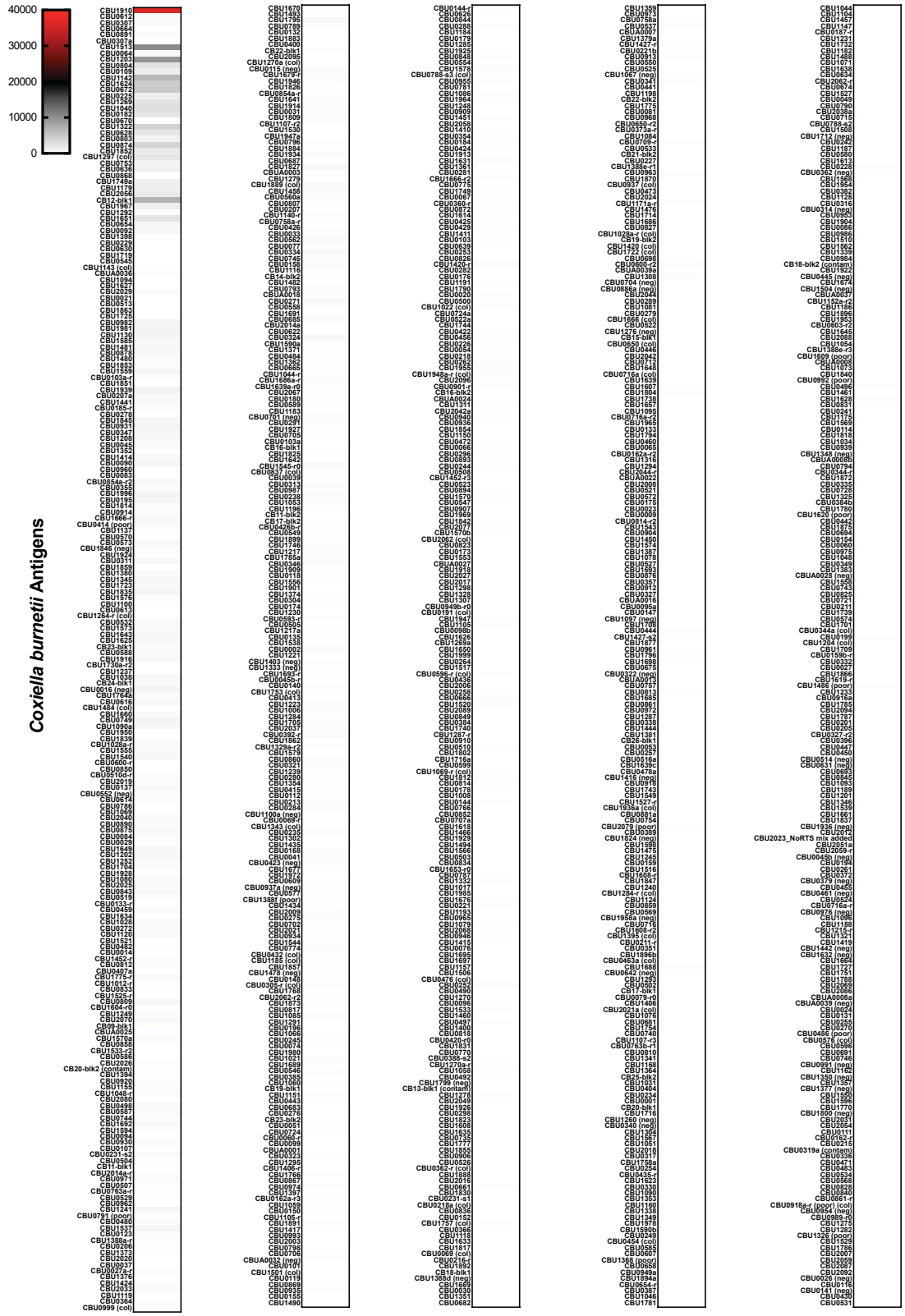

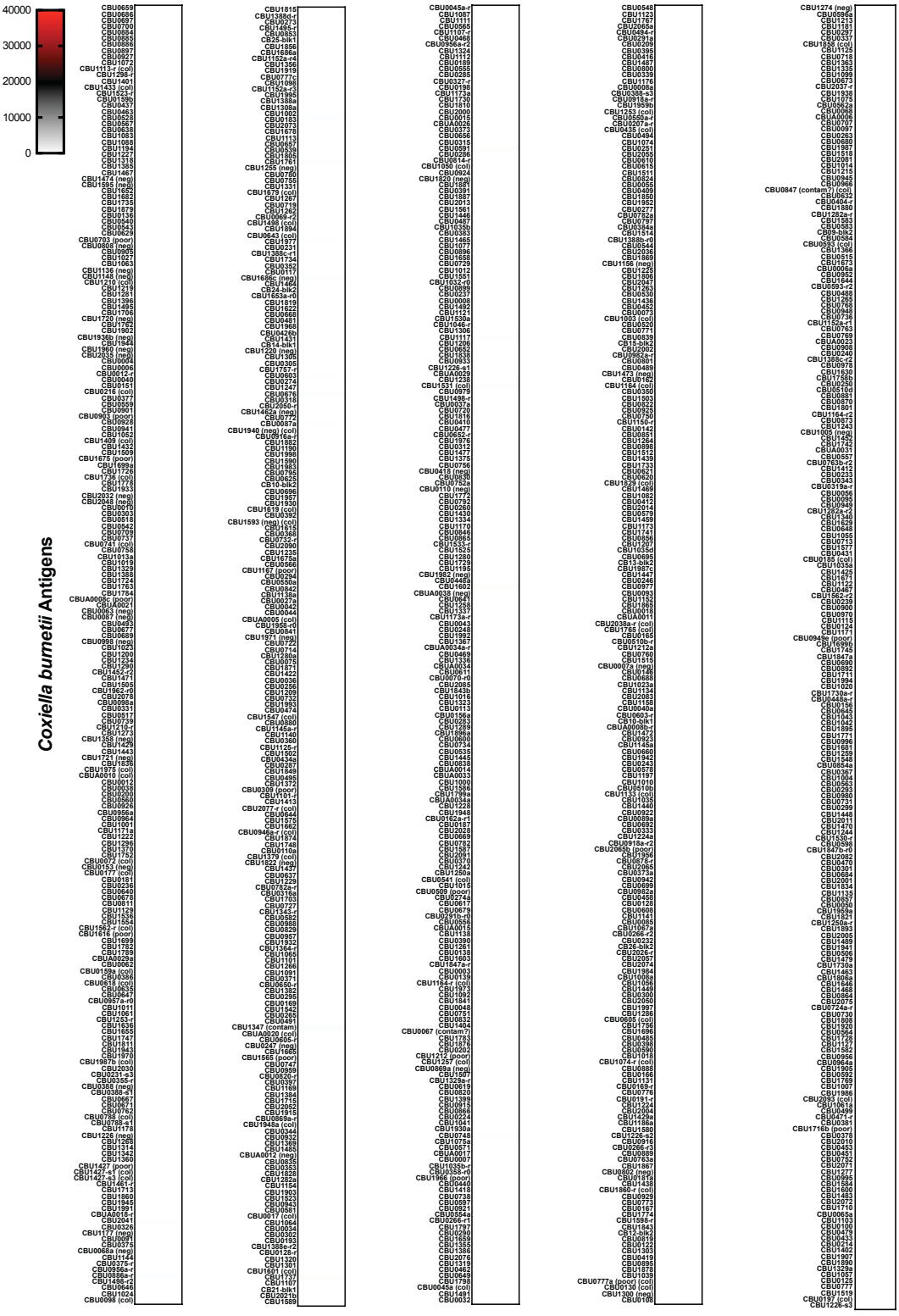

Figure 4.10 Antibody Microarray Heat Map Data from Q-Vax Vaccinated Mouse Serum. Heat map of antigen-specific serum antibody levels of Q-Vax vaccinated mice as measured by proteome-wide *Coxiella burnetii* protein microarray 28 d post vaccination. n = 5, top-left legend shows signal intensity gradient.

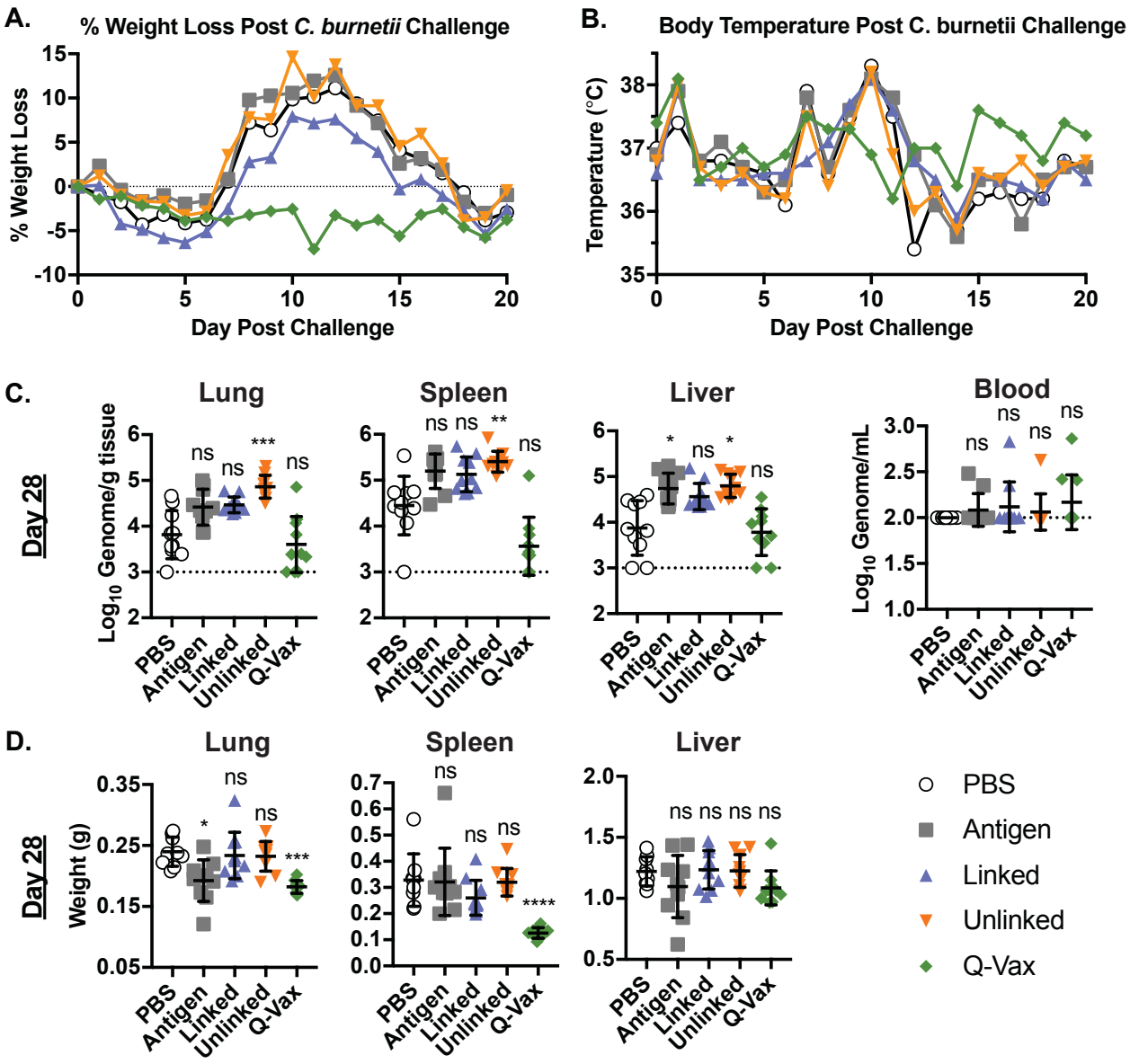

Figure 4.11 *C. burnetii* Challenge Study Following Vaccination with Linked or Unlinked TLR2/6_4_7*a*. Percent weight loss (A) and body temperature (B) of mice each day over 20 days following challenge. qPCR detection of *C. burnetii* in harvest organs and blood of mice 28 days post-challenge (C). Weight of harvested organs from mice 28 days post-challenge (D). n = 310, error bars represent SD of the mean. n = 10. Statistical analysis: one-way ANOVA, *: $p < 0.05$, **: $p < 0.01$, ***: $p < 0.001$, ****: $p < 0.0001$.

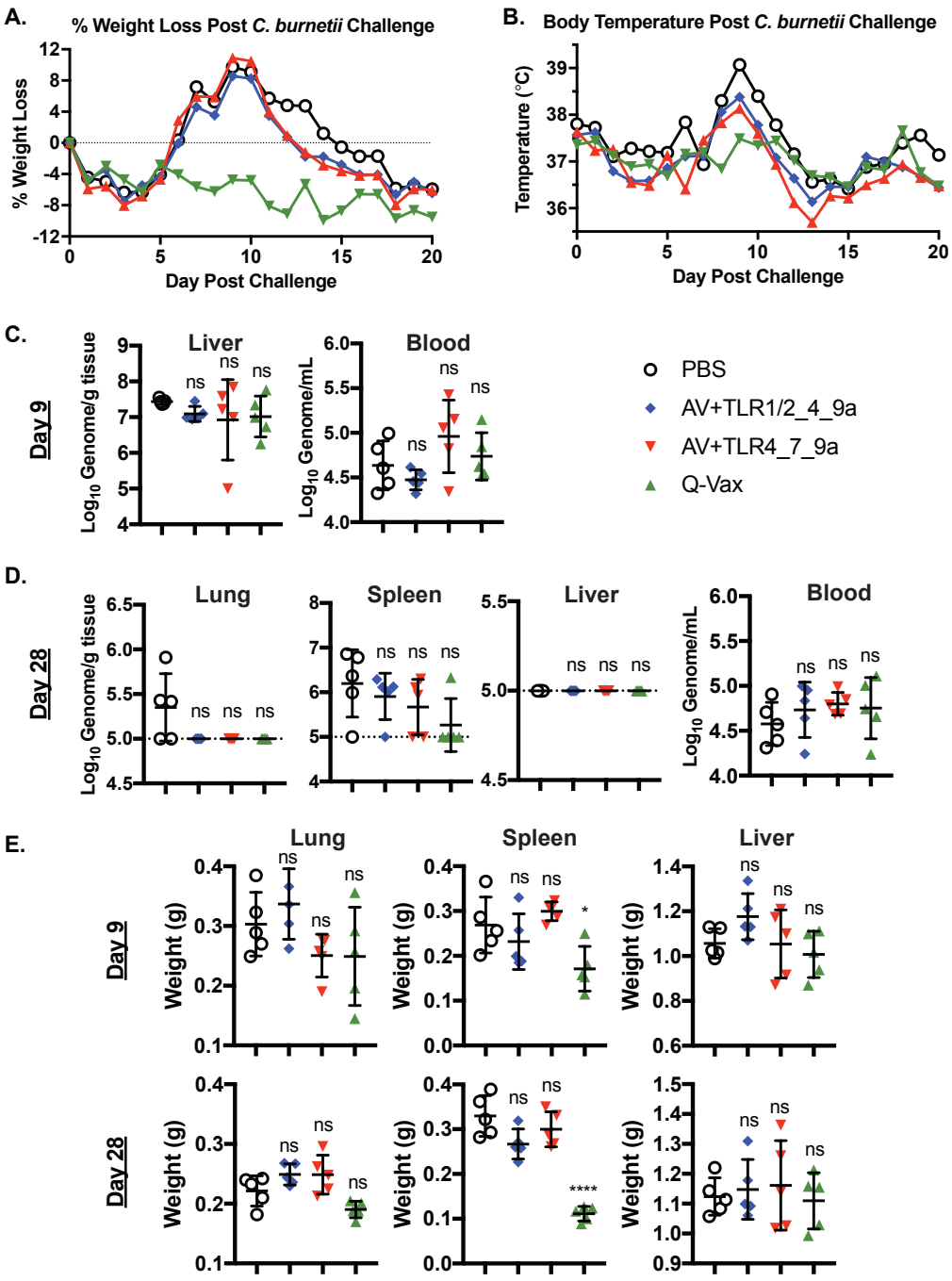

Figure 4.12 Additional *C. burnetii* Challenge Study Data of Mice Following Vaccination with TLR1/2_4_9*a* or TLR4_7_9*a* Adjuvanted Formulations. Additional *C. burnetii* challenge study data of mice following vaccination with PBS, either TLR1/2_4_9*a* or TLR4_7_9*a* mixed with 5 *C. burnetii* antigens (CBU_1910, CBU_0545, CBU_1398, CBU_0891, CBU_0307) and Addavax, or Q-Vax. Percent weight loss (A) and body temperature (B) of mice each day over 20 days following challenge. qPCR detection of *C. burnetii* in harvest organs and blood of mice either 9 days (C) 28 days post-challenge (D). Weight of harvested organs from mice 9 or 28 days post-challenge (E). n = 310, error bars represent SD of the mean. Day 0-9, n = 10, day 10-28, n = 5. Statistical analysis: one-way ANOVA, *: $p < 0.05$, **: $p < 0.01$, ***: $p < 0.001$, ****: $p < 0.0001$.

4.12 References

(1) Bond, K. A.; Franklin, L. J.; Sutton, B.; Firestone, S. M. Q-vax Q fever vaccine failures, Victoria, Australia 1994–2013. *Vaccine* **2017**, *35* (51), 7084–7087.

(2) Reeves, P. M.; Paul, S. R.; Sluder, A. E.; Brauns, T. A.; Poznansky, M. C. Q-vaxcelerate: a distributed development approach for a new Coxiella burnetii vaccine. *Hum. Vaccin. Immunother.* **2017**, *13* (12), 2977–2981.

(3) Ruiz, S.; Wolfe, D. N. Vaccination against Q fever for biodefense and public health indications. *Front. Microbiol.* **2014**, *5*, 726.

(4) Moyer, T. J.; Zmolek, A. C.; Irvine, D. J. Beyond antigens and adjuvants: formulating future vaccines. *J. Clin. Invest.* **2016**, *126* (3), 799–808.

(5) Foged, C. Subunit vaccines of the future: the need for safe, customized and optimized particulate delivery systems. *Ther. Deliv.* **2011**, *2* (8), 1057–1077.

(6) Vartak, A.; Sucheck, J. S. Recent advances in subunit vaccine carriers. *Vaccines* . 2016.

(7) Pulendran, B. Learning immunology from the yellow fever vaccine: innate immunity to systems vaccinology. *Nat. Rev. Immunol.* **2009**, *9*, 741–747.

(8) Mogensen, T. H. Pathogen recognition and inflammatory signaling in innate immune defenses. *Clin. Microbiol. Rev.* **2009**, *22* (2), 240–273.

(9) Dowling, J. K.; Mansell, A. Toll-like receptors: the swiss army knife of immunity and vaccine development. *Clin Trans Immunol*. Australasian Society for Immunology Inc. May 20, 2016, p e85.

(10) Tom, J. K.; Dotsey, E. Y.; Wong, H. Y.; Stutts, L.; Moore, T.; Davies, D. H.; Felgner, P. L.; Esser-Kahn, A. P. Modulation of innate immune responses via covalently linked TLR agonists. *ACS Cent. Sci.* **2015**, *1* (8), 439–448.

(11) Wu, T. Y.-H. Strategies for designing synthetic immune agonists. *Immunology* **2016**, *148* (4), 315–325.

(12) Lynn, G. M.; Laga, R.; Darrah, P. A.; Ishizuka, A. S.; Balaci, A. J.; Dulcey, A. E.; Pechar, M.; Pola, R.; Gerner, M. Y.; Yamamoto, A. In vivo characterization of the physicochemical properties of polymer-linked TLR agonists that enhance vaccine immunogenicity. *Nat. Biotechnol.* **2015**, *33*, 1201–1210.

(13) J van Schaik, E.; Chen, C.; Mertens, K.; Weber, M.; Samuel, J. Molecular pathogenesis of the obligate intracellular bacterium Coxiella burnetii. *Nat. Rev. Microbiol.* **2013**, *11* (8), 561–573.

(14) Eldin, C.; Mélenotte, C.; Mediannikov, O.; Ghigo, E.; Million, M.; Edouard, S.; Mege, J.-L.; Maurin, M.; Raoult, D. From Q fever to Coxiella burnetii infection: a paradigm change. *Clin. Microbiol. Rev.* **2017**, *30* (1), 115–190.

(15) Beare, P. A.; Chen, C.; Bouman, T.; Pablo, J.; Unal, B.; Cockrell, D. C.; Brown, W. C.; Barbian, K. D.; Porcella, S. F.; Samuel, J. E.; et al. Candidate antigens for Q fever serodiagnosis revealed by immunoscreening of a Coxiella burnetii protein microarray. *Clin. Vaccine Immunol.* **2008**, *15* (12), 1771–1779.

(16) Vigil, A.; Ortega, R.; Nakajima-Sasaki, R.; Pablo, J.; Molina, D. M.; Chao, C.-C.; Chen, H.-W.; Ching, W.-M.; Felgner, P. L. Genome-wide profiling of humoral immune response to Coxiella burnetii infection by protein microarray. *Proteomics* **2010**, *10* (12), 2259–2269.

(17) Vigil, A.; Chen, C.; Jain, A.; Nakajima-Sasaki, R.; Jasinskas, A.; Pablo, J.; Hendrix, L.; Samuel, J.; Felgner, P. Profiling the humoral immune response of acute and chronic Q fever by protein microarray. *Mol. Cell. Proteomics* **2011**, *10*, M110.006304.

(18) Vranakis, I.; Papadioti, A.; Tselentis, Y.; Psaroulaki, A.; Tsiotis, G. The contribution of proteomics towards deciphering the enigma of Coxiella burnetii. *Proteomics – Clin. Appl.* **2013**, *7* (1–2), 193–204.
(19) Barr, T. A.; Brown, S.; Mastroeni, P.; Gray, D. B cell intrinsic Myd88 signals drive IFN-γ production from T cells and control switching to IgG2c. *J. Immunol.* **2009**, *183* (2), 1005–1012.
(20) G Shannon, J.; A Heinzen, R. Adaptive Immunity to the obligate intracellular pathogen Coxiella burnetii; 2008; Vol. 43.
(21) Capo, C.; Mege, J.-L. Role of innate and adaptive immunity in the control of Q fever. *Adv. Exp. Med. Biol.* **2012**, *984*, 273–286.
(22) Bechah, Y.; Verneau, J.; Ben Amara, A.; Barry, A. O.; Lépolard, C.; Achard, V.; Panicot-Dubois, L.; Textoris, J.; Capo, C.; Ghigo, E.; et al. Persistence of Coxiella burnetii, the agent of Q fever, in murine adipose tissue. *PLoS One* **2014**, *9* (5), e97503.
(23) Baumgärtner, W.; Dettinger, H.; Schmeer, N. Spread and distribution of Coxiella burnetii in c57bl/6j (h-2b) and balb/cj (h-2d) mice after intraperitoneal infection. *J. Comp. Pathol.* **1993**, *108* (2), 165–184.
(24) Bewley, K. R. Animal models of Q fever (Coxiella burnetii). *Comp. Med.* **2013**, *63* (6), 469–476.
(25) Waag, D. M.; England, M. J.; Pitt, M. L. M. Comparative efficacy of a Coxiella burnetii chloroform:methanol residue (cmr) vaccine and a licensed cellular vaccine (Q-vax) in rodents challenged by aerosol. *Vaccine* **1997**, *15* (16), 1779–1783.
(26) Zhang, G.; Russell-Lodrigue, K. E.; Andoh, M.; Zhang, Y.; Hendrix, L. R.; Samuel, J. E. Mechanisms of vaccine-induced protective immunity against Coxiella burnetii infection in balb/c mice. *J. Immunol.* **2007**, *179* (12), 8372–8380.
(27) Leone, M.; Bechah, Y.; Meghari, S.; Lepidi, H.; Capo, C.; Raoult, D.; Mege, J.-L. Coxiella burnetii infection in c57bl/6 mice aged 1 or 14 months. *FEMS Immunol. Med. Microbiol.* **2007**, *50*, 396–400.
(28) Nakamura, T.; Kamogawa, Y.; Bottomly, K.; Flavell, R. A. Polarization of IL-4- and IFN-gamma-producing CD4+ T cells following activation of naive CD4+ T cells. *J. Immunol.* **1997**, *158* (3), 1085 LP – 1094.
(29) Bradley, L.; K. and Dalton, D.; M. A., C. A Direct Role for IFN-γ in Regulation of Th1 Cell Development; 1996; Vol. 157.
(30) Ciabattini, A.; Pettini, E.; Fiorino, F.; Pastore, G.; Andersen, P.; Pozzi, G.; Medaglini, D. Modulation of primary immune response by different vaccine adjuvants. *Front. Immunol.* **2016**, *7*, 427.
(31) Awate, S.; Babiuk, L. A.; Mutwiri, G. Mechanisms of action of adjuvants. *Front. Immunol.* **2013**, *4*, 114.
(32) Lightowlers, M. W.; Rolfe, R.; Gauci, C. G. Taenia saginata:vaccination against cysticercosis in cattle with recombinant oncosphere antigens. *Exp. Parasitol.* **1996**, *84* (3), 330–338.
(33) Willadsen, P.; Smith, D.; Cobon, G.; McKenna, R. V. Comparative vaccination of cattle against boophilus microplus with recombinant antigen bm86 alone or in combination with recombinant bm91. *Parasite Immunol.* **1996**, *18* (5), 241–246.
(34) Duffy, P. E.; Kaslow, D. C. A novel malaria protein, pfs28, and pfs25 are genetically linked and synergistic as falciparum malaria transmission-blocking vaccines. *Infect. Immun.* **1997**, *65* (3), 1109–1113.

(35) Darghouth, M. A.; Boulter, N. R.; Gharbi, M.; Sassi, L.; Tait, A.; Hall, R. Vaccination of calves with an attenuated cell line of theileria annulata and the sporozoite antigen spag-1 produces a synergistic effect. *Vet. Parasitol.* **2006**, *142* (1), 54–62.
(36) Campbell, J. Development of the CpG adjuvant 1018: a case study. In *Methods in molecular biology (Clifton, N.J.)*; 2017; Vol. 1494.
(37) Sekeyová, Z.; Kowalczewska, M.; Vincentelli, R.; Decloquement, P.; Flores-Ramirez, G.; Skultety, L.; Raoult, D. Characterization of antigens for q fever serodiagnostics. *Acta Virol.* **2010**, *54*, 173–180.
(38) Xiong, X.; Meng, Y.; Wang, X.; Qi, Y.; Li, J.; Duan, C.; Wen, B. Mice immunized with bone marrow-derived dendritic cells stimulated with recombinant Coxiella burnetii com1 and mip demonstrate enhanced bacterial clearance in association with a th1 immune response. *Vaccine* **2012**, *30* (48), 6809–6815.
(39) Xiong, X.; Wang, X.; Wen, B.; Graves, S.; Stenos, J. Potential serodiagnostic markers for Q fever identified in Coxiella burnetii by immunoproteomic and protein microarray approaches. *BMC Microbiol.* **2012**, *12* (35), 1–10.
(40) Baeten, L. A.; Podell, B. K.; Sluder, A. E.; Garritsen, A.; Bowen, R. A.; Poznansky, M. C. Standardized guinea pig model for Q fever vaccine reactogenicity. *PLoS One* **2018**, *13* (10), e0205882.
(41) Kersh, G. J.; Fitzpatrick, K. A.; Self, J. S.; Biggerstaff, B. J.; Massung, R. F. Long-term immune responses to Coxiella burnetii after vaccination. *Clin. Vaccine Immunol.* **2013**, *20* (2), 129–133.
(42) Zhang, G.; Samuel, J. E. Vaccines against Coxiella infection. *Expert Rev. Vaccines* **2004**, *3* (5), 577–584.
(43) Williams, J. C.; Peacock, M. G.; Waag, D. M.; Kent, G.; England, M. J.; Nelson, G.; Stephenson, E. H. Vaccines against Coxiellosis and Q fever development of a chloroform:methanol residue subunit of phase I Coxiella burnetii for the immunization of animals. *Ann. N. Y. Acad. Sci.* **1992**, *653* (1), 88–111.
(44) Zhang, Y. X.; Zhi, N.; Yu, S. R.; Li, Q. J.; Yu, G. Q.; Zhang, X. Protective immunity induced by 67 k outer membrane protein of phase I Coxiella burnetii in mice and guinea pigs. *Acta Virol.* **1994**, *38* (6), 327–331.
(45) Wilkins, A. L.; Kazmin, D.; Napolitani, G.; Clutterbuck, E. A.; Pulendran, B.; Siegrist, C.-A.; Pollard, A. J. AS03- and MF59-adjuvanted influenza vaccines in children. *Front. Immunol.* **2017**, *8*, 1760.
(46) Portuondo, D. L. F.; Ferreira, L. S.; Urbaczek, A. C.; Batista-Duharte, A.; Carlos, I. Z. Adjuvants and delivery systems for antifungal vaccines: current state and future developments. *Med. Mycol.* **2014**, *53* (1), 69–89.
(47) Lee, S.; Nguyen, M. T. Recent advances of vaccine adjuvants for infectious diseases. *Immune Netw* **2015**, *15* (2), 51–57.
(48) Beljanski, V.; Chiang, C.; Kirchenbaum, G. A.; Olagnier, D.; Bloom, C. E.; Wong, T.; Haddad, E. K.; Trautmann, L.; Ross, T. M.; Hiscott, J. Enhanced influenza virus-like particle vaccination with a structurally optimized RIG-I agonist as adjuvant. *J. Virol.* **2015**, *89* (20), 10612–10624.
(49) Goff, P. H.; Eggink, D.; Seibert, C. W.; Hai, R.; Martínez-Gil, L.; Krammer, F.; Palese, P. Adjuvants and immunization strategies to induce influenza virus hemagglutinin stalk antibodies. *PLoS One* **2013**, *8* (11), e79194.
(50) Sasaki, E.; Momose, H.; Hiradate, Y.; Furuhata, K.; Takai, M.; Asanuma, H.; Ishii, K. J.;

Mizukami, T.; Hamaguchi, I. Modeling for influenza vaccines and adjuvants profile for safety prediction system using gene expression profiling and statistical tools. *PLoS One* **2018**, *13* (2), e0191896.

(51) Calabro, S.; Tritto, E.; Pezzotti, A.; Taccone, M.; Muzzi, A.; Bertholet, S.; De Gregorio, E.; O'Hagan, D. T.; Baudner, B.; Seubert, A. The adjuvant effect of MF59 is due to the oil-in-water emulsion formulation, none of the individual components induce a comparable adjuvant effect. *Vaccine* **2013**, *31* (33), 3363–3369.

CHAPTER 5

Site-Specific TLR Agonist-Antigen Conjugation

5.1 Introduction

TLR agonists (TLR*a*), are powerful immunostimulants due to their ability to drive innate and acquired immunity and are therefore sought after as adjuvants in vaccines.[1] However, administration of TLR agonists can result in toxic side-effects *in vivo* due to their high potency.[2–4] To mitigate these adverse effects, TLR agonists can be covalently conjugated to an antigen. This ensures simultaneous delivery of antigen and adjuvant to the same antigen presenting cell, which directs the response toward the antigen, thereby lowering the required dose for an effective immune response.[5,6] These self-adjuvanting vaccines induce stronger cellular immune responses and are less toxic than vaccines comprised of co-administered antigen and adjuvant.[5]

Willie-Reece and coworkers demonstrated the promise for TLR7/8 agonist-antigen conjugates as a subunit HIV vaccine.[7] An amine functionalized resiquimod (3M-012) was photocrosslinked with HIV Gag protein. The conjugate was shown to potently stimulate T and B cell responses, in mice and non-human primates, toward the antigen whereas the un-conjugated mixture did not. A thiol-functionalized 3M-012 was also crosslinked via thiol-maleimide chemistry to HIV envelope protein.[8] Despite high immunostimulatory activity, the conjugation blocked antibody responses toward desired antigen epitopes. Recently, the same lab demonstrated that protective T cell responses *via* TLR7/8-antigen conjugates required aggregation of the conjugate.[9] In addition, Holbrook and coworkers conjugated an amine functionalized Resiquimod to influenza virus *via* a bifunctional NHS-maleimide-PEG-linker.[10] This and follow up studies demonstrated the Resiquimod-influenza conjugate vaccine generated efficacious influenza immunity in non-human primate neonates, a difficult vaccination model.[10,11] In addition, Clauson

and colleagues demonstrated that non-specific CpG (TLR9*a*) conjugation to ovalbumin resulted in improved immune responses toward the antigen.[12] However, they found that only conjugates with a 1:1 ratio of CpG:ovalbumin resulted in robust adaptive immune responses while increasing ratios of CpG:ovalbumin resulted in aggregation and diminished immune responses. These studies highlight both the clinical potential of TLR-agonist conjugates and the need to develop controlled, site-specific methods for agonist conjugation to improve the magnitude of antigen-specific immune responses while preserving native antigen recognition.

The benefits of TLR agonist conjugation can only be achieved if the conjugation does not perturb the interaction between the agonist and receptor. Therefore, effective strategies are required that facilitate TLR agonist conjugation with retention, or improved, TLR agonist potency. Thus, we sought to develop site-specific methods to conjugate TLR agonists to *C. burnetii* antigens. Through site-specific conjugation, the immunogenicity of the antigen could be improved without compromising epitope recognition. In addition, previous studies have shown that conjugation is effective at improving T cell responses. Since it appears that T cell responses are particularly important for protection to *C. burnetii*, we think that TLR agonist-antigen conjugation is a promising approach for subunit vaccination for this disease. Here, we describe our efforts to develop a versatile site-specific conjugation strategy for a Q-Fever vaccine.

5.2 Non-specific NHS Mediated Conjugation

Synthesis of TLR7*a*-CBU_1910 and TLR9*a*-CBU_1910. The first conjugation strategy we employed was to non-specifically modify the antigen, as has been performed previously,[7,13] using non-specific NHS chemistry. This strategy suffers from drawbacks, such as blocking antibody epitopes and heterogenous products.[8] However, these samples are needed for controls for any site-specific method we develop. Thus, we chose to generate these compounds and to quickly test if TLR agonist-antigen conjugates would be useful in the *C. burnetii* vaccine model and for future experiments. We started with our most abundant and immunogenic *C. burnetii* protein, CBU_1910. The protein was first functionalized with NHS-activated azido-acetic acid. The functionalization could be tracked by mass spectrometry and SDS-PAGE (**Fig. 5.1B and C**). As expected, functionalization resulted in a heterogenous mixture of protein functionalized with 4-11 azide moieties per CBU_1910 (**Fig. 5.1C**). Not only do the number of azides per protein vary, but the specific lysines modified with the azide within each mass peak vary, demonstrating the heterogenous nature of the sample.

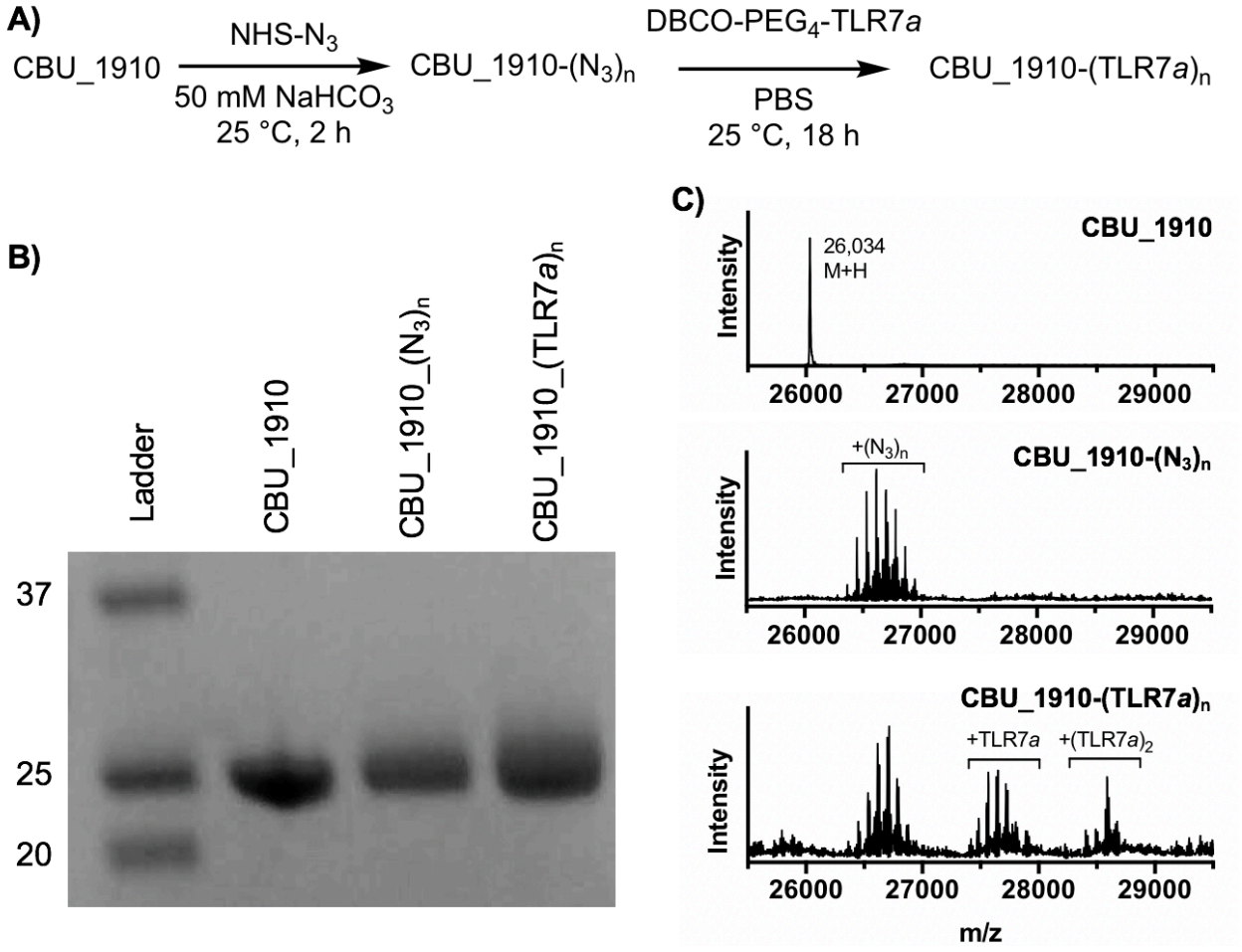

Figure 5.1 Reaction Scheme and Characterization of CBU_1910-TLR7*a*. A) Reaction scheme of CBU_1910 functionalization with NHS-azido-acetic acid (NHS-N_3) and then DBCO-PEG_4-TLR7*a* to afford the TLR7*a*-CBU_1910 conjugate. B) SDS-PAGE gel stained with Coomassie Blue of CBU_1910 stock, azide functionalized, or TLR7*a* functionalized. C) Mass spectrometry following the azide and TLR7*a* functionalization.

Following azide functionalization, the protein was reacted with either DBCO-PEG_4-TLR7*a* or BCN-TLR9*a* to form the conjugate *via* strain promoted azide-alkyne cycloaddition. The mass shifts (+ 83 per azide functionalization, +894 per TLR7*a* functionalization) were not large enough to be observed by SDS-PAGE (**Fig. 5.1B, 5.2B**). We attempted to analyze the extent of TLR7*a* conjugation by mass spectrometry, however, the spectra became too complicated to easily ascertain the conjugation extent (**Fig. 5.1C**). However, we were able to determine an approximate

labeling efficiency by UV-Vis and BCA assay, as the DBCO-PEG_4-TLR7*a* has a characteristic absorbance at 322 nm. Ultimately, we produced 24 nmole of CBU_1910-TLR7*a* (3.7 TLR7*a*/protein).

To conjugate TLR9*a* to the azide-CBU_1910, we generated a BCN-functionalized TLR9*a* by reacting an amino-functionalized CpG1826 with NHS-BCN. Upon incubation of the BCN-TLR9*a* with azide-CBU_1910, we produced 20 nmoles of CBU_1910-TLR9*a* (1.7 TLR9*a*/protein, **Fig. 5.2A**). In this case, the mass shift was sufficient to quantify the labeling by SDS-PAGE and by FPLC (**Fig. 5.2B and C**). With these two TLR agonist-antigen conjugates in hand, we tested their immunogenicity *in vivo*.

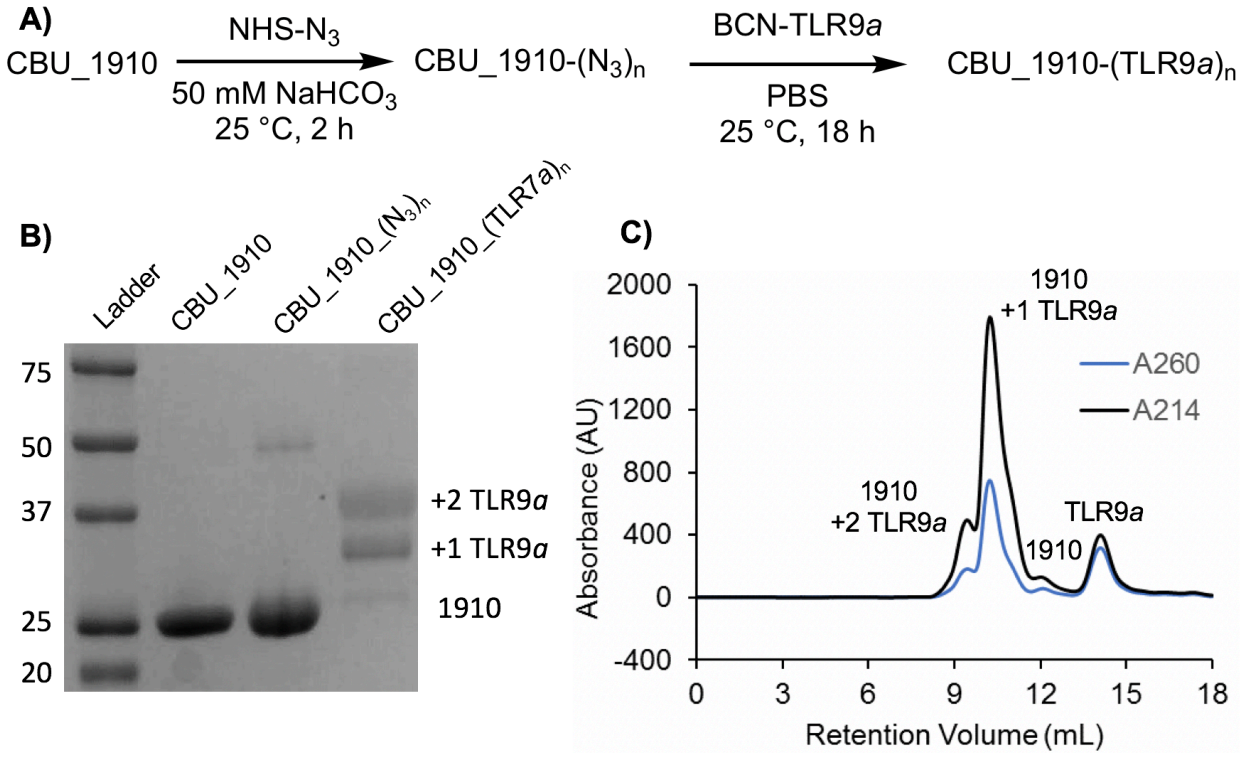

Figure 5.2 Reaction Scheme and Characterization of CBU_1910-TLR9*a*. A) Reaction scheme of CBU_1910 functionalization with NHS-azido-acetic acid (NHS-N_3) and then BCN-TLR9*a* to afford the TLR9*a*-CBU_1910 conjugate. B) SDS-PAGE gel stained with Coomassie Blue of CBU_1910 stock, azide functionalized, or TLR9*a* functionalized. C) FPLC monitoring the extent

of TLR9a conjugation in the crude reaction mixture.

***In vivo* immunogenicity studies**

Previous studies have reported that antigen conjugates with TLR7*a* or TLR9*a* improve the T cell response toward the antigen *in vivo* compared to the unconjugated control.[7,13] We sought to confirm this observation with our CBU_1910 TLR7*a* or TLR9*a* conjugates. Thus, we vaccinated mice with CBU_1910, CBU_1910_TLR9*a* (conjugated) CBU_1910 + TLR9*a* (unconjugated), CBU_1910 _TLR7*a* (conjugated), or CBU_1910 + TLR7*a* (unconjugated). Based on our previous work in preparing the vaccines for challenge studies, we also included the emulsion, AddaVax™ (AV), in the formulations. Following vaccination and boost on day 14, we took down the mice on day 21 of the experiment and harvested their lymph nodes and serum. We found that all vaccinated groups had a trend of higher numbers of immune cells isolated from the lymph node (**Fig. 5.3A**). The conjugates showed lower numbers of $CD4^+$, $CD8^+$, and $B220^+$ cells from the lymph node than the corresponding unconjugated controls. The conjugates also appeared to have fewer immune cells than the antigen + AV only control. In addition, all of the vaccine groups showed higher IFN-γ stimulation upon lymphocyte antigen recall than PBS (**Fig. 5.3B**). However, the only group that appeared to stimulate a significant amount was the CBU_1910 + TL9*a*. Finally, we also measured the antibody levels generated by the formulations in the serum. All of the groups, other than PBS, showed high levels of CBU_1910 specific antibody in the serum (**Fig. 5.3C**). However, all of the groups adjuvanted with TLR agonist, conjugated or unconjugated, showed a bias for IgG2c subtypes, suggesting a shift in immune response bias to a more TH1 type response, compared to antigen + AV only (**Fig. 5.3D**). Overall, these results suggest there wasn't much improvement in antigen-specific immune stimulation from conjugating the agonists to antigen, unlike previously reported studies. This result could, in part, be due to our methods of conjugation, which result in

decreases in TLR agonist activity. Including AV in the formulation may have also masked any effects of conjugation. More studies are needed to determine optimal conjugation methods and linkers. Later in this Chapter, we discuss our efforts to site-specifically conjugate TLR agonists to antigens. However, we had the opportunity to test the non-specific TLRa-CBU1910 conjugates in a *C. burnetii* challenge study to observe if they could function generate protective immunity in mice.

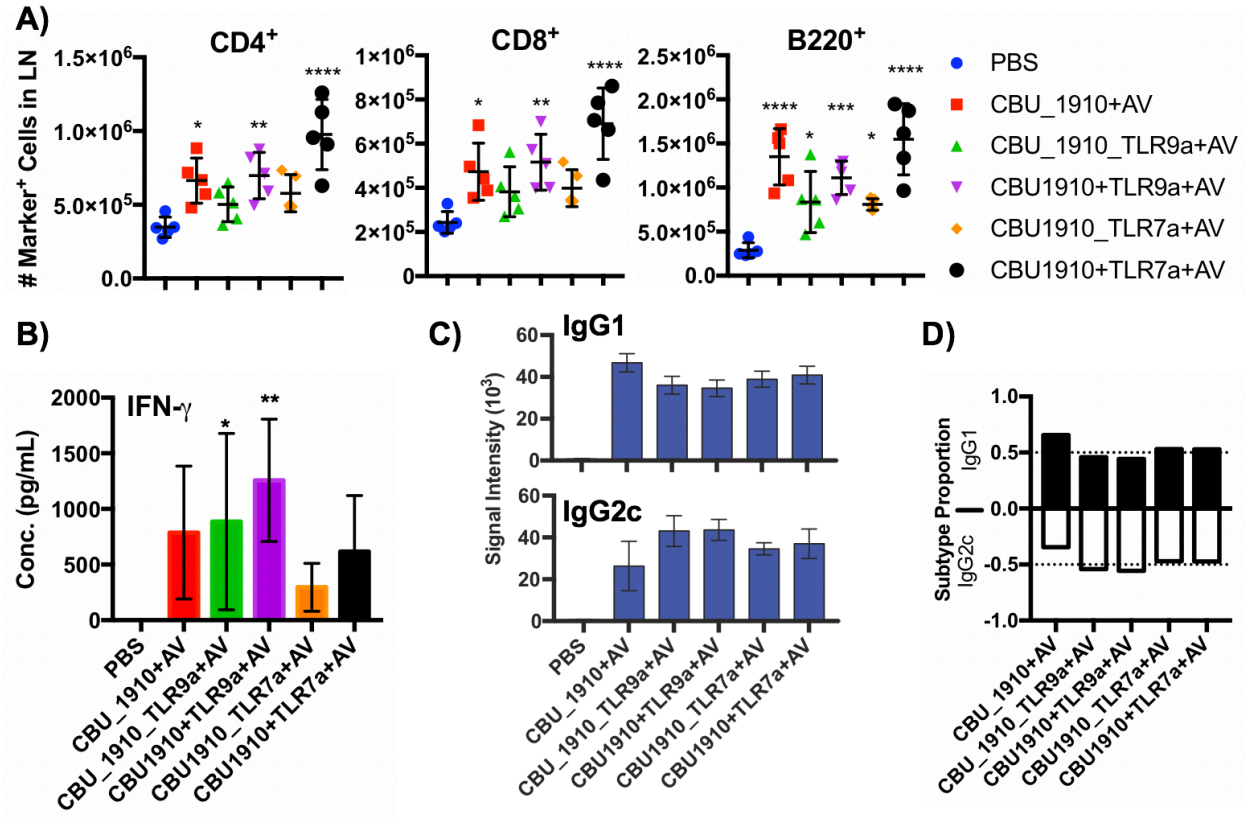

Figure 5.3 Immunogenicity Evaluation of TLR7 or 9*a*-CBU1910 Conjugates. A) Number of CD4+, CD8+, B220+ cells isolated from lymph nodes (LN) of vaccinated mice administered indicated formulation by flow cytometry on d21 following vaccination. B) Cytokine secretion upon antigen recall of inguinal lymphocytes. C) Antibody signal intensity from protein microarray analysis. D) Calculated proportions of antibody subtypes. n=5 C57BL/6 mice. Statistical analysis: one-way ANOVA, *: $p < 0.05$, **: $p < 0.01$, ***: $p < 0.001$, ****: $p < 0.0001$ all compared to PBS.

C burnetii challenge study

To assess the efficacy of the TLR*a*-CBU_1910 conjugates, we performed a *C. burnetii* challenge study. Mice were vaccinated on day 0 then boosted on day 14 with a mixture of CBU_1910_TLR7*a* and CBU_1910_TLR9*a* in AV, challenged on day 42 with aerosolized *C. burnetii*, and sacrificed on day 51. The vaccine group did not show any improvement in weight loss or body temperature to infection compared to PBS control (data not shown). However, the TLR agonsit-CBU_1910 conjugates appeared to result in a significant decrease of organisms detected by qPCR in the spleens and lungs of challenged mice (**Fig. 5.4**) This experiment demonstrates that there may be promise for a TLR agonist-antigen conjugate as a subunit vaccine for Q-Fever, but that further optimization is required.

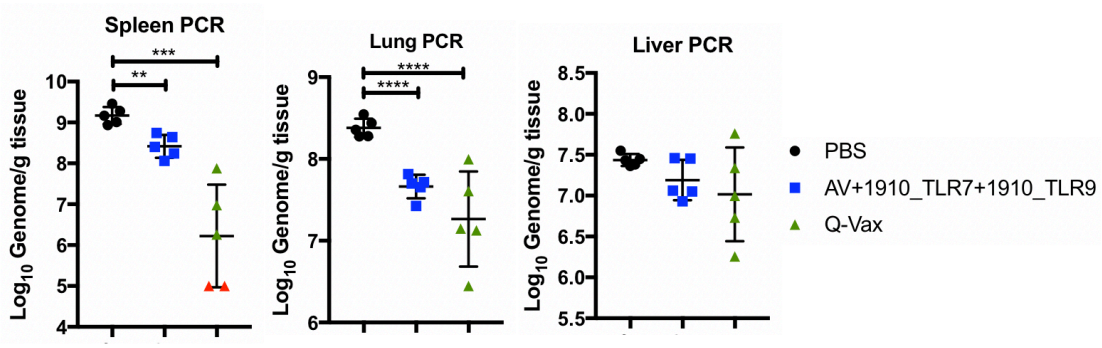

Figure 5.4 Protection from C. burnetii Upon Vaccination with TLR*a*-CBU1910 Conjugates. Protection from *C. burnetii* as assessed by qPCR of *C. burnetii* gene marker from harvested spleens, lungs, or livers on d 51 following vaccination (day 9 post challenge), n=5. Statistical analysis: one-way ANOVA, *: $p < 0.05$, **: $p < 0.01$, ***: $p < 0.001$, ****: $p < 0.0001$. AV=AddaVax™.

5.3 Initial Attempts at Site-specific TLR Agonist-Antigen Conjugation

In our first attempt at site specific modification, we selected sortase chemistry. Sortase is an enzyme that can conjugate N-terminal triglycine with C-terminal LPXTG polypeptide sequences.[14] For this work, we installed a sortase tag on the C terminus of CBU_1910, followed by a his_6 tag. This method was designed so that following sortase functionalization, the his_6 tag would be removed and the product recovered follow spin filtration and incubation with Ni-NTA resin.[15] We

used this method to append a tri-glycine-azide to the protein. Following incubation with BCN-TLR9*a*, CBU_1910-TLR9*a* conjugate was clearly observed by SDS-PAGE. Although we observed these initially promising results, after several attempts we concluded that the reaction did not scale well, and required extensive optimization for each protein we sought to conjugate. Thus we decided to try different approaches, that would be more amenable to readily generating several TLR agonist-antigen conjugates.

Although the sortase method did not sufficient material for TLR-antigen conjugation, other chemistries have been developed that may be more well suited for this purpose. The Francis lab at reported using 2-pyridine caroxyaldehyde (2PCA) chemistry to selectively modify the N-terminus of proteins.[16] By modifying the 2PCA molecule to include a functional handle for conjugation of TLR agonists, many proteins with a free N-terminus can be modified without the need to incorporate additional tags. To do this, we synthesized a novel 2PCA-azide. We found that this compound could readily functionalize GFP, a model test protein, and could be detected by mass spectrometry. We then tried to functionalize several proteins with 2PCA-azide. These included the vaccination model proteins ovalbumin and hen egg lysozyme and C. burnetii protein CBU_1910 and CBU_0345. Disappointingly, functionalization was only observed with CBU_0345. Although we demonstrated N terminal functionalization with a click chemistry handle on GFP and a *C. burnetii* antigen, we found that this approach was not as widely amenable to various proteins as we had previously hoped. The chemistry showed no reactivity with ovalbumin, hen egg lysozyme, or CBU_1910. Upon further analysis of the 2PCA mechanism and the characteristics of these proteins, it is clear that they are not ideal for 2PCA functionalization. Ovalbumin is obtained from eggs, which results in N-acylation of the N terminus. The hen egg lysozyme was recombinantly expressed in *E. coli*, so N terminal acylation was not an issue. However, the N terminus in wt HEL

is tied up in a intermolecular interaction with the side chain of a neighboring residue. Finally, with CBU_1910, the second residue in the protein is a proline, preventing the cyclization step. In addition, we found that a significant portion of the CBU_1910 has a cleaved methionine on the N terminus, resulting in the proline being the first amino acid in the sequence, which is also not amenable to 2PCA chemistry. Thus, the 2PCA approach was not suitable to meet our project goals of functionalizing a range of proteins as we had hoped and was not pursued further.

5.4 tris-NTA Mediated TLR Agonist-Antigen Complexation

To address the issue of versatility for a site-specific conjugation approach, we developed a new strategy for protein-TLR conjugation. This strategy could potentially be used on all recombinant proteins bearing a his tag, including our entire library of *C. burnetii* proteins expressed for microarray printing. His tags are frequently utilized to purify recombinant proteins through binding to Ni-NTA resin following expression. Other studies have shown that a tris-NTA construct can bind his-tagged proteins with low nano-molar affinity, on par or stronger than antibody-ligand binding.[17–19] Although the biotin and amino functionalized tris-NTA molecules are available commercially, they are prohibitively expensive - $3,355/mg biotin-tNTA and $2,003/mg amino-tNTA. Thus, we needed to develop a tNTA synthetic strategy to have sufficient material for TLR agonist-antigen complexation experiments and to introduce new chemical handles.

Scheme 5.1 Functionalized Tris-NTA Synthetic Scheme

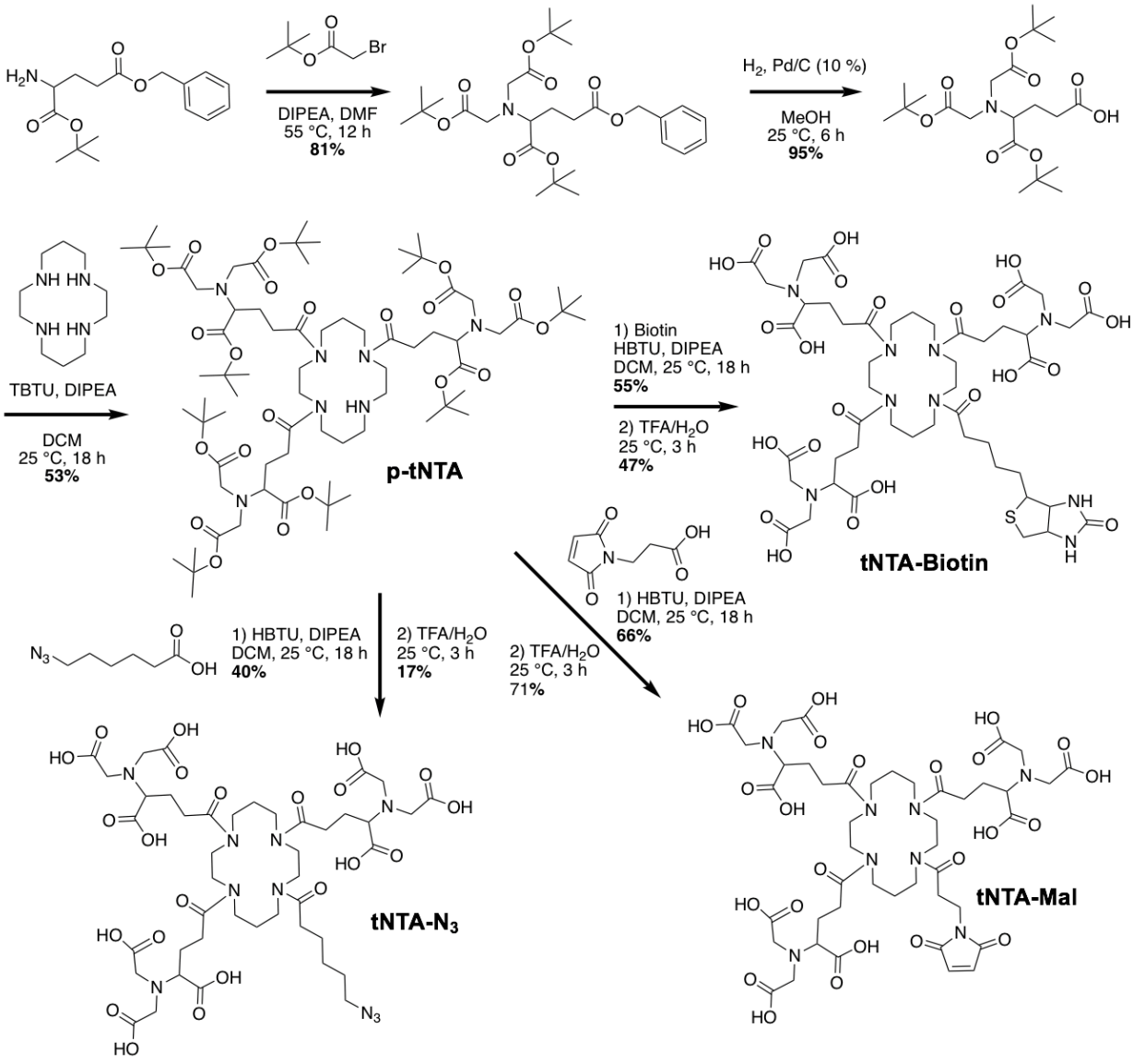

Following literature precedent, we performed a gram scale synthesis of the protected tNTA precursor (p-tNTA).[17] From there, we developed our own biotin functionalized tNTA (tNTA-Biotin) resulting in 80 mg of product. In addition, we were able to develop novel tNTA molecules at the tens of mg scale, including azide-, maleimide-, amino- and carboxy- tNTAs. These

compounds allow us to conjugate functionalized TLR agonists to the tNTA, followed by complexation with his-tagged antigens. tNTA-biotin has been particularly useful for our collaborators, the Felgner Lab, in generating high-throughput vaccine tests and for diagnostic assays. The other functionalized tTNAs have allowed us to generate conjugates with TLR agonists for complexing antigens.

Scheme 5.2 Synthesis of Ni-tNTA-TLR9*a* and Complexation with CBU_1910

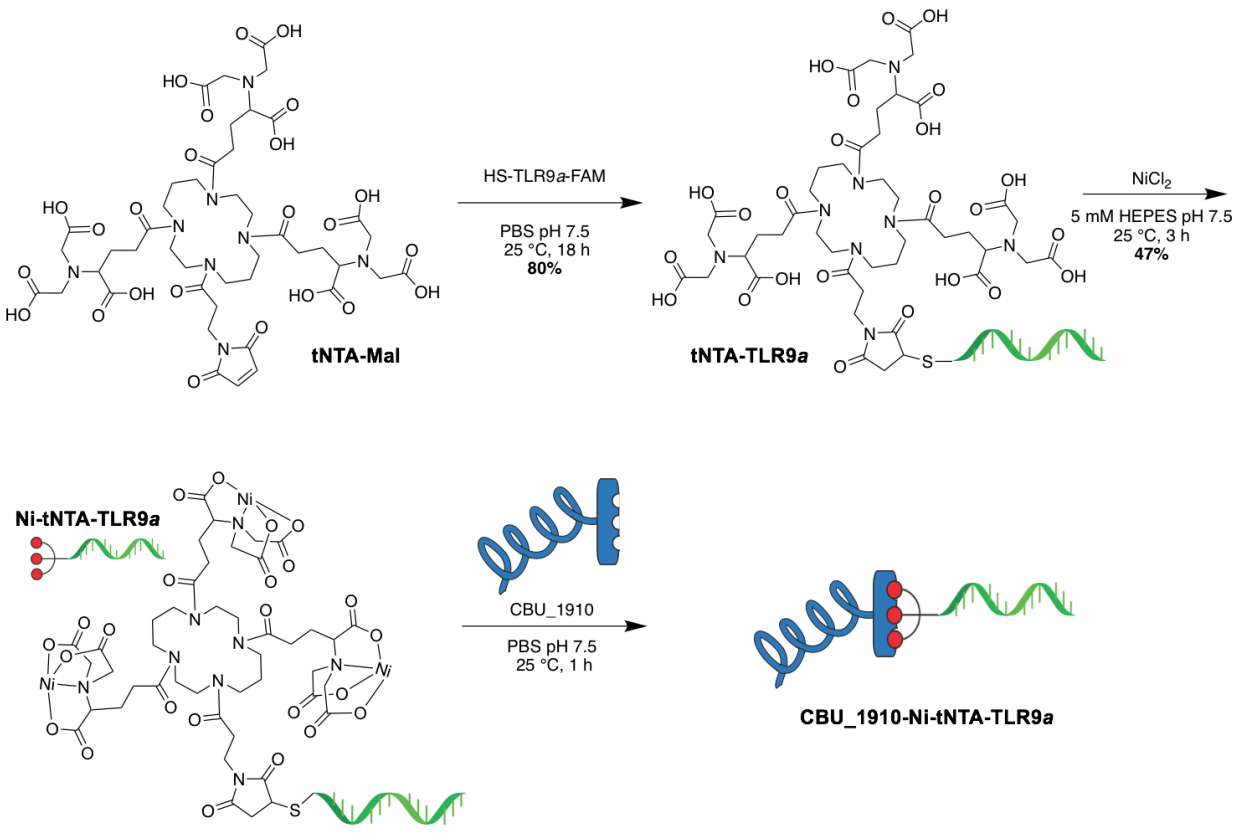

To generate tNTA-TLR agonists, we started with synthesizing tNTA-TLR9*a* (**Scheme 5.2**). For this, we used thiol-functionalized, single-stranded CpG1826 DNA-FAM (HS-TLR9*a*) which was ordered through IDT. Following TCEP reduction of the disulfide protecting group, HS-TLR9*a*

was conjugated to tNTA-Mal *via* Michael addition in 80% yield. Following conjugation, the NTA moieties were loaded with Ni^{2+} following incubation with $NiCl_2$ solution in 47% yield. We found that it was essential to use a non-phosphate buffer (like PBS), as precipitation of nickel phosphate salts would occur. However, following desalting of excess nickel, the Ni-loaded tNTA-TLR9*a* were soluble in PBS. Finally, the Ni-loaded tNTA-TLR9*a* was incubated with CBU_1910 in PBS to afford the CBU_1910-TLR9*a* complex. Given the unique nature of these molecules, we needed to develop analytical methods to confirm and evaluate the reactions.

Confirming the success of the various steps of the synthesis proved challenging. To solve this issue, we worked with the UCI Mass Spectrometry Facility to develop protocols for the oligonucleotide conjugates. In doing so, we were able to characterize the conjugates and follow the reaction process by mass spectrometry with single-Dalton resolution (**Fig. 5.5A**). In addition, we were able to apply these MS protocols to observe the formation of the intact, protein-tNTA-TLR9a complex (**Fig. 5.5B**). This was a notable achievement, as this complex is formed by non-covalent bonds, but survives the ionization process. To achieve this, we used a size exclusion column in place of the reverse phase columns typically used on the instrument which result in disruption of the complex. In addition, we had to use pH 7.4 ammonium acetate buffer, as the typical low pH formic acid buffers, which are preferred for ionization of proteins, results in protonation of the NTA and dissociation of the Ni^{2+}.

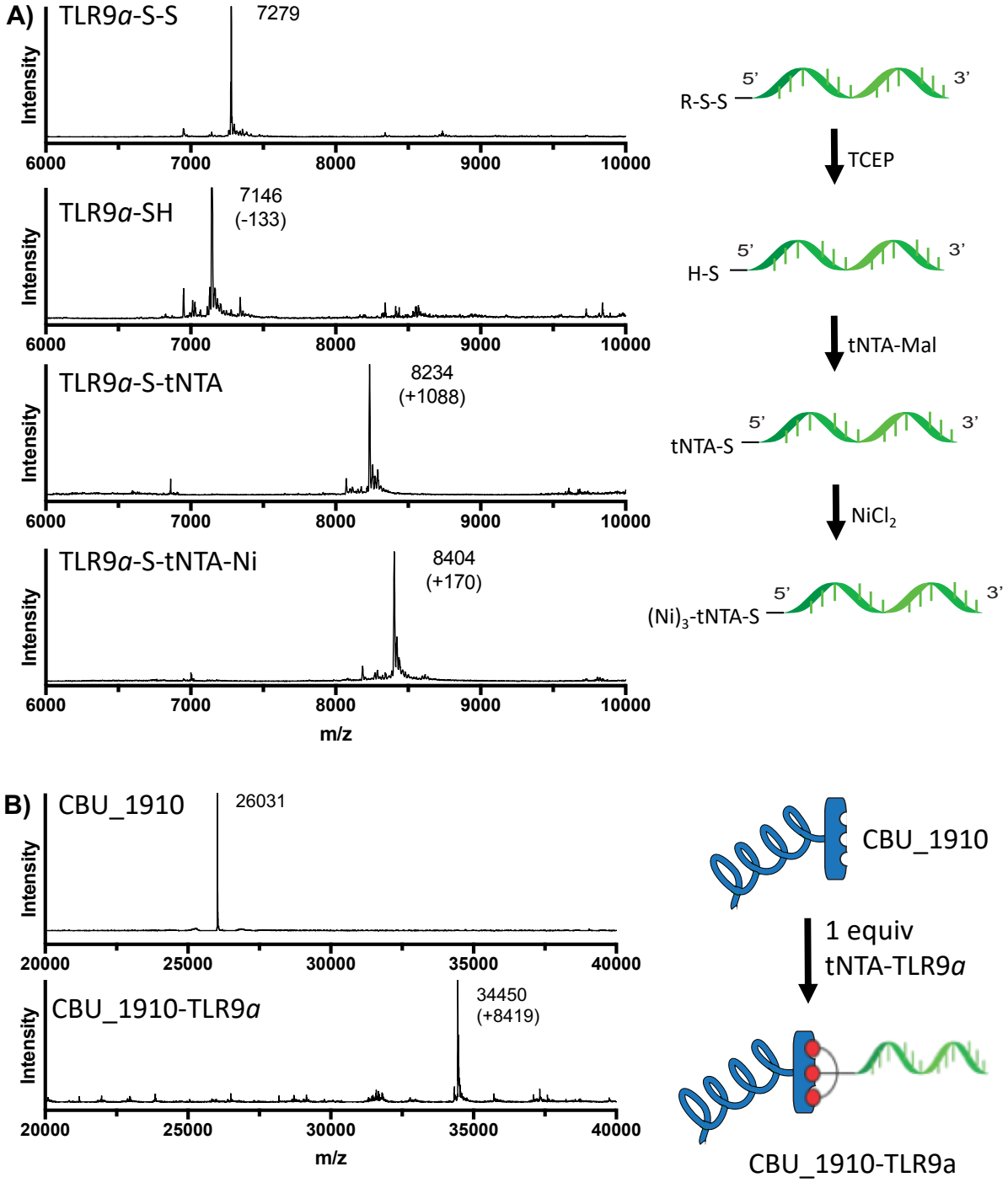
A)
TLR9α-S-S
7279
Intensity
6000
7000
8000
9000
10000
TLR9α-SH
7146
(-133)
TLR9α-S-tNTA
8234
(+1088)
TLR9α-S-tNTA-Ni
8404
(+170)
m/z
R-S-S
5'
3'
TCEP
H-S
tNTA-Mal
tNTA-S
NiCl2
(Ni)3-tNTA-S
B)
CBU_1910
26031
20000
25000
30000
35000
40000
CBU_1910-TLR9α
34450
(+8419)
1 equiv
tNTA-TLR9α
CBU_1910-TLR9a

Figure 5.5 Mass Spectrometry of Ni-tNTA-TLR9a Synthetic Intermediates and Complexing with CBU_1910. A) Mass spectra following progress of Ni-tNTA-TLR9*a* synthesis. B) Mass spectra of CBU_1910 and CBU_1910-TLR9*a* complex.

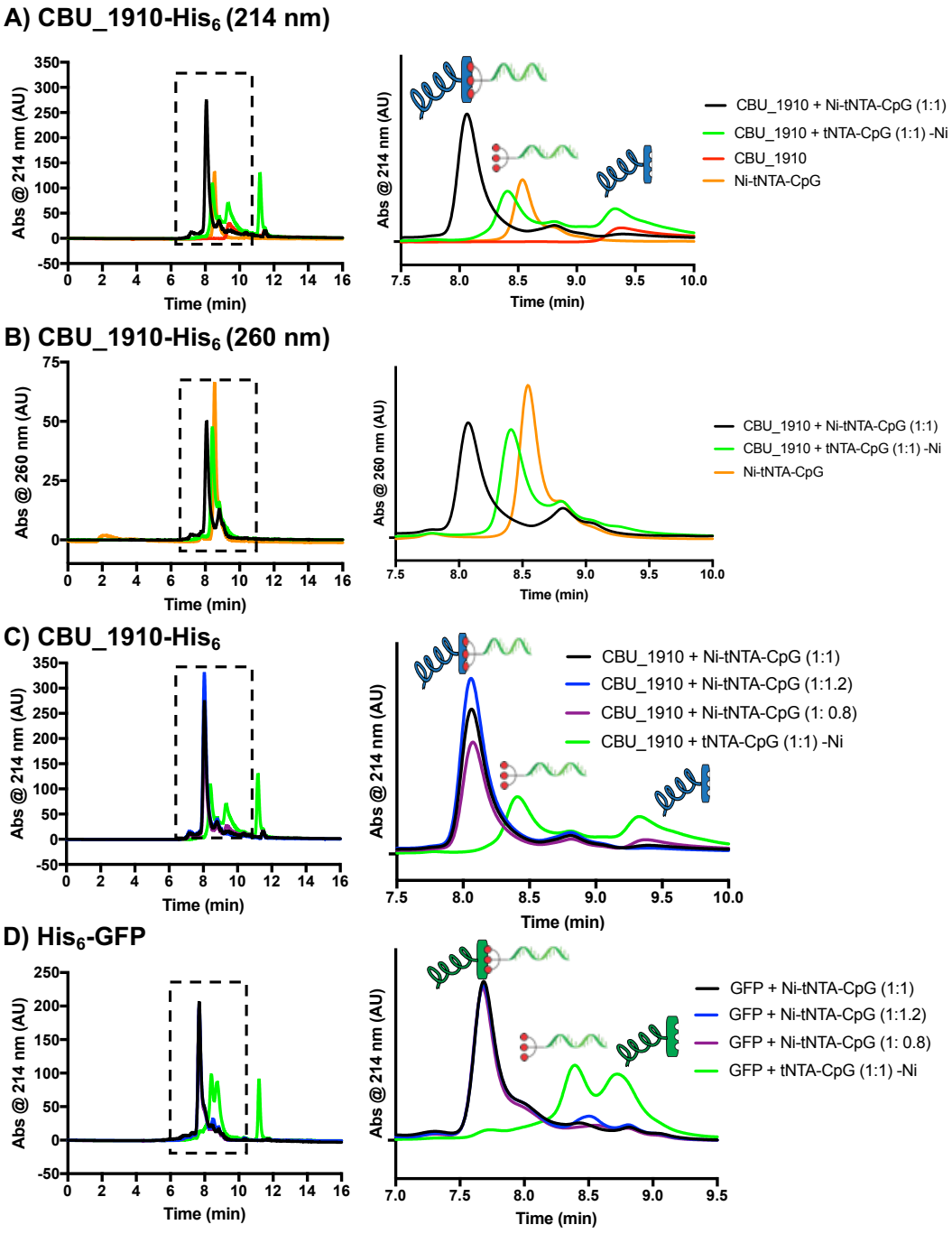

Figure 5.6 Size Exclusion Chromatography of Ni-Tris-NTA-Protein Complexes. SEC measured at A) 214 nm and B) 260 nm of CBU_1910 complexation with Ni-tNTA-TLR9*a* in PBS.

SEC measured at 214 nm of varying concentrations of Ni-tNTA-TLR9*a* with C) CBU_1910 or D) GFP in PBS.

To probe the extent of tNTA-TLR*a* complexation, we tracked the complexation of antigens and tNTA-TLR9*a* using size exclusion chromatography (SEC) with a UV detector. Upon incubation of CBU_1910 and Ni-tNTA-TLR9*a* a peak at 8 minutes was observed in both the 214 and 260 nm channels, which was sooner than peaks observed in the absence of Ni or with CBU_1910 and Ni-tNTA-TLR9*a* alone (**Fig. 5.6A and B**). The appearance of this single, faster-eluting peak suggests complexation of the antigen and the tNTA-TLR9*a*. Surprisingly, the 8 kDa Ni-tTNA-TLR9*a* eluted faster than the 26 kDa protein, potentially due to aggregation or repulsive interactions with the column. Adding a small excess (1.2 : 1) of the tNTA-TLR9*a* to CBU_1910 resulted in high conversion of the protein to the protein-tNTA complex. Incubating Ni-tNTA-TLR9*a* with GFP also resulting in formation of complex as evidenced by SEC (**Fig. 5.6 D**).

Scheme 5.3 Synthesis of tNTA-TLR7*a*

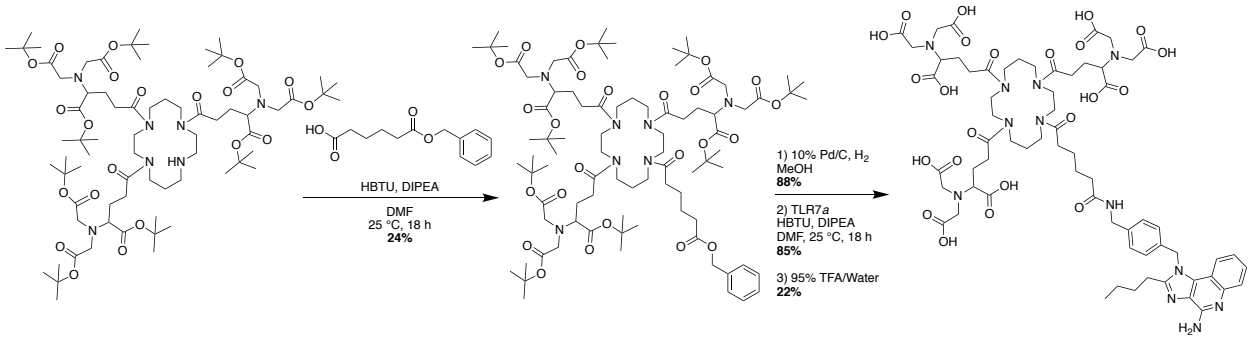

To further explore TLR agonist conjugation, we synthesized tNTA-TLR7*a* and tNTA-TLR2/6*a*. p-tNTA was coupled to a mono-Cbz protected bis-hexanoic acid *via* HBTU activation in 24% yield (**Scheme 5.3**). Following Cbz deprotection in 88% yield, TLR7*a* was conjugated using HBTU in 85% yield. Finally, TFA deprotection of the O-*t*Bu groups resulted in tNTA-

TLR7*a* in 22% yield. The next steps with this compound are nickel loading and complexation with antigen, however, purifying the Ni-tNTA-TLR7*a* from excess Ni^{2+} has proven challenging.

Scheme 5.4 Synthesis of tTNA-TLR2/6*a*

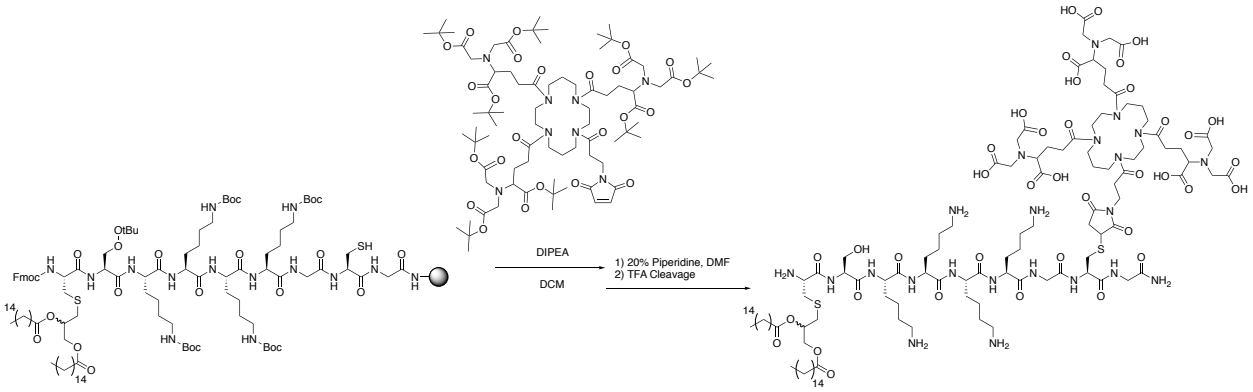

tNTA-TLR2/6 was synthesized *via* Michael addition between the resin bound peptide and tTNA-Mal, similar to the TLR tri-agonist conjugation approach developed in Chapter 2 (**Scheme 5.4**). The product was recovered following piperidine deprotection of Fmoc and resin cleavage/peptide deprotection with TFA. Conditions for nickel loading are ongoing, as our initial loading attempt resulted in precipitation.

Although the Ni loading has not been completed for tNTA-TLR7*a* and tNTA-TLR2/6*a*, we accessed the effect of tNTA conjugation with the agonist on the immunostimulatory capability of the agonist by Raw Blue NF-κB assay (**Fig. 5.7**). Unlike the Tri-agonist conjugations described in chapter 3, TLR7*a* and TLR2/6*a* conjugation did not result in dramatic loss of potency, an encouraging sign for TLR agonist-antigen complex activity.

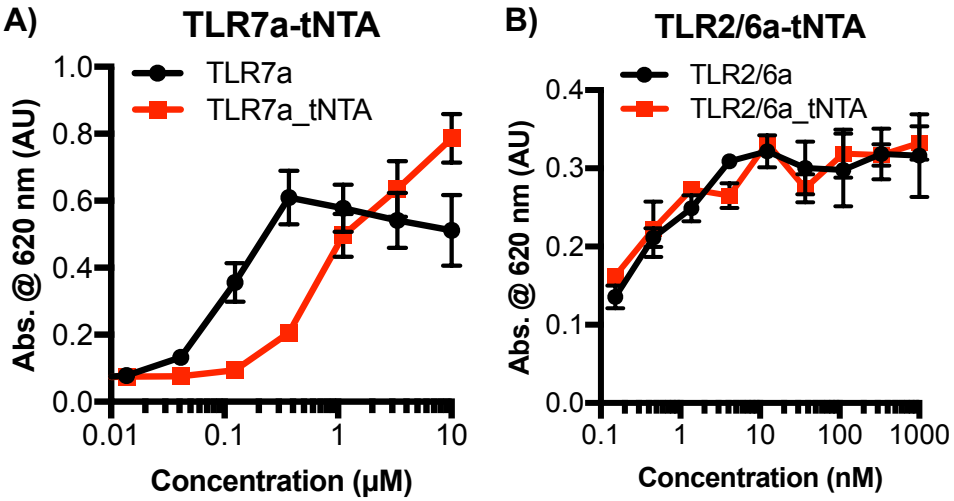

Figure 5.7 NF-κB Stimulatory Activity of TLR7*a*-tNTA and TLR2/6*a*-tNTA. A) Dose response curves of TLR7a and TLR7*a*-tNTA and B)TLR2/6a and TLR2/6*a*-tNTA on a NF-κB RAW-Blue 264.7 macrophage cell assay. Cells were incubated with each compound for 18 h at 37 °C. Supernatant was removed, incubated with QUANTI-Blue for 1 h and the absorbance at 620 nm measured. Error bars represent SD. Samples were run in triplicate.

5.5 Future Directions

Although the complexation of TLR agonist and antigen *via* tNTA has shown to be highly versatile and useful for specific applications, there are still inherent limitations. First, Ni^{2+} is required for complexation, which limits the practicality of the design as Ni^{2+} can be toxic *in vivo* and cause allergic reactions.[20] In addition, the complexation is non-covalent. Although the binding of Ni-tNTA and protein has been shown to be very strong *in vitro*, a study attempting to use this approach for vaccination showed that there was little benefit *in vivo*, and suggested that the binding appears to be short lived in the serum.[21] However, both of these issues could be addressed if the Ni-NTA protein complex could be made covalent, followed by removal of Ni^{2+}.

Recently, Vance and coworkers demonstrated an antibody-drug conjugate technique utilizing a photocrosslinker.[22] The benzophenone (Bpa) photocrosslinker was incorporated into a cyclic peptide which was found to bind non-covalently to the constant region of an antibody. Upon irradiation, the Bpa preferentially forms a covalent bond with methionine. This approach could be applied to tNTA conjugation with antigens bearing N terminal his_6 tags, as the N terminal residue directly adjacent the his tag from recombinant expression is a methionine (**Fig. 5.8A**). To test this approach, a Bpa containing tNTA-TLR9*a* was synthesized (**Fig. 5.8B**) and confirmed by LCMS (**Fig. 5.8C**). Attempts to conjugate this molecule to His_6-GFP are underway. Following generation of this molecule, *in vivo* experiments can begin, comparing the effects of vaccination with unlinked, tNTA complexed, and Bpa-tNTA- conjugated TLR agonists and antigen.

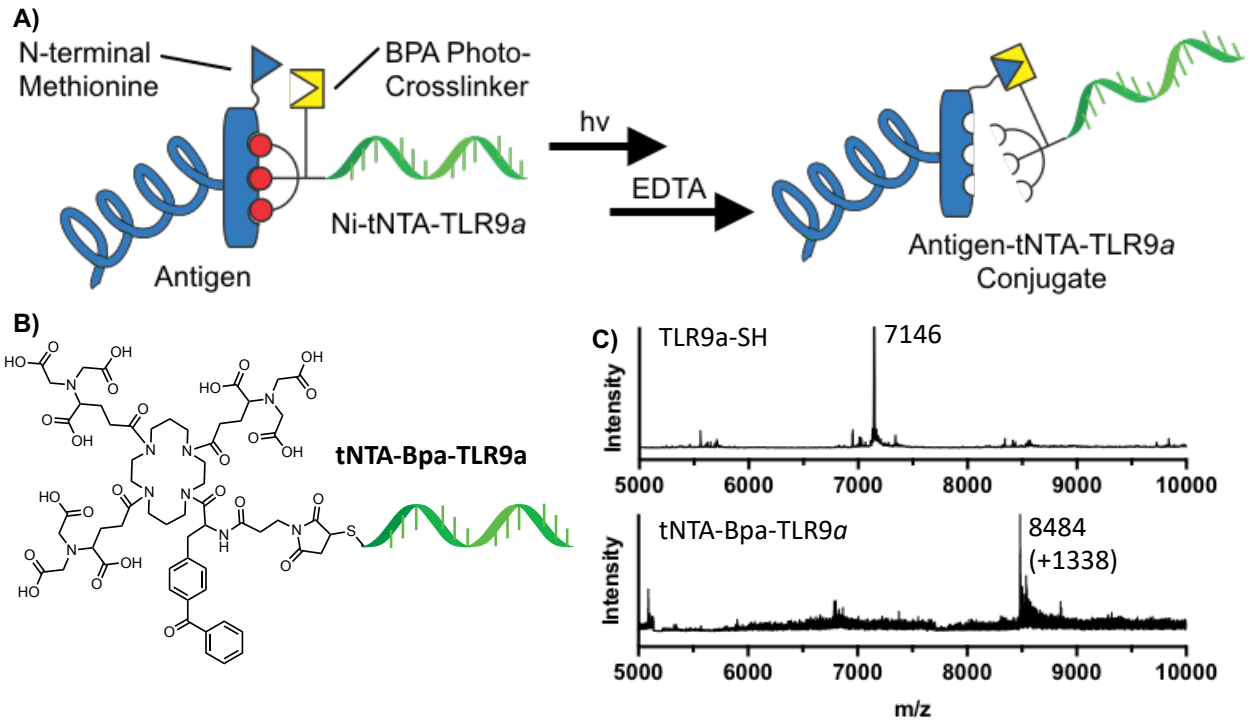

Figure 5.8 Design and Initial Results of Bpa Crosslinked tNTA-TLR Agonist-Antigens. A) Illustration of reaction scheme of Bpa functionalized tNTA-TLR9a with His tagged antigen. UV irradiation and incubation with EDTA results in a site-specific, Ni-free conjugate. B) Chemical

structure of tNTA-Bpa-TLR9*a* C) MS confirmation of generation of tNTA-Bpa-TLR9*a*.

5.6 Conclusions

TLR agonist conjugation to antigens is a promising approach to improve the antigen specific immune responses generated by the immune system. This has been demonstrated using non-specific conjugation approaches to proteins with remarkable results in vaccination experiments.[7,13] Site-specific conjugation is a promising way to improve this technology, however, no methods have been described for the site-specific conjugation of TLR agonists to protein antigens. Here, we have described our efforts and success of generating these constructs through a variety of methods. Although conjugates could be generated by sortase chemistry and by 2PCA chemistry, we found these methods to be inefficient and not amenable to several of our proteins. Thus, we turned to a complexation approach using tNTA and his_6 tag binding. We demonstrated the ability to form antigen-TLR9a complexes and developed methods to characterize these compounds. Finally, we showed our work in further developing this method with Bpa photocrosslinking as a potential solution to the limitations of the tNTA approach. This work provides a roadmap to some of the considerations to make when creating TLR agonist-antigen conjugates and can serve to be inform future studies in subunit vaccine design.

5.7 Experimental Methods

Materials and Instrumentation. Reagents were purchased from Sigma-Aldrich, ThermoFisher, Quanta Biodesign, Anaspec, or Acros Organics and used as is unless otherwise noted. Single stranded CpG-ODN1826 (Azide-C6-5′-TCCATGACGTTCCTGACGTT-3′-6-FAM or Azide-C6-5′-TCCATGACGTTCCTGACGTT-3′-OH) and CpG-ODN1826 (Cap-S-S-5’-

TCCATGACGTTCCTGACGTT-3'-6-FAM) with a phosphorothioated backbone was purchased from IDT. Buffers and media for cell culture were purchased from Fisher Life Technologies. Centrifugal Filter Devices (3k and 10k MWCO) were purchased from Millipore. Compounds were filtered using 0.22 μM syringe filters (Restek). ^{1}H and ^{13}C NMR spectra were taken on a Bruker CRYO500 NMR spectrometer (500 MHz) and analyzed using MestreNova software. Spectra are referenced to solvent peak for ^{1}H NMR (CD_3OD = 3.33 ppm, $(CD_3)_2SO$ = 2.50 ppm, $CDCl_3$ = 7.26 ppm) and ^{13}C NMR (CD_3OD = 49.00 ppm, $(CD_3)_2SO$ = 39.52 ppm, CDCl3 = 77.16 ppm). Analytical high-performance liquid chromatography (HPLC) was performed using an Agilent 1260 Infinity HPLC with a Phenomenex Luna 5 μm C8 100 Å 150 x 4.6 mm LC column. Preparative HPLC was performed on a Gilson Preparative HPLC System with 333 HPLC Pumps and GX-271 liquid handler using a Phenomenex Luna 5 μm C8(2) 100 Å 150 x 21.2 mm LC column. High resolution mass spectrometry (HRMS) was performed by the University of California, Irvine Mass Spectrometry Center. MALDI TOF was performed on an AB SCIEX TOF/TOF 5800 System instrument. SEC was performed on an Agilent analytical HPLC equipped with a Phenomenex Yarra SEC-2000 3 μm particle size, 145 A pore size, 1k-300k MW range, 300x7.8 mm column. Silica Gel Chromatography was performed using RediSep Rf normal silica columns on a Teledyne-Isco CombiFlash Rf auto column instrument. Gel electrophoresis was carried out using 10% Mini-PROTEAN TBE-urea gels or 12% Mini-PROTEAN TGX precast protein gels in a MiniPROTEAN tetra cell (BIO-RAD). Data was analyzed using student T test or one-way ANOVA in Graph Pad Prism software. All values were reported as mean ± SD, where error bars represent biological replicates.

Technical Note on Oligo Mass Spectrometry

Positive mode analysis of oligonucleotide conjugates was performed on a Waters Xevo G2 XS Q-TOF mass analyzer (Waters, Milford, MA, USA). A 5 min run in 50 mM ammonium acetate pH 7.4 was used to elute each sample off a Waters BEH 200 A 150 mm SEC stationary phase at 0.1 ml/min. Waters Masslynx MaxEnt1 software was used to deconvolute the charge-state ladder into an accurate MS1 mass.

Technical Note on ESI-MS of Oligonucleotide Conjugates

Positive mode analysis of oligonucleotide conjugates was performed on a Waters Xevo G2 XS Q-TOF mass analyzer (Waters, Milford, MA, USA). A 5 min run in 50 mM ammonium acetate pH 7.4 was used to elute each sample off a Waters BEH 200 A 150 mm SEC stationary phase at 0.1 ml/min. Waters Masslynx MaxEnt1 software was used to deconvolute the charge-state ladder into an accurate MS1 mass.

Technical Note on ESI-MS of Proteins

Positive mode analysis of proteins was performed on a Waters Xevo G2 XS Q-TOF mass analyzer (Waters, Milford, MA, USA). A 5 min gradient, 1.5 min ramp from 0%B to 97 %B, was used to elute each sample off a Waters BEH phenyl 300 A stationary phase at 0.2 ml/min. Mobile buffers were prepared gravimetrically; phase A consisted of 0.1% formic acid (FA) in water while phase B was 0.1% FA in acetonitrile. Waters Masslynx MaxEnt1 software was used to deconvolute the charge-state ladder into an accurate MS1 mass.

Mice

5-6 week old female C57BL/6 mice were purchased from Charles River Laboratories International, Inc. Mice were housed in SPF facility with a 12 hour dark/light cycle with autoclaved bedding and irradiated food. All handling of mice at both UCI and USAMRIID was performed under an approved Institutional Animal Care and Use Committee protocol. 5 or 8 mice were given a priming dose (day 0) and boosted 2 weeks later (day 14). Mice were administered 1 nmole of each TLR agonist-antigen conjugate or unconjugated mixed in liquid formulations. In relevant vaccine formulations AddaVax™ (InvivoGen, San Diego, CA) was added at 50% of total vaccine volume. Fifty microliters of vaccine formulations were delivered intramuscularly in the thigh using a 31gauge needle (BD Insulin Syringes, Laguna Hills, CA, USA; 3/10cc).

Ethics statement: All animal protocols were approved by the Institutional Animal Care and Use Committee of the University of California, Irvine. Animal research at the United States Army Medical Research Institute of Infectious Diseases (USAMRIID) was conducted under an animal use protocol approved by the USAMRIID Institutional Animal Care and Use Committee (IACUC) in compliance with the Animal Welfare Act, PHS Policy, and other Federal statutes and regulations relating to animals and experiments involving animals. The facility where this research was conducted is accredited by the Association for Assessment and Accreditation of Laboratory Animal Care International (AAALACi) and adheres to principles stated in the Guide for the Care and Use of Laboratory Animals (National Research Council, 2011).

Tissue Collection and Analysis

Plasma/Serum

Animals were anesthetized under 2-2.5% isoflurane and 2 L/min of oxygen flow under standard atmospheric pressure for these experiments. Plasma was collected on days 0, 1, 14, 15 from isoflurane anesthesized mice via cheek bleed using a 25-gauge needle (BD PrecisionGlide Needle). Blood was collected in Microvette CB 300 LH lithium heparin tubes (Sarstedt; Aktiengesellschaft & Co., Sparks, NV, USA) and plasma was separated at 2000xg for 5 min at 4°C. Serum was collected on termination day (day 17/21) via cardiac puncture of carbon dioxide euthanized mice using a 29 gauge needle (Insulin Syringe; Exelint International Co., Redondo Beach, CA, USA; 1mL), and separated at 2000xg for 10 minutes at 4°C. Plasma and serum samples were stored at -20°C for further analysis.

Flow cytometry analysis of immune cell populations

Spleen and draining inguinal LN samples were collected from mice on day 17 or 21. Whole spleens and LNs were passed through 40μm nylon mesh strainers (Fisherbrand®, Waltham, MA, USA) and rinsed with PBS to make single cell suspensions. Single cell suspensions of spleen cells were treated with ACK lysing buffer (ThermoFisher Scientific) for 5 min at room temperature to remove red blood cells. 1 x 10^6 cells, in FACS staining buffer (BioLegend), were transferred to a V-bottom plate (VWR, Radnor, PA). Fc receptors were blocked using anti-mouse CD16/32 (Biolegend) and B220 cells were stained using APC/Cy7 anti-mouse B220 (Biolegend). CD4 cells were stained using FITC anti-mouse CD4 (Biolegend). CD8 cells were stained using PE/Cy7 anti-mouse CD8a (Biolegend). Samples were analyzed by flow cytometry using ACEA NovoCyte Flow Cytometer and analyzed using NovoExpress software and GraphPad Prism.

T cell Recall Response

1 x 10^6 splenocytes/mL were incubated in CytoOne (USA Scientific, Ocala, FL, USA) flat bottom tissue culture plates (USA Scientific). Cells were stimulated with 10μg/mL of *C. burnetii* antigen in RPMI supplemented with 10% FBS, 2% penicillin and streptomycin, and 0.2% 2-mercaptoethanol (complete RPMI) and incubated for 48 h at 37 ^{o}C at 5% CO_2. IFN-γ or IL-4 levels were analyzed in undiluted supernatants by ELISA (Biolegend) according to the manufacturer's instructions. For ELISpot Analysis, 2 x 10^5 splenocytes/well were incubated with 10μg/mL of *C. burnetii* antigen in complete RPMI in double color IL-4/IFN-γ ELISpot plates (Immunospot; CTL, Shaker Heights, OH, USA) for 48 hours at 37°C at 5% CO_2. Plates were processed using manufacturer's instructions and analyzed using CTL ImmunoSpot scanning services.

Vaccine Efficacy in Live *C. burnetii* Challenge Model

Vaccination and blood collection: Groups of 10 mice were given a priming dose (day 0) via intramuscular injection with either 3 recombinant protein vaccines (CBU_1910 alone, CBU_1910 and TLR tri-agonist 2/6_4_7a, or CBU_1910 and TLR agonists 2/6+4+7a), positive control Q-Vax, or saline control. Blood was collected from vaccinated mice on day 0 (baseline) and day 14 (just before boost except Q-Vax® vaccinated mice) and 70 (at the end of study).

Aerosol exposure: On the day of *C. burnetii* challenge (day 42), mice were moved to ABSL3 and housed there for the rest of the study. *C. burnetii* Nine Mile was propagated by the Diagnostic Systems Division in ACCM-2 (Sunrise Science Products) under micro-aerobic conditions for seven days. The bacteria were concentrated by centrifugation and brought up in ACCM-2. Mice were placed in wire mesh cages per their vaccination group and challenged via whole-body exposure chamber as described previously (Zumbrun et al.). Aerosols were performed using a 3-

jet Collison nebulizer within a Class III Biosafety cabinet under control of the Automated Bioaerosol System. Starting concentrations and all glass impinger (AGI) samples were taken to enumerate bacteria concentration via PCR. All mice were exposed to a target dose of 10^{11} CFU/mL aerosolized *C. burnetii* Nine Mile strain 6 weeks following last vaccination.

Synthetic Procedures.

Non-specific (NHS) Azide Functionalization of CBU_1910

CBU_1910 (10 mg, 380 nmol) was diluted with 50 mM $NaHCO_3$ (850 uL). NHS-azido acetic acid (1.5 mg, 7600 nmol) was added to the solution and the reaction stirred for 2 h. The reaction was then purified by spinning through a 10k MWCO amicon spin filter and washing 5 X with PBS. The product was characterized by mass spectrometry, which showed a range of 4-11 azides/protein. Recovered 5.5 mg product (207 nmol, 54% yield).

Non-specific TLR7a Functionalization of CBU_1910_azide. CBU_1910_azide (3.0 mg, 115 nmol) was diluted with PBS (2.3 mL). DBCO-PEG_4-TLR7*a* (917 nmol) in DMF (459 uL) was added to the solution, and the reaction mixed for 18 h. The reaction was then purified by spinning through a 10k MWCO amicon spin filter and washing 5 X with PBS. The product was characterized by mass spectrometry, which showed a range of 0-3 TLR7*a*/protein and UV Vis and BCA showed 3.7 TLR7*a*/protein. Recovered 0.6 mg product (24 nmol, 21% yield).

Non-specific TLR9a Functionalization of CBU_1910_azide. CBU_1910_azide (1.0 mg, 38 nmol) in PBS (169 mL) was mixed with BCN-TLR9*a* (75 nmol) in PBS (1.2 mL) and the reaction mixed for 18 h. The reaction was then purified by spinning through a 10k MWCO amicon spin filter and washing 5 X with PBS. The product was characterized by mass spectrometry, which

showed a range of 0-3 TLR7*a*/protein and UV Vis and BCA showed 1.8 TLR9*a*/protein. Recovered 0.8 mg product (18 nmol, 47% yield).

Tris-NTA procedures.

p-tNTA was synthesized as previously described.[17]

pTris-NTA Biotin. Biotin (44 mg, 0.18 mmol) and HBTU (68 mg, 0.18 mmol) was dissolved in DMF (5.0 mL) and DIPEA (0.5 mL). After five minutes, p-tNTA (216 mg, 0.15 mmol) was added and the reaction was stirred overnight. The solvent was evaporated and the product purified by silica chromatography. Column Conditions: 40 g silica gel column, Mobile phase A: DCM, Mobile Phase B: Methanol. Gradient: percent mobile phase B: 0-5 min 0%, 5-10 min 10% ramp, 10-18 min 10%. Product eluted last at 11.5 min. The fractions containing product were collected, the solvent removed by rotary evaporation, and dried over high vacuum. The product was recovered and analyzed by ESI-MS (138 mg, 55% yield)**.** Predicted $[M+Na]^+$: 1689.0 m/z Observed $[M+Na]^+$: 1688.3 m/z.

Tris-NTA Biotin. pTris-NTA Biotin (216mg, 0.150 mmol) was dissolved in 95% TFA in water (5 mL) and stirred for 2 h. The TFA was removed by rotary evaporation and the residue added to 40 mL of cold diethyl ether to precipitate the product. The mixture was centrifuged to recover the product pellet. The pellet was dissolved in 50% water/ACN, sterile filtered through a nylon 0.22 um filter, and the product recovered by lyophilizing in aliquoted eppendorf tubes (82 mg, 47% yield). The product was confirmed by LCMS. Predicted $[M+Na]^+$: 1162.4 m/z Observed $[M+Na]^+$:

1162.6 m/z.

pTris-NTA-Mal. Maleimido-propionic acid (44 mg, 0.26 mmol) and HBTU (99 mg, 0.26 mmol) was dissolved in DMF (9.5 mL) and DIPEA (0.5 mL). After five minutes, p-tNTA (288 mg, 0.20 mmol) was added and the reaction was stirred overnight. The solvent was evaporated and the product purified by silica chromatography. Column Conditions: 40 g silica gel column, Mobile phase A: hexanes, Mobile Phase B: ethyl acetate. Gradient: percent mobile phase B: 0-4 min 0%, 4-8 min 100% ramp, 8-22 min. Product eluted as a broad peal at 15-22 min. The fractions containing product were collected, the solvent removed by rotary evaporation, and dried over high vaccum. The product was recovered and analyzed by LCMS (142 mg, 45% yield). Predicted $[M+Na]^+$: 1613.9 m/z Observed $[M+Na]^+$: 1612.9 m/z.

Tris-NTA-Mal. p-tNTA-Mal (216 mg, 0.15 mmol) was dissolved in 95% TFA in water (5 mL) and stirred for 2 h. The TFA was removed by rotary evaporation and the residue added to 40 mL of cold diethyl ether to precipitate the product. The mixture was centrifuged to recover the product pellet. The pellet was dissolved in 50% water/ACN, sterile filtered through a nylon 0.22 um filter, and lypoholized in aliquoted eppendorf tubes. The product was confirmed by LCMS (82 mg, 47% yield). The product was recovered and analyzed by LCMS (142 mg, 45% yield). Predicted $[M+Na]^+$: 1087.4 m/z Observed $[M+Na]^+$: 1086.4 m/z.

pTris-NTA-Azide. 6-azidohexanoic acid (43 mg, 0.270 mmol) and HBTU (103 mg, 0.270 mmol)

were dissolved in DMF (4.5 mL) and DIPEA (0.5 mL). The solution was stirred for 5 minutes, and then combined with pTNA (300 mg, 0.208 mmol) and the solution was stirred for 18 h. The solvent was evaporated and the product purified by silica chromatography. Column Conditions: 40 g silica gel column, Mobile phase A: hexanes, Mobile Phase B: ethyl acetate. Gradient: percent mobile phase B: 0-3 min 0%, 3-10 min 100% ramp, 10-18 min 100%. Product eluted as a broad peak at 12-13 min. Fractions containing product were collected, the solvent removed by rotary evaporation, and dried over high vacuum. The product was recovered and analyzed by LCMS (130 mg, 40% yield). Predicted $[M+Na]^+$: 1602.0 m/z Observed $[M+Na]^+$: 1602.8 m/z.

Tris-NTA-Azide. p-tNTA-azide was dissolved in 95% TFA in water (5 mL) and stirred for 2 h. The TFA was removed by rotary evaporation and the residue added to 40 mL of cold diethyl ether to precipitate the product. The mixture was centrifuged to recover the product pellet. The pellet was dissolved in 50% water/ACN, sterile filtered through a nylon 0.22 um filter, and lypoholized in aliquoted eppendorf tubes. The product was confirmed by LCMS (14 mg, 17% yield). Predicted $[M+H]^+$: 1075.4 m/z Observed $[M+H]^+$: 1074.5 m/z.

tNTA-TLR9*a* Conjugation. Cap-S-S-CPG-FAM (0.252 mM, 270 μL, 68.0 nmol) solution, TCEP (53.0 mM, 128 μL, 680 nmol) solution and PBS (300 μL) were combined in a 1.5 mL Eppendorf tube. The solution was agitated for 4 h at room temperature. The solution was then spun for 10 min at 14,000 x g in a 3k MWCO amicon spin filter. HEPES 5 mM buffer pH 7.5 (400 μL) was added to the retained solution, spun again, and repeated 3X. The collected solution was mixed with tNTA-maleimide in DMF solution (3.5 mM, 58.4 μL, 144 nmol) and agitated overnight at room temperature. HEPES (300 μL) was added and the solution, the solution washed 3X in a 3k MWCO

amicon spin filter, adding HEPES buffer to 500 μL total each time. The solution was collected to recover the final product (55 nmols, 80 % yield) and analyzed by HPLC and ESI-MS. The product was quantified by UV Vis absorbance at 260 nm. See **Fig. 5.6**.

tNTA-TLR9*a* Ni-Loading. tNTA-TLR9*a* solution (0.273 mM, 110 μL, 30.0 nmol) was mixed with $NiCl_2$ solution (0.5 M, 1.8 μL, 1000 nmol) in HEPES 5 mM pH 7.5 buffer and incubated for 3 h. The reaction was diluted to 500 uL with HEPES 5 mM pH 7.5 and washed 3X in a 3k MWCO amicon spin filter, adding HEPES buffer to 500 μL total each time, and then an addition 3X with PBS. The solution was collected to recover the final product (17 nmols, 57 % yield) and analyzed by ESI-MS. The product was quantified by UV Vis absorbance at 260 nm. See **Fig. 5.6**.

Ni-tNTA-TLR9*a* Complexation with Antigens.

CBU_1910 (1 mg/mL stock, 13.1 μL, 0.5 nmol) or GFP (70 μM stock, 5.7 μL, 0.4 nmol) was mixed with 0.8-1.2 equivs Ni-tNTA-TLR9*a* solution (90 μM stock) in PBS buffer and incubated for 1 h. The reaction was immediately analyzed by SEC and MS. Predicted CBU_1910-TLR9a Complex MW: 979.5 m/z. Observed $[M+2Na]^{2+}$: 979.1 m/z. See **Fig. 5.6**.

Synthesis of pTNA-COO-CbZ. Mono-Cbz-Adipic acid (61 mg, 260 μmol) and HBTU (99 mg, 260 μmol) were dissolved in DMF (9.5 mL) and DIPEA (0.5 mL). The solution was stirred for 5 minutes, and then added to p-TNTA (288 mg, 200 μmol) and the solution was stirred for 18 h. The solvent was evaporated and the product purified by silica chromatography. Column Conditions: 40 g silica gel column, Mobile phase A: hexanes, Mobile Phase B: ethyl acetate. Gradient: percent mobile phase B: 0-3 min 0%, 3-10 min 100% ramp, 10-18 min 100%. Product eluted as a broad

peak between 12-17 min. Fractions collected, the solvent removed by rotary evaporation, and dried over high vacuum to recover the product (80 mg, 24% yield). The product was characterized by ESI- MS. Predicted $[M+2Na]^{2+}$: 852.0 m/z. Observed $[M+2Na]^{2+}$: 851.4 m/z.

CbZ Deprotection of pTNA-COO-CbZ. 10% Pd/C (1 mg) was added to a flame dried RBF and purged with N_2. Methanol (20 mL) was added, followed by pTNA-COO-CbZ (83 mg, 50 μmol) dissolved in methanol (5 mL). The solution was purged again with N_2. A hydrogen balloon was then added and the reaction stirred for 6 h. The reaction solution was ran over a celite plug to remove Pd/C. The methanol was removed by rotary evaporation and the product recovered following drying under vacuum (69 mg, 88% yield). The product was characterized by MS. Predicted $[M+2Na]^{2+}$: 807.0 m/z. Observed $[M+2Na]^{2+}$: 806.9 m/z.

Synthesis of p-tNTA-TLR7*a*. p-TNT-COOH (69 mg, 44 μmol) and HBTU (22 mg, 57 μmol) were dissolved in DMF (9.5 mL) and DIPEA (0.5 mL). The solution was stirred for 5 minutes, and then TLR7*a* (21 mg, 57 μmol) was added and the solution was stirred for 18 h. The solvent was evaporated and the product purified by silica chromatography. Column Conditions: 40 g silica gel column, Mobile phase A: hexanes, Mobile Phase B: ethyl acetate. Gradient: percent mobile phase B: 0-3 min 0%, 3-10 min 100% ramp, 10-15 min 100%, 15-20 min switched to 90% ethyl acetate + 10% methanol. Product eluted at 13 min. Fractions collected, rotovapped, and dried over high vacuum to recover the product (72 mg, 85% yield). Predicted $[M+2Na]^{2+}$: 977.3 m/z. Observed $[M+2Na]^{2+}$: 977.3 m/z.

OtBu deprotection of p-tNTA-TLR7*a*. p-tNTA-TLR7*a* (55 mg, 29 μmol) was dissolved in 95%

TFA in water (5 mL) and stirred for 2 h. The TFA was removed by rotary evaporation and the residue added to 40 mL of cold diethyl ether to precipitate the product. The mixture was centrifuged to recover the product pellet. The pellet was dissolved in 50% water/ACN, sterile filtered through a nylon 0.22 um filter, and lypoholized in aliquoted eppendorf tubes and the product recovered (8.9 mg, 22% yield). The product was confirmed by LCMS. Predicted $[M+2H]^{2+}$: 703.3 m/z. Observed $[M+2H]^{2+}$: 703.6 m/z.

Synthesis of tNTA-TLR2/6*a*. The on-resin Michael addition was performed analogously to that of the TLR triagonists decribed in chapter 2. Fmoc-Pam_2CS(OtBu)K$(Boc)_4$GC(Mmt)G-Resin (50 mg resin, 0.039 mmol peptide) described above was swollen in DCM (10 mL) for 30 min and then the DCM drained. Cys(Mmt) was deprotected by washing the resin several times with 1% TFA/DCM (5 mL each wash) over 1 h. The resin was washed 3 X with DCM (10 mL) and 3 X with DMF (10 mL). p-tNTA-Mal (160 mg, 0.10 mmol) was dissolved in DMF (2 mL) with DIPEA (0.5 mL) and added to the resin . The reaction was incubated overnight, and the resin washed 3 X with DMF (10 mL). The Fmoc was deprotected using 20% piperidine in DMF (2 X 10 mL), washed 3 X with DMF (10 mL), and 3 X with DCM (10 mL). The peptide was cleaved from the resin with 95 % TFA/water (2 mL) for 2 h, and the resin washed 2 X with the 95% TFA solution (2 mL). The cleavage solutions were combined and the peptide was precipitated in ice cold diethyl ether (40 mL), and centrifuged (10 min, 4 °C). The resulting crude product was dried and purified by preparatory HPLC. The fractions containing product were pooled and lyophilized to obtain the purified product (2.5 mg, 1 μmol). The product confirmed by LCMS. Predicted $[M+3H]^{3+}$:858.8 m/z. Observed $[M+2H]^{3+}$: 859.5 m/z.

Synthesis of p-tNTA-Bpa. Fmoc-BPA-OH (79 mg, 0.16 mmol) and HBTU (61 mg, 0.16 mmol) were dissolved in DMF (2 mL) and DIPEA (1 mL). The solution was stirred for 5 minutes, and then added to p-tNTA (150 mg, 0.11 mmol) dissolved in 1 mL DMF. The reaction solution was stirred for 18 h. The solvent was evaporated and the product purified by silica chromatography. Column Conditions: 80 g silica gel column, Mobile phase A: hexanes, Mobile Phase B: ethyl acetate. Gradient: percent mobile phase B: 0-6 min 50%, 6-11 min 100% ramp, 11-19 min 100%. Product eluted at 10.5 min. Fractions collected, the solvent evaporated by rotary evaporation, and dried over high vacuum to recover the product (28 mg, 16 % yield). Product confirmed by ESI-MS. The product was characterized by MS. Predicted $[M+2Na]^{2+}$: 979.5 m/z. Observed $[M+2Na]^{2+}$: 979.1 m/z.

Fmoc deprotection of p-tNTA-Bpa-Mal. p-tNTA-Bpa (26 mg, 16 μmol) was dissolved in 25% diethyl amine in DCM (8 mL) and stirred for 6 h. The solvent was removed by rotary evaporation and the product purified by silica chromatography. Column Conditions: 12 g silica gel column, Mobile phase A: hexanes, Mobile Phase B: ethyl acetate. Gradient: percent mobile phase B: 0-2 min 50%, 2-4 min 100% ramp, 4-9 min 100%, 9-12 min switched to 90% ethyl acetate + 10% methanol. Product eluted at 9.8 min. Fractions collected, the solvent evaporated by rotary evaporation, and dried over high vacuum to recover the product (17 mg, 68 % yield). Product confirmed by MS. Predicted $[M+2Na]^{2+}$: 868.5 m/z. Observed $[M+2Na]^{2+}$: 867.8 m/z.

Synthesis of p-tNTA_Bpa-Mal. Mal-propionic acid (16 mg, 96 μmol) and HBTU (36 mg, 96 μmol) were dissolved in DMF (2 mL) and DIPEA (1 mL). The solution was stirred for 5 minutes, and then added to p-tNTA-Bpa-Mal (54 mg, 32 μmol) dissolved in 1 mL DMF. The reaction

solution was stirred for 18 h. The solvent was evaporated and the product purified by silica chromatography. Column Conditions: 80 g silica gel column, Mobile phase A: hexanes, Mobile Phase B: ethyl acetate. Gradient: percent mobile phase B: 0-2 min 10%, 2-12min 100% ramp, 12-20 min 100%. Product eluted as a broad peak from 15-19 min. Fractions collected, the solvent evaporated by rotary evaporation, and dried over high vacuum to recover the product (16 mg, 28 % yield). Product confirmed by ESI-MS. The product was characterized by MS. Predicted $[M+Na]^+$: 1865.0 m/z. Observed $[M+Na]^+$: 1864.8 m/z.

Deprotection of p-tNTA_Bpa-Mal. p-tNTA_Bpa-Mal (16 mg) was dissolved in 95% TFA in water and stirred for 2 h. The solution was evaporated and the product precipitated in cold diethyl ether. The product was characterized by MS. Predicted $[M+H]^+$: 1338.5 m/z. Observed $[M+H]^+$: 1337.7 m/z.

TLR9a Conjugation to tNTA-Bpa-Mal. Cap-S-S-CPG-FAM (0.252 mM, 159 μL, 40.0 nmol) solution, TCEP (7.6 mg/mL, 151 μL, 4000 nmol) solution and PBS (300 μL) were combined in a 1.5 mL Eppendorf tube. The solution was agitated for 4 h at room temperature. The solution was then spun for 10 min at 14,000 x g in a 3k MWCO amicon spin filter. HEPES 5 mM buffer pH 7.5 (400 μL) was added to the retained solution, spun again, and repeated 3X. The collected solution was mixed with tNTA-Bpa-Mal in DMF solution (approx. 10 mg/mL, 21 μL, approx. 160 nmol) and agitated overnight at room temperature. HEPES (300 μL) was added and the solution, the solution washed 3X in a 3k MWCO amicon spin filter, adding HEPES buffer to 500 μL total each time. The solution was collected to recover the final product (55 nmols, 80 % yield) and analyzed by ESI-MS. Predicted MW: 8484. Observed deconvoluted mass: 8484.

5.8 References

(1) Steinhagen, F.; Kinjo, T.; Bode, C.; Klinman, D. M. TLR-based immune adjuvants. *Vaccine* **2011**, *29* (17), 3341–3355.

(2) Lampkin, B. C.; Levine, A. S.; Levy, H.; Krivit, W.; Hammond, D. Phase II trial of a complex polyriboinosinic-polyribocytidylic acid with poly-l-lysine and carboxymethyl cellulose in the treatment of children with acute leukemia and neuroblastoma: a report from the children's cancer study group. *Cancer Res.* **1985**, *45* (11), 5904–5909.

(3) Pockros, P. J.; Guyader, D.; Patton, H.; Tong, M. J.; Wright, T.; McHutchison, J. G.; Meng, T.-C. Oral resiquimod in chronic HCV infection: safety and efficacy in 2 placebo-controlled, double-blind phase IIa studies. *J. Hepatol.* **2007**, *47* (2), 174–182.

(4) Robinson, R. A.; DeVita, V. T.; Levy, H. B.; Baron, S.; Hubbard, S. P.; Levine, A. S. A phase I-II trial of multiple-dose polyriboinosic-polyribocytidylic acid in patieonts with leukemia or solid tumors. *J. Natl. Cancer Inst.* **1976**, *57* (3), 599–602.

(5) Fujita, Y.; Taguchi, H. Overview and outlook of toll-like receptor ligand–antigen conjugate vaccines. *Ther. Deliv.* **2012**, *3* (6), 749–760.

(6) Blander, J. M.; Medzhitov, R. Toll-dependent selection of microbial antigens for presentation by dendritic cells. *Nature* **2006**, *440*, 808–812.

(7) Wille-Reece, U.; Flynn, B. J.; Loré, K.; Koup, R. A.; Kedl, R. M.; Mattapallil, J. J.; Weiss, W. R.; Roederer, M.; Seder, R. A. HIV gag protein conjugated to a toll-like receptor 7/8 agonist improves the magnitude and quality of Th1 and CD8+ t cell responses in nonhuman primates. *Proc. Natl. Acad. Sci. U. S. A.* **2005**, *102* (42), 15190–15194.

(8) Feng, Y.; Forsell, M. N. E.; Flynn, B.; Adams, W.; Loré, K.; Seder, R.; Wyatt, R. T.; Karlsson Hedestam, G. B. Chemical cross-linking of HIV-1 env for direct TLR7/8 ligand conjugation compromises recognition of conserved antigenic determinants. *Virology* **2013**, *446*, 56–65.

(9) Kastenmüller, K.; Wille-Reece, U.; Lindsay, R. W. B.; Trager, L. R.; Darrah, P. A.; Flynn, B. J.; Becker, M. R.; Udey, M. C.; Clausen, B. E.; Igyarto, B. Z.; et al. Protective T cell immunity in mice following protein-TLR7/8 agonist-conjugate immunization requires aggregation, type I IFN, and multiple DC subsets. *J. Clin. Invest.* **2011**, *121* (5), 1782–1796.

(10) Holbrook, B. C.; Kim, J. R.; Blevins, L. K.; Jorgensen, M. J.; Kock, N. D.; D'Agostino, R. B.; Aycock, S. T.; Hadimani, M. B.; King, S. B.; Parks, G. D.; et al. A novel r848-conjugated inactivated influenza virus vaccine is efficacious and safe in a neonate nonhuman primate model. *J. Immunol.* **2016**, *197* (2), 555–564.

(11) Holbrook, B. C.; D'Agostino, R. B.; Tyler Aycock, S.; Jorgensen, M. J.; Hadimani, M. B.; Bruce King, S.; Alexander-Miller, M. A. Adjuvanting an inactivated influenza vaccine with conjugated r848 improves the level of antibody present at 6 months in a nonhuman primate neonate model. *Vaccine* **2017**, *35* (45), 6137–6142.

(12) Clauson, R. M.; Berg, B.; Chertok, B. The content of CpG-dna in antigen-cpg conjugate vaccines determines their cross-presentation activity. *Bioconjug. Chem.* **2019**, *30* (3), 561–567.

(13) Wille-Reece, U.; Wu, C.; Flynn, B. J.; Kedl, R. M.; Seder, R. A. Immunization with hiv-1 gag protein conjugated to a TLR7/8 agonist results in the generation of HIV-1 gag-specific Th1 and CD8+ T cell responses. *J. Immunol.* **2005**, *174* (12), 7676–7683.

(14) Guimaraes, C. P.; Witte, M. D.; Theile, C. S.; Bozkurt, G.; Kundrat, L.; Blom, A. E. M.; Ploegh, H. L. Site-specific c-terminal and internal loop labeling of proteins using sortase-

mediated reactions. *Nat. Protoc.* **2013**, *8*, 1787.
(15) Popp, M. W.-L.; Antos, J. M.; Ploegh, H. L. Site-specific protein labeling via sortase-mediated transpeptidation. *Curr. Protoc. protein Sci.* **2009**, *Chapter 15*, Unit-15.3.
(16) MacDonald, J. I.; Munch, H. K.; Moore, T.; Francis, M. B. One-step site-specific modification of native proteins with 2-pyridinecarboxyaldehydes. *Nat. Chem. Biol.* **2015**, *11*, 326.
(17) Lata, S.; Reichel, A.; Brock, R.; Tampé, R.; Piehler, J. High-affinity adaptors for switchable recognition of histidine-tagged proteins. *J. Am. Chem. Soc.* **2005**, *127* (29), 10205–10215.
(18) Lata, S.; Gavutis, M.; Tampé, R.; Piehler, J. Specific and stable fluorescence labeling of histidine-tagged proteins for dissecting multi-protein complex formation. *J. Am. Chem. Soc.* **2006**, *128* (7), 2365–2372.
(19) Huang, Z.; Hwang, P.; Watson, D. S.; Cao, L.; Szoka Jr, F. C. Tris-nitrilotriacetic acids of subnanomolar affinity toward hexahistidine tagged molecules. *Bioconjug. Chem.* **2009**, *20* (8), 1667–1672.
(20) Saito, M.; Arakaki, R.; Yamada, A.; Tsunematsu, T.; Kudo, Y.; Ishimaru, N. Molecular mechanisms of nickel allergy. *Int. J. Mol. Sci.* **2016**, *17* (2), 202.
(21) Watson, D. S.; Platt, V. M.; Cao, L.; Venditto, V. J.; Szoka, F. C. Antibody response to polyhistidine-tagged peptide and protein antigens attached to liposomes via lipid-linked nitrilotriacetic acid in mice. *Clin. Vaccine Immunol.* **2011**, *18* (2), 289–297.
(22) Vance, N.; Zacharias, N.; Ultsch, M.; Li, G.; Fourie, A.; Liu, P.; LaFrance-Vanasse, J.; Ernst, J. A.; Sandoval, W.; Kozak, K. R.; et al. Development, optimization, and structural characterization of an efficient peptide-based photoaffinity cross-linking reaction for generation of homogeneous conjugates from wild-type antibodies. *Bioconjug. Chem.* **2019**, *30* (1), 148–160.